

Characterization of Catalysts for Lignin Depolymerization and 1,3-Butanediol Dehydration by using Pulse Chemisorption and Temperature Programmed Desorption

Simon Derveaux

Student number: 01802535

Supervisors: Prof. dr. ir. Philippe Heynderickx, Prof. dr. An Verberckmoes

Master's dissertation submitted in order to obtain the academic degree of
Master of Science in de industriële wetenschappen: chemie

Academic year 2022-2023

Dankwoord

Veel mensen hebben direct of indirect bijgedragen aan het voltooien van deze scriptie, wat het laatste mijlpaal is voor het behalen van mijn diploma als Industrieel Chemisch Ingenieur. Ik uit mijn dankbaarheid aan iedereen die in grote of kleine mate invloed heeft gehad op mijn academische studie. Ik wil in het bijzonder een aantal mensen bedanken die mij enorm hebben geholpen bij het maken van deze scriptie. Ik wil mijn promotoren, Prof. dr. An Verberckmoes en Prof. dr. ir. Philippe Heynderickx, bedanken voor hun steun, suggesties en feedback. Daarnaast ben ik erg dankbaar voor de doctoraatsstudenten Boyana Atanasova en Loïc Eloi, die mij hebben voorzien van waardevolle informatie, katalysatorstalen, feedback, inzichten en altijd behulpzaam waren bij het beantwoorden van mijn vragen.

Verder wil ik mijn waardering uiten aan doctoraatsstudent Alireza Ranjbari, die mij heeft begeleid in het laboratorium en bij het gebruik van de apparatuur. Ik wil GUGC bedanken voor de mogelijkheid om mijn onderzoek in Zuid-Korea uit te voeren. Het is een geweldige ervaring geweest en ik bedank iedereen die mijn tijd hier onvergetelijk heeft gemaakt. Ik wil ook mijn mede-scriptiestudenten, Margaux Nemegeer, Dries Wouters en Xander De Cleene, bedanken voor hun advies en gezelschap. Ik heb veel geweldige mensen ontmoet, die te talrijk zijn om op te noemen. Ik hoop jullie allemaal weer te ontmoeten en wens jullie het allerbeste toe. Tot slot wil ik mijn ouders en broer bedanken voor hun onvoorwaardelijke steun.

Acknowledgments

A lot of people contributed directly or indirectly to the accomplishment of this thesis, which is the last milestone in obtaining my degree as an Industrial Chemical Engineer. I express my gratitude to everyone who had a major or minor influence on my academic journey. I wish to thank some people in particular who helped me very hard to finish this thesis. I would like to thank my promotors Prof. dr. An Verberckmoes and Prof. dr. ir. Philippe Heynderickx for the support, suggestions and feedback. In addition to this, I am deeply thankful to doctoral students Boyana Atanasova and Loïc Eloi who supplied me with a lot of valuable information, catalyst samples, feedback, insights and were always helpful to answer my questions.

Further, I want to show my appreciation to doctoral student Alireza Ranjbari, who initiated and guided me in the lab and with the use of the equipment. I wish to thank GUGC for the possibility to fulfill my research in South-Korea. It has been an amazing experience, and I thank everyone who made my time here unforgettable. I would like to thank my fellow thesis students, Margaux Nemegeer, Dries Wouters, and Xander De Cleene, for their advice and company. I met a lot of amazing people, who are too numerous to sum up. I hope to meet you all again and wish you all the best. Lastly, I want to thank my parents and brother for their unwavering support.

De auteur geeft de toelating om deze masterproef voor consultatie beschikbaar te stellen en delen van de masterproef te kopiëren voor persoonlijk gebruik. Elk ander gebruik valt onder de bepalingen van het auteursrecht, in het bijzonder met betrekking tot de verplichting de bron uitdrukkelijk te vermelden bij het aanhalen van resultaten uit deze masterproef.

The author gives permission to make this master dissertation available for consultation and to copy parts of this master dissertation for personal use. In all cases of other use, the copyright terms have to be respected, in particular with regard to the obligation to state explicitly the source when quoting results from this master dissertation.

(8th of June 2023)

Deze masterproef vormt een onderdeel van een examen. Eventuele opmerkingen die door de beoordelingscommissie tijdens de mondelinge uiteenzetting van de masterproef werden geformuleerd, werden niet verwerkt in deze tekst.

This master's dissertation is part of an exam. Any comments formulated by the assessment committee during the oral presentation of the master's dissertation are not included in this text.

Abstract

This master's thesis characterizes catalysts for two reactions that can aid in the shift towards renewable biomass as a source for chemical production, driven by the limited supply of fossil fuels and the potential to reduce CO₂ emissions. The focus is on two promising reactions: the mild reductive depolymerization of lignin and the dehydration of 1,3-butanediol to butadiene.

CO pulse chemisorption is employed to determine the Pd dispersion on Pd and PdCu samples on the supports Al₂O₃, SiO₂ and AC, used for the depolymerization of lignin. Pd dispersion values ranging from 1.58 to 22.17% were reported. It was found that the dispersion in the monometallic catalysts was highest for Pd/AC, followed by Pd/Al₂O₃ and Pd/SiO₂. The bimetallic PdCu/Al₂O₃ was the most dispersed bimetallic catalyst and showed the highest dispersion value of all the catalysts. PdCu/AC and PdCu/SiO₂ show lower values. TEM-EDX analysis confirmed the relationship between smaller surface particles and higher Pd dispersion, with an exception observed in Pd/Al₂O₃. When analyzing a reactor study on the same samples, the non-acidic catalyst with the highest dispersion, Pd/AC, showed the fastest depolymerization to high M_w reduction. The catalyst with the highest dispersion of all and acidic support, PdCu/Al₂O₃, had the fastest initial depolymerization, however, the rate slowed down over time.

The zeolite ZSM-5, modified ZSM-5 and two methods to prepare hybrid ZSM-5 with CeO₂ are characterized in order to review their acid and basic properties. NH₃- and CO₂-TPD (temperature programmed desorption) are employed to characterize respectively the acidity and basicity of the ZSM-5 and hybrid samples. Increasing the Si/Al ratio and incorporating Boron were employed to decrease the acid density and strength of the ZSM-5 zeolite, because acidic tempered ZSM-5 has displayed a higher activity and selectivity to BD in the dehydration reaction of 1,3-BDO. Hybrid CeO₂ with ZSM-5 catalysts were also prepared. The results showed a significant reduction in acid sites and desorption energy values, indicating successful acid density and strength reduction. The hybrid CeO₂/ZSM-5 catalyst demonstrated a higher degree of acidic tempering compared to ZSM-5@CeO₂, but showed far less basic site incorporation. Overall, the proposed modifications and hybrid catalysts successfully tempered acidity. The hybrid ZSM-5@CeO₂ showed significant basic properties. The modified and hybrid ZSM-5 catalysts could improve the dehydration reaction of 1,3-BDO to BD and should be further investigated.

Keywords: Catalysis, NH₃-TPD, CO₂-TPD, CO pulse chemisorption, lignin depolymerization, dehydration of 1,3-butanediol

Characterization of Catalysts for Lignin Depolymerization and 1,3-Butanediol Dehydration by using Pulse Chemisorption and Temperature Programmed Desorption

Simon Derveaux

Supervisors: Prof. dr. ir. Philippe Heynderickx, Prof. dr. An Verberckmoes

Abstract: The Pd dispersion of Pd and PdCu supported on Al₂O₃, SiO₂ and active carbon (AC), used as catalysts for the lignin depolymerization is determined using CO pulse chemisorption. The Pd dispersion values range from 1.58% to 22.17%. Pd/AC exhibits the highest dispersion among monometallic catalysts, followed by Pd/Al₂O₃ and Pd/SiO₂. PdCu/Al₂O₃ is the most dispersed bimetallic catalyst and shows the highest dispersion of all the samples. PdCu/AC and PdCu/SiO₂ show lower dispersion. TEM-EDX¹ confirms the correlation between smaller surface particles and higher Pd dispersion, except for Pd/Al₂O₃. In a reactor study², the non-acidic catalysts with the highest dispersion, being Pd/AC, shows the fastest depolymerization to high molecular mass (M_w) reduction. PdCu/Al₂O₃, with high dispersion and acidic support, exhibits the fastest initial depolymerization rate, but slows down over time.

ZSM-5 is analyzed for the use in the 1,3-butanediol dehydration to butadiene. Modifications and preparing hybrid ZSM-5 with CeO₂ is employed to temper the acidity, which has proven to improve the conversion and selectivity to butadiene. Basic properties from CeO₂ are attempted to be incorporated in the hybrid catalysts. NH₃- and CO₂-TPD are employed to characterize the acid and basic sites respectively. Results from the Ghent campus are compared for confirmation. An increased SiO₂/Al₂O₃ ratio and boron incorporation decreased the acid density and strength of the catalysts. The hybrid CeO₂/ZSM-5 (dispersion of ZSM-5 on CeO₂) demonstrates better acid tempering but less basic site incorporation compared to ZSM-5@CeO₂ (core-shell structure with ZSM-5 as core and CeO₂ as shell). The modifications and hybrid catalysts successfully temper the acid properties of ZSM-5. ZSM-5@CeO₂ shows significant basic properties.

Keywords: Catalysis, CO pulse chemisorption, lignin depolymerization, NH₃-TPD, CO₂-TPD, dehydration of 1,3-BDO

I. INTRODUCTION

In recent years, numerous researches have focused on shifting chemical production from petroleum-based sources to renewable biomass resources, driven by the finite nature of fossil fuel reserves and the potential to mitigate CO₂ emissions. This study examines catalysts for two promising reactions: the mild reductive lignin depolymerization and 1,3-butanediol dehydration to butadiene. These reactions play a significant role in green chemistry and yield valuable platform chemicals as products. The study aims to characterize and evaluate the active sites on the catalysts.

Important for the lignin depolymerization, the Pd dispersion of monometallic Pd and bimetallic PdCu supported on Al₂O₃, SiO₂ and AC is determined using CO pulse chemisorption. TEM-EDX (Transmission Electron Microscopy Energy-Dispersive X-ray spectroscopy) and reactor study data, provided by Ghent university, are linked to the obtained results in order to gain a better understanding between the Pd dispersion and the catalytic performance of the catalysts.

Zeolite ZSM-5 samples are modified and used in hybrid CeO₂ catalysts with the goal of tempering their acid density and strength, which has been reported to increase the conversion of 1,3-butanediol (1,3-BDO) and selectivity to butadiene (BD). Basic properties are attempted to be incorporated by preparing hybrid catalysts with CeO₂. The acidic and basic properties are characterized using NH₃-TPD (Temperature Programmed Desorption) and CO₂-TPD respectively. By evaluating the properties, promising modifications and hybrid methods can be selected for further research for the dehydration of 1,3-butanediol.

¹ TEM-EDX data provided by Ghent University (Boyana Atanasova)

² Lignin depolymerization reactor study data provided by Ghent University (Boyana Atanasova)

II. MATERIALS AND METHODS

A. Catalysts for the lignin depolymerization

1) Materials³

Monometallic Pd and bimetallic PdCu catalysts supported on Al₂O₃, SiO₂ and AC (active carbon) were prepared using incipient wetness impregnation with metal precursors Pd(NO₃)₂·8H₂O and Cu(NO₃)₂·6H₂O. The six samples are dried at 60°C for 16 hours. The Al₂O₃ and SiO₂ supported samples are calcined at 450°C for four hours under air while the AC supported samples are calcined under the same conditions but under N₂ [1]. The metal loading was aimed to be 5wt% and have a Pd/Cu ratio of 3/2 for the bimetallic catalysts. The actual metal loading was determined by ICP-AES⁴ (Inductively Coupled Plasma Atomic Emission Spectroscopy). The results are listed in Table 1.

Table 1: metal loading of the catalysts

Catalyst	Pd (wt%)	Cu (wt%)	Tot. (wt%)
Pd/Al ₂ O ₃	3.05	/	3.05
Pd/AC	4.27	/	4.27
Pd/SiO ₂	3.41	/	3.41
PdCu/Al ₂ O ₃	2.02	1.54	3.56
PdCu/AC	3.88	2.97	6.85
PdCu/SiO ₂	2.16	1.54	3.70

2) Characterization of the catalysts

The Pd dispersion is determined using CO pulse chemisorption. This is performed by using the AutoChem II 2920 with a TCD (Thermal Conductivity Detector). Ca. 100 mg sample per analysis is loaded. A pretreatment is performed by heating the sample to 200°C under He. The sample is reduced at 200°C under a 10% H₂/Ar flow to convert the surface Pd into their metallic form so that CO will chemisorb on the particles. A fixed volume of 1% or 10% CO/He is pulsed over the sample each 1.5 min at a stable temperature of 35°C. The amount of surface Pd on the samples is calculated by correlating the adsorbed gas volume to the amount of surface Pd, with a Pd/CO stoichiometry factor of two [2]. The Pd dispersion (D) is then determined by equation 1.

$$D = \frac{\text{moles of metal on surface } (N_s)}{\text{total moles of metal in sample } (N_t)} \quad (1)$$

The average particle size of the catalysts is determined using TEM-EDX. The dispersion and particle size results are linked by using equation 2 [3].

$$D = 6 \cdot \frac{v_m}{a_m \cdot d_{VA}} \quad (2)$$

³ The catalysts were provided by Ghent University and not prepared by the writer of this thesis

⁴ ICP-AES data provided by Ghent University (INCAT)

Here d_{VA} is the average particle size and a_m and v_m are respectively the surface area occupied on a polycrystalline surface and the volume occupied in the bulk of the metal by a Pd atom.

B. Catalysts for the 1,3-BDO dehydration

1) Materials⁵

Eight samples are characterized. These include commercial ZSM-5, ZSM-5 with a SiO₂/Al₂O₃ ratio of ca. 25 and 150, boron incorporated samples with (theoretically) half the Al₂O₃ replaced by B, pure CeO₂ and two different hybrid ZSM-5 with CeO₂ catalysts. The synthesis of the ZSM-5 and boron incorporated samples is based on the method of de Reviere et al. (2020) [4]. The synthesis of pure CeO₂ and the hybrid catalysts is based on the method of De Saegher et al. (2020) [5] and Di et al. (2022) [6] respectively. Two hybrid catalysts are prepared starting from the prepared ZSM-5 with SiO₂/Al₂O₃ ratio 25. CeO₂/ZSM-5 corresponds to the sample where ZSM-5 is dispersed on CeO₂, with each 50/50 wt%. ZSM-5@CeO₂ corresponds to the core-shell catalysts, with ZSM-5 as the core and CeO₂ as the shell. The actual SiO₂/Al₂O₃ and B/Al₂O₃ ratios were determined using ICP-OES⁶ (Inductively Coupled Plasma Optical Emission Spectroscopy). The analyzed catalysts with actual SiO₂/Al₂O₃ and/or B/Al₂O₃ ratios and characterized properties are listed in Table 2.

Table 2: catalysts for the 1,3-BDO dehydration

Catalyst	Actual Si/Al ratio	Actual B/Al ratio	Characterized properties
Comm. ZSM-5	24	/	acidity
ZSM-5@25	15	/	acidity
ZSM-5@150	153	/	acidity
ZSM-5@25_B	47	0.2	acidity
ZSM-5@150_B	356	0.9	acidity
CeO ₂	/	/	basicity
CeO ₂ /ZSM-5	/	/	acidity, basicity
ZSM-5@CeO ₂	/	/	acidity, basicity

2) Characterization of the catalysts

NH₃- and CO₂-TPD are employed to characterize the acidic and basic properties of the catalysts respectively. This is performed by using the AutoChem II 2920 with a TCD. Similar methods were used. The samples are pretreated at 550°C under He in order to remove water. NH₃ is loaded by flowing 5% NH₃/He at 120°C, while CO₂ is loaded by flowing 5% CO₂/He at 40°C. Weakly physisorbed probe gas is removed by flushing with He. Lastly, the analysis starts by linearly increasing the temperature until 550°C. TPD spectra were recorded at heating rates 10, 15 and 20°C/min.

⁵ The catalysts were provided by Ghent University (Loïc Eloï) and not prepared by the writer of this thesis

⁶ ICP-OES data provided by Ghent University (Diederik Leenknecht)

3) TPD spectra interpretation

Noise removal by adjacent-averaging smoothing and baseline correction is performed in the Origin data treatment software. After, modelled Gaussian peaks for the different site strengths are obtained by deconvolution of the signal. The parameters a_i (scaling factor), σ_i (standard deviation) and μ_i (time at peak maximum) in equation 3 are determined so that the residual sum of squared of the experimental data points and the modelled data points are minimized. N is the number of peaks and t the time in minutes.

$$f(t) = \sum_{i=1}^N \frac{a_i}{\sigma_i \cdot \sqrt{2\pi}} \cdot e^{-\frac{(t-\mu_i)^2}{2\sigma_i^2}} \quad (3)$$

By performing the TPD experiments at different heating rates, the first order Arrhenius curves for each sample can be plotted. The Arrhenius equation is reformulated to equation 4 [7,8]. β is the heating rate, R the gas constant, T_{\max} the temperature at maximum desorption and A the pre-exponential factor in the Arrhenius equation. The desorption energy E_d corresponds to the strength of the active sites.

$$2 \cdot \ln(T_{\max}) - \ln(\beta) = -\frac{E_d}{R} \left(\frac{1}{T_{\max}} \right) + \ln(A) \quad (4)$$

The slope of $2 \cdot \ln(T_{\max}) - \ln(\beta)$ versus $1/T_{\max}$ equals $-E_d/R$, so that the desorption energy for the peaks can be determined.

III. RESULTS AND DISCUSSION

A. Metal dispersion study on catalysts for lignin depolymerization

1) Pd dispersion

The Pd dispersion of the catalysts is determined using CO pulse chemisorption. The results are listed in Table 3. The error (standard deviation) is calculated using a 1% error on the loop temperature and the standard deviation on the peak areas of the saturated peaks. The average particle size at the surface of the samples, determined by TEM-EDX, is also displayed.

Table 3: Pd dispersion results

Catalyst	Pd dispersion (%)	Particle size (nm)
Pd/Al ₂ O ₃	8.89 ± 0.27	7
PdCu/Al ₂ O ₃	22.17 ± 0.23	10
Pd/SiO ₂	2.13 ± 0.04	14
PdCu/SiO ₂	1.58 ± 0.05	15
Pd/AC	12.68 ± 0.16	13
PdCu/AC	10.46 ± 0.26	12

The Pd dispersion is greatly influenced by both the catalyst support and the presence of the co-metal Cu. Both the mono- and bimetallic SiO₂ supported catalysts show very low dispersion. For the monometallic Pd catalysts, the dispersion is the highest for Pd/AC, followed by Pd/Al₂O₃ and Pd/SiO₂. The bimetallic PdCu/Al₂O₃ exhibits the highest dispersion of all the catalysts, with a value of 22.17%. The bimetallic PdCu/AC and PdCu/SiO₂ show lower dispersion.

2) Dispersion relation to particle size

The dispersion values were linked to the particle size, determined by TEM-EDX. The average particle and dispersion for all the catalysts are shown in Figure 1.

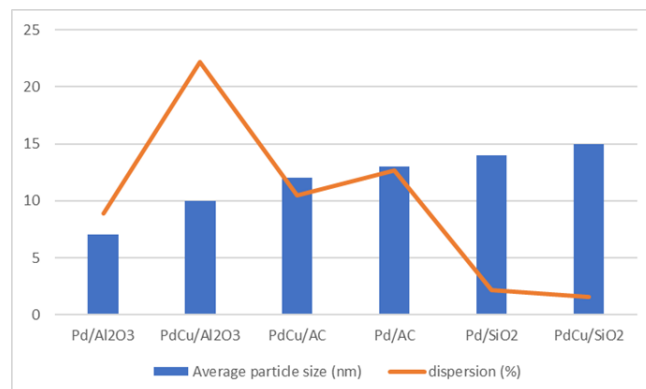


Figure 1: average particle size and Pd dispersion for the catalysts

Normally, smaller average particles on the surface correspond to a higher dispersion rate. This trend was confirmed, with some slight deviations. Only Pd/Al₂O₃ did not comply with this theory by showing a far too low dispersion. The dispersion in function of the average particle size is shown in Figure 2, with the exclusion of the data for Pd/Al₂O₃. The standard deviation on the dispersion was too small to be visible on the graph.

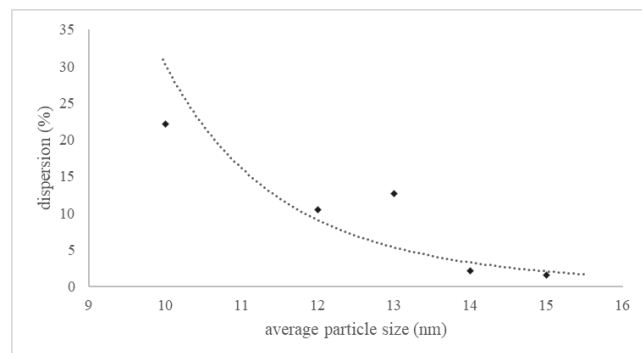


Figure 2: Dispersion in function of the average particle size of the surface species (Pd/Al₂O₃ excluded)

The outline of this curve has a similar shape as the theoretical one, derived from equation (2). However, the values of the experimental data points deviate significantly from the theoretical ones, with a shift to higher average particle size. For the bimetallic catalysts, this is partly because the size determined by TEM-EDX makes no difference between Pd and Cu particles, while the dispersion is only in regard to Pd. It is also possible that the assumptions in equation (2) are not correct for this catalyst. For example, hemispheric particles on the surface are assumed. In addition to this, the measurements itself are complex techniques where small variations in experimental procedures, data analysis or equipment can lead to significant deviations on the results.

3) Dispersion relation to reactor results

The results of a reactor study⁷ on the samples are linked to the dispersion results from this thesis. The mild depolymerization of lignin was performed in a batch reactor at 200°C and 10 bar, containing 0.05 g catalyst. The lignin was solved in a 70/30% ethanol water mixture in a concentration of 20 mg/ml. The mean molecular mass (M_w) of the depolymerized lignin is determined using GPC (Gel permeation Chromatography) at different reaction times. The M_w in function of the batch time (amount of Pd on catalyst multiplied by the reaction time) is visualized in Figure 3.

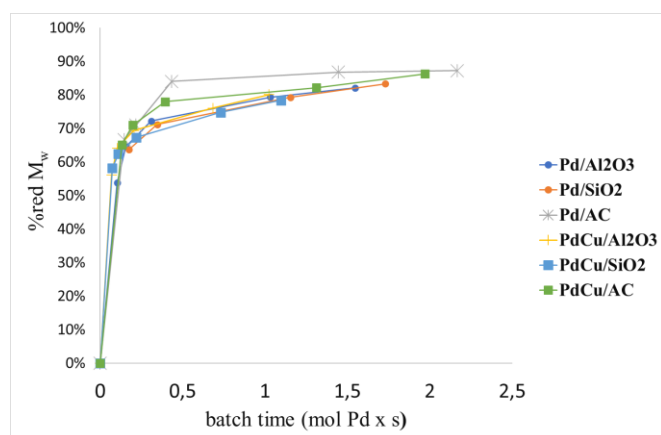


Figure 3: lignin depolymerization reaction results

It is observed that the catalysts with the highest dispersion on a non-acidic support, being Pd/AC, displays the fastest depolymerization to a high M_w reduction of around 85%. The fastest initial depolymerization is observed for PdCu/Al₂O₃, which possesses an acidic support and has the highest reported dispersion of all the catalysts in this study. However, the depolymerization rate decreases and a far longer time is needed to reach a M_w reduction of 85%. Interestingly, a similar fast initial rate is observed for the non-acidic PdCu/SiO₂, while showing a very low dispersion. In conclusion, Pd/AC, with a non-acidic support and a relatively high dispersion of 12.68% compared to the other non-acidic catalysts, seems the most efficient for the depolymerization of lignin to a high M_w reduction. The initial rate is not the fastest, but the depolymerization rate stays high for a long time. A clear relation between the Pd dispersion, nature of the support and the reaction activity was not yet found. Further research to understand the complex reaction mechanism is needed.

B. Acidity and basicity study on catalysts for the 1,3-BDO dehydration

1) Issues regarding the TPD spectra

The obtained TPD spectra are strongly deformed and a nod in the baseline at a temperature of around 400°C is observed, leading to difficulties in obtaining quantitative results. Attempts were made to mitigate this issue by using more sample, different heating rates, reconnecting the gasses, baseline stabilization, data treatment... but no solution was found.

⁷ Lignin depolymerization reactor study data provided by Ghent University (Boyana Atanasova)

The baseline was chosen to go through the minimum point between the peaks, which in reality is not true. This made it impossible to obtain quantitative results for the concentration of active sites. A comparison between the catalysts could be made, however probably with a significant error on the results. As an example, the recorded NH₃-TPD spectrum of commercial ZSM-5 with heating rate 10°C/min and the corrected and deconvoluted spectrum are shown in Figure 4 and Figure 5.

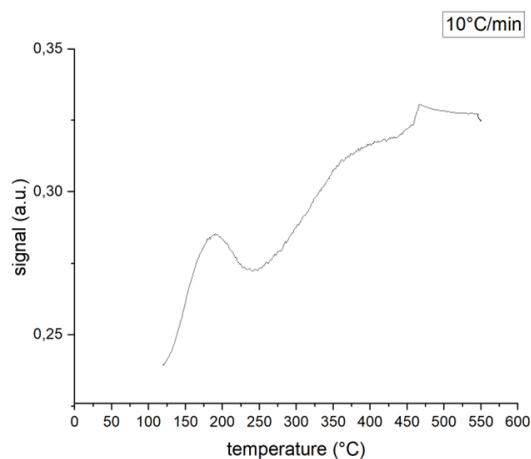


Figure 4: recorded NH₃-TPD spectrum of commercial ZSM-5 (10°C/min)

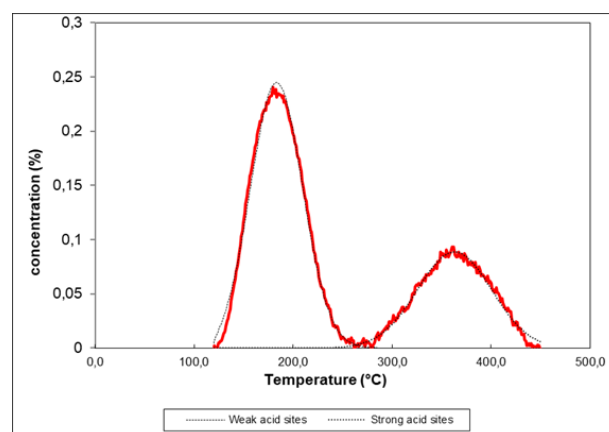


Figure 5: corrected and deconvoluted NH₃-TPD spectrum of commercial ZSM-5 (10°C/min)

To confirm the comparative results and to be able to report quantitative values for the active site density, NH₃-TPD results on the same samples performed at the Ghent campus⁸ were discussed. As an example for the CO₂-TPD spectra, the recorded spectrum of CeO₂ with heating rate 15°C/min and the corrected and deconvoluted spectrum are shown in Figure 6 and Figure 7.

⁸ NH₃-TPD on the samples at the Ghent campus was performed by doctoral student Loïc Eloi

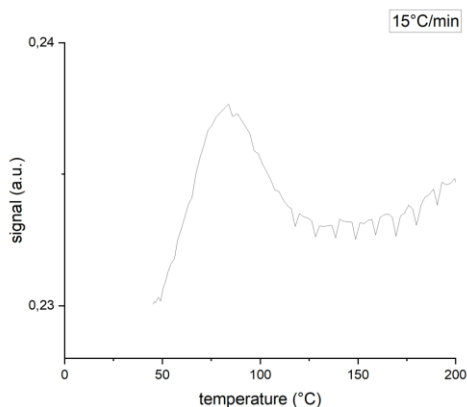


Figure 6: recorded CO₂-TPD spectrum of CeO₂ (15°C/min)

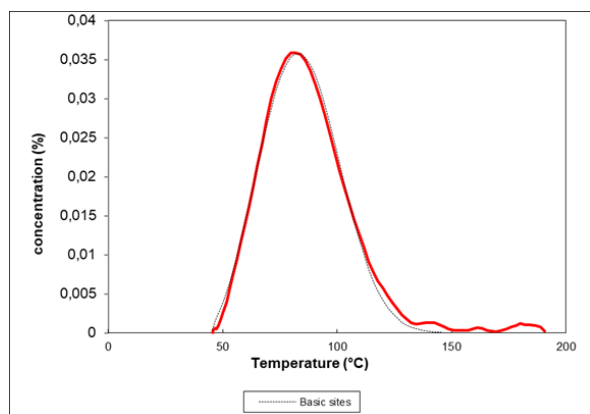


Figure 7: corrected and deconvoluted CO₂-TPD spectrum of CeO₂ (15°C/min)

Because only one peak is observed in the TPD spectrum, the baseline correction is probably more correctly performed. Hence, the obtained density values are quantitatively more valuable than those of the NH₃-TPD study.

2) Acidity study with NH₃-TPD

NH₃-TPD is performed on all the samples, except CeO₂. The absolute values of the acid density in this thesis are not representative of the actual value, due to the problems stated above. Only comparative conclusions between the samples are useful. However, the determined E_d values are probably correct and useful because the deformed spectra still permit to localize the peak temperatures. These results are listed in Table 4. The experimental error is calculated from the standard deviation on E_d of commercial ZSM-5, which has been analyzed twice.

Table 4: determined E_d values of the catalysts

Catalyst	Strength of the strong acid site E _d (kJ/mol)
Comm. ZSM-5	132.59 ± 2.51
ZSM-5@25	133.95 ± 2.51
ZSM-5@150	98.97 ± 2.51
ZSM-5@25_B	113.46 ± 2.51
ZSM-5@150_B	84.58 ± 2.51
CeO ₂ /ZSM-5	98.80 ± 2.51
ZSM-5@CeO ₂	134.6 ± 2.51

The conclusions of the NH₃-TPD analysis are as follows. When increasing the Si/Al ratio from 25 to 150, a decrease in weak and strong acidic sites of respectively 82.1% and 51.2% is observed. A slightly higher decrease is observed in the Ghent study, but a comparable trend is observed. In this study, E_d decreased from 133.95 kJ/mol to 98.97 kJ/mol when increasing the Si/Al from 25 to 150. These results correspond with the values of 135.1 kJ/mol and 103.3 kJ/mol, reported by Gunst et al. (2020) [9]. The modification thus leads to a successful lowering of the acid density and strength.

Boron was incorporated into the ZSM-5@25 and ZSM-5@150 catalysts. The acid density results for ZSM-5@25_B in this thesis seemed to be incorrect and were refuted. The Ghent study reported a total acid density decrease of 34.6%, with an equal decrease for the weaker and stronger sites. The E_d value of the boron incorporated sample is 113.46 kJ/mol, compared to 133.95 kJ/mol for ZSM-5@25. The Ghent study reported E_d values of respectively 84 kJ/mol and 115 kJ/mol, thus showing a significant difference. However, the same trend is observed. The results of ZSM-5@150_B seemed more reliable. In this thesis and the Ghent thesis, the decrease in the weaker sites (weak and medium strength) is 51.7% and 55.8% respectively. The decrease in strong sites is 71.4% and 36% respectively. This indicates that the decrease in the strong acid site density in this thesis was too high. This thesis determined a decrease in E_d from 98.97 kJ/mol for ZSM-5@150 to 84.58 kJ/mol for ZSM-5@150_B. The boron incorporation in ZSM-5 samples thus successfully tempered the acidity, by both decreasing the acid density and strength of the catalysts.

The hybrid CeO₂/ZSM-5 in this research showed a decrease of 61.1% and 79.6% for the weak and strong sites respectively compared to ZSM-5. The Ghent study reported a decrease of 72% and 40%. The decrease in stronger acid sites in this thesis seems thus to be higher expected. The determined E_d value in this research is 98.80 kJ/mol, compared to 133.95 kJ/mol for pure ZSM-5. The acid density and strength of the hybrid CeO₂/ZSM-5 is thus successfully decreased.

The acid density of the hybrid ZSM-5@CeO₂ was found to increase in this research. This is highly unlikely and does not corresponds with the result of the Ghent campus. Hence, this result is refuted. No significant change in E_d is found. This cannot be confirmed with data from Ghent, so that this observation is highly uncertain. The Ghent campus reported a total acid density decrease of 27.4%, which is far lower than the decrease of the hybrid CeO₂/ZSM-5. The acidic tempering of the hybrid CeO₂/ZSM-5 is thus more effective than in ZSM-5@CeO₂.

3) Basicity study with CO₂-TPD

CO₂-TPD was performed on the two hybrid catalysts and pure CeO₂. No Ghent results are available, so that no comparison is possible. Because only one peak is observed in the TPD spectrum, the baseline correction is probably more correctly performed. Hence, the obtained density values are quantitatively more valuable than those of the NH₃-TPD study. Pure CeO₂ showed one basic peak at a temperature of around 80°C. This is lower than the reported temperature of 110°C by Yoshikawa et al. (2016) for a similar heating rate [10]. The basic density is 11.82 μmol/g_{cat}.

ACKNOWLEDGEMENTS

The author would like to thank doctoral students Boyana Atanasova and Loïc Eloi for the provided analysis and reactor data.

REFERENCES

- [1] B. Kraushaar-Czarnetzki and S. P. Müller, "Shaping of Solid Catalysts Objectives of Catalyst Shaping," *Synthesis of Solid Catalysts*, pp. 173–199, 2009, Accessed: Jan. 16, 2023. [Online]. Available: https://books.google.com/books/about/Synthesis_of_Solid_Catalyst_s.html?hl=nl&id=5ejCa9HGf2oC
- [2] P. Canton, G. Fagherazzi, M. Battagliarin, F. Menegazzo, F. Pinna, and N. Pernicone, "Pd/CO Average Chemisorption Stoichiometry in Highly Dispersed Supported Pd/ γ -Al₂O₃ Catalysts," *Langmuir*, vol. 18, no. 17, pp. 6530–6535, Aug. 2002, doi: 10.1021/LA015650A.
- [3] G. Bergeret and P. Gallezot, "Particle Size and Dispersion Measurements," vol. 2, p. 10, 2008, doi: 10.1002/9783527610044.hetcat0038f.
- [4] A. de Reviere, T. Vandevyvere, M. K. Sabbe, and A. Verberckmoes, "Renewable Butene Production through Dehydration Reactions over Nano-HZSM-5/ γ -Al₂O₃ Hybrid Catalysts," *Catalysts* 2020, Vol. 10, Page 879, vol. 10, no. 8, p. 879, Aug. 2020, doi: 10.3390/CATAL10080879.
- [5] T. De Saegher *et al.*, "Monometallic Cerium Layered Double Hydroxide Supported Pd-Ni Nanoparticles as High Performance Catalysts for Lignin Hydrogenolysis," *Materials* 2020, Vol. 13, Page 691, vol. 13, no. 3, p. 691, Feb. 2020, doi: 10.3390/MA13030691.
- [6] Z. Di, H. Wang, R. Zhang, H. Chen, Y. Wei, and J. Jia, "ZSM-5 core-shell structured catalyst for enhancing low-temperature NH₃-SCR efficiency and poisoning resistance," *Appl Catal A Gen*, vol. 630, p. 118438, Jan. 2022, doi: 10.1016/J.APCATA.2021.118438.
- [7] M. Niwa and N. Katada, "New Method for the Temperature-Programmed Desorption (TPD) of Ammonia Experiment for Characterization of Zeolite Acidity: A Review," *The Chemical Record*, vol. 13, no. 5, pp. 432–455, Oct. 2013, doi: 10.1002/TCR.201300009.
- [8] P. A. Webb, "Introduction to Chemical Adsorption Analytical Techniques and their Applications to Catalysis," 2003.
- [9] D. Gunst, M. Sabbe, M. F. Reyniers, and A. Verberckmoes, "Study of n-butanol conversion to butenes: Effect of Si/Al ratio on activity, selectivity and kinetics," *Appl Catal A Gen*, vol. 582, Jul. 2019, doi: 10.1016/J.APCATA.2019.05.035.
- [10] K. Yoshikawa, M. Kaneeda, and H. Nakamura, "Development of Novel CeO₂-based CO₂ adsorbent and analysis on its CO₂ adsorption and desorption mechanism," *Energy Procedia*, vol. 114, pp. 2481–2487, Jul. 2017, doi: 10.1016/J.EGYPRO.2017.03.1400.

The hybrid CeO₂/ZSM-5 catalyst showed only 6% of the basic concentration compared to pure CeO₂, with a value of 0.81 $\mu\text{mol/g}_{\text{cat}}$. The basic properties of CeO₂ are thus barely incorporated in the hybrid catalyst. The strength of the basic peak is decreased, with a shift in peak maximum to around 70°C for a heating rate of 15°C/min. The E_d value was not determined due to a technical error.

The hybrid catalyst ZSM-5@CeO₂ shows a better incorporation of basic sites compared to CeO₂/ZSM-5. The basic site density is 37.3% of the density in pure CeO₂, with a value of 4.41 $\mu\text{mol/g}_{\text{cat}}$. A weaker basic site strength is observed, with an E_d value of 99.45 kJ/mol compared to 110.83 kJ/mol for pure CeO₂. This method for the preparation of a hybrid catalysts with the goal of incorporating basic properties is thus superior. This is probably due to the fact that CeO₂ is the shell in the core-shell structure, and thus more exposed at the surface of the catalysts. However, a lower acidic tempering was reported for this catalysts compared to CeO₂/ZSM-5.

IV. CONCLUSION

The Pd dispersion for the supported metal catalysts, used in the lignin depolymerization is determined using CO pulse chemisorption. Dispersion values ranging from 1.58% to 22.17% are reported. PdCu/Al₂O₃ exhibited the highest Pd dispersion, while the SiO₂ supported catalysts show very low dispersion. The determined dispersion from this thesis was linked to the average particle size of the surface species determined by TEM-EDX. Reactor data for the lignin depolymerization was discussed. Pd/AC, the catalyst with the highest dispersion on a non-acidic support, displayed the fastest depolymerization to a high M_w reduction of around 85%. PdCu/Al₂O₃, the catalysts with an acidic support and the highest reported dispersion of all the samples, exhibited a very fast initial depolymerization rate. However, as the reaction progresses, the depolymerization rate decreases so that a high M_w reduction of 85% is reached after a longer time compared to Pd/AC.

NH₃- and CO₂-TPD was employed to characterize the acid and basic properties on catalysts for the dehydration of 1,3-BDO. Increasing the SiO₂/Al₂O₃ and the boron incorporation in ZSM-5 significantly lowered the acid density and strength on the samples. The lowest reported E_d value of the strong acid site is 84.58 kJ/mol for ZSM-5@150_B, which is a significant decrease from the value of 133.95 kJ/mol for ZSM-5@25. The tempering of the acidity is more effective in the CeO₂/ZSM-5 hybrid catalyst than in ZSM-5@CeO₂. However, ZSM-5@CeO₂ exhibited a far higher basic site incorporation, with basic concentrations of respectively 4.41 and 0.81 $\mu\text{mol/g}_{\text{cat}}$. The modifications and hybrid catalysts possibly have a beneficial influence on the ZSM-5 catalysts with the aim of increasing the conversion of 1,3-BDO and the selectivity to butadiene.

Karakterisering van katalysatoren voor de depolymerisatie van lignine en de dehydratie van 1,3-butaandiol met behulp van pulschemisorptie en temperatuur-geprogrammeerde desorptie

Simon Derveaux

Promotoren: Prof. dr. ir. Philippe Heynderickx, Prof. dr. An Verberckmoes

Abstract: De Pd-dispersie van Pd en PdCu op de dragers Al_2O_3 , SiO_2 en actief koolstof (AC), gebruikt als katalysatoren voor de lignine depolymerisatie, is bepaald met behulp van CO pulschemisorptie. De Pd-dispersiewaarden variëren van 1.58% tot 22.17%. Pd/AC vertoont de hoogste dispersie onder de monometaal katalysatoren, gevolgd door Pd/ Al_2O_3 en Pd/ SiO_2 . PdCu/ Al_2O_3 is de meest gedispergeerde bimetaalkatalysator en vertoont de hoogste dispersie van alle stalen. PdCu/AC en PdCu/ SiO_2 vertonen een lagere dispersie. TEM-EDX¹ bevestigt de correlatie tussen kleinere oppervlakte-deeltjes en hogere Pd-dispersie, behalve voor Pd/ Al_2O_3 . In een reactorstudie² vertoont de niet-zure katalysator met de hoogste dispersie, namelijk Pd/AC, de snelste depolymerisatie tot een hoge moleculaire massa (M_w) reductie. PdCu/ Al_2O_3 , met hoge dispersie en een zure drager, vertoont de snelste initiële depolymerisatie snelheid, maar deze vertraagt na verloop van tijd.

ZSM-5 is geanalyseerd voor gebruik als katalysator bij de dehydratie van 1,3-butaandiol tot butadieen. Modificaties en de bereiding van hybride ZSM-5 met CeO_2 werd toegepast om de zuurtegraad te temperen, wat de conversie en selectiviteit naar butadieen kan verhogen. Er wordt getracht basische eigenschappen van CeO_2 in te brengen in de hybride katalysatoren. NH_3 - en CO_2 -TPD worden gebruikt om respectievelijk de zure en basische sites te karakteriseren. De resultaten van de Gent campus worden ter bevestiging vergeleken. Een verhoogde $\text{SiO}_2/\text{Al}_2\text{O}_3$ -verhouding en boorintegratie verminderden de zuurdensiteit en sterkte van de katalysatoren. De hybride $\text{CeO}_2/\text{ZSM-5}$ (dispersie van ZSM-5 op CeO_2) toont een betere zuurtempering maar een lagere integratie van basische sites in vergelijking met ZSM-5@ CeO_2 (core-shell structuur met ZSM-5 als kern en CeO_2 als schil). In conclusie, de modificaties en hybride katalysatoren temperen met succes de zure eigenschappen van ZSM-5. ZSM-5@ CeO_2 vertoont significante basische eigenschappen.

Slutelbegrippen: Katalyse, CO pulschemisorptie, lignine depolymerisatie, NH_3 -TPD, CO_2 -TPD, dehydratie van 1,3-BDO

I. INTRODUCTIE

In de afgelopen jaren hebben talloze onderzoeken zich gericht op het verschuiven van de chemische productie van bronnen op basis van aardolie naar hernieuwbare biomassa-bronnen, gedreven door de eindigheid van fossiele brandstofreserves en het potentieel om CO_2 -uitstoot te verminderen. Deze studie onderzoekt katalysatoren voor twee veelbelovende reacties: de milde reductieve lignine depolymerisatie en de dehydratie van 1,3-butaandiol tot butadieen. Deze reacties spelen een belangrijke rol in de groene chemie en leveren waardevolle platformchemicaliën op als producten. Het onderzoek heeft tot doel de actieve sites op de katalysatoren te karakteriseren en te evalueren.

De Pd-dispersie op de katalysatoren is belangrijk voor de lignine depolymerisatie. Dit wordt bepaald voor monometaal Pd en bimetaal PdCu ondersteund op de dragers Al_2O_3 , SiO_2 en actieve koolstof (AC) met behulp van CO pulschemisorptie. TEM-EDX (Transmission Electron Microscopy Energy-Dispersive X-ray spectroscopy) en reactorstudiegegevens, verstrekt door de Universiteit Gent, worden gekoppeld aan de verkregen resultaten om een beter begrip te krijgen omtrent de Pd-dispersie en de katalytische prestaties van de katalysatoren.

Zeoliet ZSM-5 stalen worden gemodificeerd en gebruikt in hybride CeO_2 katalysatoren met het doel hun zuurdichtheid en sterkte te temperen, wat de omzetting van 1,3-butaandiol (1,3-BDO) en de selectiviteit naar butadieen (BD) kan verhogen. Er wordt getracht basische eigenschappen in te brengen door hybride katalysatoren met CeO_2 te bereiden. De zure en basische eigenschappen worden gekarakteriseerd met respectievelijk NH_3 -TPD (Temperature Programmed Desorption) en CO_2 -TPD. Door evaluatie van de eigenschappen kunnen veelbelovende modificaties en hybride methoden worden geselecteerd voor verder onderzoek naar katalysatoren voor de dehydratie van 1,3-butaandiol.

¹ TEM-EDX data aangeleverd door Universiteit Gent (Boyana Atanasova)

² Lignine depolymerisatie reactor data aangeleverd door Universiteit Gent (Boyana Atanasova)

A. Katalysatoren voor de depolymerisatie van lignine

1) Materialen³

Monometaal Pd en bimetaal PdCu katalysatoren op de dragers Al₂O₃, SiO₂ en AC (actieve koolstof) werden bereid met behulp van *incipient wetness impregnation* met de metaalprecursoren Pd(NO₃)₂·8H₂O en Cu(NO₃)₂·6H₂O. De zes stalen zijn gedurende 16 uur bij 60°C gedroogd. De Al₂O₃ en SiO₂ gedragen stalen zijn vier uur gecalcineerd bij 450°C onder lucht, terwijl de AC gesteunde stalen onder dezelfde omstandigheden zijn gecalcineerd, maar dan onder N₂ [1]. Voor de metaalkatalysatoren werd gestreefd naar een metaalbelasting van 5wt% en een Pd/Cu-verhouding van 3/2 voor de bimetallic stalen. De werkelijke metaalbelasting werd bepaald door ICP-AES⁴ (Inductively Coupled Plasma Atomic Emission Spectroscopy). De resultaten zijn opgelijst in tabel 1.

Tabel 1: metaal belading van de katalysatoren

Katalysator	Pd (wt%)	Cu (wt%)	Tot. (wt%)
Pd/Al ₂ O ₃	3.05	/	3.05
Pd/AC	4.27	/	4.27
Pd/SiO ₂	3.41	/	3.41
PdCu/Al ₂ O ₃	2.02	1.54	3.56
PdCu/AC	3.88	2.97	6.85
PdCu/SiO ₂	2.16	1.54	3.70

2) Karakterisatie van de katalysatoren

De Pd-dispersie is bepaald met behulp van CO pulschemisorptie. Dit gebeurt met behulp van de AutoChem II 2920 met een TCD (Thermal Conductivity Detector). Ca. 100 mg monster per analyse werd geladen. Een voorbehandeling werd uitgevoerd door het staal te verwarmen tot 200°C onder He. Het staal werd gereduceerd bij 200°C onder 10% H₂/Ar om de oppervlakte Pd species om te zetten in hun metaalvorm zodat CO kan chemisorberen op de deeltjes. Een vast volume van 1% of 10% CO/He wordt elke 1,5 min bij een stabiele temperatuur van 35°C over het monster gepulseerd. De hoeveelheid oppervlakte-Pd op de monsters wordt berekend door het geadsorbeerde gasvolume te correleren met de hoeveelheid oppervlakte-Pd, met een Pd/CO stoichiometriefactor van twee [2]. De Pd-dispersie (D) wordt dan berekend uit vergelijking 1.

$$D = \frac{\text{mol metaal op oppervlakte } (N_s)}{\text{totaal mol metaal in staal } (N_t)} \quad (1)$$

De gemiddelde deeltjesgrootte van de katalysatoren werd bepaald met behulp van TEM-EDX. De resultaten van de dispersie en de deeltjesgrootte zijn gekoppeld met behulp van vergelijking 2 [3].

$$D = 6 \cdot \frac{v_m}{a_m \cdot d_{VA}} \quad (2)$$

Hier is d_{VA} de gemiddelde deeltjesgrootte en a_m en v_m zijn respectievelijk de oppervlakte ingenomen op een polykristallijn oppervlak en het volume ingenomen in de bulk van het metaal door een Pd-atoom.

B. Katalysatoren voor de dehydratie van 1,3-BDO

1) Materialen⁵

Acht stalen zijn gekarakteriseerd. Deze omvatten commerciële ZSM-5, ZSM-5 met een SiO₂/Al₂O₃-verhouding van ca. 25 en 150, stalen met boor geïncorporeerd waarbij (theoretisch) de helft van het Al₂O₃ is vervangen door B, pure CeO₂ en twee verschillende hybride ZSM-5 met CeO₂ katalysatoren. De synthese van de ZSM-5 en de met boor ingewerkte stalen is gebaseerd op de methode van de Reviere et al. (2020) [4]. De synthese van zuivere CeO₂ en de hybride katalysatoren is gebaseerd op de methode van respectievelijk De Saegher et al. (2020) [5] en Di et al. (2022) [6]. Twee hybride katalysatoren werden bereid op basis van het bereide ZSM-5 met SiO₂/Al₂O₃-verhouding 25. CeO₂/ZSM-5 is het staal waarbij ZSM-5 is gedispergeerd op CeO₂, met elk 50/50 wt%. ZSM-5@CeO₂ is een *core-shell* katalysator, met ZSM-5 als *core* (kern) en CeO₂ als *shell* (schil). De werkelijke SiO₂/Al₂O₃ verhoudingen en B/Al₂O₃ werden bepaald met ICP-OES⁶ (Inductively Coupled Plasma Optical Emission Spectroscopy). De geanalyseerde katalysatoren, de werkelijke SiO₂/Al₂O₃-, en/of de B/Al₂O₃-verhoudingen en de gekarakteriseerde eigenschappen staan vermeld in tabel 2.

Tabel 2: Katalysatoren voor de dehydratie van 1,3-BDO

Katalysator	Reële Si/Al ratio	Reële B/A ratio	Gekarakteriseerde eigenschappen
Comm. ZSM-5	24	/	Zuurheid
ZSM-5@25	15	/	Zuurheid
ZSM-5@150	153	/	Zuurheid
ZSM-5@25_B	47	0.2	Zuurheid
ZSM-5@150_B	356	0.9	Zuurheid
CeO ₂	/	/	Basisheid
CeO ₂ /ZSM-5	/	/	Zuurheid, basisheid
ZSM-5@CeO ₂	/	/	Zuurheid, basisheid

2) Karakterisatie van de katalysatoren

NH₃- en CO₂-TPD worden gebruikt om de zure, respectievelijk basische eigenschappen van de katalysatoren te karakteriseren. Hierbij wordt gebruik gemaakt van de AutoChem II 2920 met een TCD. Vergelijkbare methoden werden gebruikt. De monsters werden voorbehandeld bij 550°C onder He om water te verwijderen. NH₃ wordt geladen door 5% NH₃/He te laten vloeien bij 120°C, terwijl CO₂ wordt geladen door 5% CO₂/He te laten vloeien bij 40°C. Zwak fysisch geadsorbeerd analysegas wordt verwijderd door te flushen met He.

³De gedragen Pd katalysatoren zijn beschikbaar gesteld door Universiteit Gent en dus niet bereid door de auteur van deze thesis.

⁴ICP-AES data aangeleverd door Universiteit Gent (INCAT)

⁵De katalysatoren werden beschikbaar gesteld door Universiteit Gent (Loïc Eloi) en dus niet gemaakt door de auteur van deze thesis

⁶ICP-OES data aangeleverd door Universiteit Gent (Diederik Leenknecht)

Tenslotte begint de analyse met een lineaire verhoging van de temperatuur tot 550°C. TPD-spectra werden opgenomen bij opwarmnelheden van 10, 15 en 20°C/min.

3) Interpretatie van de TPD spectra

De ruis op de spectra werd gereduceerd in de Origin dataverwerking software door *adjacent-averaging smoothing*. De basislijncorrectie werd ook uitgevoerd in dezelfde software. Daarna werden gemodelleerde Gaussische pieken voor de verschillende actieve site sterktes verkregen door deconvolutie van het signaal. De parameters a_i (schaalfactor), σ_i (standaardafwijking) en μ_i (tijd bij piekmaximum) in vergelijking 3 worden zo bepaald dat de residuele som van het kwadraat van de experimentele datapunten en de gemodelleerde datapunten wordt geminimaliseerd. N is het aantal pieken en t de tijd in minuten.

$$f(t) = \sum_{i=1}^N \frac{a_i}{\sigma_i \cdot \sqrt{2\pi}} \cdot e^{-\frac{(t-\mu_i)^2}{2\sigma_i^2}} \quad (3)$$

Door de TPD-experimenten uit te voeren bij verschillende opwarmnelheden kunnen de eerste orde Arrhenius-curven voor elk monster worden uitgezet. De Arrhenius-vergelijking is geherformuleerd tot vergelijking 4 [7,8]. β is de opwarmnelheid, R de gasconstante, T_{max} de temperatuur bij maximale desorptie en A de pre-exponentiële factor in de Arrhenius-vergelijking. De desorptie-energie E_d is een maat voor de sterkte van de actieve sites.

$$2 \cdot \ln(T_{max}) - \ln(\beta) = -\frac{E_d}{R} \left(\frac{1}{T_{max}} \right) + \ln(A) \quad (4)$$

De helling van $2 \cdot \ln(T_{max}) - \ln(\beta)$ in functie van $1/T_{max}$ is gelijk aan $-E_d/R$, zodat de desorptie-energie voor de pieken kan worden bepaald.

III. RESULTATEN EN DISCUSSIE

A. Metaaldispersie studie op katalysatoren voor de lignine depolymerisatie

1) Pd dispersie

De Pd-dispersie van de katalysatoren werd bepaald met behulp van CO pulschemisorptie. De resultaten staan vermeld in tabel 3. De fout (standaardafwijking) is berekend met een fout van 1% op de loop-temperatuur en de standaardafwijking op de piekoppervlakken van de verzadigde pieken. De gemiddelde deeltjesgrootte op het oppervlak van de stalen, bepaald met TEM-EDX, wordt ook weergegeven.

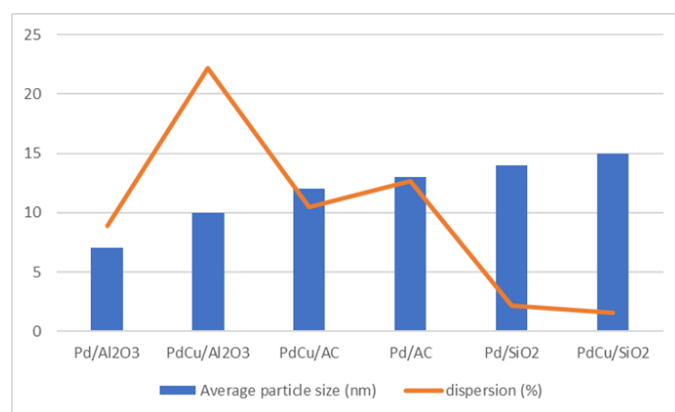
Tabel 3: Pd dispersie resultaten

Katalysator	Pd dispersie (%)	Deeltjesgrootte (nm)
Pd/Al ₂ O ₃	8.89 ± 0.27	7
PdCu/Al ₂ O ₃	22.17 ± 0.23	10
Pd/SiO ₂	2.13 ± 0.04	14
PdCu/SiO ₂	1.58 ± 0.05	15
Pd/AC	12.68 ± 0.16	13
PdCu/AC	10.46 ± 0.26	12

De Pd-dispersie wordt sterk beïnvloed door zowel de katalysatordrager als de aanwezigheid van het co-metaal Cu. Zowel de mono- als de bimetaal SiO₂-gedragen katalysatoren vertonen een zeer lage dispersie. Voor de monometallische Pd-katalysatoren is de dispersie het hoogst op Pd/AC, gevolgd door Pd/Al₂O₃ en Pd/SiO₂. Het bimetallische PdCu/Al₂O₃ vertoont de hoogste dispersie van alle katalysatoren, met een waarde van 22.17%. De bimetallische PdCu/AC en PdCu/SiO₂ vertonen een lagere dispersie.

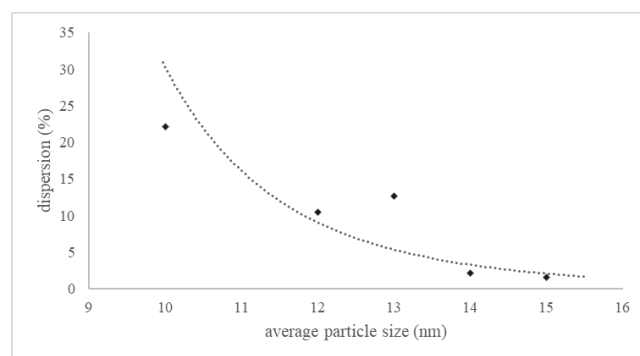
2) Dispersierelatie tot de deeltjesgrootte

De dispersiewaarden werden gekoppeld aan de deeltjesgrootte, bepaald met TEM-EDX. De gemiddelde deeltjesgrootte en dispersie van alle katalysatoren is zichtbaar in figuur 1.



Figuur 1: gemiddelde deeltjesgrootte en Pd dispersie van de katalysatoren

Normaliter komen kleinere gemiddelde deeltjes aan het oppervlak overeen met een hogere dispersie. Deze trend werd bevestigd, met enkele kleine afwijkingen. Alleen Pd/Al₂O₃ voldeed niet aan deze theorie door een veel te lage dispersie te vertonen. De dispersie in functie van de gemiddelde deeltjesgrootte is weergegeven in figuur 2, met uitzondering van de data voor Pd/Al₂O₃. De standaardafwijking van de dispersie was te klein om in de grafiek zichtbaar te zijn.



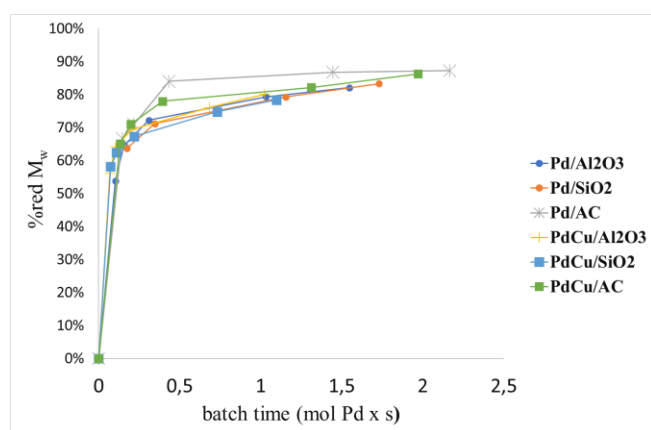
Figuur 2: Dispersie in functie van de gemiddelde deeltjesgrootte van de oppervlakte partikels

Deze curve heeft een soortgelijke vorm als de theoretische, afgeleid uit vergelijking (2). De waarden van de experimentele datapunten wijken echter aanzienlijk af van de theoretische, met een verschuiving naar een hogere gemiddelde deeltjesgrootte.

Voor de bimetaalkatalysatoren komt dit deels doordat de door TEM-EDX bepaalde grootte geen verschil maakt tussen Pd- en Cu-deeltjes, terwijl de dispersie alleen betrekking heeft op Pd. Het is ook mogelijk dat de aannames in vergelijking (2) niet juist zijn voor deze katalysator. Er wordt bijvoorbeeld uitgegaan van halfronde deeltjes aan het oppervlak. Bovendien zijn de metingen complexe technieken waarbij kleine variaties in experimentele procedures, gegevensanalyse of apparatuur tot aanzienlijke afwijkingen op de resultaten kunnen leiden.

3) Dispersierelatie tot de reactorresultaten

De resultaten van een reactorstudie⁷ op de monsters zijn gekoppeld aan de dispersieresultaten uit deze thesis. De milde depolymerisatie van lignine werd uitgevoerd in een batchreactor bij 200°C en 10 bar, met 0.05 g katalysator. De lignine werd opgelost in een mengsel van 70/30% ethanol en water in een concentratie van 20 mg/ml. De gemiddelde moleculaire massa (M_w) van de gedepolymeriseerde lignine is bepaald met behulp van GPC (Gel Permeatie Chromatografie) bij verschillende reactietijden. De M_w in functie van de batch-tijd (hoeveelheid Pd op de katalysator vermenigvuldigd met de reactietijd) wordt gevisualiseerd in Figuur 3.



Figuur 3: lignine depolymerisatie reactor resultaten

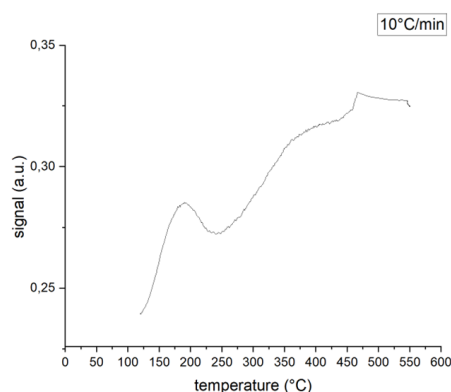
De katalysator met de hoogste dispersie op een niet-zure drager, namelijk Pd/AC, vertoont de snelste depolymerisatie tot een hoge M_w -reductie van ongeveer 85%. De snelste initiële depolymerisatie wordt waargenomen voor PdCu/Al₂O₃, dat een zure drager heeft en de hoogst gerapporteerde dispersie van alle katalysatoren in deze studie. De depolymerisatiesnelheid neemt echter af en er is veel meer tijd nodig om een M_w -reductie van 85% te bereiken. Interessant is dat een vergelijkbare snelle beginsnelheid wordt waargenomen voor het niet-zure PdCu/SiO₂, terwijl de dispersie zeer laag is. In conclusie, Pd/AC, met een niet-zure drager en een relatief hoge dispersie van 12.68%, lijkt vergeleken met de andere katalysatoren, het meest efficiënt voor de depolymerisatie van lignine tot een hoge M_w -reductie. De beginsnelheid is niet de snelste, maar de depolymerisatie snelheid blijft lang hoog.

Een duidelijk verband tussen de Pd-dispersie, de aard van de drager en de reactieactiviteit werd nog niet gevonden. Verder onderzoek om het complexe reactiemechanisme te begrijpen is nodig.

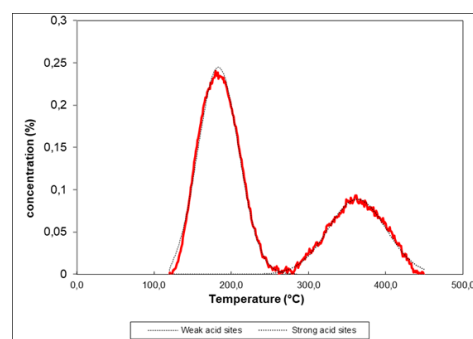
B. Zuurheid en basisheid studie op katalysatoren voor de dehydratie van 1,3-BDO

1) Problemen omtrent de TPD spectra

De verkregen TPD-spectra zijn sterk vervormd en bij een temperatuur van ongeveer 400°C wordt een knik in de basislijn waargenomen, waardoor het moeilijk is kwantitatieve resultaten te verkrijgen. Er werden pogingen ondernomen om dit probleem te verhelpen door meer staal te gebruiken, andere opwarmingsnelheden, de gassen opnieuw aan te sluiten, basislijnstabilisatie, dataverwerking... maar er werd geen oplossing gevonden. De basislijn werd gekozen om door het minimumpunt tussen de pieken te gaan, wat in werkelijkheid niet correct is. Dit maakte het onmogelijk om kwantitatieve resultaten te verkrijgen voor de concentratie van de actieve sites. Een vergelijking tussen de katalysatoren kon worden gemaakt, maar waarschijnlijk met een aanzienlijke fout op de resultaten. Als voorbeeld wordt het opgenomen NH₃-TPD spectrum van commercieel ZSM-5 met opwarmingsnelheid 10°C/min en het gecorrigeerde en gedeconvolueerde spectrum getoond in Figuur 4 en 5.



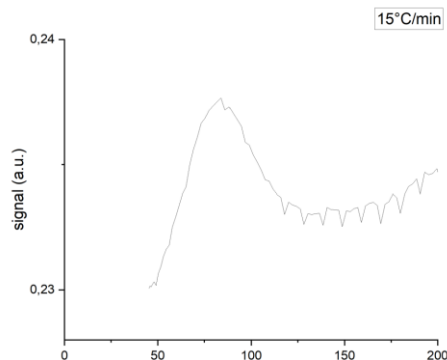
Figuur 4: opgenomen NH₃-TPD spectrum van commercieel ZSM-5 (10°C/min)



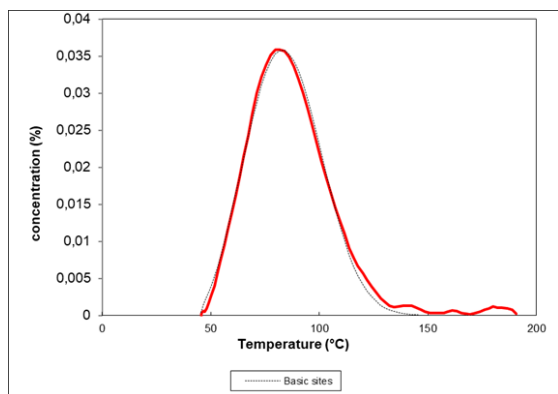
Figuur 5: gecorrigeerd en gedeconvolueerd NH₃-TPD spectrum van commercieel ZSM-5 (10°C/min)

⁷ Lignine depolymerisatie reactor studie data aangeleverd door Universiteit Gent (Boyana Atanasova)

Om de vergelijkende resultaten te bevestigen en kwantitatieve waarden voor de dichtheid van de actieve sites te kunnen rapporteren, werden NH₃-TPD resultaten op dezelfde stalen, uitgevoerd op de campus in Gent⁸, besproken. Als voorbeeld van de CO₂-TPD spectra wordt het opgenomen spectrum van CeO₂ met opwarmingsnelheid 15°C/min en het gecorrigeerde en gedeconvolueerde spectrum getoond in Figuur 6 en 7.



Figuur 6: opgenomen CO₂-TPD spectrum van CeO₂ (15°C/min)



Figuur 7: gecorrigeerd en gedeconvolueerd CO₂-TPD spectrum van CeO₂ (15°C/min)

Omdat er maar één piek wordt waargenomen in het TPD-spectrum, is de basislijncorrectie waarschijnlijk correcter uitgevoerd. Daarom zijn de verkregen concentraties kwantitatief waardevoller dan die van de NH₃-TPD studie.

2) Studie van de zuurheid met NH₃-TPD

NH₃-TPD is uitgevoerd op alle monsters, behalve op CeO₂. De absolute waarden van de zuurdichtheid in deze thesis zijn niet representatief voor de werkelijke waarde, als gevolg van bovengenoemde problemen. Alleen vergelijkende conclusies tussen de katalysatoren zijn nuttig. De bepaalde E_d waarden zijn echter waarschijnlijk wel correct en nuttig omdat de vervormde spectra nog steeds toelaten de piektemperaturen te lokaliseren. Deze resultaten staan vermeld in tabel 4.

De experimentele fout is berekend op basis van de standaardafwijking van E_d van commercieel ZSM-5, dat tweemaal werd geanalyseerd.

Tabel 4: bekomen E_d waarden of the katalysatoren

Katalysator	Sterkte van de sterk zure sites E _d (kJ/mol)
Comm. ZSM-5	132.59 ± 2.51
ZSM-5@25	133.95 ± 2.51
ZSM-5@150	98.97 ± 2.51
ZSM-5@25_B	113.46 ± 2.51
ZSM-5@150_B	84.58 ± 2.51
CeO ₂ /ZSM-5	98.80 ± 2.51
ZSM-5@CeO ₂	134.6 ± 2.51

De conclusies van de NH₃-TPD analyse zijn als volgt. Bij een verhoging van de Si/Al-verhouding van 25 tot 150 wordt een afname van de zwakke en sterk zure sites van respectievelijk 82.1% en 51.2% waargenomen. In de studie uit Gent wordt een iets grotere afname waargenomen, maar een vergelijkbare trend. In deze studie nam E_d af van 133.95 kJ/mol tot 98.97 kJ/mol bij een toename van het Si/Al van 25 tot 150. Deze resultaten komen overeen met de waarden van 135.1 kJ/mol en 103.3 kJ/mol, gerapporteerd door Gunst et al. (2020) [9]. De modificatie leidt dus tot een succesvolle verlaging van de zuurdichtheid en de sterkte.

In de katalysatoren ZSM-5@25 en ZSM-5@150 werd boor ingewerkt. De zuurdichtheidsresultaten voor ZSM-5@25_B in deze thesis leken onjuist en werden weerlegd. De studie in Gent rapporteerde een totale zuurdichtheidsdaling van 34.6%, met een gelijke daling voor de zwakkere en sterkere sites. De E_d waarde van het met boor verwerkte monster is 113.46 kJ/mol, vergeleken met 133.95 kJ/mol voor ZSM-5@25. De Gent studie rapporteerde E_d waarden van respectievelijk 84 kJ/mol en 115 kJ/mol, een significant verschil. Dezelfde trend wordt echter waargenomen. De resultaten van ZSM-5@150_B leken betrouwbaarder. In deze thesis en het onderzoek uit Gent bedraagt de afname van de zwakkere sites (zwakke en middelsterke) respectievelijk 51.7% en 55.8%. De afname van de sterke sites is respectievelijk 71.4% en 36%. Dit wijst erop dat de afname van de dichtheid van de sterke zure sites in dit proefschrift te hoog was. Deze thesis bepaalde een afname in E_d van 98.97 kJ/mol voor ZSM-5@150 tot 84.58 kJ/mol voor ZSM-5@150_B. De boorintegratie in ZSM-5-monsters temperde dus met succes de zuurgraad, door zowel de zuurdichtheid als de sterkte van de zure sites te verlagen.

De hybride CeO₂/ZSM-5 in dit onderzoek vertoonde een afname van 61.1% en 79.6% voor respectievelijk de zwakke en sterke sites vergeleken met ZSM-5. Het Gentse onderzoek rapporteerde een afname van 72% en 40%. De afname van sterkere zure sites in dit proefschrift lijkt dus hoger verwacht. De bepaalde E_d waarde in dit onderzoek is 98.80 kJ/mol, vergeleken met 133.95 kJ/mol voor ZSM-5. De zuurdichtheid en sterkte van de hybride CeO₂/ZSM-5 is dus met succes afgenomen.

De zuurdichtheid van de hybride ZSM-5@CeO₂ scheen in dit onderzoek toe te nemen. Dit is hoogst onwaarschijnlijk en komt niet overeen met het resultaat van de Gent campus. Dit resultaat wordt daarom weerlegd.

⁸ NH₃-TPD op de stalen op campus Gent werd uitgevoerd door doctoraat student Loïc Eloi

Er werd geen significante verandering in E_d gevonden. Dit kan niet worden bevestigd met gegevens uit Gent, zodat deze vaststelling niet zeker is.

Het onderzoek uit Gent rapporteerde een totale daling van de zuurdichtheid met 27.4%, wat veel lager is dan de daling van de hybride $\text{CeO}_2/\text{ZSM-5}$. De zure tempering van de hybride $\text{CeO}_2/\text{ZSM-5}$ is dus effectiever dan bij ZSM-5@CeO_2 .

3) Studie van de basisheid met CO_2 -TPD

CO_2 -TPD werd uitgevoerd op de twee hybride katalysatoren en op zuiver CeO_2 . Er zijn geen Gentse resultaten beschikbaar, zodat geen vergelijking mogelijk is. Omdat er maar één piek wordt waargenomen in het TPD-spectrum, is de basislijncorrectie waarschijnlijk correcter uitgevoerd. Daarom zijn de verkregen waarden voor de site concentraties kwantitatief waardevoller dan die van de NH_3 -TPD studie. Zuiver CeO_2 vertoonde één basispiek bij een temperatuur van ongeveer 80°C . Dit is lager dan de gerapporteerde temperatuur van 110°C door Yoshikawa et al. (2016) voor een vergelijkbare opwarmingsnelheid [10]. De concentratie aan basische sites is $11.82 \mu\text{mol/g}_{\text{cat}}$.

De hybride $\text{CeO}_2/\text{ZSM-5}$ katalysator vertoonde slechts 6% van de basische site concentratie in vergelijking met zuiver CeO_2 , met een waarde van $0.81 \mu\text{mol/g}_{\text{cat}}$. De basische eigenschappen van CeO_2 zijn dus nauwelijks opgenomen in de hybride katalysator. De sterkte van de basispiek is afgenomen, met een verschuiving van het piekmaximum naar ongeveer 70°C voor een opwarmingsnelheid van $15^\circ\text{C}/\text{min}$. Door een technische fout is de E_d -waarde niet bepaald.

De hybride katalysator ZSM-5@CeO_2 vertoont een betere integratie van basische sites dan $\text{CeO}_2/\text{ZSM-5}$. De concentratie van de basische sites is 37.3% van de concentratie in zuiver CeO_2 , met een waarde van $4.41 \mu\text{mol/g}_{\text{cat}}$. Er wordt een zwakkere basische site sterkte waargenomen, met een E_d waarde van 99.45 kJ/mol vergeleken met 110.83 kJ/mol voor zuiver CeO_2 . Deze methode voor de bereiding van een hybride katalysator met als doel de integratie van basische eigenschappen is dus superieur. Dit is mogelijk toe te schrijven aan het feit dat CeO_2 de schil is in de *core-shell* structuur, en dus meer blootgesteld is aan het oppervlak van de katalysator. Voor deze katalysator werd echter een lagere zuurgraad reductie gerapporteerd dan voor $\text{CeO}_2/\text{ZSM-5}$.

IV. CONCLUSIE

De Pd-dispersie van de gedragen metaalkatalysatoren, gebruikt als katalysator in de lignine depolymerisatie, werd bepaald met behulp van CO pulschemisorptie. De dispersiewaarden variëren van 1.58% tot 22.17%. $\text{PdCu}/\text{Al}_2\text{O}_3$ vertoonde de hoogste Pd-dispersie, terwijl de SiO_2 -gedragen katalysatoren een zeer lage dispersie vertoonden. De vastgestelde dispersie uit deze thesis werd gekoppeld aan de gemiddelde deeltjesgrootte van de oppervlakte deeltjes die met TEM-EDX werden bepaald. Reactorgegevens voor de lignine depolymerisatie werden besproken. Pd/AC , de katalysator met de hoogste dispersie op een niet-zure drager, vertoonde de snelste depolymerisatie tot een hoge M_w -reductie van ongeveer 85%. $\text{PdCu}/\text{Al}_2\text{O}_3$, de katalysator met een zure drager en de hoogste dispersie van alle monsters, vertoonde een zeer snelle initiële depolymerisatie snelheid.

Naarmate de reactie vordert, neemt de depolymerisatie snelheid echter af, zodat een hoge M_w -reductie van 85% pas na langere tijd wordt bereikt in vergelijking met Pd/AC .

NH_3 - en CO_2 -TPD werden gebruikt om de zure en basische eigenschappen op katalysatoren voor de dehydratie van 1,3-BDO te karakteriseren. Het verhogen van de $\text{SiO}_2/\text{Al}_2\text{O}_3$ verhouding en de boorintegratie in ZSM-5 verlaagde de zuurconcentratie en sterkte in de stalen aanzienlijk. De laagste gerapporteerde E_d -waarde van de sterk zure site is $84,58 \text{ kJ/mol}$ voor ZSM-5@150_B , wat een significante daling is ten opzichte van de waarde van $133,95 \text{ kJ/mol}$ voor ZSM-5@25 . De tempering van de zuurdensiteit is effectiever in de hybride katalysator $\text{CeO}_2/\text{ZSM-5}$ dan in ZSM-5@CeO_2 . ZSM-5@CeO_2 vertoonde echter een veel hogere basische site-integratie, met concentraties van respectievelijk 4.41 en $0.81 \mu\text{mol/g}_{\text{cat}}$. De modificaties en hybride katalysatoren hebben mogelijk een gunstige invloed op de ZSM-5 katalysatoren met het doel de conversie van 1,3-BDO en de selectiviteit naar butadien te verhogen.

DANKWOORD

De auteur dankt doctoraatsstudenten Boyana Atanasova en Loïc Eloi voor de geleverde analyse- en reactordata.

REFERENTIES

- [1] B. Kraushaar-Czarnetzki and S. P. Müller, "Shaping of Solid Catalysts Objectives of Catalyst Shaping," *Synthesis of Solid Catalysts*, pp. 173–199, 2009, Accessed: Jan. 16, 2023. [Online]. Available: https://books.google.com/books/about/Synthesis_of_Solid_Catalysts.html?hl=nl&id=5ejCa9HGf2oC
- [2] P. Canton, G. Fagherazzi, M. Battagliarin, F. Menegazzo, F. Pinna, and N. Pernicone, "Pd/CO Average Chemisorption Stoichiometry in Highly Dispersed Supported Pd/ γ - Al_2O_3 Catalysts," *Langmuir*, vol. 18, no. 17, pp. 6530–6535, Aug. 2002, doi: 10.1021/LA015650A.
- [3] G. Bergeret and P. Gallezot, "Particle Size and Dispersion Measurements," vol. 2, p. 10, 2008, doi: 10.1002/9783527610044.hetcat0038i.
- [4] A. de Reviere, T. Vandevyvere, M. K. Sabbe, and A. Verberckmoes, "Renewable Butene Production through Dehydration Reactions over Nano-HZSM-5/ γ - Al_2O_3 Hybrid Catalysts," *Catalysts 2020, Vol. 10, Page 879*, vol. 10, no. 8, p. 879, Aug. 2020, doi: 10.3390/CATAL10080879.
- [5] T. De Saegher et al., "Monometallic Cerium Layered Double Hydroxide Supported Pd-Ni Nanoparticles as High Performance Catalysts for Lignin Hydrogenolysis," *Materials 2020, Vol. 13, Page 691*, vol. 13, no. 3, p. 691, Feb. 2020, doi: 10.3390/MA13030691.
- [6] Z. Di, H. Wang, R. Zhang, H. Chen, Y. Wei, and J. Jia, "ZSM-5 core-shell structured catalyst for enhancing low-temperature NH_3 -SCR efficiency and poisoning resistance," *Appl Catal A Gen*, vol. 630, p. 118438, Jan. 2022, doi: 10.1016/J.APCATA.2021.118438.
- [7] M. Niwa and N. Katada, "New Method for the Temperature-Programmed Desorption (TPD) of Ammonia Experiment for Characterization of Zeolite Acidity: A Review," *The Chemical Record*, vol. 13, no. 5, pp. 432–455, Oct. 2013, doi: 10.1002/TCR.201300009.
- [8] P. A. Webb, "Introduction to Chemical Adsorption Analytical Techniques and their Applications to Catalysis," 2003.
- [9] D. Gunst, M. Sabbe, M. F. Reyniers, and A. Verberckmoes, "Study of n-butanol conversion to butenes: Effect of Si/Al ratio on activity, selectivity and kinetics," *Appl Catal A Gen*, vol. 582, Jul. 2019, doi: 10.1016/J.APCATA.2019.05.035.
- [10] K. Yoshikawa, M. Kaneda, and H. Nakamura, "Development of Novel CeO_2 -based CO_2 adsorbent and analysis on its CO_2 adsorption and desorption mechanism," *Energy Procedia*, vol. 114, pp. 2481–2487, Jul. 2017, doi: 10.1016/J.EGYPRO.2017.03.1400.

Table of contents

Dankwoord	
Acknowledgments	
Abstract	
Extended abstract	
List of figures	
List of tables	
List of symbols and abbreviations	
1 Literature study.....	1
1.1 Introduction: relevance of biomass-derived chemicals	1
1.2 Depolymerization of lignin	2
1.2.1 Oxidative catalytic depolymerization.....	4
1.2.2 Reductive catalytic depolymerization	5
1.2.3 Influence of catalyst acidity and metal dispersion on reductive catalytic depolymerization of lignin	6
1.2.4 Bimetallic catalysts	12
1.3 Dehydration of 1,3-butanediol to 1,3-butadiene.....	13
1.3.1 Zeolites and ZSM-5	14
1.3.2 Direct dehydration of 1,3-butanediol over a zeolite catalyst (ZSM-5)	16
1.3.3 Modification of ZSM-5 with Boron.....	20
1.3.4 Stepwise conversion of 1,3-butanediol to butadiene.....	21
1.3.5 Hybrid catalyst containing CeO ₂ and zeolites	22
1.4 Temperature-programmed techniques.....	26
1.4.1 Temperature-programmed reduction (TPR).....	26
1.4.2 Temperature-programmed oxidation (TPO).....	27
1.4.3 Temperature-programmed desorption (TPD).....	28
1.4.4 Pulse chemisorption.....	30
1.5 Summary of TP techniques and catalyst active sites.....	31
1.6 Research questions and research approach.....	34
2 Materials and methods.....	35
2.1 Materials.....	35
2.1.1 Characterization of catalysts for the mild reductive catalytic depolymerization of lignin	35

2.1.2	Characterization of catalysts for the dehydration of 1,3-butanediol	37
2.1.3	Used (analysis) gasses and other chemicals.....	40
2.2	Methods.....	41
2.2.1	Instrument: AutoChem II 2920 and TCD detector	41
2.2.2	Preparation of the samples	42
2.2.3	Reductive catalytic depolymerization of lignin: metal dispersion study	43
2.2.4	Dehydration of 1,3-butanediol: acidity and basicity study	47
2.2.5	Overview of the samples and performed experiments	52
3	Results and discussion	53
3.1	Metal dispersion study on catalysts for the mild reductive catalytic depolymerization of lignin.....	53
3.1.1	Metal dispersion.....	53
3.1.2	Influence of the supports	55
3.1.3	Influence of the addition of Cu to form bimetallic PdCu catalyst.....	57
3.1.4	Comparison with TEM-EDX results: particle size	60
3.1.5	Dispersion relation with catalysts activity	65
3.2	Acidity and basicity study on catalysts for the dehydration of 1,3-butanediol	68
3.2.1	NH ₃ and CO ₂ gas concentration calibration	68
3.2.2	Spectra interpretation and issues	70
3.2.3	Acidity study with NH ₃ -TPD	75
3.2.4	Basicity study with CO ₂ -TPD	92
3.2.5	ZSM-5 modifications and hybrid catalysts effect on the dehydration of 1,3-BDO 95	
3.3	Future research.....	97
3.3.1	Supported metal catalysts for the depolymerization of lignin	97
3.3.2	ZSM-5 catalysts for the dehydration of 1,3-BDO	97
4	Conclusion.....	99
4.1	Supported metal catalysts for the depolymerization of lignin.....	99
4.2	ZSM-5 catalysts for the dehydration of 1,3-BDO	100
5	Sustainability review	102
5.1	Green catalysis.....	102
5.2	The SDG's and green catalysis	104
	References.....	106
	Appendices	119

Appendix A: CO pulse chemisorption spectra	119
Appendix B: TEM-EDX results on supported metal catalysts	122
Appendix C: NH ₃ -TPD acidity results from Ghent campus	124
Appendix D: NH ₃ -TPD spectra from Ghent campus	125
Appendix E: Arrhenius plots for E _d determination of the strong acid sites (Ghent campus)	127
Appendix F: analysis conditions for NH ₃ -TPD at the home campus (Ghent)	128
Appendix G: corrected and deconvoluted NH ₃ -TPD spectra (respective heating ratio of 10, 15, 20°C/min).....	129
Appendix H: Arrhenius plots for E _d determination of the strong acid sites.....	136
Appendix I: corrected and deconvoluted CO ₂ -TPD spectra (respective heating ratio of 10, 15, 20°C/min).....	140
Appendix J: Arrhenius plots for E _d determination of the basic sites.....	143

List of figures

Figure 1: lignin molecule representation	3
Figure 2: main lignin monomers (monolignols) [9]	3
Figure 3: vanillin structure [13]	4
Figure 4: yield in function of the quantity of acid sites on the catalysts	6
Figure 5: weight-average molecular weight in function of acid sites on the catalysts.....	7
Figure 6: NH ₃ -TPD profiles of the catalysts [30]	8
Figure 7: phenolic monomers produced per acid site as function of metal dispersion	9
Figure 8: phenolic monomers produced per surface Pd site as function of acid site quantity	10
Figure 9: relation between the phenolic monomer yield and Pd dispersion ([CO]/[Pd]) on the mostly non-acidic Pd/SiO ₂ catalysts [30].....	10
Figure 10: adsorption of lignin on (a) highly dispersed Pd and (b) on poorly dispersed, bulk Pd [30]	11
Figure 11: proposed reaction scheme for the 1,3-BDO dehydration [45]	14
Figure 12: structure of ZSM-5 zeolite [53]	15
Figure 13: proposed reaction scheme for the direct dehydration of 1,3-butanediol	17
Figure 14: selectivity of the ZSM-5 catalysts.....	17
Figure 15: deactivation study of ZSM-5@260 [32] C _{BDO} : conversion of 1,3-BDO; S _{BD} : selectivity to BD; S _{PP} : selectivity to propylene; S _{3B1ol} : selectivity to 3-buten-1-ol [43]	18
Figure 16: NH ₃ -TPD spectra of (a) ZSM-5@30, (b) ZSM-5@64, (c) ZSM-5@106 and (d) ZSM-5@260 [43].....	19
Figure 17: total acid density in function of SiO ₂ /Al ₂ O ₃ ratio	19
Figure 18: NH ₃ -TPD profiles of HZSM-5 and B/HZSM-5 [60]	20
Figure 19: possible reaction mechanism for dehydration of 1,3-BDO over CeO ₂ [64].....	22

Figure 20: reaction results for dehydration of 1,3-BDO with different Ce@MOR catalysts [67]	23
Figure 21: impact of acid properties on conversion and selectivity to BD for the 1,3-BDO dehydration	24
Figure 22: catalyst efficiency in function to the fraction of medium acidic sites on the Ce@MOR catalysts	25
Figure 23: evolution of catalytic performance for Ce@MOR catalysts [67]	25
Figure 24: H ₂ -TPR spectrum [72]	27
Figure 25: NH ₃ -TPD spectra for MOR and ZSM-5 [81]	29
Figure 26: example of a pulse chemisorption spectrum [84] S _u : unsaturated peaks; S _s : saturated peaks	30
Figure 27: AutoChem II	42
Figure 28: U-tube loaded with quartz wool and sample, placed in the furnace	43
Figure 29: NH ₃ -TPD of ZSM-5 with separate and consecutive temperature ramps [107]	48
Figure 30: reduction profiles for silica supported catalysts [121]	58
Figure 31: average particle size and dispersion for the catalysts	61
Figure 32: Plot of dispersion as a function of mean diameter d _{VA} for Ni, Pt and Pd, as stated by eq. (7) [106]	63
Figure 33: Plot of determined dispersion in this research as a function of mean diameter d _{VA} of the surface species	64
Figure 34: Plot of determined dispersion in this research as a function of mean diameter d _{VA} of the surface species (Pd/Al ₂ O ₃ excluded)	65
Figure 35: batch reactor results for the lignin depolymerization	67
Figure 36: signal vs time (with rising NH ₃ concentration)	69
Figure 37: signal vs time (with rising CO ₂ concentration)	69
Figure 38: gas concentration calibration curves blue curve: NH ₃ /He; orange curve: CO ₂ /He	69
Figure 39: obtained spectrum on empty tube	70
Figure 40: recorded NH ₃ -TPD spectrum of commercial ZSM-5	71
Figure 41: recorded NH ₃ -TPD spectrum of ZSM-5@25_B	71
Figure 42: baseline correction for commercial ZSM-5	72
Figure 43: corrected spectrum for commercial ZSM-5	72
Figure 44: baseline correction for ZSM-5@25_B	73
Figure 45: corrected spectrum for ZSM-5@25_B	73
Figure 46: NH ₃ -TPD spectra of commercial and prepared ZSM-5@25	78
Figure 47: NH ₃ -TPD spectra ZSM-5@25 and ZSM-5@150	80
Figure 48: NH ₃ -TPD spectrum for ZSM-5@25 (Ghent campus)	81
Figure 49: NH ₃ -TPD spectrum for ZSM-5@150 (Ghent campus)	81
Figure 50: NH ₃ -TPD spectra of ZSM-5@25 and ZSM-5@25_B	83
Figure 51: NH ₃ -TPD spectra of ZSM-5@150 and ZSM-5@150_B	84
Figure 52: NH ₃ -TPD spectrum for ZSM-5@25_B (Ghent campus)	85
Figure 53: NH ₃ -TPD spectrum for ZSM-5@150_B (Ghent campus)	86
Figure 54: NH ₃ -TPD spectra of ZSM-5@25 and CeO ₂ /ZSM-5	88
Figure 55: NH ₃ -TPD spectra of ZSM-5@25 and ZSM-5@CeO ₂	89
Figure 56: NH ₃ -TPD spectrum for CeO ₂ /ZSM-5 (Ghent campus)	90

Figure 57: NH ₃ -TPD spectrum for ZSM-5@CeO ₂ (Ghent campus).....	90
Figure 58: CO ₂ -TPD spectra of CeO ₂ and CeO ₂ /ZSM-5.....	94
Figure 59: CO ₂ -TPD spectra of CeO ₂ and ZSM-5@CeO ₂	95
Figure 60: 12 principles of green chemistry.....	102
Figure 61: sustainable development goals.....	104
Figure 62: Pd/Al ₂ O ₃ CO pulse chemisorption spectrum (1% CO).....	119
Figure 63: Pd/Al ₂ O ₃ CO pulse chemisorption spectrum (10% CO).....	119
Figure 64: PdCu/Al ₂ O ₃ CO pulse chemisorption spectrum (10% CO/He).....	120
Figure 65: Pd/SiO ₂ CO pulse chemisorption spectrum (1% CO/He).....	120
Figure 66: PdCu/SiO ₂ CO pulse chemisorption spectrum (10% CO/He).....	120
Figure 67: Pd/AC CO pulse chemisorption spectrum (10% CO/He).....	121
Figure 68: PdCu/AC CO pulse chemisorption spectrum (10% CO/He).....	121
Figure 69: CO pulse chemisorption spectrum of an empty tube with quartz wool (10%CO/He)	121
Figure 70: particle size distribution of Pd/Al ₂ O ₃	122
Figure 71: particle size distribution of Pd/SiO ₂	122
Figure 72: particle size distribution of Pd/AC.....	122
Figure 73: particle size distribution of PdCu/Al ₂ O ₃	123
Figure 74: particle size distribution of PdCu/SiO ₂	123
Figure 75: particle size distribution of PdCu/AC.....	123
Figure 76: NH ₃ -TPD spectrum for ZSM-5@25 (Ghent campus).....	125
Figure 77: NH ₃ -TPD spectrum for ZSM-5@150 (Ghent campus).....	125
Figure 78: NH ₃ -TPD spectrum for ZSM-5@25_B (Ghent campus).....	125
Figure 79: NH ₃ -TPD spectrum for ZSM-5@150_B (Ghent campus).....	126
Figure 80: NH ₃ -TPD spectrum for CeO ₂ /ZSM-5 (Ghent campus).....	126
Figure 81: NH ₃ -TPD spectrum for ZSM-5@CeO ₂ (Ghent campus).....	126
Figure 82: Arrhenius plot for ZSM-5@25 (acid site) at Ghent campus.....	127
Figure 83: Arrhenius plot for ZSM-5@25_B (acid site) at Ghent campus.....	127
Figure 84: NH ₃ -TPD spectrum of commercial ZSM-5 (10°C/min).....	129
Figure 85: NH ₃ -TPD spectrum of commercial ZSM-5 (15°C/min).....	129
Figure 86: NH ₃ -TPD spectrum of commercial ZSM-5 (20°C/min).....	129
Figure 87: NH ₃ -TPD spectrum of ZSM-5@25 (10°C/min).....	130
Figure 88: NH ₃ -TPD spectrum of ZSM-5@25 (15°C/min).....	130
Figure 89: NH ₃ -TPD spectrum of ZSM-5@25 (20°C/min).....	130
Figure 90: NH ₃ -TPD spectrum of ZSM-5@150 (10°C/min).....	131
Figure 91: NH ₃ -TPD spectrum of ZSM-5@150 (15°C/min).....	131
Figure 92: NH ₃ -TPD spectrum of ZSM-5@150 (20°C/min).....	131
Figure 93: NH ₃ -TPD spectrum of ZSM-5@25_B (10°C/min).....	132
Figure 94: NH ₃ -TPD spectrum of ZSM-5@25_B (15°C/min).....	132
Figure 95: NH ₃ -TPD spectrum of ZSM-5@25_B (20°C/min).....	132
Figure 96: NH ₃ -TPD spectrum of ZSM-5@150_B (10°C/min).....	133
Figure 97: NH ₃ -TPD spectrum of ZSM-5@150_B (15°C/min).....	133
Figure 98: NH ₃ -TPD spectrum of ZSM-5@150_B (20°C/min).....	133
Figure 99: NH ₃ -TPD spectrum of CeO ₂ /ZSM-5 (10°C/min).....	134

Figure 100: NH ₃ -TPD spectrum of CeO ₂ /ZSM-5 (15°C/min).....	134
Figure 101: NH ₃ -TPD spectrum of CeO ₂ /ZSM-5 (20°C/min).....	134
Figure 102: NH ₃ -TPD spectrum of ZSM-5@CeO ₂ (10°C/min).....	135
Figure 103: NH ₃ -TPD spectrum of ZSM-5@CeO ₂ (15°C/min).....	135
Figure 104: NH ₃ -TPD spectrum of ZSM-5@CeO ₂ (20°C/min).....	135
Figure 105: Arrhenius plot for commercial ZSM-5 (1) (acid site).....	136
Figure 106: Arrhenius plot for commercial ZSM-5 (2) (acid site).....	136
Figure 107: Arrhenius plot for ZSM-5@25 (acid site)	137
Figure 108: Arrhenius plot for ZSM-5@150 (acid site)	137
Figure 109: Arrhenius plot for ZSM-5@25_B (acid site)	138
Figure 110: Arrhenius plot for ZSM-5@150_B (acid site)	138
Figure 111: Arrhenius plot for CeO ₂ /ZSM-5 (acid site)	139
Figure 112: Arrhenius plot for ZSM-5@CeO ₂ (acid site)	139
Figure 113: CO ₂ -TPD spectrum of CeO ₂ (10°C/min).....	140
Figure 114: CO ₂ -TPD spectrum of CeO ₂ (15°C/min).....	140
Figure 115: CO ₂ -TPD spectrum of CeO ₂ (20°C/min).....	140
Figure 116: CO ₂ -TPD spectrum of CeO ₂ /ZSM-5 (10°C/min).....	141
Figure 117: CO ₂ -TPD spectrum of CeO ₂ /ZSM-5 (15°C/min).....	141
Figure 118: CO ₂ -TPD spectrum of ZSM-5@CeO ₂ (10°C/min).....	142
Figure 119: CO ₂ -TPD spectrum of ZSM-5@CeO ₂ (15°C/min).....	142
Figure 120: CO ₂ -TPD spectrum of ZSM-5@CeO ₂ (20°C/min).....	142
Figure 121: Arrhenius plot for CeO ₂ (basic site).....	143
Figure 122: Arrhenius plot for ZSM-5@CeO ₂ (basic site).....	144

List of tables

Table 1: reaction results of dehydration of 1,3-BDO at 300°C [43]	16
Table 2: reaction results for dehydration of 1,3-BDO with different Ce@MOR catalysts [67]	23
Table 3: acid properties from NH ₃ -TPD study	24
Table 4: summary of the most important active sites and techniques that can be used to characterize the catalysts.....	33
Table 5: characteristics of the used supports	35
Table 6: theoretical catalysts loading.....	36
Table 7: metal loading determined by ICP-AES.....	36
Table 8: used chemicals for the zeolite synthesis	37
Table 9: used chemical for the hybrid catalysts with core-shell topology.....	39
Table 10: actual SiO ₂ /Al ₂ O ₃ ratios, measured by OES	39
Table 11: used gasses and other chemicals in the AutoChem experiments and their properties [97].....	40
Table 12: experimental overview.....	52
Table 13: dispersion and active metal surface results of the CO pulse chemisorption study.	54
Table 14: particle size from TEM-EDX (ranked with rising average particle size).....	61
Table 15: comparison between particle size found by TEM-EDX and from dispersion results	62

Table 16: gas calibration curves parameters	70
Table 17: acid density results from NH ₃ -TPD experiments.....	76
Table 18: NH ₃ -TPD desorption energy results	76
Table 19: comparison for T _{max} in this thesis and at home campus Ghent (at 10°C/min)	77
Table 20: acid site concentration results of commercial and prepared ZSM-5@25	78
Table 21: acid site concentration results of ZSM-5@25 and ZSM-5@150	79
Table 22: acid site concentration results of ZSM-5@25 and ZSM-5@150 (Ghent campus) ...	81
Table 23: acid site concentration results of ZSM-5@25, ZSM-5@150 and the Boron incorporated catalysts.....	83
Table 24: acid site concentration results of ZSM-5@25_B and ZSM-5@150_B (Ghent campus)	85
Table 25: acid site concentration results of ZSM-5@25 and the hybrid catalysts	88
Table 26: acid site concentration results of ZSM-5@25 and hybrid catalysts (Ghent campus)	90
Table 27: CO ₂ -TPD desorption energy results.....	93
Table 28: basic density results from CO ₂ -TPD experiments.....	93
Table 29: NH ₃ -TPD results of the samples, analyzed on Ghent campus.....	124
Table 30: peak temperature of spectra with heating ratio 10°C/min, from Ghent campus .	124

List of symbols and abbreviations

Symbols

A	Angstrom
A	fraction of active gas in the mixture
a	cross-sectional area of the active metal atom
A	pre-exponential factor
A_f	area of the saturated peaks
A_i	area of peak i
a_i	scaling factor
a_m	surface area occupied by metal atom on surface
C_{BDO}	conversion of 1,3-BDO
$C_{\beta-O}$	β -O-4 aryl ether bond
D	dispersion
d_{VA}	mean particle size
E_d	desorption energy
h	high temperature peak
l	low temperature peak
M_w	weight-average molecular mass
n	stoichiometry factor
N	number of peaks
N_a	Avogadro's number
N_s	number of exposed surface metal atoms
N_t	total number of metal atoms in the sample
P_{std}	standard pressure
R	gas constant
S_{3B1ol}	selectivity to 3-buten-1-ol
S_{BD}	selectivity to BD
S_{PE}	selectivity to propylene
S_s	saturated peaks (pulse chemisorption)
S_u	unsaturated peaks (pulse chemisorption)
t	time
T	temperature
T_{loop}	loop temperature
T_{std}	standard temperature
V_{ads}	volume of adsorbed active gas
V_g	molar gas volume
V_{inj}	injected volume of active gas
V_{loop}	loop volume
V_m	volume occupied by metal atom in the bulk of the metal

X_{BDO}	conversion of 1,3-BDO
μ_i	mean value
σ_i	standard deviation
β	heating rate

Abbreviations

1BoI	1-butanol
2BoI	2-butanol
3B1oI	3-butene-1-ol
3B2oI	3-butene-2ol
AC	active carbon
AD	distilled water
AIP	aluminum isopropoxide
BD	butadiene
BDO	butanediol
BET	Brunauer-Emmett-Teller
EtOH	ethanol
FID	flame ionization detector
FTIR	Fourier transform infrared spectroscopy
GPC	gel permeation chromatography
HMT	hexa methylene tetramine
ICP-AES	Inductively Coupled Plasma Atomic Emission Spectroscopy
ICP-OES	Inductively Coupled Plasma Optic Emission Spectroscopy
KL	Kraft lignin
LDH	layered double hydroxide
MEK	methyl ethyl ketone
MeOH	methanol
MOF	metal-organic framework
MOR	mordenite
MS	mass spectrometer
MS	Mass spectroscopy
MTG	methanol to gasoline process
MVK	methyl vinyl ketone
MW	molecular weight
OL	organosolv lignin
PP	propylene
PVP	poly vinyl pyrrolidone
RSSQ	Residual Sum of Squares

SDA	Structure Directing Agent
SDG	sustainable development goals
STP	standard temperature and pressure
TCD	thermal conductivity detector
TEM- EDX	transmission electron microscopy energy- dispersive X-ray
TEOS	tetra ethyl ortho silicate
TOS	time on stream
TPAOH	tetra propyl ammonium hydroxide
TPD	temperature programmed desorption
TPO	temperature programmed oxidation
TPR	temperature programmed reduction
XPS	X-ray photoelectron spectroscopy
XRD	X-ray diffraction
ZSM-5	Zeolite Socony Mobil-5

1 Literature study

1.1 Introduction: relevance of biomass-derived chemicals

In recent years, there has been a growing body of research aimed at transitioning chemical production away from petroleum-based sources and towards renewable biomass resources. This shift is driven by two primary factors: the finite nature of fossil fuel reserves and the potential to mitigate carbon dioxide (CO₂) emissions, as biomass consumes CO₂ during its growth [1]. To illustrate the need for this shift, it is stated that at the current consumption rate, the fossil oil reserves will be depleted in 50 years [2].

Within this context, this master's thesis focuses on two crucial reactions to obtain important bulk chemicals from renewable sources: the depolymerization of lignin and the dehydration of 1,3-butanediol to butadiene. These processes hold significant importance in the field of green chemistry and offer valuable products as outcomes. In order to comprehend their significance and explore the potential applications of the resulting conversions, this study will first provide an in-depth discussion of these reactions. The key for enabling the transition towards biomass derived chemicals lies in the development of performant heterogenous catalysts [3]. To facilitate this, the specific active sites required for each reaction will be identified.

Subsequently, the thesis delves into the implementation of temperature programmed techniques and pulse chemisorption to characterize promising catalysts employed in these reactions. By employing these techniques, various properties of the catalysts can be elucidated, providing insights into their activity and efficiency. The correlation between these properties and the resulting chemical properties will also be explored, establishing a comprehensive understanding of the catalysts' performance.

Overall, this master's thesis aims to contribute to the advancement of renewable chemical production by investigating key reactions, their associated active sites, and the characterization of catalysts through temperature programmed techniques. By doing so, it strives to enhance our understanding of green chemistry and pave the way for more sustainable and environmentally friendly chemical synthesis.

1.2 Depolymerization of lignin

All plants contain lignin, which is a complex natural aromatic polymer visible in Figure 1 [4]. Lignin is the most abundant natural aromatic polymer, thus promising in the use as a renewable source [5]. Lignin occurs in the cell wall and generally accounts for about 20-30% of the total mass of the plant. The amount of lignin present depends on the type of plant [6]. The other main components are cellulose and hemicellulose. Lignin can be extracted from biomass, and it is a byproduct of the paper and pulp industry, among others. Nowadays, it is mainly burned to recover energy. However, it can also be used as the basis for various basic chemicals. These are then called biomolecules, and these are of significant importance for the pathway to green chemistry [7]. This makes it possible to produce chemicals starting not from carbon fuels, but from bio-compounds. Lignin can be used to produce bioplastics, biofuel, biofertilizers, food additives, value-added chemicals, textiles, lubricants, adhesives, etc. [8]. The monomers (also called monolignols) that make up the polymer mainly are p-coumaryl alcohol, coniferyl alcohol, and sinapyl alcohol, whose structures are shown in Figure 2. These three components are arranged irregularly in the lignin molecule [9]. The complexity and heterogeneity of lignin make for technical challenges for its efficient valorization [10]. To obtain the useful products, lignin must first be extracted from the biomass source and this lignin-rich stream is then depolymerized so that smaller platform chemicals are formed. These platform chemicals can then serve as a substrate for the selective production of various high-value products.

A promising source is the paper manufacturing industry. Here, lignin is present in large quantities in the wastewater. The pulping process produces around 50 million tons of lignin each year, and only a fraction of this lignin is isolated and used for other applications, except as low-value fuel to generate electricity and heat [8]. The most used pulping process is the Kraft Process, here strong alkali is used to break the bonds that link lignin, hemicellulose and cellulose in the wood chips. This lignin is classified as 'Kraft lignin'. Further separation steps and precipitation by acidification of the stream (called Black Liquor) lead to a lignin-rich product [11]. Another pulping process is the organic solvent treatment that dissolves lignin with solvents like ethanol or methanol in water. The obtained lignin is named 'organosolv lignin' [12].

Lignin is foremost a promising candidate as a sustainable source of phenolics [13]. To obtain the wanted basic chemicals, this process must ensure that the aromatic rings of the obtained products remain intact. In addition, the more functional groups are left on the product, the easier it is to further modify the compound by functionalization.

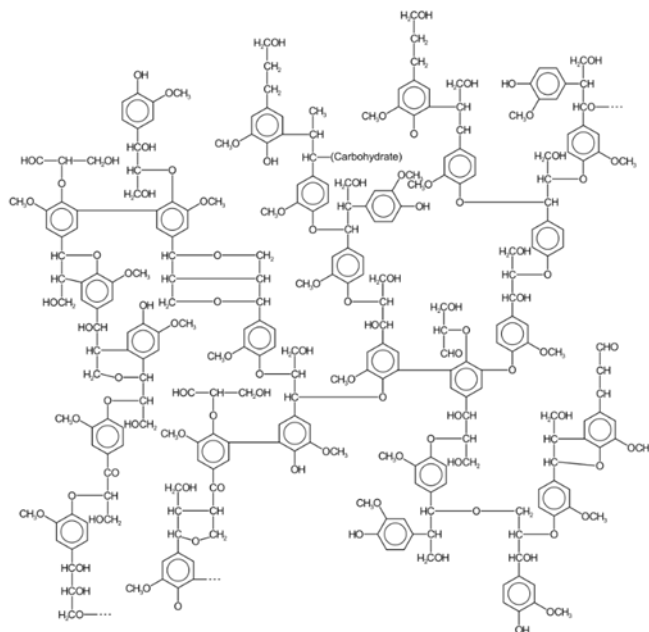


Figure 1: lignin molecule representation

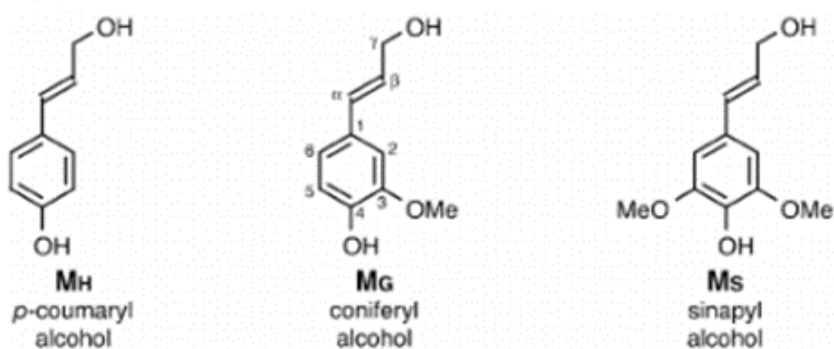


Figure 2: main lignin monomers (monolignols) [9]

Depolymerization of lignin aims to decompose the compound so that smaller products are formed. This is a conversion of high-molecular-weight lignin to low-molecular-mass monomers. For this to happen, the intermolecular C-C or C-O-C bonds of the compounds have to break. Due to the lower bond dissociation energy of the ether bond, the cleavage of the β -O-4 aryl ether bond (C_{β} -O) is mainly performed [13]. This can be achieved by various processes, mostly by depolymerization with elevated temperatures in the absence of oxygen (pyrolysis) or the use of catalysts [7][14]. Depolymerization generally leads to a number of phases, the waste carbon phase, the aqueous phase, the oil phase, and the lignin leftover. The oil fraction contains most of the phenolic monomers, which are useful chemical compounds and thus make it the most valuable fraction [15]. The most important and researched methods for the depolymerization of lignin are depolymerization in supercritical fluids, pyrolysis (high temperature with absence of oxygen), and conversion with metallic, acidic, or base catalysts. The method and conditions should be optimized to lead to the largest formation of oil and the lowest quantity of byproducts [7].

Catalytic processes for the depolymerization can be oxidative or reductive. Both methods will be briefly discussed to understand their advantages and disadvantages. This thesis mainly focusses on the use of metallic catalysts on various supports for the mild reductive lignin depolymerization.

1.2.1 Oxidative catalytic depolymerization

The oxidative depolymerization has long been focusing on the production of vanillin [13], shown in Figure 3. Currently, vanillin is one of the only phenolic compounds manufactured on an industrial scale from biomass [16]. New techniques can however possibly produce a variety of aromatic products. Vanillin is used as a flavoring agent in food [17], but the biggest amount is used as an intermediate for bio-based polymers [18].

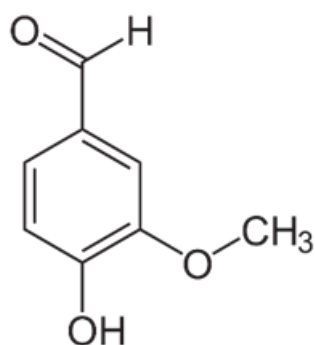


Figure 3: vanillin structure [13]

The oxidative depolymerization used to be catalyzed with homogeneous metal ion catalysts like Cu in alkali conditions [19]. Recently, new innovations using metal oxides like CuO and TiO₂ as heterogeneous catalysts have proven to be an improvement due to their good characteristics and the easy recovery of heterogeneous catalysts in comparison to homogeneous catalysts [20]. An advantage of oxidative depolymerization is that it requires milder conditions. Reaction temperatures for the oxidative catalytic depolymerization of lignin are often around 100°C, which lowers energy costs. The oxidative reaction-pathway also leads to more aromatic products with an active functional group, like aldehydes. This makes it possible to modify the compounds by functionalizing them [21]. A disadvantage is that the oxidation needs to be tempered to prevent over-oxidation that can lead to ring-opening. This is an unwanted reaction in the formation of aromatic chemicals [22].

1.2.2 Reductive catalytic depolymerization

In reductive catalytic depolymerization, lignin is dissolved in organic solvents like MeOH, EtOH or organic solvents mixed with water due to its low solubility in pure water [23]. Used catalysts are Ni, Ru, Pt or Pd-based that can be modified with metals like Fe, Mo and Cu. Common supports are active carbon (AC) and γ -Al₂O₃ [24]. Other metal oxides like SiO₂ and zeolites such as ZSM-5 and SBA-15 are also options [25]. The role of the metal is the dissociation of H₂ that can be fed to the reactor or originates from the solvent (alcohols). The hydrogen-atoms promote the catalytic hydrogenolysis of lignin and hydrogenate reactive intermediates. This limits the condensation of smaller molecules to larger compounds and thus prevents coke-forming. The role of the supports is to break the intramolecular O-4 aryl ether bonds (C_β-O). The most important properties of the supports are the strength and amount of strong acid sites and the surface area of the catalyst [13].

Unlike oxidative depolymerization, the side-chain functional groups of the formed products can be reduced and this leads to the formation of less valuable compounds. This is because they are far less easily modified by functionalization than compounds with a lot of reactive functional groups. The conditions of the reaction, being the temperature and pressure, also have an influence on this, as a more harsh environment can lead to a higher reduction rate of the functional groups [25]. Reductive depolymerization usually leads to higher yields and selectivity to phenolic monomers than oxidative depolymerization [26][13]. The typical main phenolic monomers produced during reductive catalyzed depolymerization are propenyl-substituted phenols, propyl substituted phenols and propanol substituted phenols. Etherified and saturated products are also formed [27]. The formed products have uses for the production of polymer materials, thermoplastics, adhesives and coatings [28].

Reducing the cost of the metal catalysts is a big challenge in order to make the process economically viable. The used metals Pd, Pt and Ru are noble metals and, therefore, they are expensive. Introduction of cheaper transition metals like Fe and Cu in the catalysts can lower the process-costs significantly, while sometimes even enhancing the catalyst performance, which will be discussed later [13]. For comparison, the cost per mole is around €6800 for Pt, €2000 for Pd and only €12, €5 and €0.004 for the non-noble metals Ni, Cu and Fe respectively [29]. (Partly) non-noble metal catalyst will lead to more cost-efficient processes.

In this thesis, the heterogeneous reductive catalytic depolymerization of lignin will be studied. More concrete, Pd- and PdCu-metal catalysts on three supports (Al₂O₃, SiO₂ and active carbon) will be characterized with focus on the active sites for this reaction. The main parameters are the metal dispersion and the acidity of the supports. Active acid sites are critical for the lignin depolymerization because they can break the ether C_β-O bonds. The metal active sites are required to initiate the depolymerization by adsorbing and dissociating hydrogen which is needed for the hydrogenolysis of the ether bonds so that the cleavage can be achieved [30].

1.2.3 Influence of catalyst acidity and metal dispersion on reductive catalytic depolymerization of lignin

Kim et al. (2017) studied the catalytic depolymerization of organosolv lignin on supported 5% Ru catalysts [31]. Used supports were SiO_2 , Al_2O_3 and zeolites ZSM-5 and H β . The catalyst acidity was measured using NH_3 -TPD with a TCD and a quadrupole MS as detectors. The metal dispersion was measured using CO chemisorption with a TCD. The quantity of acid sites was the highest on the zeolite catalysts Ru/H β and Ru/ZSM-5, with values of respectively 1375 and 1113 $\mu\text{mol}/\text{g}_{\text{catalyst}}$. Ru/ Al_2O_3 had an acid concentration of 60 $\mu\text{mol}/\text{g}_{\text{catalyst}}$, while Ru/ SiO_2 showed close to none acid sites. A batch reactor study was performed using GC/MS and GC/FID to identify and quantify the reaction products. The depolymerization yield to small hydrocarbons in function of the total acidity is shown in Figure 4.

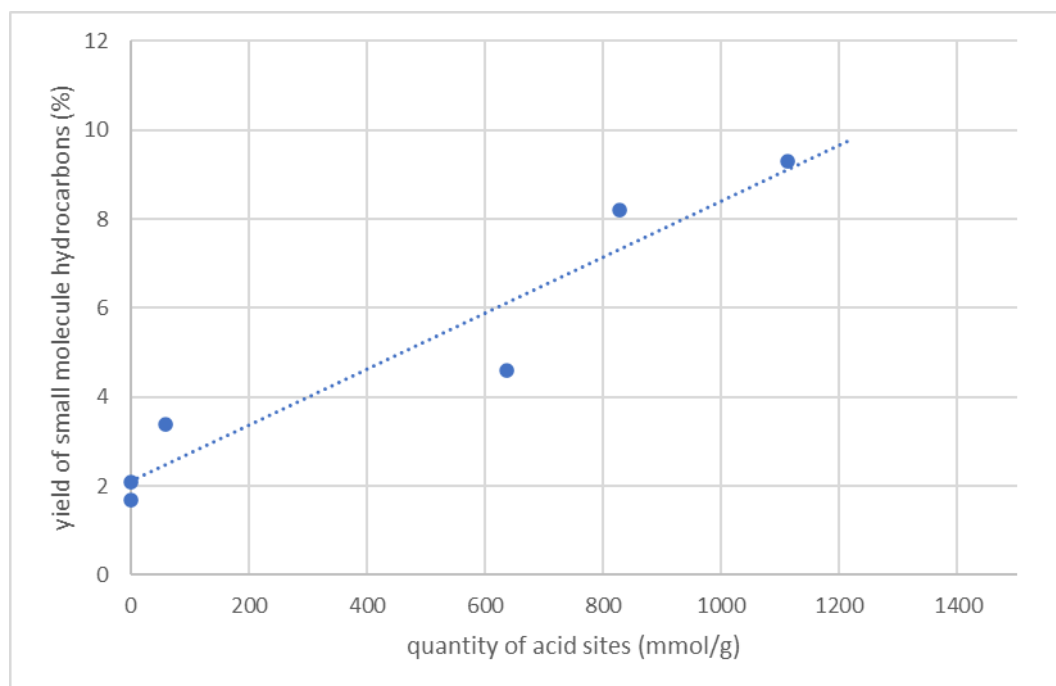


Figure 4: yield in function of the quantity of acid sites on the catalysts

It is clear that the total quantity of acidic sites has a positive influence on the catalyst activity. The weight-average molecular weight (M_w) of the depolymerization products was found using GPC (gel permeation chromatography). From Figure 5 it is clear that the depolymerization products have a lower molecular weight with rising amount of acidic sites. The depolymerization has thus proceeded further [31]. However, it should be noted that too much acidic sites can lead to the loss of the aromatic products, by forming cyclohexane instead of phenolic or benzene compounds. A too low acid concentration will lead to a low activity, but when too high a loss in aromatic products can occur.

The balance between these two factors should be optimized. In this study, no distinction between weak and strong acidic sites was made.

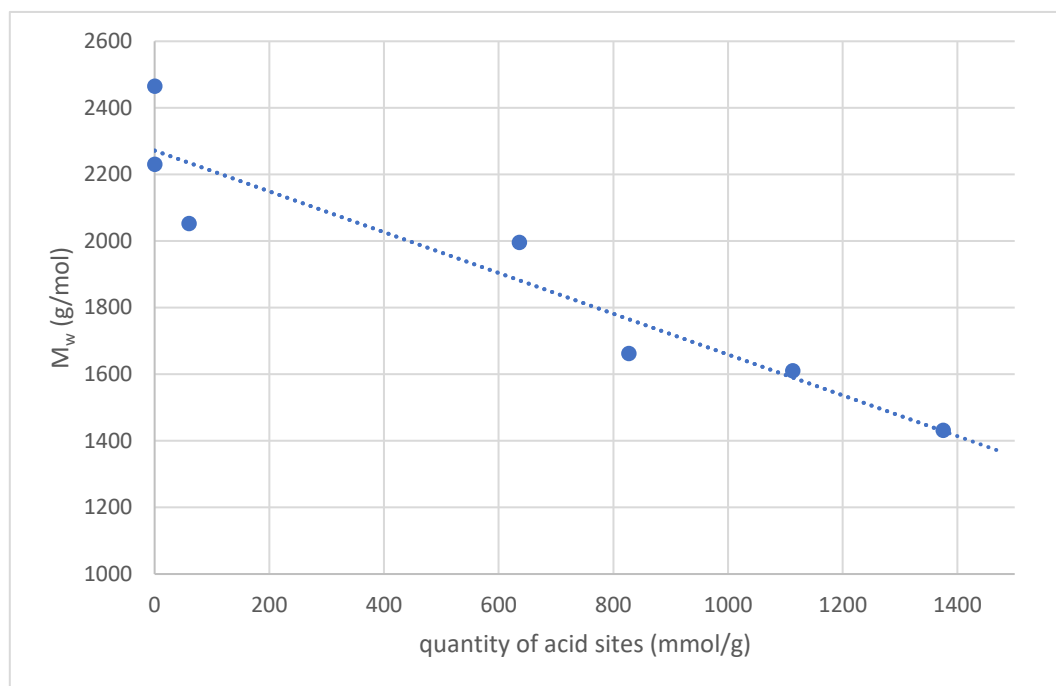


Figure 5: weight-average molecular weight in function of acid sites on the catalysts

A reliable correlation between the metal dispersion and catalytic activity was not found in this study and will be discussed later. However, when using metal-free catalysts, a very low yield of small hydrocarbons was obtained. This leads to the conclusion that metal particles on the solid acid supports are required for the depolymerization [31].

An et al. (2022) modified a Ru/Al₂O₃ solid catalyst by incorporating W. NH₃-TPD revealed that this modification enhanced the catalysts acidic strength. It was found that stronger acidity led to a higher yield and more formation of small molecular products. Stronger acidity promotes the cleavage of both intramolecular ether C_β-O bonds and even C-C bonds that have a higher bond dissociation energy. The selectivity to small molecules increases with rising acidic strength [32].

A recent study by Karnitski et al. (2022) studied the influence of both the acidity and Pd dispersion of a number of supported mono metal Pd catalysts, including Pd-Al₂O₃, Pd-SiO₂ and Pd on zeolite H β with 1 wt% Pd [30]. NH₃-TPD and CO-pulse chemisorption were used to characterize the catalysts. Pd/SiO₂ showed the highest Pd dispersion of 0.466, expressed as [CO]/[Pd] (mol/mol). Pd-Al₂O₃ showed a lower dispersion of 0.379 while the zeolite supported Pd/H β showed a very low dispersion of 0.068. The recorded NH₃-TPD profiles are shown in Figure 6. It is visible that the zeolite H β has a very high amount of acid sites, while Pd/SiO₂ has very few.

The quantity of surface acid sites per catalyst mass showed a reversed order in comparison with the Pd dispersion. Pd/H β has a very high acid density of 1164 $\mu\text{mol/g}$, followed by Pd/Al $_2$ O $_3$ and Pd/SiO $_2$ with values of 130 and 73 $\mu\text{mol/g}$ [30].

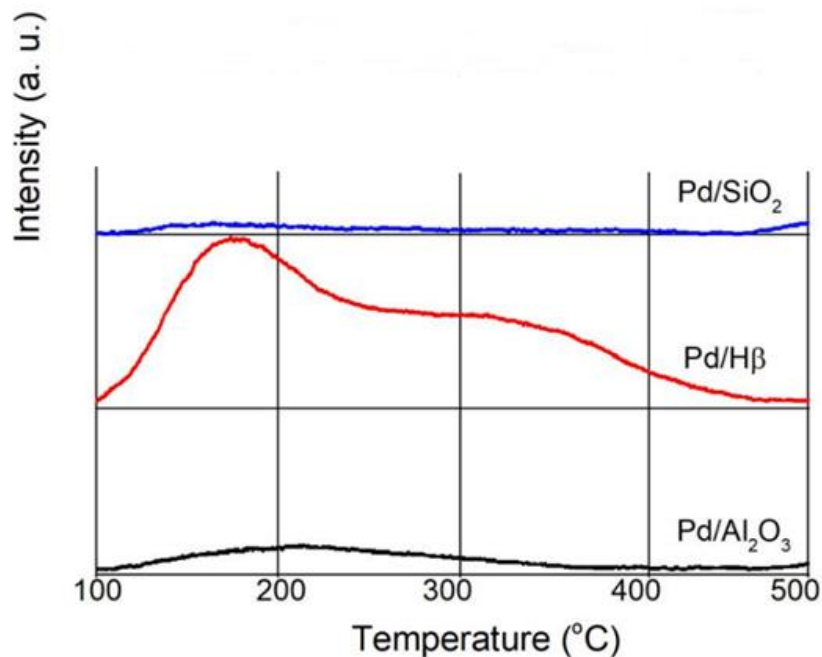


Figure 6: NH $_3$ -TPD profiles of the catalysts [30]

A reactor study for the lignin depolymerization was performed, using a GC-MS and GC-FID to qualify and quantify the depolymerization products. Both oak-extracted organosolv lignin (OL) and concentrated kraft lignin (KL) were used in the study, leading to slightly different results but showing the same global trends. The goal of the depolymerization of lignin is the formation of high-value phenolic monomers. High monomer yield was obtained with Pd/Al $_2$ O $_3$ and Pd/SiO $_2$, but significantly less activity was observed with Pd/H β . This indicates that the lignin depolymerization activity is not only determined by the quantity of acid sites but also by the properties of the surface metal sites. The porosity of the support material plays a crucial role in determining the active metal surface area, which in turn has a significant impact on the overall activity of the catalyst [33]. Notably, supports such as SiO $_2$ and Al $_2$ O $_3$ possess larger pores than H β , a characteristic that heavily influences the effectiveness of the catalyst [34], [35].

Furthermore, the microporous nature of zeolite structures restricts the diffusion of bulky lignin molecules within the pores. As a result, the reaction primarily occurs on the external surface of the catalyst, reducing the active metal surface area per gram of zeolite. This ultimately leads to lower activity levels, as the limited surface area hinders the catalyst's effectiveness in catalyzing the reaction.

Regarding the Pd catalyst on an acidic support, the amount of produced phenolic monomers per total acid sites of the catalyst ($\text{g}_{\text{monomer}}/\mu\text{mol}_{\text{acid sites}}$) strongly improved with a high amount of Pd on the surface, as shown in Figure 7. This metal dispersion is correlated with the amount of CO chemisorbed per mole Pd $[\text{CO}]/[\text{Pd}]$, and is the ratio of the amount of Pd available on the surface of the catalysts to the total amount of Pd in the catalyst [36].

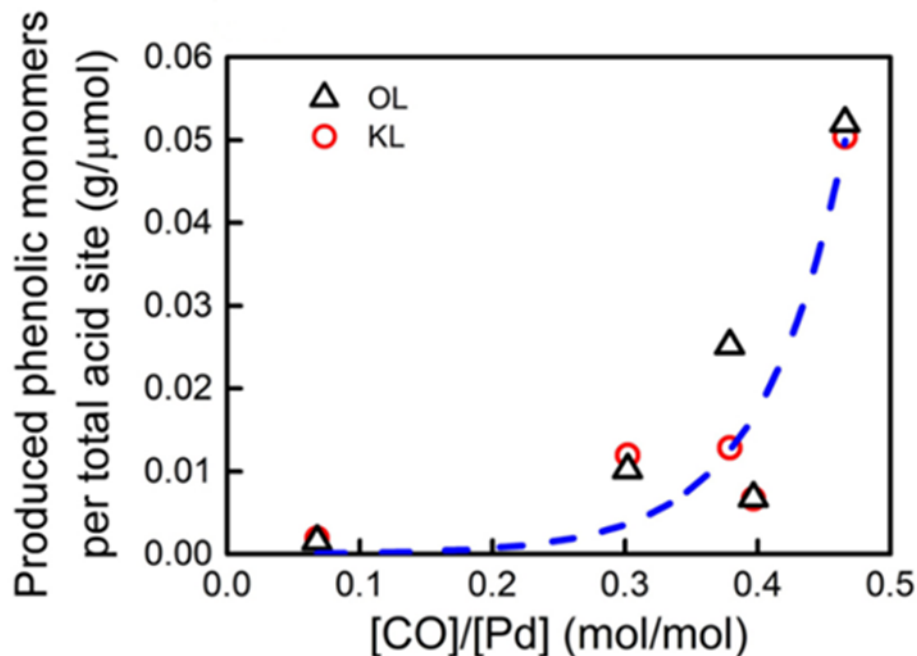


Figure 7: phenolic monomers produced per acid site as function of metal dispersion

The higher activity is probably due to more favorable H_2 adsorption [30]. When no surface Pd is observed, depolymerization does not occur so that no phenolic monomers are formed. The relation between the amount of phenolic monomers produced per gram surface Pd as a function of the total acid site quantity is shown in Figure 8. The blue line represents the fitted reactor data and is an estimation of the trend. The positive trend shows that acid sites facilitate lignin depolymerization. However, it can also be observed that when the quantity of total acid sites is zero, depolymerization will still occur. This indicates that Pd atoms can still depolymerize lignin without the presence of acid sites, be it with low efficiency. In conclusion, it is found that surface Pd atoms promoted depolymerization even in the absence of active acid sites, while the absence of surface Pd atoms inhibited the process [30].

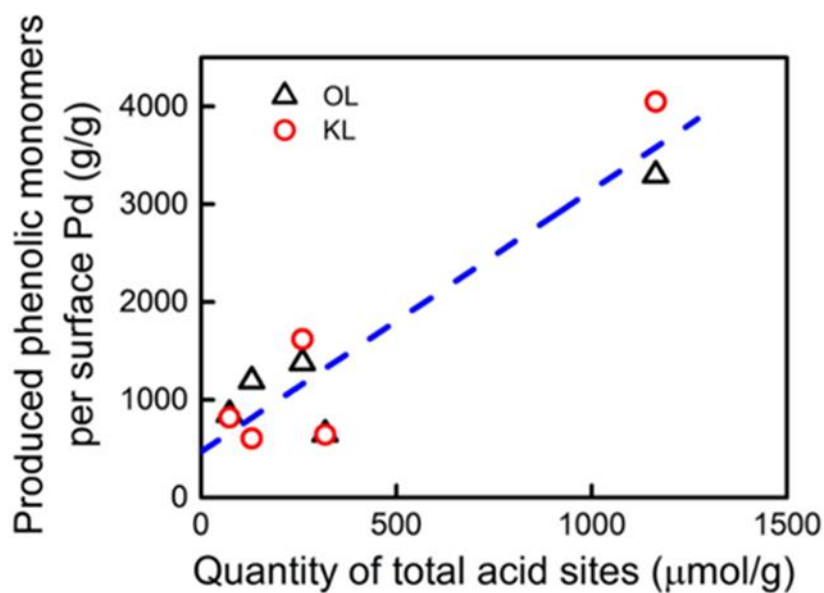


Figure 8: phenolic monomers produced per surface Pd site as function of acid site quantity

To study the catalyst efficiency of Pd on a non-acidic support, SiO_2 with different metal dispersion ratios was synthesized [30]. This support possesses very few acidic sites so that the depolymerization will be mostly Pd-catalyzed. The metal dispersion of the catalysts was manipulated by varying the reduction time and temperature. The BET surface area and pore size distributions of these catalysts were not significantly different. The depolymerization on acidic sites is thus mostly ruled out for this catalysts. This in contrast to Al_2O_3 that has more acidic sites and can be described as an acidic support [30]. The relation between the phenolic monomer yield and Pd dispersion on the mostly non-acidic Pd/ SiO_2 is shown in Figure 9.

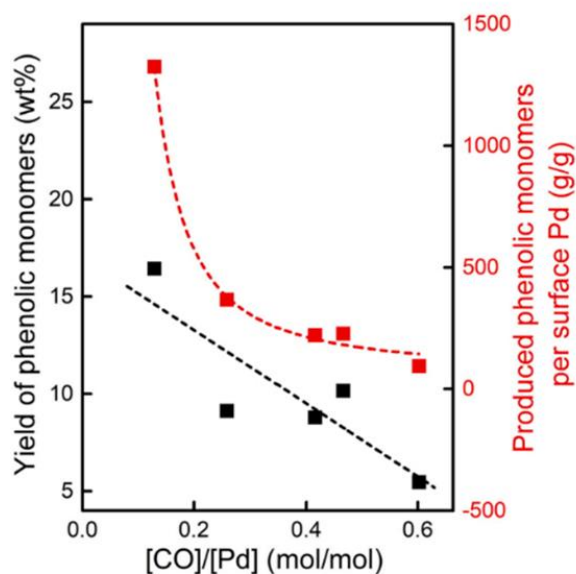


Figure 9: relation between the phenolic monomer yield and Pd dispersion ($[\text{CO}]/[\text{Pd}]$) on the mostly non-acidic Pd/ SiO_2 catalysts [30]

The reactor study revealed higher yields of phenolic monomers and larger quantities of phenolic monomers per surface Pd for lower Pd dispersion values. These results are surprising, as previous findings seemed to indicate that more dispersed metals on the supports lead to more activity for the lignin depolymerization reaction. The most well-dispersed catalyst with a [CO]/[Pd] value of ca. 0.6 achieved monomer yields of only 5%. In comparison, the non-catalyzed depolymerization under these conditions had a similar yield of 5.5%. This leads to the indication that well-dispersed Pd on non-metallic catalysts had no significant effect on the depolymerization reaction. These observations lead to the assumption that the depolymerization of lignin proceeds more easily on the surface of low-dispersed bulk Pd than on well-dispersed, small Pd particles. This can possibly be explained by the better decomposition of multidentate lignin that adsorbs on multiple sites of the bulk Pd surface.

The adsorption of lignin on highly and poorly dispersed Pd is shown in Figure 10. The depolymerization reaction can initiate on more sites on one lignin molecule when bulk Pd particles are present, while highly dispersed particles initiate the dissociation on one or few sites [30].

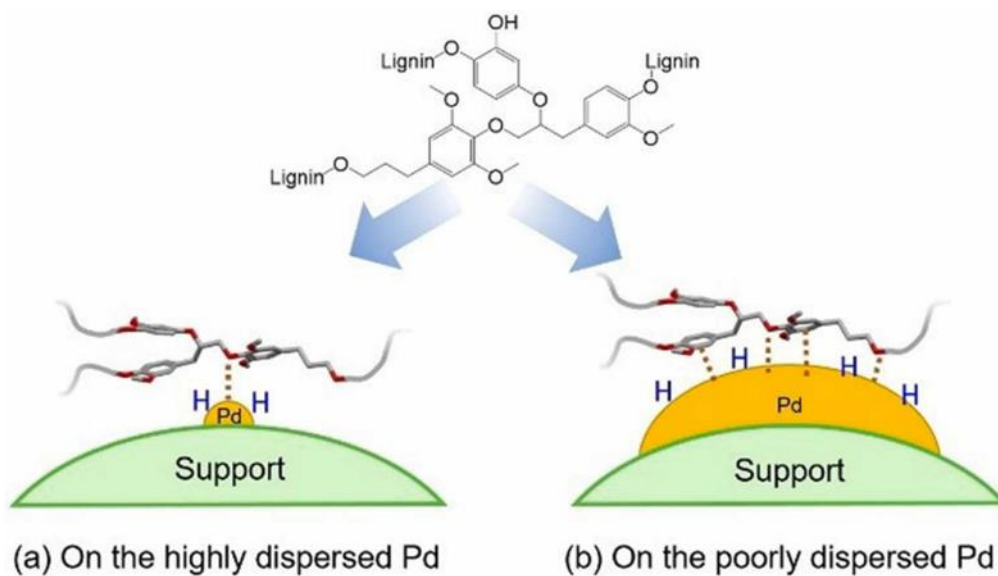


Figure 10: adsorption of lignin on (a) highly dispersed Pd and (b) on poorly dispersed, bulk Pd [30]

The former results lead to the following hypothesis: the reductive catalytic depolymerization of lignin can be promoted with metallic catalysts (e.g. with Pd). On acidic supports (e.g. Al_2O_3) a higher metal dispersion leads to higher activity, while on mostly non-acidic supports (e.g. SiO_2) a lower dispersion leads to higher activity. In this case, bulk metal sites promote the depolymerization. The reason for this distinction is possibly due to the existence of multiple reaction-paths, which each their own optimal catalyst-characteristics. Further research will be needed to confirm this statement and to find the most effective catalyst choice, being acidic supported with high metal dispersion or mostly non-acidic supported with low metal dispersion.

1.2.4 Bimetallic catalysts

The use of bimetallic catalysts can be a valuable option for enhancing and reducing the cost of the depolymerization of lignin. This is frequently done by using a non-noble metal like Ni or Cu in combination with noble metals like Ru or Pd. The concept behind bifunctional heterogeneous catalysis states on the fact that two distinct active sites function in tandem to perform a surface-catalyzed reaction. The most common method however, states on the modification of one of the metals by adding a second, co-metal. For example, by adding the second metal, the surface dispersion of the main metal can be altered [37].

Adding a second metal to form a bimetallic catalyst offers many possibilities, and is thus an interesting strategy. The effect can be classified in three categories: an increase in catalytic activity, modification of the selectivity or an improvement of the catalyst stability. There are five phenomena that make these improvements possible. In geometric (ensemble) the adding of the second metal effects alter the geometry of the active sites. In electronic (ligand) effects, the second metal alters the electron properties by electron transfer between the metals. Stabilizing effects lead to a more stable metal by for example inhibiting sintering or suppressing cokes formation on the catalyst. In synergistic effects, both metal species participate in the chemical bonding to reaction intermediates and transition states. In the last effect, the bi-functional effect, each metal species provides a different function in the reaction mechanism. Generally, geometric and electronic effects affect the catalytic activity and stability, while stabilizing effects improve the stability. Synergistic and bi-functional effects can lead to an improvement in reaction rates, but can also lead to new, possibly improved, reaction pathways [38].

Jiang et al. (2019) researched the use of SiO₂ supported Pd, Ni and bimetallic equimolar PdNi catalysts for the depolymerization of lignin into monomeric phenols [39]. The catalysts were characterized with electron microscopy, X-ray diffraction (XRD) and X-ray photoelectron spectroscopy. A reactor study for the depolymerization of lignin was performed. The bimetallic PdNi/SiO₂ yielded the highest total amount of monophenols and thus showed the highest activity. XRD showed that the bimetallic PdNi catalyst has more Pd and Ni in metallic form compared to the monometallic Pd or Ni catalysts. There are thus more contact opportunities between the active metal sites and hydrogen providing substrates. This significantly promotes the formation of atomic H and enables the hydrogenolysis process of the ether C_β-O bonds which is of great importance for the lignin depolymerization into monophenols [32]. The reduced cost of this bimetallic catalyst in comparison to the pure Pd catalyst is also a great advantage to make the process viable [39].

Sitthisa et al. (2011) used monometallic Pd and bimetallic PdCu supported on SiO₂, prepared by incipient wetness impregnation, for the hydrogenation of furfural to furfuryl alcohol [40]. On Pd/SiO₂, the reaction pathway favored decarbonylation to furan. On the bimetallic PdCu/SiO₂, the conversion was halved, but hydrogenation became the preferred reaction pathway. This resulted in furfuryl alcohol production and the hydrogenation yield almost doubled. The adding of Cu thus proved to be a valuable asset.

In conclusion, the use of bimetallic catalysts can significantly improve the conversion, selectivity or stability of reactions. A number of different phenomena are responsible for these effects. The catalysts can be modified by experimenting with different co-metals.

1.3 Dehydration of 1,3-butanediol to 1,3-butadiene

Butadiene (BD) is mostly used as a (co-)monomer for synthetic rubber and elastomers [41]. In 2012, the global use was 10 million metric tons and continues to grow each year. A lot of researched and used routes to obtain 1,3-butadiene (from now on referred to as butadiene) are based on the conversion of ethanol. This study will focus on a promising route that uses 1,3-butanediol (from now on referred to as 1,3-BDO). This is increasingly appealing because of the rising availability of bio-derived BDO from renewable feedstocks [42] and the increasing importance of producing 'green chemicals'. 1,3-BDO can be obtained by fermentation of glucose, sucrose and glycerol in the presence of certain organisms. [43],[44]. The selective double dehydration to form butadiene from 1,3-BDO requires specific catalysis, which leaves a lot of unanswered questions.

A proposed reaction scheme of the 1,3-BDO dehydration is shown in Figure 11. A mixture of intermediates from the first dehydration and side-products from non-wanted reactions (cracking and isomerization) is obtained [45]. There is thus a great need for an active and selective catalyst to maximize the efficiency of the process. The intermediates (3-buten-1-ol, 2-buten-1-ol and 3-buten-2-ol) differentiate because of the regioselectivity in the first dehydration. This leads to three different mono-alcohols. The most stable of the products can be predicted by *Zaitsev's rule*. The rule states that the most substituted product is favorably formed because a more stable carbocation is obtained [46]. Because of this and the fact that dehydration is the most favorable from secondary alcohols for the same reason, it is predicted that 3-buten-2-ol is the least probable intermediate. 2-buten-1-ol is the more stable in comparison to 3-buten-1-ol so that the formation is the highest for 2-buten-1-ol, lower for 3-buten-1-ol and the lowest for 3-butene-2-ol. Unwanted side-reactions that occur are cracking of 3-buten-1-ol, generating propylene and formaldehyde, and isomerization of 3-buten-2-ol, generating methyl ethyl ketone (MEK) [45].

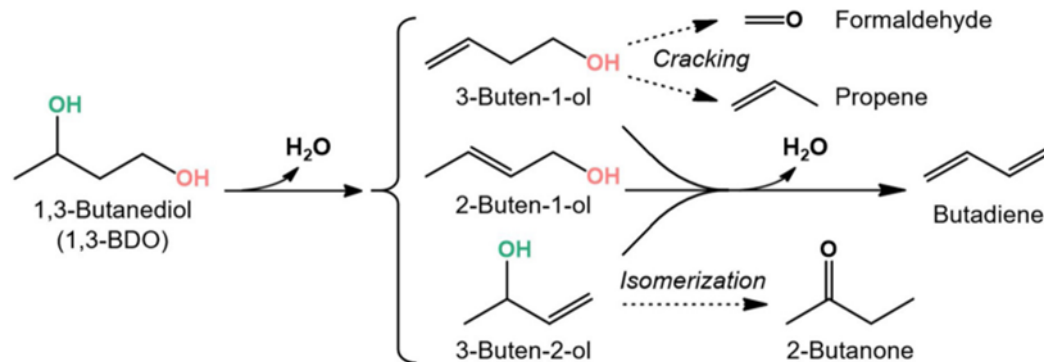


Figure 11: proposed reaction scheme for the 1,3-BDO dehydration [45]

The use of acid catalysts leads to the formation of the three previously discussed enol-intermediates. It is found that 3-buten-2-ol and 2-buten-1-ol are selectively converted to butadiene. However, this is not the case for 3-buten-1-ol. This is due to the fact that this is the least active among the three formed intermediates. The compound is hence also a significant by-product of the reaction. The more 3-buten-1-ol is formed, the lower the selectivity to butadiene will be [45].

Utilizing a mildly basic rare earth metal oxide, such as cerium(IV)oxide (CeO₂) offers a promising solution [43]. This is applied in a two-stage approach where the second step then uses Brønsted acids like silica-alumina (zeolites). Optimization of this technique results in a higher selectivity toward 3-buten-2-ol and 2-buten-1-ol in the first step, and therefore, a higher butadiene selectivity over the silica-alumina [42], [47]. This will be further discussed in the section about the stepwise conversion of 1,3-BDO.

1.3.1 Zeolites and ZSM-5

A frequently used type of catalysts are zeolites. These are aluminosilicate compounds with a structure of interlinked tetrahedra of alumina (AlO₄) and silica (SiO₄). They form a regularly formed porous crystal structure with the elements Al, O, Si and metals like Mg, K and Na which compensate the negative charges in the structure. Zeolites can be naturally occurring, formed in volcanic or sedimentary rocks [48]. An example is mordenite (MOR) that is mostly used as a catalyst in the petrochemical industry for the acid-catalyzed isomerization of alkanes and aromatics [49]. Most used zeolites are however synthetically developed for specific purposes. Examples are zeolites X and Y, used for catalytic cracking and ZSM-5, also known as pentasil-zeolite that is used in for example the methanol to gasoline process (MTG) [50], [51].

Zeolites are stable and high-temperature and high-pressure resistant materials. They are very useful due to their porous structure that makes it possible to trap other molecules like water and alkali or alkaline-earth metal cations.

The cations are not permanently part of the crystal structure, they can be exchanged for other positively charged ions. Cation-exchange water softeners are an important example of this. Here Ca- and Mg-ions are exchanged with Na-ions originating from the zeolite. Zeolites also act as molecular sieves, because the regular openings in the structure can selectively trap compounds of certain sizes or linearity [52]. This makes it possible to use them as shape-selective catalysts in for example catalytic crackers to turn large hydrocarbons into diesel, kerosene, waxes and gasoline [48].

An interesting zeolite for the catalysis of the dehydration of 1,3-BDO is the medium-pore ZSM-5, shown in Figure 12 [53].

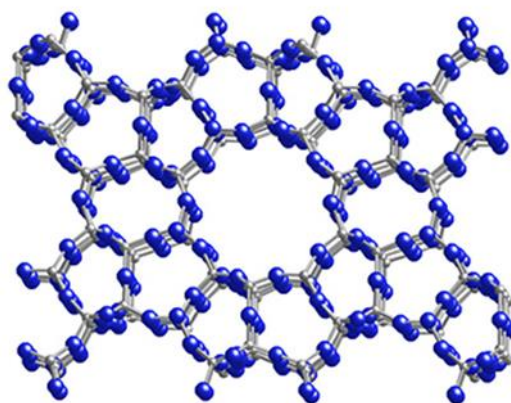


Figure 12: structure of ZSM-5 zeolite [53]

Due to its acidity ZSM-5 can be used as a catalyst in acid-catalyzed reactions. It can be modified by ion exchange or using different silica/alumina ratio, making it a very versatile zeolite and thus useful for many applications [54]. The molecular sieve has 3D channel systems. The chemical formula of ZSM-5 is $\text{Na}_n\text{Al}_n\text{Si}_{96-n}\text{O}_{192} \cdot 16\text{H}_2\text{O}$. The variable n is a number between 0 and 28. This leads to a variable $\text{SiO}_2/\text{Al}_2\text{O}_3$ ratio [55]. ZSM-5 is a pentasil zeolite, which is the name for zeolites that forms 5-membered oxygen rings in the crystal structure. The zeolite is especially useful for shape selectivity. Only molecules that fit in its channel system can enter the zeolite or can be formed as products. Bigger molecules that are formed within are trapped and are converted to smaller molecules or in the worst case block the pores [54]. This can lead to deactivation of the catalyst and should be minimized. In what follows, ZSM-5 will be studied as it is a promising catalyst for the dehydration of 1,3-BDO to 1,3-BD.

1.3.2 Direct dehydration of 1,3-butanediol over a zeolite catalyst (ZSM-5)

ZSM-5 zeolites with a high SiO₂/Al₂O₃ molar ratio have a low-density of Lewis acid sites while showing the presence of Brönsted acid sites with an intermediate strength. ZSM-5 appears to be a valuable option to convert 1,3-BDO into BD with relatively high yields [43].

A study by Jing et al. [43] researched the performance of a number of catalysts. The focus in this work will be on the use of ZSM-5 zeolites, the other catalysts will not be discussed here. The studied ZSM-5 catalysts are ZSM-5@30, ZSM-5@64, ZSM-5@106 and ZSM-5@260. The last number is the SiO₂/Al₂O₃ molar ratio. The amount and strength of the acid sites in these catalysts was analyzed with NH₃-TPD on an AutoChem II 2920 system and with a TCD and MS as detectors. The 1,3-BDO dehydration in presence of the catalysts was performed in a fixed-bed reactor at 300°C. The results of the reactor study are shown in Table 1.

Table 1: reaction results of dehydration of 1,3-BDO at 300°C [43]

	conversion (%)	selectivity (%)								BD productivity (g _{BD} /g _{cat} ·h)
		MEK	MVK	1BoI	2BoI	3B1oI	3B2oI	Propylene	BD	
ZSM5@30	90	2.1	0.7	0.7	0.3	12	2.5	25	40	3
ZSM5@64	95+	2	1.2	1.2	0.4	10	2.6	30	43	3.6
ZSM5@106	95+	8.2	1.2	0.8	0.4	9.4	2.6	23	45	3.8
ZSM5@260	95+	1.8	1.3	1	0.3	8.7	2.3	24	60	5.1

The main products are butadiene, propylene and 3-buten-1-ol. A hypothesized reaction route is shown in Figure 13.

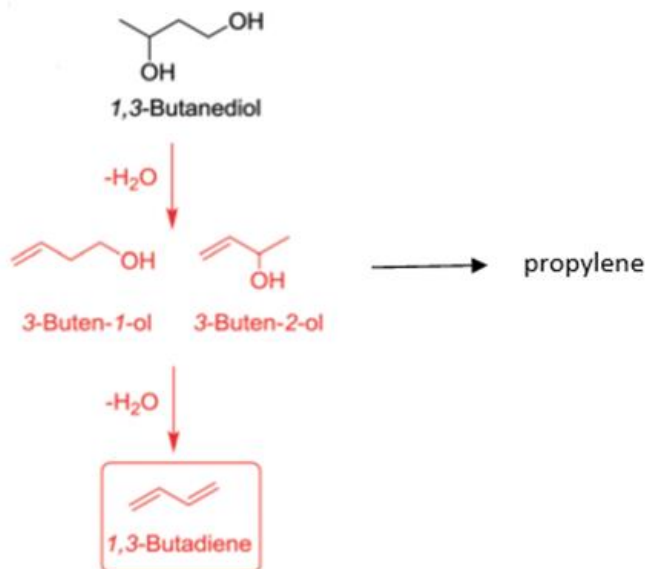


Figure 13: proposed reaction scheme for the direct dehydration of 1,3-butanediol

The first step is the dehydration of 1,3-BDO to 3-buten-1-ol and 3-butene-2-ol with the second step being two parallel reactions. These are the dehydration of 3-buten-1-ol into the wanted product BD and the carbon-carbon bond cleavage of 3-buten-1-ol or 3-butene-2-ol to propylene. There are also a number of smaller by-products in lower quantities formed: methyl ethyl ketone (MEK), methyl vinyl ketone (MVK), 1-butanol, 2-butanol and 3-butene-2-ol. The selectivity of each catalyst is visualized in Figure 14.

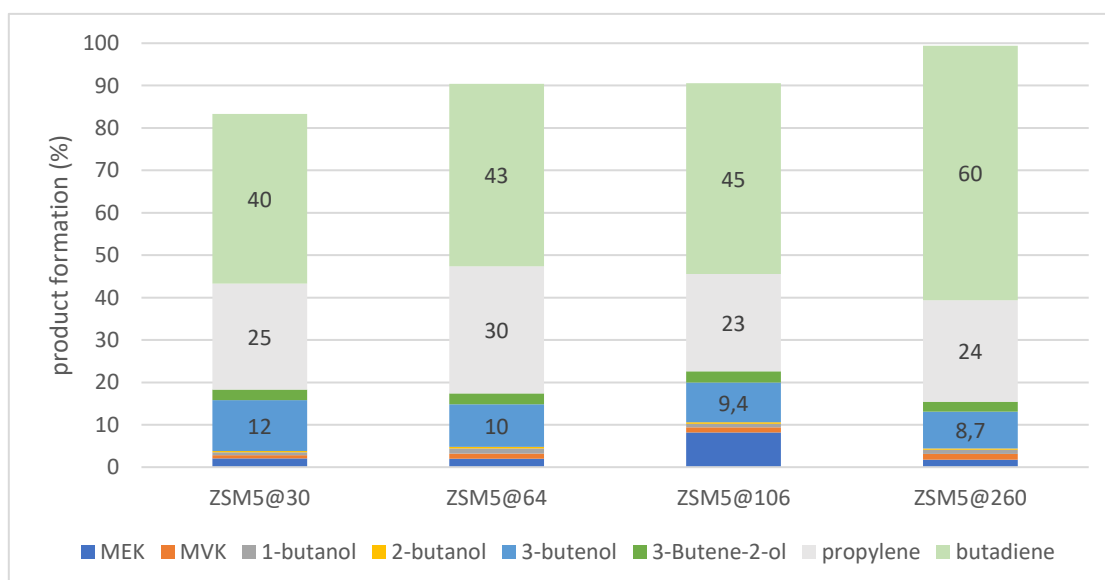


Figure 14: selectivity of the ZSM-5 catalysts

Figure 14 shows a steady rise in conversion and selectivity to BD with higher $\text{SiO}_2/\text{Al}_2\text{O}_3$ molar ratio.

Due to the formation of other by-products in low quantities, the sum of the selectivity values does not equal the conversion. All the catalysts show a conversion close to 100%, except for ZSM-5@30.

ZSM-5@260 seems the most promising catalyst choice from these results at a temperature of 300°C. A catalytic stability test was performed at the same temperature. This showed that there is a slow deactivation after 24 hours of reaction time, but the selectivity to BD remains almost constant. This is shown in Figure 15.

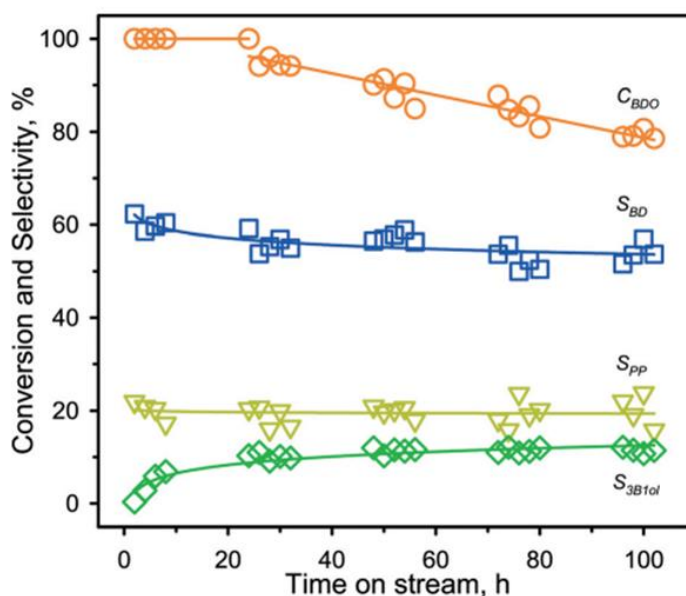


Figure 15: deactivation study of ZSM-5@260 [32] C_{BDO} : conversion of 1,3-BDO; S_{BD} : selectivity to BD; S_{PP} : selectivity to propylene; S_{3B1ol} : selectivity to 3-buten-1-ol [43]

The reaction mechanism is thus not influenced by the deactivation of the catalyst. The deactivation is likely due to less attainable acid sites as a result of plugging of the pores by certain formed species [43], [56].

The NH_3 -TPD spectra in the temperature range of 130°C to 600°C of the ZSM-5 catalysts are shown in Figure 16. The acidic sites are ranked in terms of strength: weak sites (130-280°C), medium sites (280-450°C) and strong sites (450-600°C). As visible from the curves, higher SiO_2/Al_2O_3 ratios led to a lower temperature for the peak maximum. This means that a higher ratio correspond to lower acidic site strength. The catalysts show mostly weak and medium acidity. The total acid density also decreases with rising SiO_2/Al_2O_3 ratio. This is visualized in Figure 17. Tempering the acidity can lead to a higher conversion and selectivity to BD, as can be seen when linking the results of Figure 14 with the acid properties of the catalysts from Figure 16 and Figure 17. The catalysts with the least amount of acidic sites and the weakest sites (ZSM-5@260) performs best with the highest conversion and selectivity to BD.

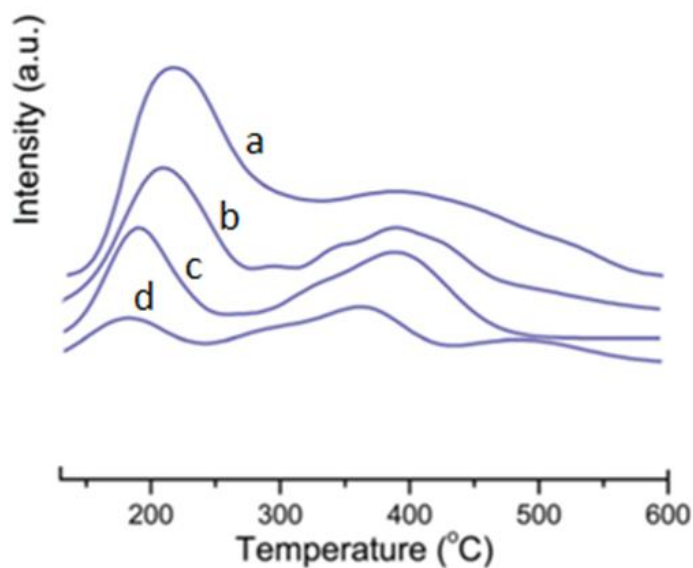


Figure 16: NH_3 -TPD spectra of (a) ZSM-5@30, (b) ZSM-5@64, (c) ZSM-5@106 and (d) ZSM-5@260 [43]

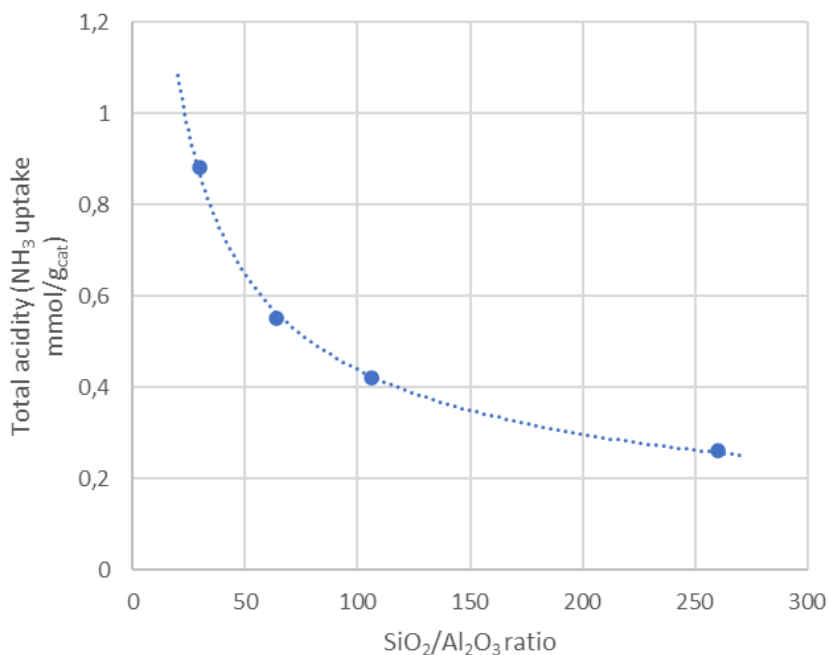


Figure 17: total acid density in function of $\text{SiO}_2/\text{Al}_2\text{O}_3$ ratio

However, no distinction between Lewis or Brönsted acid sites can be made with NH_3 -TPD. This can be done with FTIR spectroscopy with a specific probe molecule, often pyridine [57]. This method is outside the scope of this thesis, but the results will be discussed. It is found that the ratio of the amount of Brönsted on Lewis sites (B/L) is 1.25; 3.28; 1.94 and 6.16 for the catalysts in order of rising $\text{SiO}_2/\text{Al}_2\text{O}_3$ ratio, respectively. It is stated that the highest proportion of Brönsted acid sites with medium strength in ZSM-5@260 is responsible for the highest selectivity for BD with this catalyst. In conclusion, the zeolite with the highest $\text{SiO}_2/\text{Al}_2\text{O}_3$ ratio (ZSM-5@260) is the most promising for the direct dehydration of 1,3-butanediol into butadiene over aluminosilicate catalysts.

1.3.3 Modification of ZSM-5 with Boron

A promising option to further temper the acidity is the incorporation of boron in the ZSM-5 catalyst. This can be done by partly using B instead of Al when synthesizing the catalyst or by adding B by incipient wetness impregnation on a pure ZSM-5 catalyst.

The first option has been studied for the catalytic methanol to olefin conversion and xylene formation [58]. A study by Sayed et al. states that boron-associated sites in the ZSM-5 catalyst showed weak acidity in comparison of Al-associated sites. The characterization is performed by infrared spectroscopy. [58]. The replacing of Al by B leads to a decrease of the zeolite acidic strength, which can possibly improve the selectivity to BD in the dehydration of 1,3-BDO. The shape selectivity of the ZSM-5 catalyst remains unaffected [58]. A slightly different approach is performed by Imelik et al. [59]. Here B is incorporated in an already synthesized ZSM-5 catalyst. This latter option is an easier way to modify ZSM-5 with different amounts of B. Their study also showed a decrease in acid strength when adding B to the zeolite.

Li et al. characterized ZMS-5 catalyst modified by silicalite-1-coating and boron to influence the acidity for the alkylation-reaction of toluene with methanol [60]. The boron modified ZSM-5 will be discussed. The catalyst was prepared by incipient wetness impregnation of ZSM-5 with an aqueous solution of boron acid. The acidity is mapped with NH_3 -TPD. The profiles of the unmodified HZSM-5 and boron-modified B/HZSM-5 are shown in Figure 18.

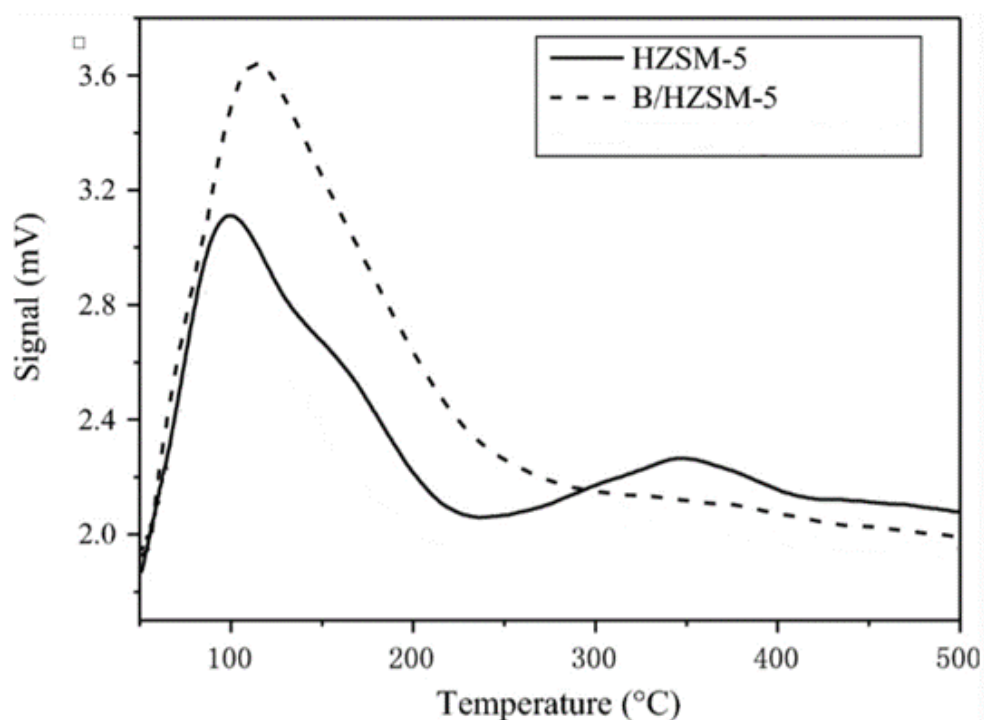


Figure 18: NH_3 -TPD profiles of HZSM-5 and B/HZSM-5 [60]

Two main peaks for the unmodified catalyst is visible, one corresponding to weaker acidic sites around a temperature of 100°C and one corresponding to stronger acidic sites around 350°C.

It is visible that the B-modified catalyst has a higher amount of weaker acidic sites but almost none strong acidic sites in comparison to the pure HZSM-5. The percentage of weak acidity in the total acidity thus increases significantly, which lowered the conversion of toluene [60]. It is concluded that the boron modification weakened the acidity but increased the total amount of acidic sites.

The discussed studies focus mainly on the methanol conversion to olefins or alkylation of toluene and conclude that incorporating B to ZSM-5 lowers the activity of the catalysts, thus stating that this option is not favorable [58]. For the dehydration of 1,3-BDO however, tempering of the acid strength can improve the conversion and selectivity to BD. No studies have been found that discuss this particular use of B incorporation in ZSM-5 for the dehydration of 1,3-BDO, and needs further research.

1.3.4 Stepwise conversion of 1,3-butanediol to butadiene

The direct dehydration requires a specific catalyst to perform two reaction steps while being under the same reaction conditions. The catalyst can never be optimal for each step, resulting in a decrease of efficiency and a lower butadiene selectivity [1]. This can be improved by separating both dehydration steps by using a specific catalyst for each step.

The first step is the dehydration of 1,3-BDO to unsaturated C4 mono-alcohols. As stated earlier, pure CeO₂ can catalyze the dehydration to selectively produce 3-butene-2-ol and 2-buten-2-ol in a fixed-bed reactor. The catalyst is stable during a test for 5 hours at 325°C, but is less efficient at temperatures above 375°C [47]. The specific surface of CeO₂ decreases when calcined at a higher temperature. This leads to a lower conversion of 1,3-BDO, but a slightly higher selectivity for 3-butene-2-ol and 2-buten-2-ol with increasing temperature [61]. CeO₂ has a cubic fluorite topology with the {111} facet as the most stable one [62]. This facet grows with higher calcination temperature. Bigger particles also showed the {111} facet as more present and this leads to more selective conversion to 3-butene-2-ol and 2-buten-1-ol. It is stated that this facet is responsible for the dehydration reaction [63].

A possible reaction mechanism for the dehydration of 1,3-BDO over CeO₂ is shown in Figure 19 [64]. Three Ce cations are exposed at a point defect site on the CeO₂ {111} facet, which is the active site of the catalyst for this reaction. The reaction takes place due to the redox reaction of Ce⁴⁺ to Ce³⁺. This makes it possible to dehydrate the compound and release a H₂O-molecule.

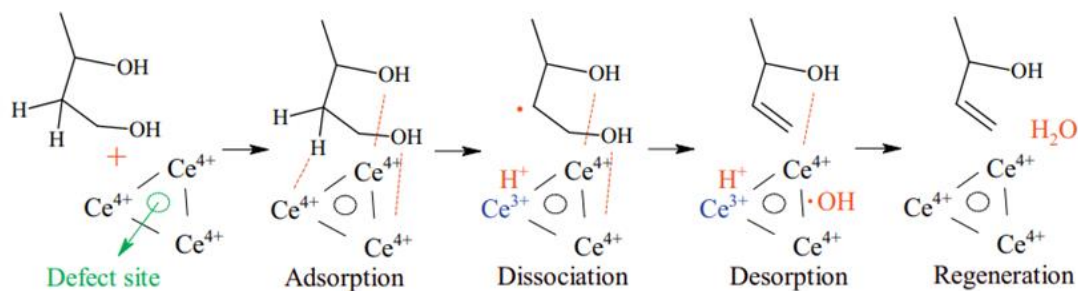


Figure 19: possible reaction mechanism for dehydration of 1,3-BDO over CeO_2 [64]

Further dehydration of mono-alcohols over CeO_2 does not proceed. They are less reactive than diols and need strong acidity [65]. A second step is thus needed for the conversion of formed mono-alcohols from the first step, 3-butene-2-ol and 2-buten-1-ol, to butadiene. This is possible over a solid acid catalyst like $\text{SiO}_2\text{-Al}_2\text{O}_3$ [66]. This catalyst shows a high activity to form BD from 3-butene-2-ol and 2-buten-1-ol. Conversion and selectivity values, exceeding 90%, are reported at initial stages. The deactivation can be solved by modification of $\text{SiO}_2\text{-Al}_2\text{O}_3$ with Ag. Ag cleaves hydrogen gas to hydrogen atoms and these atoms suppress the formation of cokes that leads to deactivation by filling the pores of the catalysts. With this modification, the activity stays stable for 5 hours instead of 1 hour without Ag [66].

1.3.5 Hybrid catalyst containing CeO_2 and zeolites

CeO_x can also be combined with a zeolite as support to form a hybrid catalyst for the dehydration of 1,3-butanediol into butadiene. Fang et al. characterized a series of CeO_x nanoparticles encapsulated in mordenite catalysts, referred to as Ce@MOR_X with X the Si/Ce ratio [67]. The catalyst is called a hybrid of CeO_x nanoparticles and MOR. The relation of the composition of the catalyst to its activity for the dehydration of 1,3-BDO to BD is discussed. The used catalysts are Ce@MOR_X with X equal to 20, 50, 100 and 200. The reaction results are shown in Table 2 and visualized in Figure 20.

Table 2: reaction results for dehydration of 1,3-BDO with different Ce@MOR catalysts [67]

catalyst	BDO conversion (%)	selectivity			BD productivity (g _{BD} /g _{cat} .h)
		3B1ol	Propylene	BD	
MOR	38	9.8	13	16	1.32
Ce@MOR_20	29	2.7	11	5.4	0.46
Ce@MOR_50	100	12	24	46	3.84
Ce@MOR_100	92	11	21	39	3.29
Ce@MOR_200	75	7.9	16	25	2.08

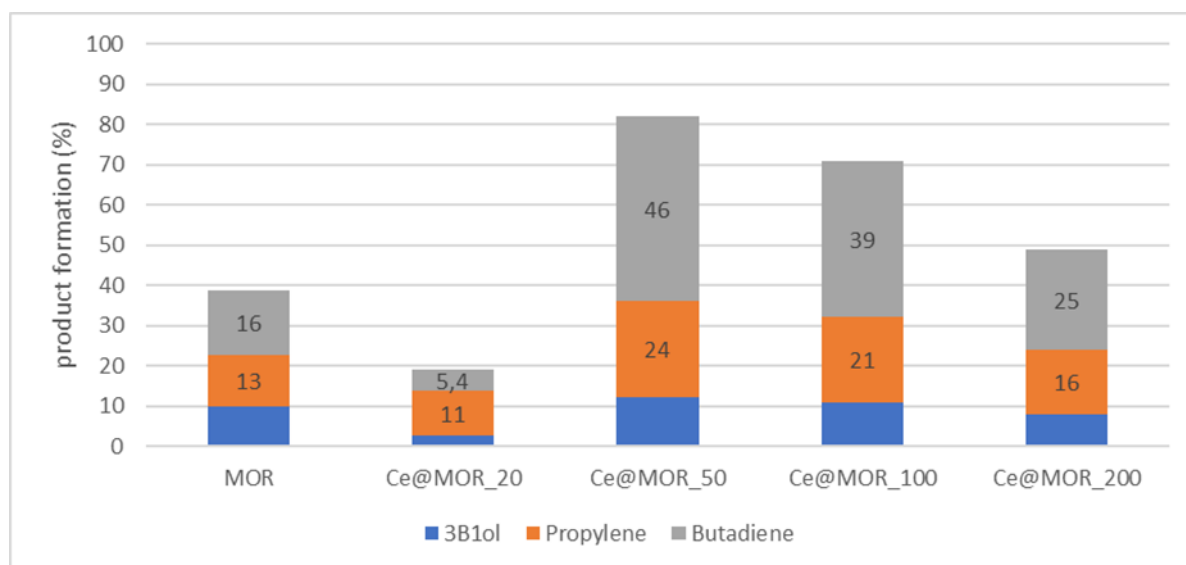


Figure 20: reaction results for dehydration of 1,3-BDO with different Ce@MOR catalysts [67]

In comparison with the pure MOR catalyst, the conversion of 1,3-BDO and the selectivity to BD can increase significantly when adding a certain amount of CeO₂ to the zeolite. The best results are found for the Ce@MOR₅₀ catalyst. Here, the BD selectivity reaches a maximum of 46% at a conversion of 100%. This is explained by NH₃-TPD results, where it was found that the ratio of medium over strong acid sites in the catalyst increased from 0.7 for the pure MOR to 4.1 for Ce@MOR₅₀, shown in Table 3 [67]. Corroborating with previous results, this improves the selective conversion of 1,3-BDO to BD.

Table 3: acid properties from NH₃-TPD study

	fraction medium acidic sites (%)	fraction strong acidic sites (%)	medium/strong acid ratio
MOR	26.9	37	0.7
Ce@MOR_50	53	13	4.1
Ce@MOR_100	50	12	4.2
Ce@MOR_200	47	17.5	2.7

A graph with the data from the study is made to visualize the impact of the acid properties on the conversion and selectivity to BD in the dehydration of 1,3-BDO catalyzed with Ce@MOR. This is shown in Figure 21. The medium/strong acid ratio is multiplied by 10 for clarification of the trends.

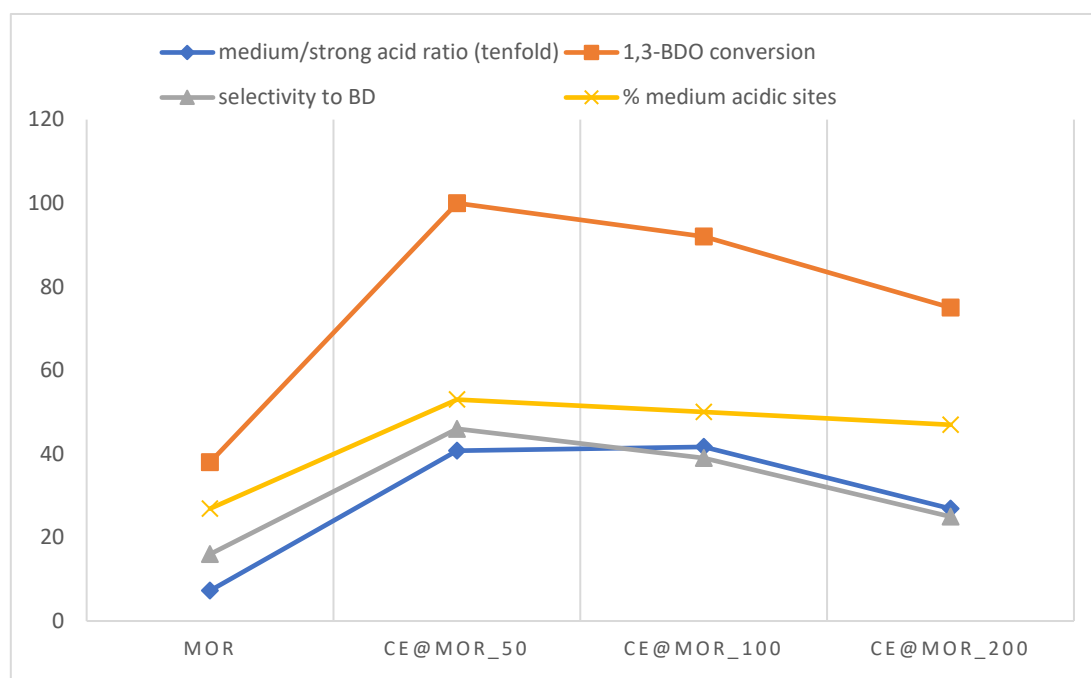


Figure 21: impact of acid properties on conversion and selectivity to BD for the 1,3-BDO dehydration

Ce@MOR₅₀ shows a maximum for 1,3-BDO conversion and selectivity to BD. This is in parity to its highest percentage of medium acidic sites and high medium/strong acid ratio. To conclude, Ce@MOR₅₀ is the best performing catalyst, closely followed by Ce@MOR₁₀₀. The high influence of the fraction medium acidic sites is shown in Figure 22.

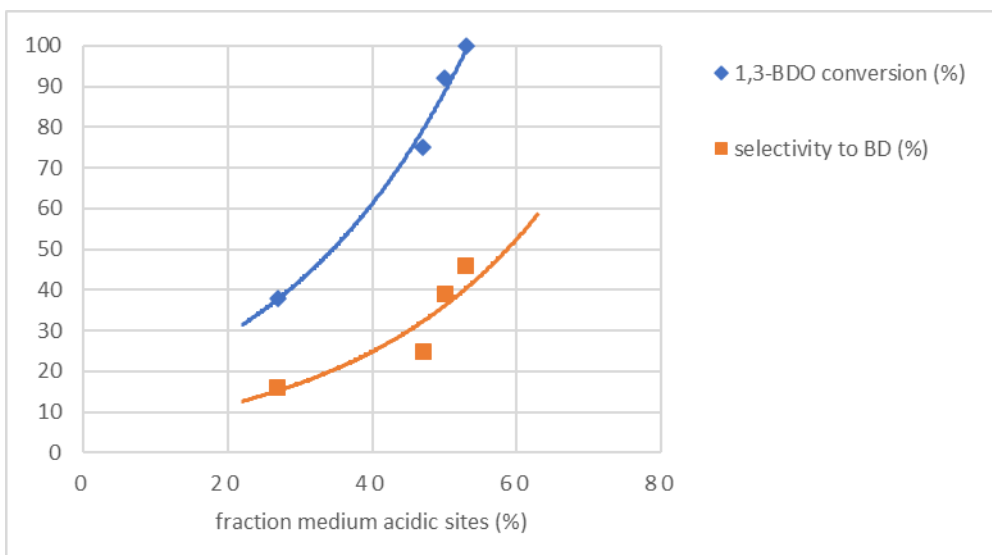


Figure 22: catalyst efficiency in function to the fraction of medium acidic sites on the Ce@MOR catalysts

A strongly rising trend of 1,3-BDO conversion and selectivity to BD with higher fraction medium acidic sites is visible. It is clear that a high fraction of medium acidic sites is optimal for the selective conversion of BDO to BD [67]. The catalyst also showed a high stability, the evolution of the catalytic performance as a function of the time of stream (TOS) is shown in Figure 23. This shows a stable conversion and selectivity to BD for the first 6 hours of the reaction with a slow decrease in selectivity to BD after 6 hours. These are acceptable results and lead to the conclusion that the hybrid Ce@MOR_50 is an effective catalyst for the dehydration of 1,3-BDO to BD [67].

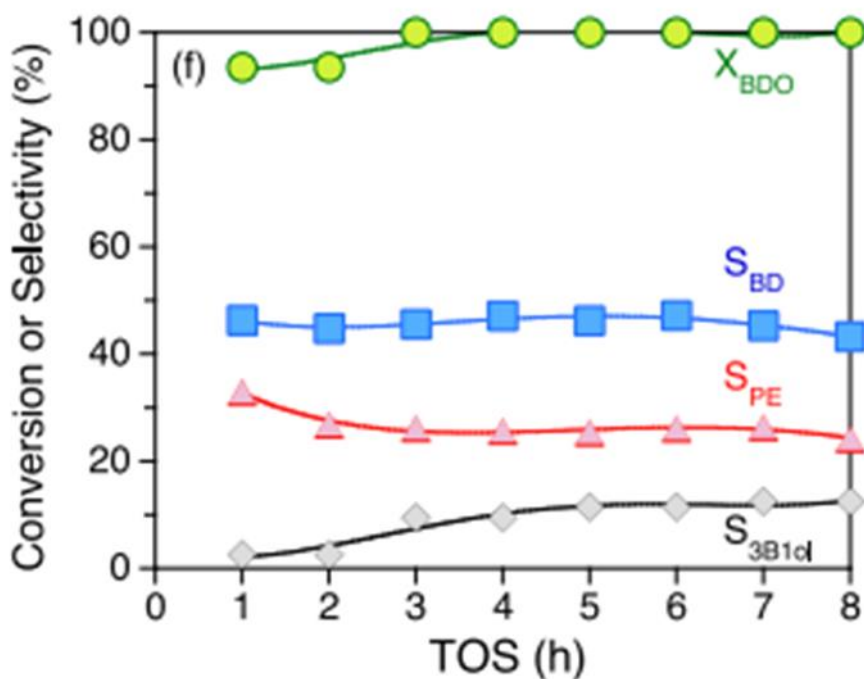


Figure 23: evolution of catalytic performance for Ce@MOR catalysts [67]

In this case, the MOR zeolite was dispersed with CeO₂ nanoparticles and referred to as CeO₂@MOR. The opposite is also possible, then the zeolite is dispersed on CeO₂ and referred to as MOR@CeO₂. This approach has been done for ZSM-5 by Prabhu et al. (2022) and led to a very stable ZSM-5@CeO₂ catalyst [68].

1.4 Temperature-programmed techniques

The characterization of solid catalysts is frequently done with various temperature-programmed techniques. These include temperature-programmed reduction (TPR), temperature-programmed oxidation (TPO), temperature-programmed desorption (TPD), and pulse chemisorption. These will be briefly explained to understand the concept of each technique.

1.4.1 Temperature-programmed reduction (TPR)

Hydrogen-TPR (H₂-TPR) is frequently used as a method for the characterization of reducible metal catalysts. It makes it possible to examine the surface chemistry of metals and metal oxides. When performing the experiment, a catalyst is dispersed upon a surface and placed in a fixed-bed, usually a glass U-shaped tube, with furnace. Impurities on the surface are removed by overflowing with carrier gas. This reducing gas (hydrogen gas with an inert gas like Ar) passes the catalyst while the temperature in the reactor linearly increases. The reduction will not occur at the starting temperature, but when a certain reduction temperature is reached, the reducing gas will lead to a reduction of the catalyst. A detector constantly analyses the outgoing H₂ concentration. The difference between the ingoing and outgoing H₂ concentration leads to the H₂ that is consumed by the reduction-reaction [69]. This can be visualized in a graph with temperature on the x-axis and the H₂ consumption (or detector signal) on the y-axis. A thermal conductivity detector (TCD) measures changes in thermal conductivity and is linked to the change in H₂-concentration [70]. This technique can be used to find the most efficient reduction conditions [71].

To illustrate this, a spectrum is shown in Figure 24. Certain characteristics can be derived after deconvolution of the spectrum into different peaks. The number of reducible species is equal to the number of spectrum peaks and the temperature at which each species reduces can be seen on the x-axis.

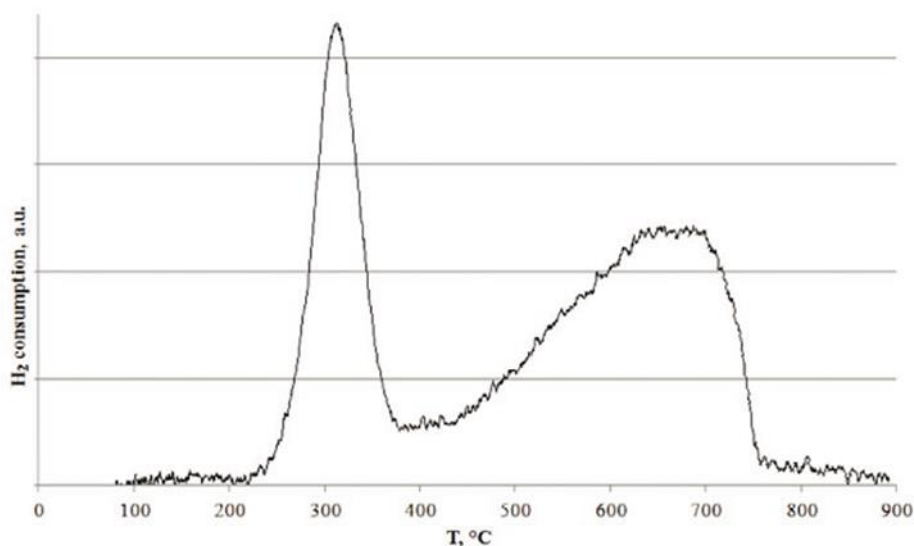


Figure 24: H₂-TPR spectrum [72]

In this example, there are two reducible species with main reduction temperatures of respectively 300°C and 650°C. The maximum reduction rate is related to the maximum H₂-consumption because this reducing gas is consumed gas to reduce the metal (oxide) catalyst. More reducible species consume more H₂ and lead to a higher peak in the spectrum. The area under the curve equals the total H₂-gas consumed for a certain mass of catalyst [70]. It is important to notice that the spectra are dependent on the heating rate, the H₂-concentration, and the flow rate of the gas. The main changes are a shift of the peaks to a higher temperature when the heating rate is higher and a shift to lower temperature when the flow rate and H₂ concentration are higher [73]. In this respect, experiments with the aim to compare catalysts amongst each other should always be performed under the same conditions [72].

1.4.2 Temperature-programmed oxidation (TPO)

TPO is less frequently used in comparison to TPR as a method to analyze metal catalysts, but can give useful insights. The concept is the same, but instead of a reducing gas, an oxidizing gas is used [74]. This is most frequently a dilute oxygen in helium flow. The temperature in the fixed-bed reactor again linearly increases. At certain temperatures, oxidation of the metal species will occur while the oxygen is reduced. The consumed oxygen is a measurement of oxidation of the species at a certain temperature and a similar curve like TPR visualizes the results [75]. This method gives an insight in the oxidizing properties of the catalyst. Metal species on a catalyst that oxidize at a lower temperature, meaning that they oxidize easier, will lead to a greater fraction of this metal that is present in the metal oxide form. This generally corresponds to a less active catalyst due to the lower concentration of metallic active sites.

1.4.3 Temperature-programmed desorption (TPD)

TPD is a useful technique for the characterization of catalysts because it allows insights in the interaction of probe molecules with the surfaces of heterogeneous catalysts. This makes it possible to evaluate active sites on catalyst surfaces [76]. A small amount of catalyst is placed on a fixed bed, usually a glass U-shaped tube. A probe molecule, together with an inert gas flows over the solid and the probe molecule adsorbs on the surface of this solid until the sample is completely saturated. Thereafter, the temperature is linearly increased and at a certain temperature, the heat will overcome the activation energy and break the bond between the adsorbate and adsorbent. Depending on the adsorption strength of the active site, the probe molecule will thus desorb at a different temperature. The desorbed molecules will then enter the stream of inert carrier gas. The probe molecule is analyzed with a downstream detector. A frequently used detector is an online quadrupole mass spectrometers and a thermal conductivity detector (TCD). The conditions of the method have a high influence on the results, it is thus important to maintain the same parameters when evaluating different catalysts [77]. One should also take this in mind when comparing absolute results of different researches.

1.4.3.1 NH₃-TPD

A frequently used technique is NH₃-TPD to analyze the strength and concentration of acidic active sites of a catalyst. In a quartz fixed-bed, the catalyst gets saturated with NH₃ by using a flow gas of the compound in an inert gas (mostly He). Before the adsorption starts, the samples are purged with He to remove excess adsorbed molecules. As the temperature increases, NH₃ starts to desorb and the outlet stream (containing He and NH₃) can be quantified with an online quadrupole mass spectrometer or a TCD detector [78].

NH₃-TPD is frequently used to get insight in the amount and strength of acidic active sites on catalyst-supports [79].

When there are multiple different surface functionalities, like Lewis or Brønsted acid sites, it is hard to identify which peak in the spectrum corresponds to this active site. Other techniques like X-ray photoelectron spectroscopy (XPS) and Fourier transform infrared (FTIR) can be used overcome this problem and identify the peaks in the TPD-spectra [77][80]. To illustrate this, a typical NH₃-spectrum will be briefly discussed.

An example of a NH₃-TPD spectrum of two earlier discussed zeolites MOR and ZSM-5 is shown in Figure 25.

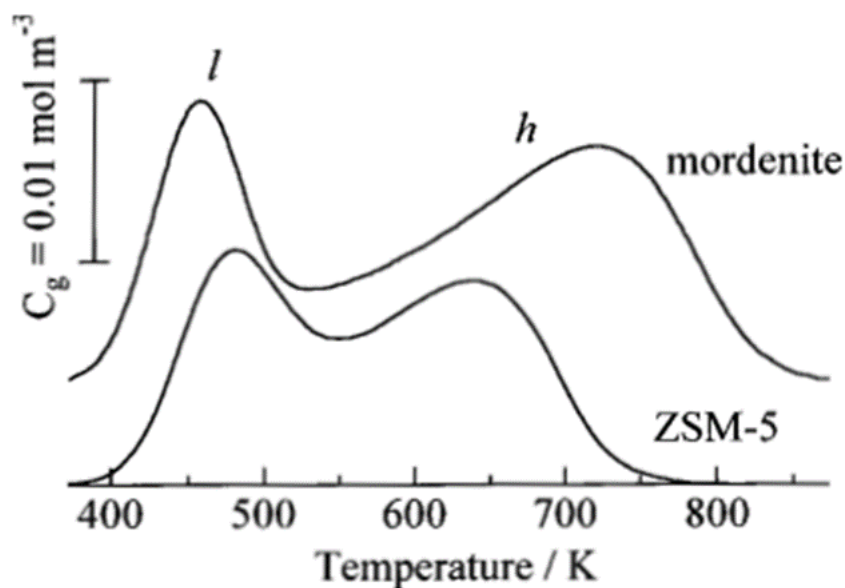


Figure 25: NH_3 -TPD spectra for MOR and ZSM-5 [81]

The acid sites can be classified into three types, namely weak, medium and strong acid sites depending on the temperature the NH_3 is desorbed. Zeolites typically show two desorption peaks, one at low and one at high temperature [81]. This is also visible for MOR and ZSM-5.

They both show a peak around 450 and 480 K respectively that corresponds to the weak acidic sites and a peak around 650 and 740 K respectively that corresponds to the strong acidic sites. It is stated that the low temperature peak is contributed to desorption of physically adsorbed or weakly held NH_3 rather than adsorbed NH_3 on acid sites that contributes to the high temperature peak [81]. MOR shows a higher amount of both weak and strong acidic sites in comparison to ZSM-5. The total amount of acidic sites is thus also higher for the MOR zeolite.

1.4.3.2 CO_2 -TPD

Similar experiments can be performed to analyze the strength and concentration of basic active sites. This is frequently done with CO_2 -TPD. Here CO_2 in He or pure CO_2 is used as reaction-gas [82]. A quadrupole MS or TCD can be used for the detection of outgoing components and thus quantification of the desorption rate at a certain temperature [79]. In analogy with NH_3 -TPD, peaks can be attributed to weak, medium and strong basic sites on the catalyst for defined temperature ranges [83].

1.4.4 Pulse chemisorption

When performing pulse chemisorption, a small metal catalyst sample is placed in a fixed-bed, usually a glass U-shaped tube, and is overflowed with an inert gas like Ar, used for H₂ pulse chemisorption or He, for CO pulse chemisorption. The reason for this distinction is that the inert gas and the adsorption gas needs a high difference in thermal conductivity, in order to obtain a higher sensitivity of the TCD. The process happens at a constant temperature. At certain times, a small and constant amount of adsorption gas (H₂ or CO) is added to the flow. By using an online TCD or MS and when the entrance concentration is known, the consumption of reaction-gas can be found. Mostly, the difference in area under the signal in a reactor without and with catalyst sample is calculated to quantify the H₂ or CO uptake [84], [85]. When the whole 'pulse' of probe molecules is consumed by the catalyst, no signal is detected. This is usually the case for the first pulse or pulses.

With each pulse, the catalyst is more saturated so that less gas is taken up by the catalyst surface. This leads to more probe molecules in the outgoing flow and thus an increase in signal intensity. When the surface is saturated, the uptake becomes zero for each pulse so that for the next pulses a constant signal is observed.

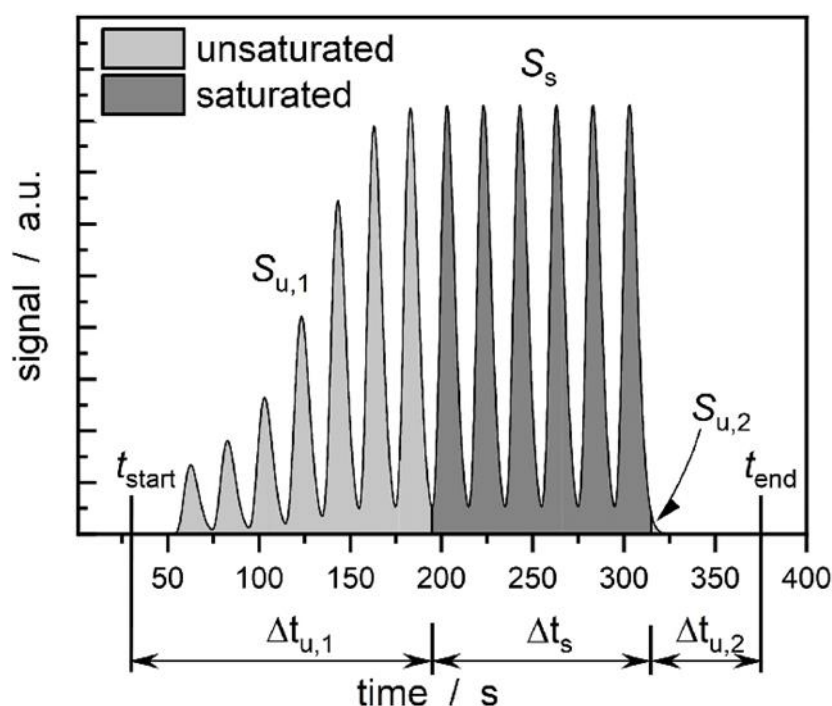


Figure 26: example of a pulse chemisorption spectrum [84]
 S_u : unsaturated peaks; S_s : saturated peaks

The signal corresponds to the signal when no catalyst is present in the reactor. The total chemisorption (uptake) is equal to the uptake in each pulse. This can be calculated by summing the difference of the pulse without catalyst present (or the signal after complete saturation) and the pulses with catalyst present [84][86].

An example of a pulse chemisorption spectrum is shown in Figure 26. The signal is given in function of time. The signal rises with each pulse until the surface is saturated. When the saturation is complete, the signal of each pulse will remain constant because no chemisorption of the probe molecule will take place [84]. The total uptake can be derived from this graph by the method stated above.

Pulse chemisorption is the most efficient method for determining metal surface areas due to its relative short analysis time in comparison to TPD [86]. It is used to determine the active surface area and percent metal dispersion (fraction of atoms exposed to the surface) and active particle size of the metal analyzed metals [87]. The metal dispersion is particularly important for catalysis, since only atoms that are available on the surface can take part in catalytic reactions [88].

CO is chosen as the adsorbate gas when H₂ can be adsorbed into the metal, which happens with Pd to form Pd-hydrides. H₂ can also significantly adsorb on certain supports like active carbon. CO can chemisorb on metals such as Fe, Ni, Ru, Pt, Pd and is frequently used to study the metal dispersion and active metal area. The pulse chemisorption data can be converted into dispersion results, which will be discussed in the chapter 'Methods'.

1.5 Summary of TP techniques and catalyst active sites

In the former chapter, a number of frequently used (temperature-programmed) techniques to characterize solid catalysts were discussed. The discussed techniques were: TPR, TPD and pulse chemisorption, with multiple variants possible. Each of these techniques makes it possible to gain an insight in one or multiple properties of these catalysts. Typical properties are: amount and strength of active acidic or base sites on the surface, reduction properties, dispersion and strength of metal active sites, surface concentrations of species... The techniques and the characteristics they map are summarized and linked to the active sites of the catalysts for the two reactions on which this thesis focusses: the reductive catalytic depolymerization of lignin and the dehydration of 1,3-BDO. The methods of the used techniques in this thesis will be further specified in 2.2: Methods.

For clarity, the main active sites on the catalysts for both reactions are summarized in this chapter. As stated earlier, the main active sites for the supported metal catalysts for the reductive catalytic depolymerization of lignin are the amount and strength of the acid sites on the supports (in case of acidic supports) and the metal dispersion. Three supports are used; Al₂O₃, SiO₂ and active carbon. Al₂O₃ is an acidic support, while SiO₂ and AC are mostly non-acidic [89]. The role of the metal is the dissociation of H₂ that can be fed to the reactor or originates from the solvent (alcohols as H-donating solvents). The hydrogen-atoms promote the catalytic hydrogenolysis of lignin and can hydrogenate reactive intermediates. This limits the condensation of smaller molecules to larger compounds and thus prevents coke-forming. The role of the supports is to assist in the breakage of the intramolecular O-4 aryl ether bonds (C_β-O).

The most important properties of the supports are the strength and amount of strong acid sites [13]. However, other properties such as porosity, hydrophobicity, structure... also have an influence on the catalytic activity.

The Pd dispersion on the supports showed to have a significant influence on the catalyst performance. A recent study showed that whether this dispersion is best low or high depends on the support [30]. The reductive catalytic depolymerization of lignin can be promoted with Pd catalysts. The study states that on acidic supports (e.g. Al_2O_3) a higher metal dispersion leads to higher activity, while on mostly non-acidic supports (e.g. SiO_2 and AC [89]) a lower dispersion leads to higher activity. In this case, bulk metal sites promote the depolymerization. The reason for this distinction is possibly due to the existence of multiple reaction-paths, which each their own optimal catalyst-characteristics. Further research will be needed to confirm this statement and to find the most effective catalyst choice, being acidic supported with high metal dispersion, mostly non-acidic supported with low metal dispersion or other combinations. The Pd dispersion can also be influenced by the use of bimetallic catalysts.

For the dehydration of 1,3-BDO, it is discussed that a higher amount and fraction of medium strength Brönsted acid sites leads to a higher conversion and selectivity to BD. The focus in this thesis are zeolite catalysts, particularly ZSM-5. Tempering the acidity of the zeolite catalysts is here of great importance for a performant dehydration reaction to BD. Possibilities to achieve this is by varying the $\text{SiO}_2/\text{Al}_2\text{O}_3$ molar ratio of ZSM-5 or the incorporation of Boron. It can also be attempted by using hybrid catalysts of ZSM-5 and CeO_2 , which has mild acidic and significant basic properties [90].

The discussed TP techniques and what characteristics they clarify are shown in Table 4. A more detailed experimental plan, with performed methods for each catalyst can be found in 2.2: Methods.

Table 4: summary of the most important active sites and techniques that can be used to characterize the catalysts

Technique	Reductive catalytic depolymerization of lignin	Dehydration of 1,3-BDO
NH₃-TPD <i>Amount and strength of acid sites</i>	Acid density and strength of the supported metal catalysts (not researched in this thesis)	Acid density and strength of the zeolite and hybrid catalysts
CO₂-TPD <i>Amount and strength of basic sites</i>	/	Base density and strength of the zeolite/CeO ₂ catalysts and pure CeO ₂
CO-pulse chemisorption <i>Metal dispersion, active metal surface</i>	Dispersion of Pd on the supports (Al ₂ O ₃ , SiO ₂ , AC) and active metal surface	/
TPR <i>Reduction properties</i>	Reduction properties of the catalysts (not researched in this thesis)	/

1.6 Research questions and research approach

The world is facing numerous challenges in terms of energy and sustainability, and the use of renewable sources for platform chemicals plays a crucial role in addressing these challenges. Platform chemicals are the building blocks for the production of various chemicals, materials and fuels. In this context, the depolymerization of lignin to monomeric phenols and the dehydration of 1,3-butanediol to butadiene are important processes that have the potential to provide sustainable and renewable feedstocks for various industrial applications. In this thesis, the focus will be on the investigation of some promising catalysts used for two specific processes, the reductive catalytic depolymerization of lignin and the dehydration of 1,3-butanediol. The research will aim to answer the following questions:

Reductive catalytic depolymerization of lignin:

- How does the used support (Al_2O_3 , SiO_2 and AC) influence the Pd dispersion and active metal area on the catalysts?
- How does the use of bimetallic PdCu on the supports influence the Pd dispersion and active metal area on the catalysts?

Research approach: a Pd dispersion and active area study of the supported Pd and PdCu catalysts will be performed using CO-pulse chemisorption.

Dehydration of 1,3-BDO:

- How does the $\text{SiO}_2/\text{Al}_2\text{O}_3$ ratio of the ZSM-5 zeolite influence the catalyst's acidity?
- How does the incorporation of Boron in the zeolite structure influence the acidity of the catalyst?
- What are the basic properties of pure CeO_2 and how can the use of hybrid $\text{CeO}_2/\text{ZSM-5}$ influence the catalysts acidity and basicity?

Research approach: ZSM-5 with different $\text{SiO}_2/\text{Al}_2\text{O}_3$ molar ratios, incorporated Boron in the zeolite or using hybrid CeO_2 with ZSM-5 will be characterized using NH_3 -TPD to research if the tempering of the acidity of these zeolites is a viable option to optimize the dehydration of 1,3-BDO to BD. The influence of using hybrid CeO_2 with ZSM-5 on the basic properties will also be researched.

This research will try to contribute to a better understanding of these catalysts and provide valuable insights for the development of sustainable and renewable feedstocks for various industrial applications.

2 Materials and methods

2.1 Materials

2.1.1 Characterization of catalysts for the mild reductive catalytic depolymerization of lignin

2.1.1.1 Supported metal catalysts synthesis¹

Six supported metal catalysts were prepared and characterized. These were Pd and PdCu on the supports Al₂O₃, SiO₂ and active carbon (AC). Pristine catalyst supports were bought from companies with high purity and their characteristics are listed in Table 5. The metal catalysts were synthesized through *incipient wetness impregnation*. In this method, the active metal precursor is dissolved in water. The concentration of the solution is calculated to lead to the wanted metal loading on the support after impregnation and removal of the solvent. The used precursors are Pd(NO₃)₂·8H₂O and Cu(NO₃)₂·6H₂O. The solution is then added to the support in a volume equal to the total pore volume of the support. This is done slowly (during ca. 20 min) to let capillary action draw the solution into the pores and obtain a good spreading of the metal. The catalyst is then dried at 60°C for 16 hours and calcined at 450°C for 4 hours under air (γ-Al₂O₃ and SiO₂) or N₂ (AC) to remove the volatile solvent so that the metal is deposited on the support surface [91]. All six catalysts have approx. 5 wt% metal loaded and the bimetallic catalysts have a Pd/Cu ratio of approx. 3/2 wt%. The calculated composition is shown in Table 6. The samples are the same as used by Ward Samoy in his master's dissertation: "*Characterization of catalytic active sites via temperature-programmed techniques (2022)* [92].

Table 5: characteristics of the used supports

	γ-Al ₂ O ₃	SiO ₂	Active carbon
Producing company	Sasol Puralox SCCA 150/200	CARiACT Q	Norit SAE SUPER
Specific surface area (m²/g)	195	198	1182
Pore volume (cm³/g) (specs)	0.8	1.18	0.95
Particle size distribution (μm)	[100;500]	[75;500]	[100;300]

¹The supported metal catalysts were prepared by the research group in the academic year 2021-2022. This description is informative and was not performed by the writer of this thesis.

Table 6: theoretical catalysts loading

Catalysts	Pd theoretical loading (wt%)	Cu theoretical loading (wt%)	Total theoretical metal loading (wt%)
Pd/Al ₂ O ₃	4.99	/	4.99
Pd/AC	4.97	/	4.97
Pd/SiO ₂	5.00	/	5.00
PdCu/Al ₂ O ₃	3.16	1.87	5.03
PdCu/AC	3.14	1.87	5.01
PdCu/SiO ₂	3.09	1.86	4.96

2.1.1.2 True metal loading

The theoretical metal loading does not exactly match the actual loading. The actual loading is more accurately determined by Inductively Coupled Plasma Atomic Emission Spectroscopy (ICP-AES)². The technique uses inductively coupled plasma to produce excited atoms and ions that emit electromagnetic radiation. This radiation has a wavelength characteristic of a particular element and the intensity of the emissions are proportional to the concentration of the various elements [93]. The results are shown in Table 7.

Table 7: metal loading determined by ICP-AES

Catalyst	Pd loading (wt%)	Cu loading (wt%)	Total metal loading (wt%)
Pd/Al ₂ O ₃	3.05	/	3.05
Pd/AC	4.27	/	4.27
Pd/SiO ₂	3.41	/	3.41
PdCu/Al ₂ O ₃	2.02	1.54	3.56
PdCu/AC	3.88	2.97	6.85
PdCu/SiO ₂	2.16	1.54	3.70

It is clear that there is a significant difference between the theoretical (calculated) metal loading and the more precise, observed metal loading. When discussing the results, it is important to keep in mind the difference in actual metal loading between the different catalysts. The precise amount of Pd on the catalysts should be taken into account for the dispersion and active metal area calculations, to enable for a valuable comparison between the catalysts.

² ICP-AES on the catalysts was performed by the UGhent INCAT research group and not by the writer of this thesis.

2.1.2 Characterization of catalysts for the dehydration of 1,3-butanediol

In this study, a total of eight samples were characterized, including seven (modified) ZSM-5 catalysts and pure CeO₂. The first sample examined was a commercially bought ZSM-5 catalyst from Zeolite International, which had a SiO₂/Al₂O₃ ratio of 24. This catalyst serves as a reference point for comparison with the other samples.

Two prepared ZSM-5 catalysts are characterized, with different SiO₂/Al₂O₃ ratios. The first one, referred to as ZSM-5@25, has a SiO₂/Al₂O₃ ratio of 25 (theoretical), while the second, referred to as ZSM-5@150, has a SiO₂/Al₂O₃ ratio of 150 (theoretical).

To review the effects of Boron incorporation, the same two ZSM-5 catalysts are modified with an equal amount of Boron. The modified catalysts, referred to as ZSM-5@25_B and ZSM-5@150_B, have half of the Al replaced by B (theoretical). The Si/Al ratios here resemble the amount of SiO₂ relatively to the amount of Al₂O₃ and Boron together (SiO₂/Al₂O₃+B). The amount of B and Al₂O₃ is aimed to be equal.

Additionally, two hybrid CeO₂ with ZSM-5@25 catalysts were analyzed. The first hybrid sample involved ZSM-5 dispersed on CeO₂, referred to as CeO₂/ZSM-5 with each species in 50/50% weight ratio. The second hybrid sample exhibited a core-shell topology, with ZSM-5 as the core and CeO₂ as the shell, designated as ZSM-5@CeO₂. Lastly, prepared pure CeO₂ was characterized as a separate sample to study its individual properties.

2.1.2.1 (Modified) zeolite catalysts synthesis³

The synthesis is based on the method of de Reviere et al. (2020) [94]. The used chemicals are shown in Table 8.

Table 8: used chemicals for the zeolite synthesis

Chemical	Properties	Producing company
Commercial ZSM-5	SiO ₂ /Al ₂ O ₃ ratio: 24 CAS: 1318-02-1 100%	Zeolyst
Aluminum isopropoxide (AIP)	98%	Merck Life Science
Tetra propyl ammonium hydroxide (TPAOH)	1 M in water	Merck Life Science
Sodium hydroxide (NaOH)	>98%	Merck Life Science
Tetra ethyl ortho silicate (TEOS)	>99%	Chem Lab Analytical

³The samples were synthesized in January 2023 at the INCAT research group, UGent by doctoral student Loïc Eloi and thus not prepared by the writer of this thesis.

Boron hydroxide (B(OH)₃)	99%	VWR chemicals
Ammonium nitrate (NH₄NO₃)	1 M	Chem Lab Analytical
Boric acid (H₃BO₃)	>99%	VWR Chemicals
Ce(NO₃)₃.6H₂O	434.34 g/mol	Merck Life Science
Hexa methylene tetramine (HMT)	140.186 g/mol	Merck Life Science
NaCl	58.44 g/mol	Chem Lab Analytical
Ammonium persulfate ((NH₄)₂S₂O₈)	228.18 g/mol	Merck Life Science
Ethanol	100%	Chem Lab Analytical

Synthesis of the ZSM-5 catalysts

A recipient was added with the aluminum source, AIP, and the ZSM-5 structure-directing agent (SDA) TPAOH, and stirred until completely dissolved. Water and NaOH were added while stirring, followed by the slow dropwise addition of the silica source (TEOS). The solution was then left to age for 24 hours in a closed recipient to allow AIP and TEOS to completely hydrolyze. The solution was then placed in a Teflon liner and crystallized for 96 hours at 165°C (hydrothermal treatment). The crystallized zeolite was separated from the liquid through centrifugation, repeated three times with the addition of water to the solution. The sample was dried for 20 hours at 120°C and calcined for 6 hours at 550°C. To form the protonated zeolite (HZSM-5), 10 ml/g zeolite of 1M NH₄NO₃ was added and stirred for 2 hours at 50°C, exchanging the Na ions for H ions. The solution was separated from the zeolite through centrifugation and the sample was washed with water and centrifuged, dried for 20 hours at 120°C, and finally calcined for 6 hours at 550°C.

The molar composition of the solution was 1Al:25Si:9TPAOH:0.16NaOH:495H₂O:100EtOH for ZSM-5@25, the Si/Al ratio is changed by lowering the amount of the added Al source. For ZSM-5@150, the composition of the solution was 0.17Al:25Si:9TPAOH:0.16NaOH:495H₂O:100EtOH.

Synthesis of the B incorporated ZSM-5 catalyst

The addition of boron is done by adding H₃BO₃ while stirring, right before adding the silica source TEOS. Half of the amount of Al is replaced with B. The molar composition of the solution was 0.5Al:0.5B:25Si:9TPAOH:0.16NaOH:495H₂O:100EtOH.

Synthesis of the pure CeO₂

The synthesis of pure CeO₂ is based on the method of De Saegher et al. (2020) [95]. To obtain the pure CeO₂, the following synthesis steps are followed. Ce-salt (Ce(NO₃)₃.6H₂O), HMT, (NH₄)₂S₂O₈, NaCl and water are mixed at 400 rpm and 110°C in a recipient for 24 hours. After this, the precipitate is centrifuged and washed with water three times. The precipitate is solved in ethanol and dried at room temperature for 48 hours. The formed compound is Ce-LDH (layered double hydroxide). To obtain pure CeO₂, Ce-LDH is calcined for 6 hours at 800°C, which leads to a partial decomposition to form CeO₂.

Synthesis of the CeO₂/ZSM-5 hybrid catalyst

The form the hybrid CeO₂/ZSM-5, pure CeO₂ is added 30 minutes before the hydrothermal treatment starts. The ZSM-5 with a SiO₂/Al₂O₃ ratio of 25 is used. The hybrid catalyst has an equal weight ratio of CeO₂ and ZSM-5.

Synthesis of the hybrid core-shell topology catalyst (ZSM-5@CeO₂)

The synthesis of the core-shell topology catalyst (ZSM-5@CeO₂) is based on the method of Di et al. (2022) [96]. The used chemicals are shown in Table 9.

Table 9: used chemical for the hybrid catalysts with core-shell topology

Chemical	Properties	Producing company
ZSM-5@25 (see above)	See above	
Ethanol	100%	Chemlab
Poly vinyl pyrrolidone (PVP)	MM: 40 000	Merck
Ce(NO ₃) ₃ .6H ₂ O	99%	Merck
Hexa methylene tetra amine	99%	Merck

To synthesize the core shell catalyst, 0.5 g of the previously prepared ZSM-5@25 was added to a mixture of 20 ml of ethanol and AD in a 1/1 volume ratio. The mixture was then stirred for 30 minutes before being placed in an ultrasonic bath for 10 minutes. Next, 1 g of PVP was added and the mixture was stirred until the PVP is fully dissolved. 0.3 g of Ce(NO₃)₃.6H₂O and 0.3 g of HMT were added to the mixture, which was then stirred for 2 hours at 60°C. The mixture is allowed to settle for 3 hours, after which the product is collected via centrifugation. The product is then washed with AD three times, followed by drying at 120°C for 20 hours. The final step is to calcine the product at 550°C for 6 hours.

The synthesized zeolites were characterized using Inductively Coupled Plasma Optic Emission Spectroscopy (ICP-OES) by the research group⁴ to map their actual Si/Al ratios, rather than their theoretical, targeted values. The results are shown in Table 10.

Table 10: actual SiO₂/Al₂O₃ ratios, measured by OES

Sample	Targeted value		Measured value	
	Si/Al	B/Al	Si/Al	B/Al
ZSM-5@25	25	-	15	-
ZSM-5@150	150	-	153	-
ZSM-5@25_B	50	1	47	0.2
ZSM-5@150_B	300	1	356	0.9

⁴ This OES analysis was done at the LCA (Laboratory of Chemical Analysis) research group, UGhent by Diederik Leenknecht and thus not performed by the writer of this thesis.




It is clear that some significant deviations from the targeted values are observed. The discussion of the data should thus always be done in regard to the measured, actual values.




The deviation of the measured values from the targeted values is due to the complexity of the zeolite syntheses. A significant difference in Si/Al ratio between the targeted and measured values can be observed, depending on how good the Al incorporation has been achieved. The incorporation of B is even more complex and needs an environment of pH 10-11 to have an efficient incorporation of B in the zeolite framework. The used synthesis environment was around pH 13, which led to a decreased incorporation of B. This is mostly observed in ZSM-5@25_B, where the B/Al ratio is only 0.2 instead of the aimed 1. The synthesis could in future work be improved by controlling the pH with the addition of sulfuric acid or using a higher theoretical (targeted) value of B/Al = 2 to obtain an actual value of B/Al = 1.

2.1.3 Used (analysis) gasses and other chemicals

The used analysis, preparation and carrier gasses, their properties and the method for which they are used are listed in Table 11.

Table 11: used gasses and other chemicals in the AutoChem experiments and their properties [97]

Gas	T _{BP} (°C)	Thermal conductivity (air=1)	Hazards	Use in method
Helium (He)	-268.9	5.84		Carrier gas for pulse chemisorption and TPD
Hydrogen (H ₂)	-252	7.07		Reduction gas before pulse chemisorption
Carbon monoxide (CO)	-191	0.97		Analysis gas in pulse chemisorption

Ammonia (NH₃)	-33	0.92		Analysis gas in NH ₃ -TPD
Carbon dioxide (CO₂)	-78.5	0.62		Analysis gas in CO ₂ -TPD
Argon (AR)	-185.9	0.68	/	Carrier gas for reduction with H ₂
Isopropyl alcohol	82	/		Cleaning of U-tube

2.2 Methods

2.2.1 Instrument: AutoChem II 2920 and TCD detector

The analyses (CO pulse chemisorption, NH₃- and CO₂-TPD) are all performed on the Micromeritics AutoChem II 2920. It is a fully automated instrument capable of a variety of temperature-programmed and chemical adsorption studies. The Kwikcool feature permits faster cooling to ambient temperature with the help of cooled air that is pumped into the furnace, reducing the analysis time of lengthy experiments. The instrument is shown in Figure 27. Detailed information can be found in the AutoChem II 2920 operator manual [98].

The quantification of the gasses is performed with a Thermal Conductivity Detector (TCD), incorporated in the AutoChem device. A TCD works on the principle of the difference in thermal conductivity between a reference gas and the sample gas. A TCD is a very commonly used for the quantification of gasses because of its low maintenance needs, stability and cost-effectivity.



Figure 27: AutoChem II

The sensing element is typically a filament made of a material with high thermal conductivity, like platinum or tungsten. By flowing an electric current through the filament, it is heated. The resistance of the filament corresponds with its temperature. The filament is located in a chamber filled with the reference gas, He. When the sample gas passes the detector, the thermal conductivity of the gas mixture changes and changes the rate of heat transfer from the filament [99]. Most gasses have a far lower thermal conductivity than He [100]. This leads to a change in temperature of the filament and thus change in resistance, which is recorded using a Wheatstone bridge. This change is proportional to the sample gas concentration in the gas mixture [101].

2.2.2 Preparation of the samples

The samples are loaded in a quartz U-tube. Before each analysis, the tube is rinsed with water and iso propyl alcohol and subsequently dried with warm air to obtain a clean, inert tube. The sample is then carefully placed as a layer on a quartz wool bed, which securely holds the sample in place while allowing the analysis and preparation gasses to flow through the sample bed. To ensure the tube is inert, the methods are performed on an empty tube with quartz wool. When no signal is obtained, the tube's inertness is confirmed. Once the sample, with a mass of around 100 mg (for CO pulse chemisorption) or 200 mg (for TPD), is loaded, the U-tube is placed in the furnace, as depicted in Figure 28.

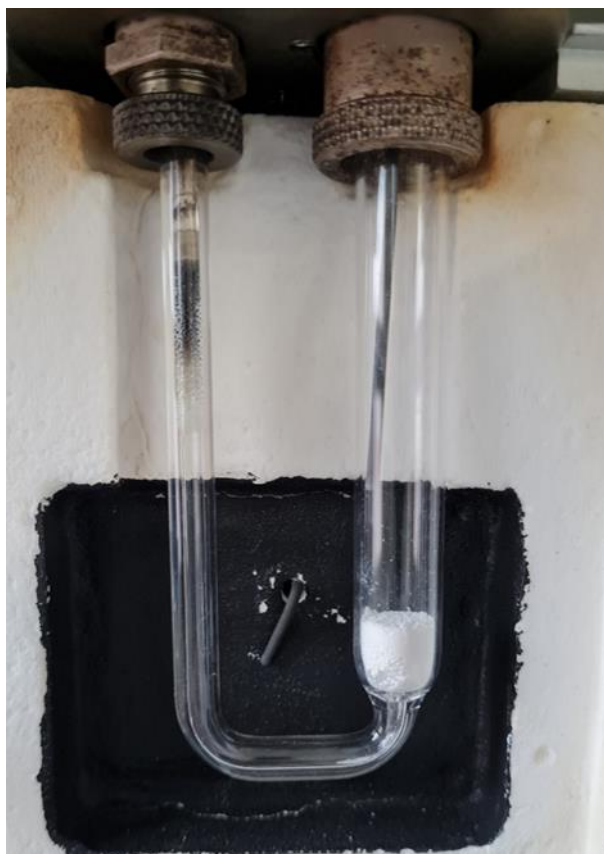


Figure 28: U-tube loaded with quartz wool and sample, placed in the furnace

2.2.3 Reductive catalytic depolymerization of lignin: metal dispersion study

Pulse chemisorption is used to determine the active surface area and percent metal dispersion (fraction of atoms exposed to the surface) and active particle size of the metal analyzed metals [87], [88]. CO pulse chemisorption is chosen as analysis technique because this method is often used with Pd loaded catalysts [102]. The goal is quantifying the dispersion of the Pd on the supported Pd and PdCu catalysts. The analysis will be done in the AutoChem II 2920 with a TCD. When performing the CO pulse chemisorption, a small catalyst sample (approx. 100 mg) is placed in quartz U-shaped tube, and is first pretreated by overflowing the gas with He under rising temperature to remove adsorbed particles. After this, the catalyst is reduced under a 10% H₂/Ar flow to convert the surface metal species into their metallic form. This is needed to bring the species in their active form and to chemisorb the CO on the Pd particles. CO is then added to the flow in small pulses, and the adsorption on the sample is monitored.

2.2.3.1 CO pulse chemisorption method

The full detailed CO pulse chemisorption method, performed on the AutoChem II, is for all the samples as follows. The only difference between the different samples is the use of 1% or 10% CO in He as pulse gas, depending on the CO uptake (corresponding with the metal dispersion) of the sample. For samples with a high dispersion, the uptake of CO is high, which is why the 10% CO/He generally generates a better spectrum. For samples with low dispersion, the uptake of CO can be too low so that the spectrum shows no significant difference in peak area, which is why 1% CO/He is generally used in this case. Which gas is used for each sample is determined by trial and error with both the analysis gasses.

Step 1: pretreatment (under inert He flow at 50 cm³/min)

- heating to 80°C at 10°C/min, wait 2 min
- heating to 120°C at 2°C/min, wait 10 min
- heating to 200°C at 10°C/min, wait 60 min
- cooling to 80°C, wait 5 min

Step 2: reduction (under 10 vol% H₂/Ar flow at 50 cm³/min)

- heating to 200°C at 10°C/min, wait 60 min
- cooling to 35°C, wait 5 min

Step 3: CO pulse chemisorption (pulses of 1 or 10 vol% CO/He)

- wait for 15 min to stabilize baseline
- start recording: t = 0.2 seconds (as advised by the AutoChem II manual)
- wait 3 min
- Repeat 20 times a CO pulse, each 1.5 min (or until 4 subsequent equal peaks are detected)

Step 4: termination (under inert He flow at 20 cm³/min)

- return to ambient temperature

2.2.3.2 Dispersion and active area calculations

In this section, it is explained how the analysis results can be turned into quantitative dispersion and active area values of the samples. After the pretreatment steps (see earlier) the experiment is started. In pulses, a small and constant amount of adsorption CO is added to the flow. This amount is dependent on the volume, pressure and temperature of the loop and the active gas concentration in the CO/He mixture. It can be calculated by using Eq (1). The adsorption process happens at a constant temperature of 35°C, slightly above ambient temperature so that this can easily be kept constant in the equipment furnace. At this temperature, no chemisorption of CO on Cu particles or on the supports will occur [103],[104]. By using an online TCD, the consumption of reaction-gas can be found. The difference in area under the signal in a reactor without and with catalyst sample is calculated to quantify the CO uptake [84], [85].

When the whole 'pulse' of probe molecules is adsorbed by the catalyst, no signal is detected. This is usually the case for the first pulse or pulses.

With each pulse, the catalyst is more saturated so that less gas is taken up by the catalyst surface. This leads to more probe molecules in the outgoing flow and thus an increase in signal intensity. When the surface is saturated, the uptake becomes zero for each pulse so that for the next pulses a constant signal is observed with maximum peaks. This signal corresponds to the signal when no catalyst is present in the reactor. The total chemisorption (uptake) is equal to the uptake in each pulse. This can be calculated by summing the difference of the signal after complete saturation and the pulses which show CO uptake [84],[86].

The dispersion (D) of the metal is defined as $\frac{N_s}{N_t}$, with N_s the number of exposed surface metal atoms and N_t the total number of metal atoms in the sample. The volume of the active gas (CO) which is injected (V_{inj}) can be calculated at STP conditions using Eq. (1).

$$V_{inj}(STP, cm^3) = V_{loop} \cdot \frac{T_{std}}{T_{loop}} \cdot \frac{P_{amb}}{P_{std}} \cdot \frac{A}{100} \quad (1)$$

Here is V_{loop} the injected loop volume in cm^3 (a loop of $0.48616 cm^3$ is installed on the equipment), T_{std} the standard temperature (273.15K), T_{amb} the temperature of the loop in K, P_{std} the standard pressure (1 atm), P_{amb} the ambient pressure of the loop in atm and A the % active gas in the gas-mixture. The used gas mixture is 1% or 10% CO in helium.

The volume of the active gas that is chemisorbed is found by using V_{inj} and the area under the peaks, calculated by Eq. (2).

$$V_{ads}(STP, cm^3/g) = \frac{V_{inj}}{m} \cdot \sum_{i=1}^n \left(1 - \frac{A_i}{A_f}\right) \quad (2)$$

Here m is the mass of the sample in grams, n the number of peaks, A_i the area of peak i and A_f the area of the peak when saturation is achieved (the mean area of the last, equal peaks).

The dispersion is defined by Eq. (3).

$$D = \frac{\text{moles of metal on surface } (N_s)}{\text{total moles of metal in sample } (N_t)} \quad (3)$$

The dispersion D can be calculated by using Eq. (4) and (5)

$$N_s \left(\frac{\text{moles}}{\text{g}} \right) = n \cdot \frac{V_{ads}}{V_g} \quad (4)$$

$$N_t \left(\frac{\text{moles}}{\text{g}} \right) = \frac{\% \text{ metal loading}}{MW \cdot 100} \quad (5)$$

Here n is the stoichiometry factor (how many adsorbate molecules are chemisorbed per metal atom), V_g the molar gas volume at STP ($22414 \text{ cm}^3/\text{mol}$) and MW the molecular weight of the metal (106.400 g/mole for Pd) [98].

The stoichiometry factor is the average chemisorption stoichiometry that has been studied for Pd on various supports and dispersion. The Pd/CO average chemisorption stoichiometry for alumina, silica and AC was found to be close to 2, so this will be used as stoichiometry factor for the experiments [105].

Lastly, the active metal surface area per gram of sample is calculated using Eq. (6).

$$A_m \left(\frac{\text{m}^2}{\text{g}} \right) = \left(\left(n \cdot \frac{V_{ads}}{V_g} \right) \cdot N_A \right) \cdot a \quad (6)$$

Here N_A is Avogadro's number ($6.023 \cdot 10^{23}$ molecules/mol) and a the cross-sectional area of the active metal atom in m^2 . The value for Pd is $0.0787 \text{ nm}^2 = 7.872 \cdot 10^{-20} \text{ m}^2$ [98].

The error on the dispersion and active metal area is (arbitrary) determined by two factors: the error (standard deviation) on A_f (mean area of the saturated peaks) and an estimated error on the loop temperature. The loop temperature is determined to be 110.9°C , but has a slight fluctuation of an estimated 1%. The error on those two factors is propagated to the dispersion and active area values.

2.2.3.3 Average particle size calculation

The metal dispersion and the particle size of the specie on the surface are correlated with each other. Bergeret et al. (2008) formulated a relation (see eq. (7)) to calculate the mean particle size when the dispersion of a metal is known. Hemispheric particles on the surface are assumed [106].

$$D = 6 \cdot \frac{v_m}{a_m \cdot d_{VA}} \quad (7)$$

Here D is the dispersion, v_m the volume occupied by the metal atom in the bulk of the metal and is equal to $\frac{MM}{\rho \cdot N_A}$, a_m the surface area occupied by the metal atom on a polycrystalline surface and d_{VA} the mean particle size [106].

2.2.4 Dehydration of 1,3-butanediol: acidity and basicity study

2.2.4.1 NH_3 and CO_2 gas concentration calibration

To enable for a quantitative determination of the acidic and basic sites on the catalysts samples, a gas concentration calibration is performed as described in the AutoChem II manual [98]. If a series of known gas concentrations is associated with the signals recorded by the TCD, then the signals recorded during the analysis can be converted to gas concentrations. From this data, it is possible to calculate the volume and amount of active gas associated with the peaks in the spectra. The signal response depends on the analyzed gas, so that a calibration curve for NH_3 and CO_2 should be composed.

A clean, empty U-tube is placed in the furnace chamber. The measurement is performed at a temperature of 30°C and the flowrates of all gases is $50 \text{ cm}^3/\text{min}$. During the automatic analysis the analyzer increases the proportion of analysis gas in 10% increments by mixing the analysis gas (5% NH_3/He or 5% CO_2/He) with carrier gas (He). The obtained calibration curve makes it possible to convert the recorded TCD signals into gas concentrations.

2.2.4.2 Acidity study: NH_3 -TPD

NH_3 -TPD is performed on all zeolite and hybrid samples but not on the pure CeO_2 sample. Seven samples are thus analyzed. The samples should be evacuated of adsorbed water prior to the analysis, so pretreatment at elevated temperature is needed. The complete method is summarized in the following steps.

Firstly, a pretreatment step was performed to remove any water present in the samples. This was achieved by subjecting the samples to a flow of inert gas, specifically He, at an elevated temperature of 550°C . The aim of this step was to ensure the removal of any residual water from the samples. Next, the adsorption of the probe molecule, NH_3 , was carried out. The samples were exposed to a continuous flow of 5% NH_3 in Helium at a fixed temperature of 120°C . This step allowed for the adsorption of NH_3 onto the surface of the samples, facilitating further analysis. Following the adsorption of NH_3 , a desorption step was conducted to remove the physisorbed NH_3 from the samples.

This was achieved by flushing the samples with a flow of inert gas, again using He. The purpose of this step is to eliminate any loosely bound NH_3 molecules.

Lastly, the temperature-programmed desorption (TPD) technique was employed to desorb the NH_3 molecules from the samples and detect them. The temperature was linearly increased until reaching 550°C . The desorbed NH_3 molecules are detected using a thermal conductivity detector (TCD). Temperature ramps were used for the TPD analysis, with three different ramp rates: $10^\circ\text{C}/\text{min}$, $15^\circ\text{C}/\text{min}$, and $20^\circ\text{C}/\text{min}$. This approach allowed for the evaluation of the desorption behavior of NH_3 from the samples under different heating rates.

It should be noted that subsequent TPD with different heating rates is only possible on compounds with a high thermal stability. When the thermal stability is not high enough, the latter analyses will be influenced by the former heating steps, leading to a decrease in acidity. In this case, there should be fresh samples for each heating step. Not all zeolites are stable enough. Beta-zeolite, for example will have very different amounts of desorbed NH_3 when no fresh sample is used. ZSM-5 however, shows a high thermal stability when heating to 550°C . This is due to its crystalline structure. The ZSM-5 samples can thus be analyzed with different heating rates on the same sample, enabling faster and easier analysis. This is visible for ZSM-5 in the TPD spectra for fresh sample between each TPD or with consecutive heating in Figure 29 [107].

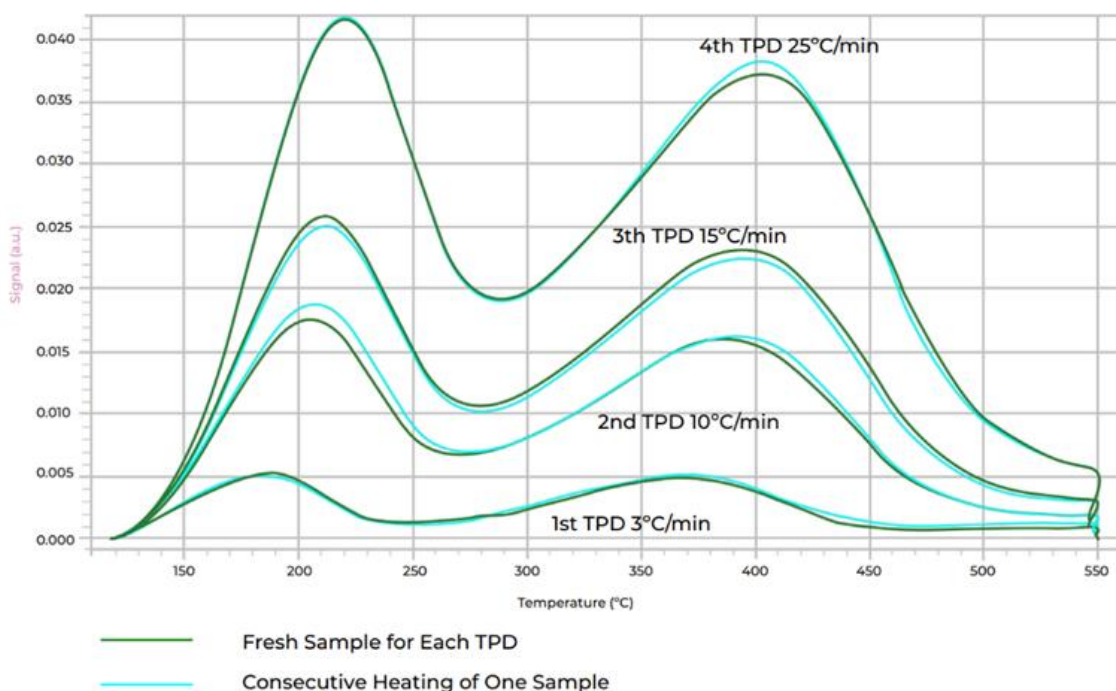


Figure 29: NH_3 -TPD of ZSM-5 with separate and consecutive temperature ramps [107]

Detailed method (equal for all samples)

Step 1: pretreatment (under inert He flow at 50 cm³/min)

- heating to 550°C at 10°C/min, wait 120 min
- cooling to 120°C at 20°C/min, wait 5 min

Step 2: NH₃ loading at 120°C (5% NH₃/He at 50 cm³/min)

- wait 30 min

Step 3: NH₃-TPD (under inert He flow at 50 cm³/min) at 10°C/min

- wait 30 min (purging non adsorbed NH₃)
- start recording with t= 0.1 s
- heating to 550°C at 10°C/min, wait 30 min
- stop recording
- return to 120°C (use Kwikcool on Autochem → fast cooling)

⇒ **Repeat loading and TPD steps for TPD heating rates of 15°C/min and 20°C/min**

Step 4: termination

- return to ambient temperature (use Kwikcool)

2.2.4.3 Basicity study: CO₂-TPD

CO₂-TPD will be performed on three samples, the two hybrid CeO₂ with ZMS-5@25 catalysts, CeO₂/ZSM-5 (ZSM-5 dispersed on CeO₂) and ZSM-5@CeO₂ (core-shell topology, being ZSM-5 core and CeO₂ shell) and on pure CeO₂. The TPD method is summarized as follows.

Firstly, a pretreatment step was performed to remove any water present in the samples. This was achieved by subjecting the samples to a flow of inert gas, specifically He, at an elevated temperature of 550°C. The aim of this step was to ensure the removal of any residual water from the samples. Next, the adsorption of the probe molecule, CO₂, was carried out. The samples were exposed to a continuous flow of 5% CO₂ in Helium at a fixed temperature of 40°C. This step allowed for the adsorption of CO₂ onto the surface of the samples, facilitating further analysis. Following the adsorption of CO₂, a desorption step was conducted to remove the physisorbed CO₂ from the samples. This was achieved by flushing the samples with a flow of inert gas, again using He. The purpose of this step is to eliminate any loosely bound CO₂ molecules.

Lastly, the temperature-programmed desorption (TPD) technique was employed to desorb the CO₂ molecules from the samples and detect them. The temperature was linearly increased until reaching 550°C. The desorbed CO₂ molecules are detected using a thermal conductivity detector (TCD). Temperature ramps were used for the TPD analysis, with three different ramp rates: 10°C/min, 15°C/min, and 20°C/min. This approach allowed for the evaluation of the desorption behavior of CO₂ from the samples under different heating rates.

Detailed method (equal for all samples)

- Step 1: pretreatment (under inert He flow at 50 cm³/min)

-heating to 550°C at 10°C/min, wait 120 min

-cooling to 40°C at 50°C/min, wait 5 min

Step 2: CO₂ loading at 40°C (under 5% CO₂/He at 50 cm³/min)

-wait 30 min

Step 3: CO₂-TPD (under inert He flow at 50 cm³/min) at 10°C/min

-wait 10 min (purging non adsorbed CO₂)

-start recording with t= 0.1 s

-heating to 550°C at 10°C/min, wait 15 min

-stop recording

-cooling to 40°C (use Kwikcool on Autochem → fast cooling)

⇒ **Repeat loading and TPD steps for TPD heating rates of 15°C/min, 20°C/min**

Step 4: termination

-return to ambient temperature (use Kwikcool)

2.2.4.4 Noise removal

On some samples, the analysis leads to spectra with a significant amount of noise. In this cases, the signal is smoothed by the use of a simple noise removal technique: *adjacent-averaging smoothing*. In this method, each smoothed data point is computed as the average from the data points within a moving window [108]. The range of this window is chosen to be 5 data points, which showed good smoothing without using a too broad window which could deform the spectra. This method is easily performed with the *Origin: Data Analysis and Graphing Software* [109]. When a lot of noise is present, smoothing can have a significant impact on the results, it should thus be attempted to minimize the noise of the analysis spectra.

2.2.4.5 Deconvolution of the TPD signal: modelling Gaussian peaks

The TPD spectra can be considered to be the sum of different peaks, corresponding to different sites of different strength. To enable for the differentiation of peaks of different maximum peak temperatures, which corresponds with the strength of the active sites, the signal is separated into modelled Gaussian peaks. The signal is then the sum of the Gaussian peaks, as formulated in Eq. (8).

$$f(t) = \sum_{i=1}^N \frac{a_i}{\sigma_i \cdot \sqrt{2\pi}} \cdot e^{-\frac{(t-\mu_i)^2}{2\sigma_i^2}} \quad (8)$$

Here N is the number of peaks, a_i a scaling factor for each peak, σ_i the standard deviation, t the time in minutes, μ_i the time in minutes at the peak maximum.

The parameters of the Gaussian peaks (a_i , σ_i , μ_i) are found by minimizing the *residual sum of squares (RSSQ)* of the experimental data points $f(t)_{i,exp}$ and the modelled data $f(t)_{i,mod}$, as depicted in Eq. (9).

$$RSSQ = \sum_{i=1}^j (f(t)_{i,exp} - f(t)_{i,mod})^2 \quad (9)$$

Here j is the number of experimental data points.

When the deconvolution is performed, the number of Gaussian peaks to be modelled can be chosen. This is done with regard to the properties of the analyzed samples.

As discussed in 1.4.3.1: NH₃-TPD, earlier studies showed that zeolites and modified zeolite samples typically have two peaks when analyzed with NH₃-TPD, one at low (ca. 150°C) and one at high temperature (ca. 350°C), which respectively correspond to the weak acidic and strong acidic sites [81], [107], [110]–[112]. The spectra will thus be deconvoluted into two modelled Gaussian peaks. These modelled peaks will make it possible to quantify the concentration of weak and strong acidic sites on the zeolite samples.

CO₂-TPD is performed on CeO₂ and hybrid CeO₂-ZSM-5 catalysts. CO₂-TPD studies of CeO₂ showed one basic peak at a temperature of ca. 100°C [113], [114]. One Gaussian peak will thus be modelled.

2.2.4.6 Quantification of desorption energy (E_d) of the active sites

The strength of the active acidic and basic sites can be quantified by the desorption energy (E_d). This is done by performing the TPD experiment at three different, linearly spread temperature ramp rates. The desorption is done at temperature ramps of 10°C/min, 15°C/min and 20°C/min. The desorption energy is calculated using a first order kinetic model [107]. By reformulating the Arrhenius equation, E_d can be found by plotting the Arrhenius curves [112], [115]–[117]. The Arrhenius equation is reformulated to Eq. (10) [112], [117].

$$2. \ln(T_{\max}) - \ln(\beta) = -\frac{E_d}{R} \left(\frac{1}{T_{\max}} \right) + \ln(A) \quad (10)$$

Here β is the heating rate (K/s), E_d the desorption energy, R the gas constant, T_{\max} the temperature (K) at maximum desorption (at the peak) and A the pre-exponential factor in the Arrhenius equation. This last factor A is not needed for the calculation of E_d in this technique.

Plotting $2. \ln(T_{\max}) - \ln(\beta)$ versus $1/T_{\max}$ (K^{-1}) leads to linear curves. The slope of this curve equals $-E_d/R$ so that the desorption energy can be derived for each peak in the TPD spectra.

2.2.5 Overview of the samples and performed experiments

An overview of all the samples and which analysis techniques that will be used on them is shown in Table 12.

Table 12: experimental overview

Experiment	Sample	Results
CO pulse chemisorption (6 samples)	Pd/Al ₂ O ₃	Influence supports
	Pd/AC	
	Pd/SiO ₂	
	PdCu/Al ₂ O ₃	Influence Cu on Pd dispersion on different supports
	PdCu/AC	
	PdCu/SiO ₂	
NH₃-TPD (7 samples)	ZSM-@25 (commercial)	Acidity of commercial ZSM-5
	ZSM-5@25	Influence SiO ₂ /Al ₂ O ₃ ratio
	ZSM-5@150	
	ZSM-5@25_B	Influence boron incorporation
	ZSM-5@150_B	
	CeO ₂ /ZSM-5	Influence of using hybrid zeolite/CeO ₂ (two methods)
	ZSM-5@CeO ₂	
CO₂-TPD (3 samples)	CeO ₂ /ZSM-5	Basicity of hybrid zeolite/CeO ₂ (two methods)
	ZSM-5@CeO ₂	
	CeO ₂	Basicity of pure CeO ₂

3 Results and discussion

The goal of this thesis is to try to find active and efficient catalyst for the reductive catalytic depolymerization of lignin and the dehydration of 1,3-butanediol. These reactions were investigated in regard to the state-of-the-art in the literature study. To be able to make a prediction about the catalytic action of a number catalysts, they are characterized to qualify and quantify their active sites.

In this thesis, only a characterization of some properties is performed. An attempt to find some promising catalysts for the reactions will be made. These catalysts will however not be tested for the reaction itself, so that further (reactor) studies will be necessary to confirm the activity and efficiency of the proposed catalysts.

3.1 Metal dispersion study on catalysts for the mild reductive catalytic depolymerization of lignin

Six catalysts for the reductive depolymerization of lignin are characterized. Samples of monometallic Pd and bimetallic PdCu supported on Al_2O_3 , SiO_2 and AC are analyzed in regard to their Pd dispersion value. The importance of this dispersion has been discussed in the literature study. The used technique was CO pulse chemisorption, which has been proven to be a useful method for the quantification of surface Pd species that can then be converted into dispersion results. The influence of the used support and the addition of Cu to form a bimetallic catalysts will be discussed. The results of this thesis are attempted to be linked to the activity for the mild reductive catalytic depolymerization of lignin. The ultimate goal is to select a promising catalyst, which could be a valuable asset in the development of this green reaction.

3.1.1 Metal dispersion

The CO pulse chemisorption was performed for all samples. The samples were all calcined at 450°C for four hours right after their preparation. Before the pulse chemisorption, a pretreatment at elevated temperature (200°C) to remove any contaminants like water and a reduction under H_2 was done. The reduction aims to convert the surface species into their metallic Pd form that will adsorb CO.

The samples Pd/ Al_2O_3 , Pd/ SiO_2 and PdCu/ SiO_2 were pulsed with 1% CO. PdCu/ Al_2O_3 , Pd/AC and PdCu-AC were pulsed with 10% CO. The choice of the active concentration of CO was dependent on the amount of CO uptake by the sample and the amount of noise in the spectrum. Of all catalysts, a clear pulse spectrum was obtained. The spectra are shown in

Appendix A: CO pulse chemisorption spectra. The pulse chemisorption spectrum of an empty tube with quartz wool is also included, to show that there is no CO uptake when no catalyst is present in the tube. The active metal (Pd) dispersion and the active metal surface were calculated by using the equations described in 2.2.3.2: Dispersion and active area calculations. The results are shown in Table 13. The focus in this thesis lies on the dispersion results, but the active metal surface area is displayed for completeness. The error (standard deviation) on the dispersion and active metal area is determined by two factors: the standard deviation on A_f (mean area of the saturated peaks) and an estimated error on the loop temperature. The loop temperature is determined to be 110.9°C, but has a slight fluctuation of an estimated 1%. The error on those two factors is propagated to the dispersion and active area values. The obtained standard deviation is very low, indicating a precise measurement of the samples.

Table 13: dispersion and active metal surface results of the CO pulse chemisorption study

Catalyst	Pd dispersion (%)	Active metal surface area (cm ³ /g)
Pd/Al₂O₃ (1% CO, most reliable)	8.89 ± 0.27	1.208 ± 0.037
Pd/Al₂O₃ (10% CO)	6.34 ± 0.09	0.86 ± 0.012
PdCu/Al₂O₃	22.17 ± 0.23	1.996 ± 0.021
Pd/SiO₂	2.13 ± 0.04	0.323 ± 0.006
PdCu/SiO₂	1.58 ± 0.05	0.152 ± 0.004
Pd/AC	12.68 ± 0.16	2.413 ± 0.031
PdCu/AC	10.46 ± 0.26	1.808 ± 0.045

Upon analyzing the data, several observations can be made. Firstly, it is evident that the dispersion and active metal surface area of the catalysts are significantly impacted by the type of catalyst support and the presence of a co-metal. The monometallic catalyst shows the highest Pd dispersion for the AC support, followed by Al₂O₃ and SiO₂, with values of respectively 12.68 ± 0.16%, 8.89 ± 0.27% and 2.13 ± 0.04%. The bimetallic PdCu catalysts exhibit a different trend in dispersion. PdCu shows the highest dispersion on Al₂O₃, followed by AC and SiO₂ with values of respectively 22.17 ± 0.23%, 10.46 ± 0.26% and 1.58 ± 0.05.

From these results, some remarks can be made. In particular, catalysts supported on SiO₂ exhibit a very low dispersion and active metal surface area. The bimetallic PdCu/Al₂O₃ shows the highest reported dispersion value of 22.17 ± 0.23%. However, monometallic Pd/Al₂O₃ shows a far lower dispersion of 8.89 ± 0.27%. This significant difference with the bimetallic catalyst is remarkable, which is why the analysis was repeated with 10% CO/He as pulse gas. However, an even lower dispersion value of 6.34 ± 0.09% was found. The analysis with 1% had more than one not saturated peak, which is why this result (dispersion value of 8.89%) will be taken as the most trustworthy and considered for the discussion.

The AC supported catalysts show intermediate dispersion values. It is also worth noting that the monometallic catalyst has slightly higher dispersion compared to the bimetallic catalyst on the AC support.

The presence of Cu as a co-metal has a significant influence on the dispersion and active metal surface area of Pd-based catalysts. It can either increase or decrease the accessibility of active metal sites, depending on the support.

3.1.2 Influence of the supports

Al₂O₃ supported catalyst

The alumina supported catalysts show a high difference between the monometallic (Pd) and bimetallic (PdCu) catalyst. A value of 8.89% and 22.17% is found for the monometallic and bimetallic catalyst respectively.

Byun et al. (2018) researched the metal dispersion by using CO pulse chemisorption on Pd/Al₂O₃ catalysts, calcined at different temperatures [118]. The Pd loading was 5 wt% which corresponds to this thesis. The catalysts were prepared using a deposition-precipitation method, which is different than the method for the preparation of the samples in this thesis (incipient wetness impregnation). In this method, a metal precursor is precipitated onto a suspended support material by increasing the pH of the aqueous solution [119]. For a calcination temperature of 500°C for 4 hours, a Pd dispersion of 20.8% was obtained. In this thesis, the catalysts were calcined at a similar, slightly lower temperature of 450°C and same calcination time. The Pd dispersion value for Pd/Al₂O₃ found in this thesis is significantly lower at 8.89%. The difference in preparation method probably has the most significant influence on the Pd dispersion difference between the studies. A review study by Mehrabadi et al. (2017) compared different preparation methods for Pd and Pt on (among others) Al₂O₃, SiO₂ and AC supports. It was stated that generally the deposition-precipitation method leads to well-dispersed particles, while incipient wetness impregnation leads to less dispersed particles with a bigger particle size [120]. This could explain the lower dispersion value found in this thesis (8.89%) compared to the reported value in the study of Byun et al. (2018) (20.8%) which used the same Pd loading and calcination conditions but different preparation method [118].

SiO₂ supported catalyst

The SiO₂ supported catalysts exhibit remarkably low dispersion values (2.13% and 1.58% for mono- and bimetallic resp.), which is worth noting. Roma et al. (2000) found a Pd dispersion value of 6.7% for Pd/SiO₂ [121]. In a study conducted by Kwon (2018) [122], low dispersion values were also reported for similar monometallic Pd catalysts supported on silica. The study aimed to characterize Pd/SiO₂ catalysts.

The results showed a Pd dispersion of around 5-6% (depending on source of the silica support), which is stated to be attributed to several factors. One possible explanation is the weak metal-support interaction and the high surface stability of SiO₂, which leads to the formation of aggregated Pd particles that cannot be evenly distributed on the support [122].

Moreover, the functional group of SiO₂, silanol (-OH), has been found to impede the reduction of Pd (and other metals) by strongly bonding with Pd ions during catalyst preparation, resulting in significantly lower Pd dispersion [122]–[126]. To address this issue, the silanol group was removed by modifying the SiO₂ prior to the catalyst preparation through thermal treatment (at 700°C, above 800°C leads to sintering) and ammonia treatment at 200°C. The effectiveness of this treatment was confirmed using FTIR, which showed almost complete removal of the silanol groups. The resulting pretreated SiO₂ was then used to prepare the catalysts, which exhibited much higher Pd dispersion values of 13% (thermal treatment) and 9% (ammonia treatment), where the not pretreated sample showed around 5-6% dispersion. This confirmed that removing the silanol group significantly increases Pd dispersion [122].

Although this modification was not possible for the samples in this study because they were already prepared, future research on SiO₂ supported metal samples could attempt to increase the dispersion value by pretreating the support prior to catalyst preparation.

However, the Pd dispersion values found in this thesis are even lower than the reported values of around 5-6%. Pd/SiO₂ showed 2.13% Pd dispersion and PdCu/SiO₂ 1.58%. It is not sure how this difference can be explained. Possible explanations are external reasons like analysis method, user and machine errors... which can further lower the dispersion value.

AC supported catalyst

AC has a ca. six times higher specific surface area than the alumina and silica supports, with values of respectively 1182, 195 and 198 m²/g. A higher specific surface area generally enables for a higher metal dispersion, although the monometallic AC supported catalyst in this thesis only shows a Pd dispersion value of 12.68%. This dispersion value is the highest of all monometallic catalysts, but is not that much higher than the monometallic Al₂O₃ supported catalyst (dispersion value of 8.89%). The specific surface area is thus not proportionately linked to the Pd dispersion. The AC supported catalysts show an intermediate Pd dispersion compared to the other supports with a slightly lower value for the bimetallic than the monometallic catalysts.

A study by Dhachapally et al. (2007) characterized Pd supported on AC with varying Pd wt% [127]. The catalysts were prepared using the wet impregnation method. The catalyst preparation review study by Mehrabadi et al. (2017) stated that the particles of surface species on catalysts prepared by wetness and incipient wetness impregnation have similar sizes and thus lead to similar dispersion values [120]. One of the tested samples had a Pd loading of 4 wt%, which is close to the Pd loading in this thesis (4.3 wt% for the monometallic catalyst).

The dried samples were reduced at 300°C, which is 100°C higher than in this thesis. Characterization by CO pulse chemisorption at room temperature showed a dispersion value of 14.4% [127].

Another study by Yong Tae et al. (2008) found a similar value of 15% [128]. The samples were prepared using a wet impregnation method and the dispersion was determined using CO pulse chemisorption at room temperature. The Pd loading was 5%, and can thus be compared to samples in this thesis.

A study by Baek et al. (2016) reported a Pd dispersion of 11.3%, determined by CO pulse chemisorption [129]. The samples were however prepared using ion exchange in an aqueous solution, which can lead to a difference to the value obtained in this thesis.

In this thesis, a value of 12.68% was obtained for the monometallic catalyst, which is in the range of other reported values, which leads to believe the calculated dispersion is realistic.

3.1.3 Influence of the addition of Cu to form bimetallic PdCu catalyst

Al₂O₃ supported bimetallic catalyst

The bimetallic PdCu/Al₂O₃ was found to have a far higher dispersion than the monometallic catalyst (22.17% and 8.89% respectively). The addition of Cu thus has a positive effect on the Pd dispersion on the alumina support.

This is also reported by Insorn et al. (2016) for alumina supported Pd and PdCu catalysts. The catalysts were prepared by incipient wetness impregnation and had a total metal loading of around 4%. An increase in dispersion value was found for a Pd/Cu ratio of 3/2, which is similar to the ratio in this thesis. The reported dispersion values are 19% for the monometallic and 27% for the bimetallic catalysts (with a Pd/Cu ratio of 3/2), which are both higher than the values found in this thesis. For a ratio lower than 1 (less Pd than Cu), a very low dispersion was found. For a ratio of 1 a similar dispersion value as the monometallic Pd/Al₂O₃ was reported. In order to obtain higher dispersion values than the monometallic catalyst, it is thus important to have a Pd/Cu ratio higher than 1 [130].

The proposed reason for the increase in Pd dispersion when adding a relatively specific amount of Cu, lower than the Pd amount, is the following. It has been stated that adding Cu to Pd/Al₂O₃ leads to both electronic and geometric modifications of the catalyst. The electronic effect is minor, as the electronic properties of Pd atoms are not strongly affected by Cu addition [131]. The geometric effect however, may induce Pd to become more exposed at the metal surface, thus showing a higher dispersion value [130]. Insorn et al. (2016) could not explain the specifics of the geometric effect, but some possibilities are proposed [130]. Pd and Cu have a similar surface free energy and form a continuous series of face-centered-cubic substitutional solid solutions up to a Cu/Pd fraction of around 0.4.

This possibly leads to a high Pd dispersion value. [132]. Another possible explanation is the following. Pd particles have a considerable amount of low-coordination sites such as edges, defects... [133]. The Cu is mostly deposited on the low-coordination sites of Pd, particular when the Cu amount was small (for example for the 3/2 Pd/Cu ratio). It is stated that this can have a beneficial effect on the metal dispersion due to the fact that more lineary bonded CO is observed [134]. This hypothesizes are not certain and needs to be further researched, in order to completely understand the geometric effects when adding Cu to the Pd/Al₂O₃ catalyst.

SiO₂ supported bimetallic catalyst

The bimetallic SiO₂ catalyst was found to have a slightly lower dispersion value than the monometallic catalyst (resp. 1.58% and 2.13%).

This corresponds with a study performed by Roma et al. (2000) [121]. 3%Pd/SiO₂ and 3%Pd-3%Cu/SiO₂ catalysts, prepared by incipient wetness impregnation, were characterized using pulse chemisorption and TEM (transmission electron microscopy) to determine their Pd dispersion. The reported Pd dispersion was 4,5% and 6,7% for the bimetallic and monometallic catalyst respectively. These values are higher than reported in this thesis (see Influence of the supports). A slightly lower value for the bimetallic catalyst is thus reported, analogue as in this thesis. The samples were also characterized using H₂-TPR. The TPR spectra of Pd/SiO₂, Cu/SiO₂ and PdCu/SiO₂ are shown in Figure 30.

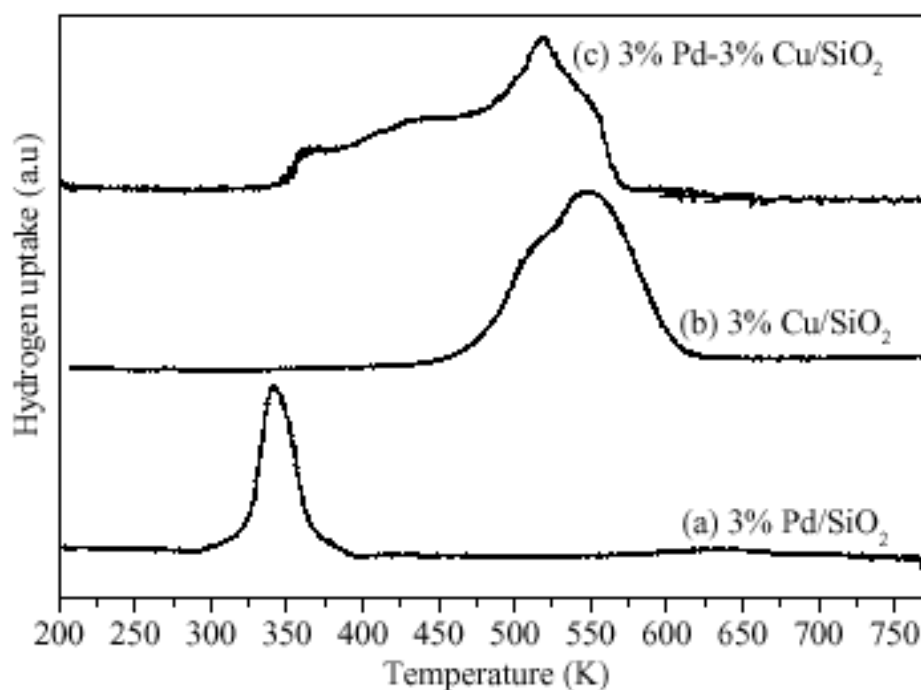


Figure 30: reduction profiles for silica supported catalysts [121]

The reduction profiles show a high shift in reduction temperature with the adding of Cu. It was stated that the addition of Cu led to a Pd-Cu interaction that increased the reduction temperature of the catalyst. A Pd-Cu alloy formation was confirmed using EXAFS (extended X-ray absorption fine-structure) [121]. The samples in this thesis were reduced only to 473K, which does not correspond with full reduction as found in the cited research. It is thus a possibility that the analyzed sample was not fully reduced. This possibly leads to a decrease in Pd dispersion for the bimetallic catalyst. This is however only a possibility, and should be further researched to ensure this statement. This could in future research be done by performing H₂-TPR.

AC supported bimetallic catalyst

The bimetallic AC catalyst was found to have a slightly lower dispersion value than the monometallic catalyst (resp. 10.46% and 12.68%), but this change is not very big. Barrabés et al. (2006) also reported no significant difference in Pd dispersion between 1% Pd/AC and 1%Pd-1%Cu/AC. It is stated that this makes it probable that there is no substantial overlaying of Cu on the surface Pd particles so that the addition of Cu does not influence the Pd dispersion too much [135].

Possible influence of the Tammann and Hüttig temperature on the metal dispersion

As discussed in the former chapters, the metal dispersion varies for each support and with the adding of Cu to form a bimetallic catalyst. It is dependent on interactions with support and co-metal. The metal dispersion on different supports has been frequently determined in numerous research works. However, due to the fact that the preparation, pretreatment before the analysis and reduction conditions are different in each study, it is difficult to compare these results. Phenomena that are for example often overlooked or not considered when discussing dispersion results are the Tammann and Hüttig temperatures of the metals.

The Tammann temperature is the temperature at which atoms in a bulk crystal lattice of the material become sufficiently mobile to diffuse readily, while the Hüttig temperature leads to the same effect on the surface. The atoms are then more chemically reactive and susceptible to recrystallization, agglomeration or sintering. The Tammann and Hüttig temperatures are estimated at respectively one-half and three-tenth of the absolute temperature of the compound's melting point [136], [137]. The dispersion is a surface property, which make the Hüttig temperature ($0,3.T_m$) an important parameter. Raising the temperature of the sample above this temperature can have an influence on the measured metal dispersion of the tested catalysts, as the desorption of adsorbed gasses on the surface often increases when the temperature of the sample reached the Hüttig temperature.

The Hüttig temperature of Pd and Cu is respectively 275°C and 134°C [138]. The samples in this thesis were pretreated at a maximum temperature of 200°C, because the Hüttig temperature was not taken into account when performing the experiments. This means that the Hüttig temperature is reached for the Cu.

The Cu species are thus possibly susceptible to recrystallization, agglomeration and sintering. This change in surface structure could also affect the Pd particles, for example by overlaying, putting pressure on or deforming them. This can lead to a change in dispersion results. The susceptibility to recrystallization, agglomeration and sintering of metals is different depending on the support and metal-support interaction strength. It is thus difficult to predict how significant these phenomenon's influence the metal dispersion.

3.1.4 Comparison with TEM-EDX results: particle size

The surface metal properties of the catalysts were also analyzed with TEM-EDX (transmission electron microscopy energy-dispersive X-ray spectroscopy). This was done by the INCAT research group (Industrial Catalysis and Adsorption Technology) at UGhent, more specific by doctoral student Boyana Atanasova. TEM-EDX measures the energy and number of characteristic X-rays generated by an electron beam that irradiates the analyzed area. This enables for an analysis of surface atoms like Pd and Cu. It is important to note that the average particle size is dependent on Pd as well as Cu species, while the calculated dispersion is only determined for the Pd species on the surface. This because CO shown no significant chemisorption on Cu particles as it does on Pd [139], [140]. The average particle size, found with TEM-EDX, can thus not directly be linked to the measured Pd dispersion.

The detailed results (particle size and distribution of the samples) can be found in Appendix B: TEM-EDX results on supported metal catalysts. The particle size distribution and the average and median particle size for all the samples can be found from Figure 70 until Figure 75.

Pd/Al₂O₃ has the smallest Pd particles with an average size of 7 nm and a narrow particle size distribution. Pd/SiO₂ has larger particles with an average value of 14 nm and a higher distribution, which means that a lot of particles are significantly smaller or bigger than the average particle size. Pd/AC showed an intermediate particle of 13 nm size but a very high distribution and even a small degree of cluster formation to form very large particles.

The bimetallic PdCu/Al₂O₃ shows similar particles as Pd/Al₂O₃, but also has limited cluster formation to bigger particles which lead to a higher average particle size of 10 and 7 nm respectively. PdCu/SiO₂ shows slightly larger particles (15 vs 14 nm) than Pd/SiO₂, and a larger distribution than PdCu/Al₂O₃. PdCu/AC shows slightly smaller particle size than Pd/AC with average values of respectively 12 and 13 nm, and a large distribution with cluster formation. The particle sizes are summarized in Table 14 (in order of rising average particle size) and visualized in Figure 31 for comparison with the dispersion results obtained of this thesis.

Table 14: particle size from TEM-EDX (ranked with rising average particle size)

Catalyst	Average particle size (nm)	Median particle size (nm)	dispersion (%)
Pd/Al₂O₃	7	7	8.89 ± 0.27
PdCu/Al₂O₃	10	10	22.17 ± 0.23
PdCu/AC	12	9	10.46 ± 0.26
Pd/AC	13	10	12.68 ± 0.16
Pd/SiO₂	14	13	2.13 ± 0.04
PdCu/SiO₂	15	14	1.58 ± 0.05

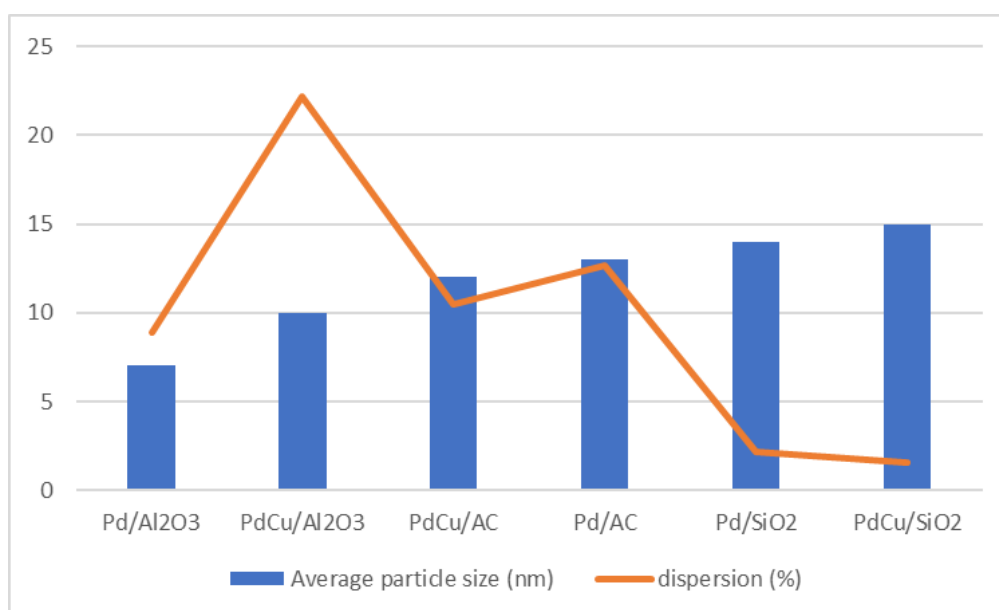


Figure 31: average particle size and dispersion for the catalysts⁵

The particle size of the surface species is related to the metal dispersion on the surface of the catalyst. In theory, this means the smaller the particle size, the higher the metal dispersion is and thus the more dispersed the metal is on the surface. The metal particles on the surface of the support material can form bigger particles or clusters, which significantly lowers the dispersion value. This trend is however not found for all the samples in this thesis.

The smallest particle size is observed for Pd/Al₂O₃, followed by PdCu/Al₂O₃ (average size of respectively 7 and 10 nm). The alumina support leads thus to the smallest particles and should correlate with the highest dispersion. This is only the case for the bimetallic catalyst, and not for the monometallic catalyst in this research.

The SiO₂ supported catalysts have the biggest average particle size of 14 nm for the monometallic and 15 for the bimetallic catalyst. This corresponds with the fact that the dispersion values are also the lowest of all supports.

⁵ The standard deviation on the dispersion values was too low to be visible by error bars on the graph.

Pd/AC and PdCu/AC have an average particle size of respectively 13 and 12 nm. This intermediate size corresponds with the intermediate dispersion value compared to the other catalysts. The dispersion value does however not follow this trend, with a slightly higher dispersion value for the monometallic catalyst (12.68% vs 10.46%) while this catalyst shows a slightly lower particle size.

As stated earlier, the determined dispersion values of the samples in this thesis can be converted into an average particle size of the surface species (see 2.2.3.3: Average particle size calculation). The values for Pd of v_m (volume of the metal atom) and a_m (surface area of the metal atom) are respectively 14.7 \AA^3 (Angstrom) and 7.93 \AA^2 [106]. From equation (7) and by using the values for Pd stated above, as explained in 2.2.3.3, the average particle size (d_{VA}) of the Pd particles can then be calculated by equation (11).

$$d_{VA} = \frac{1,112 \text{ nm}}{D} \quad (11)$$

The calculated d_{VA} values from the measured dispersion results and those from TEM-EDX are shown in Table 15.

Table 15: comparison between particle size found by TEM-EDX and from dispersion results

Catalyst	Average particle size (nm)	Dispersion (%)	d_{VA} (nm)
	(determined by TEM-EDX)		(calculated from D)
Pd/Al₂O₃	7	8.89 ± 0.27	12.5
PdCu/Al₂O₃	10	22.17 ± 0.23	5.0
Pd/SiO₂	14	2.13 ± 0.04	52.2
PdCu/SiO₂	15	1.58 ± 0.05	70.4
Pd/AC	13	12.68 ± 0.16	8.8
PdCu/AC	12	10.46 ± 0.26	10.6

It is clear that the calculated particle sizes from the dispersion results deviate significantly from the values determined by TEM-EDX for most of the samples. The results for the SiO₂ supported samples are completely different. For the bimetallic catalysts, this is partly because the size determined by TEM-EDX makes no difference between Pd and Cu particles, while the dispersion is only in regard to Pd, which influences the results. This is because the formula does not account for the presence of Cu in the PdCu catalysts, which influences the dispersion and particle size on the surface.

It is also possible that the assumptions in the conversion formula (11) to calculate the average particle size from the CO pulse chemisorption results are not correct for these catalysts.

For example, hemispheric particles on the surface are assumed, which is possibly not the reality. In addition to this, the measurements itself are complex techniques where small variations in experimental procedures, data analysis or equipment can lead to significant deviations on the results.

When plotting the dispersion in function of the average particle size, the plot as shown in Figure 32 should be obtained, as stated by eq. (11) [106]. This differs slightly for each metal depending on the parameters of each metal in eq. (7). This equation will be repeated for clarity.

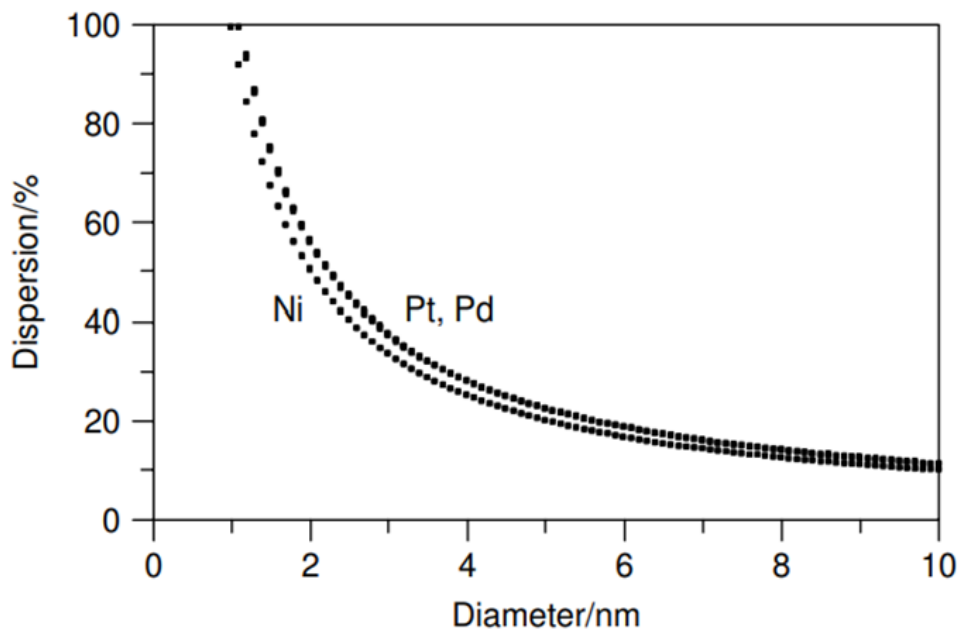


Figure 32: Plot of dispersion as a function of mean diameter d_{VA} for Ni, Pt and Pd, as stated by eq. (7) [106]

$$D = 6 \cdot \frac{v_m}{a_m \cdot d_{VA}} \quad (7, \text{repeated})$$

This same data is plotted with the dispersion results of this thesis and the average particle size from the TEM-EDX analysis, shown in Figure 33.

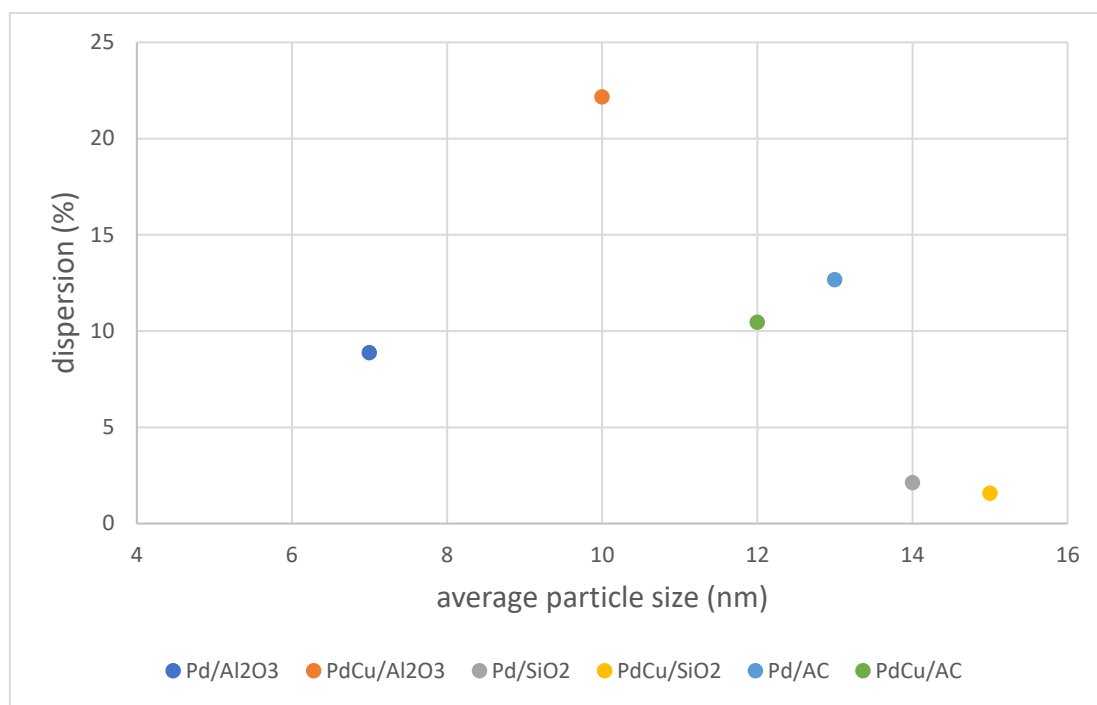


Figure 33: Plot of determined dispersion in this research as a function of mean diameter d_{VA} of the surface species⁶

The global trend (lower dispersion with rising average particle size) is followed by most of the catalysts, except for Pd/Al₂O₃, which shows a far too low dispersion in comparison with the measured particle size. The other samples show a more logical dispersion versus particle size value (with some deviations on the ideal curve as shown in Figure 32), with decreasing dispersion for higher particle size. These deviations are possibly explained due to the fact that the dispersion value cannot be completely correlated correctly to the particle size obtained by TEM-EDX (see earlier). When the results are plotted without the value for Pd/Al₂O₃, the trend visible in Figure 34 is obtained.

⁶ The standard deviation on the dispersion values was too low to be visible by error bars on the graph.

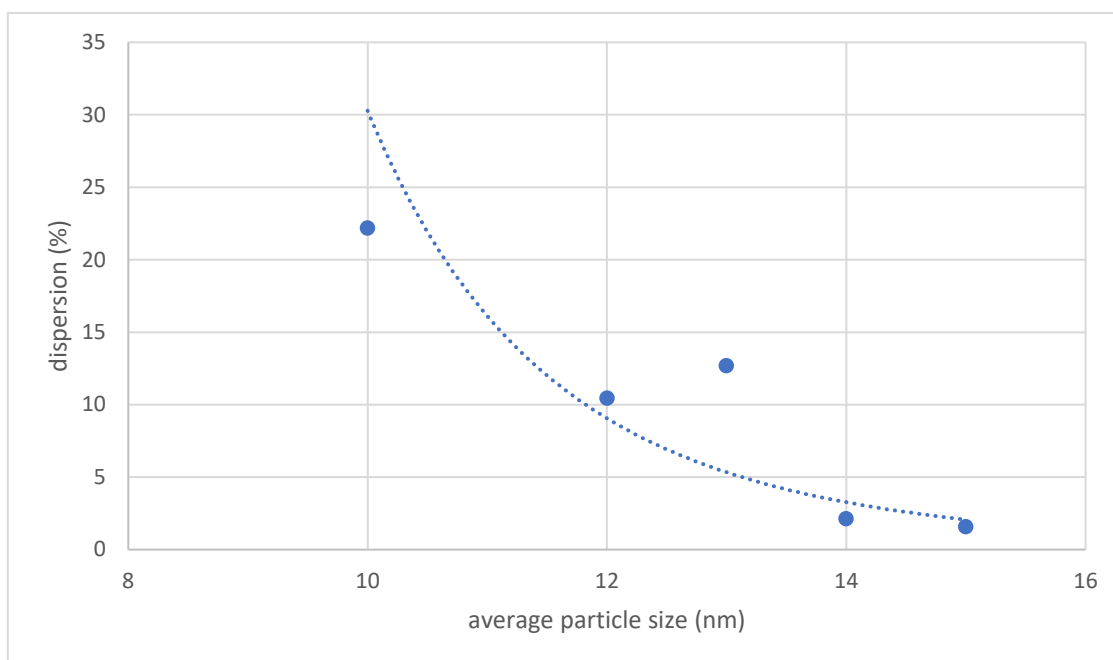


Figure 34: Plot of determined dispersion in this research as a function of mean diameter d_{VA} of the surface species (Pd/Al₂O₃ excluded)⁷

The outline of this curve has a similar shape as the theoretical one (see Figure 32). However, the values of the data points deviates significantly from the theoretical ones. A big shift to higher average particle size is observed compared to the theoretical curve.

3.1.5 Dispersion relation with catalysts activity

I did not evaluate the performance of the catalysts. However, in order to correlate the characteristics of the catalysts with their performance in the reductive catalytic depolymerization of lignin, the dispersion results are analyzed in conjunction with a reactor study. The reactor results were obtained from Boyana Atanasova, a doctoral student at the INCAT research group (Industrial Catalysis and Adsorption Technology) at UGhent.

In the batch reactor at 200°C and 10 bar, which contained 0.05 grams of catalyst, lignin depolymerization was carried out. The fed lignin was solved in a mixture of 70/30% ethanol/water in a concentration of 20 mg/ml. The mean molecular mass (M_w) of the depolymerized lignin was determined using gel permeation chromatography (GPC) after 3, 6, 20, and 30 hours. The reduction in molecular mass (%) for each catalyst was plotted as a function of batch time for each reaction. The batch time was defined as the product of the amount of Pd particles in the reactor (moles) and the reaction time (s). This was introduced to allow for a useful comparison, as the metal loading varied among the catalysts.

⁷ The standard deviation on the dispersion values was too low to be visible by error bars on the graph.

The findings are presented in Figure 35, which shows that all catalysts exhibit a similar, rapid initial depolymerization resulting in a molecular weight (M_w) reduction of around 65%. The bimetallic catalysts PdCu/Al₂O₃ and PdCu/SiO₂ both show the fastest, similar depolymerization rate in the first phase.

Following this phase, that ends at a reduction of around 65% in M_w for all the samples, a second, slower depolymerization phase starts. In this second phase, the AC supported catalysts demonstrate clearly the most rapid depolymerization, with the monometallic Pd/AC achieving an M_w reduction of approximately 87% after a batch time of just 0.5 mol Pd x s. The M_w value then remains constant. Consequently, this catalyst reaches the final depolymerization grade the quickest among all the catalysts. The bimetallic PdCu/AC exhibits a slightly slower decrease in M_w and a similar final depolymerization grade as the Pd/AC, but only after a batch time of approximately 2 mol Pd x s. The other catalysts, with Al₂O₃ and SiO₂ supports, have a similar, albeit slower depolymerization rate in this second phase. However, depolymerization continues for longer and may reach the same or almost the same final depolymerization grade as the AC supported catalysts.

In conclusion, the bimetallic catalysts PdCu/Al₂O₃ and PdCu/SiO₂ both show the fastest, similar depolymerization rate in the first phase. This phase ends for all the catalysts at around 65% in M_w reduction. In the subsequent second phase, the Pd/AC catalyst demonstrates a very rapid depolymerization resulting in a final M_w reduction grade of 87%, and leads to the conclusion that this catalyst is the most valuable when the highest depolymerization grade in the shortest amount of time should be reached. The bimetallic PdCu/AC is the second best performing catalyst, however taking four times longer to reach the same final value.

The depolymerization process with the bimetallic Al₂O₃ and SiO₂ supported catalysts can be valuable when a very fast initial depolymerization rate is desirable. To reach a high M_w reduction grade, the catalysts take a far longer time than the AC supported ones, but may ultimately result in the same or almost the same final depolymerization grade as the AC supported catalysts.

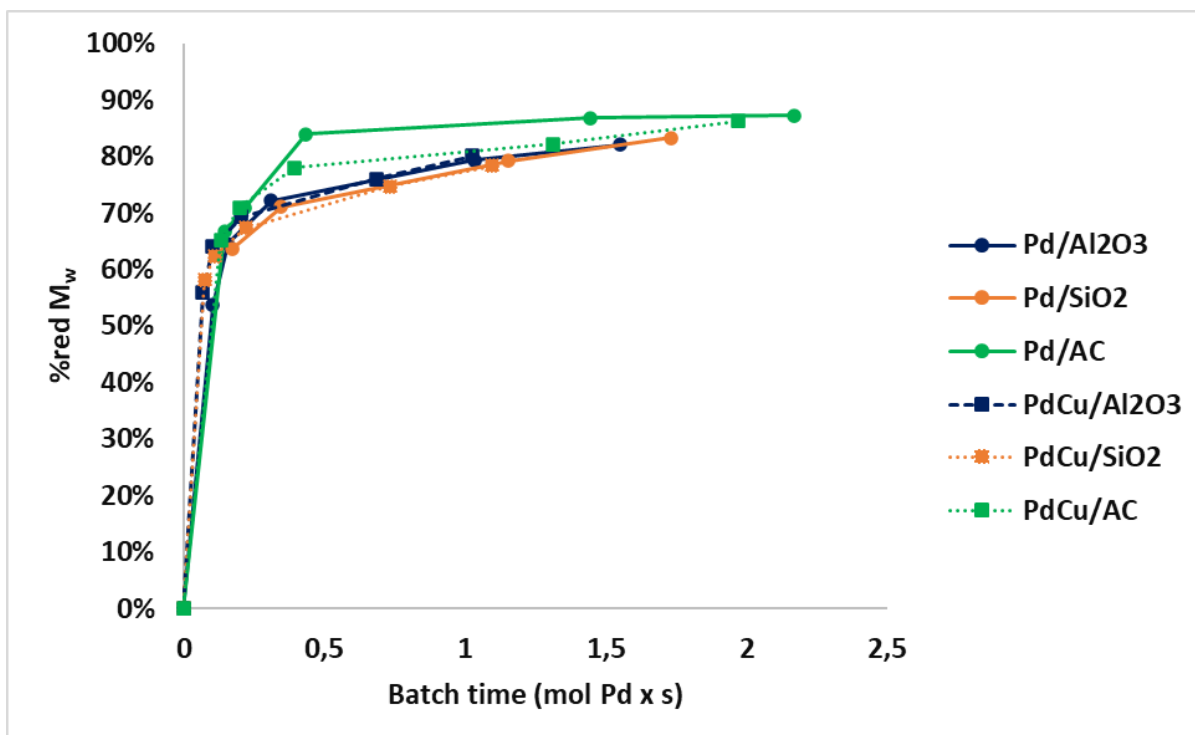


Figure 35: batch reactor results for the lignin depolymerization

A big difference of the AC support in comparison to Al₂O₃ and SiO₂ is the very high specific surface area, with values of respectively 1182, 195 and 198 m²/g. This had however, no direct correlation to the Pd dispersion (see earlier). The pore volume (resp. 0.95, 0.8 and 1.18 cm³/g) and particle size distribution (resp. 100-300, 100-500 and 75-500 μm) is not very different between the supports.

The AC supported catalyst is a mostly non-acidic support, which leads to the hypothesis that non-acidic supports have the best activity for this reaction when a high M_w reduction value is desired. In comparison to the other non-acidic support, SiO₂, AC has a much higher dispersion value. The monometallic AC catalyst has a higher dispersion than the bimetallic catalyst.

A possible conclusion is this: the highest activity (leading the fastest to a high M_w reduction rate) for the depolymerization of lignin is observed for the catalyst with the non-acidic support that shows the highest dispersion value of the catalysts characterized in this thesis.

The fastest initial depolymerization rate is found for PdCu/Al₂O₃, that has an acidic support and the highest reported dispersion of all the catalysts in this thesis. However, the depolymerization rate slows down and a high M_w reduction rate is reached after a far longer reaction time. The monometallic Pd/Al₂O₃ does not show this very fast first phase depolymerization rate. In addition to this, the non-acidic PdCu/SiO₂ also shows this fast initial rate. The fast initial M_w reduction is thus not only influenced by the acidity of the support.

Further research is needed to confirm whether a catalyst with medium to high dispersion on a non-acidic support is indeed beneficial for this reaction and how the reaction-mechanism is affected by this.

3.2 Acidity and basicity study on catalysts for the dehydration of 1,3-butanediol

For the dehydration of 1,3-BDO, it was discussed in the literature study that the acidity has an important role in the reaction. ZSM-5 is a promising catalyst, but it has been reported that tempering of the acidity has a positive influence on the selectivity of the reaction to butadiene. In the literature study, it has been reported that zeolite catalysts with lower acidic density and strength lead to a higher conversion and selectivity to BD.

The lowering of the acidic density and strength has been attempted by varying the Si/Al ratio, incorporation Boron in the ZSM-5 and using hybrid zeolite with CeO₂ catalysts. The acidity of these (modified and hybrid) ZSM-5 samples is characterized using NH₃-TPD. The basicity of hybrid CeO₂ with ZSM-5 also can influence the reaction, and is characterized using CO₂-TPD. The samples will be compared and the influence of the modifications are discussed. The results are also correlated with the data obtained on some of the same samples at the home campus (Ghent), in order to draw more correct and trustworthy conclusions. From these acidity and basicity results, a prediction of some promising catalysts for the 1,3-BDO dehydration reaction will be tried to made.

3.2.1 NH₃ and CO₂ gas concentration calibration

For each analysis gas (NH₃/He and CO₂/He) 11 data points are obtained for gas concentrations of 0% to 5% active gas, with increments of 0.5%. The 0% data point is not considered in the calibration curve.

The obtained TCD signals in function of time with rising NH₃ and CO₂ concentration are shown in Figure 36 and Figure 37, respectively.

The signal that can be corresponded with a certain concentration is determined by using the mean TCD signal of three points on each signal plateau: a point on the left, a point on the right, and a point in the middle of the horizontal part (determined by the AutoChem II software). The resulting calibration curves are shown in Figure 38.

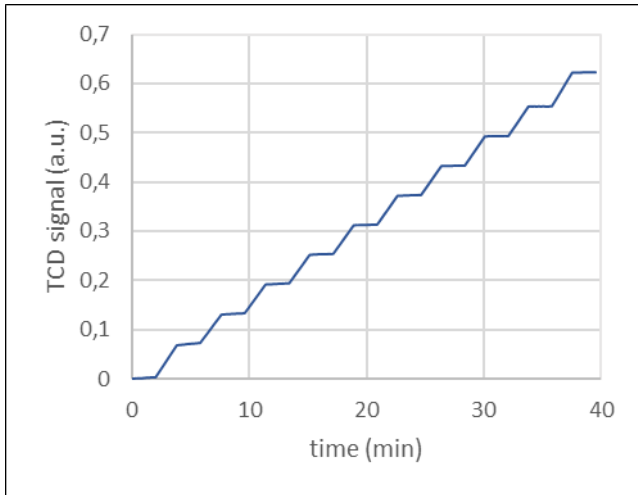


Figure 36: signal vs time (with rising NH_3 concentration)

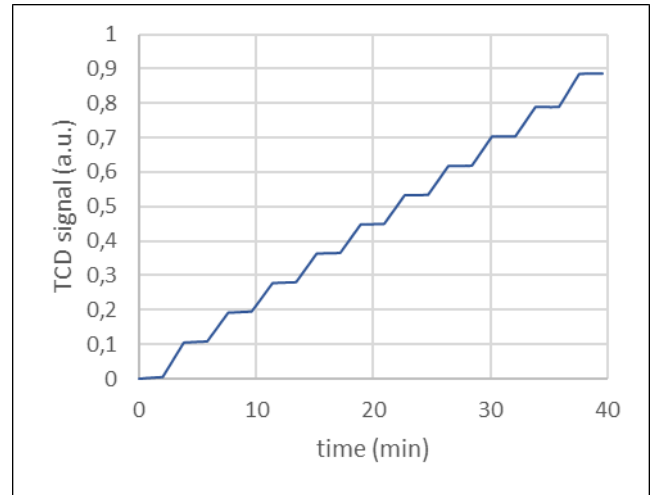


Figure 37: signal vs time (with rising CO_2 concentration)

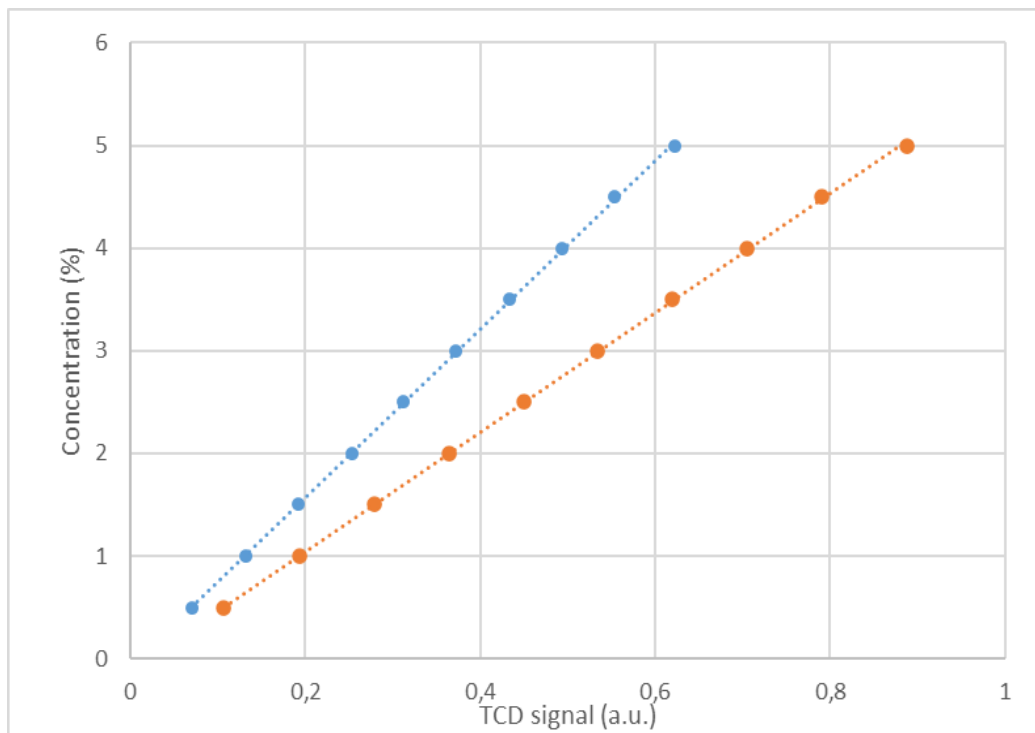


Figure 38: gas concentration calibration curves
 blue curve: NH_3/He ; orange curve: CO_2/He

The resulted parameters for the function $y = a \cdot x + b$ for each gas, where y is the concentration of the gas, a is the slope of the curve and b the intercept, are shown in Table 16. The intercept is found to be significant different from zero (with 95% confidence), and thus should be taken into account when calculating the concentration of the gas from a TCD signal. From the obtained calibration curve, the concentration of the gasses in the analysis can be calculated and enables for a quantitative analysis of the TPD results.

Table 16: gas calibration curves parameters

Gas	a (slope)	B (intercept)	R ²
NH ₃ /He	8.232 ± 0.0378	-0.077 ± 0.0146	0.9998
CO ₂ /He	5.823 ± 0.0258	-0.121 ± 0.0142	0.9998

3.2.2 Spectra interpretation and issues

3.2.2.1 NH₃-TPD

Due to some (probably technical or even software) problems with the AutoChem equipment, the obtained TPD spectra are deformed due to a very unstable baseline and a nod in the spectrum at elevated temperature, which varied for each analysis. The spectrum on an empty tube (with quartz wool but no catalyst) is shown in Figure 39. The temperature unit is always degrees Celsius (°C). However, this baseline varied between each analysis, so that correcting for this was found to be not possible.

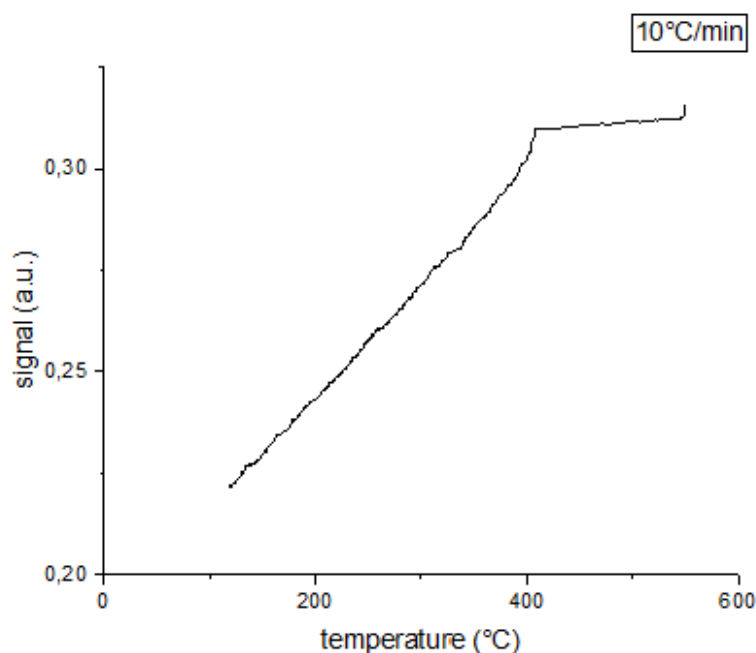


Figure 39: obtained spectrum on empty tube

Various attempts were made to try to mitigate this problem, by using other heating rates, using more sample, reconnecting the gasses, long waiting time for baseline stabilization... but without result.

An effort to try to find a correlation between the location of the nod and the conditions was also not successful, as the temperature at which this occurs seemed to be random. It was thus decided to discuss the results with the obtained spectra, of which two examples for NH₃-TPD are shown in Figure 40 and Figure 41.

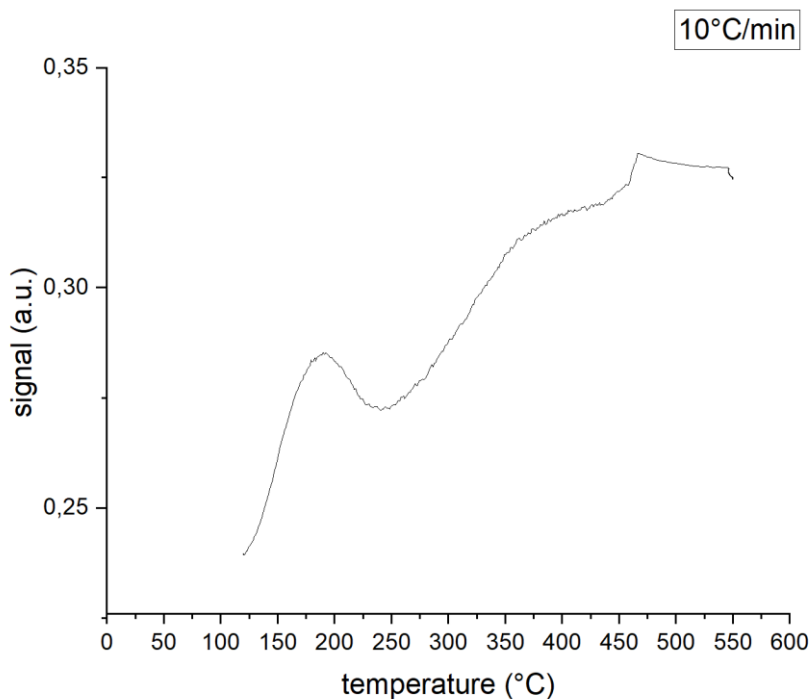


Figure 40: recorded NH₃-TPD spectrum of commercial ZSM-5

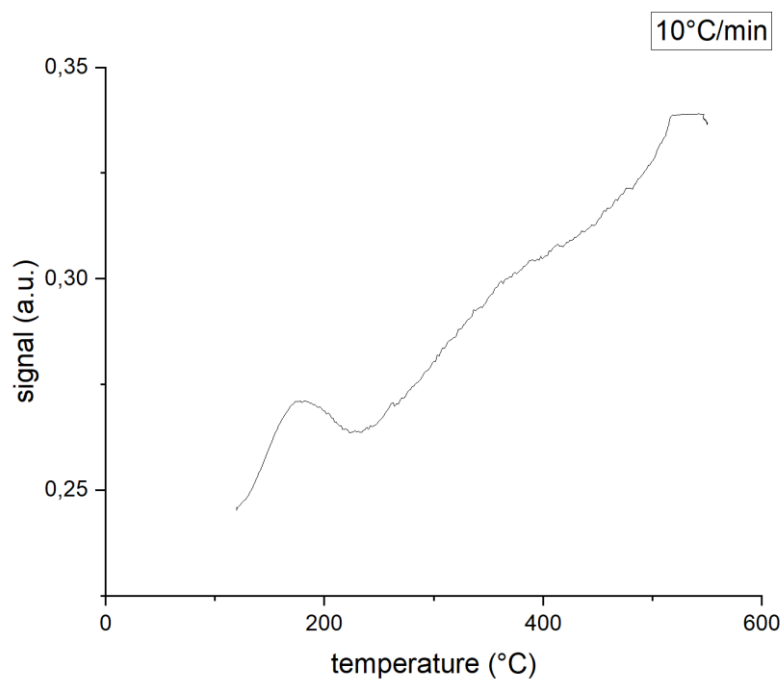


Figure 41: recorded NH₃-TPD spectrum of ZSM-5@25_B

The baseline correction cannot be done correctly, but was tried to be done for all spectra in the most similar way possible, in order to be able to draw conclusion and compare the catalysts between each other. This is done in the following way. It is attempted to take a straight baseline by using the upper left point of the graph and the point where the second peak seems to be at its minimum. As an example, the baseline and corrected spectrum for the commercial ZSM-5 are shown in Figure 42 and Figure 43.

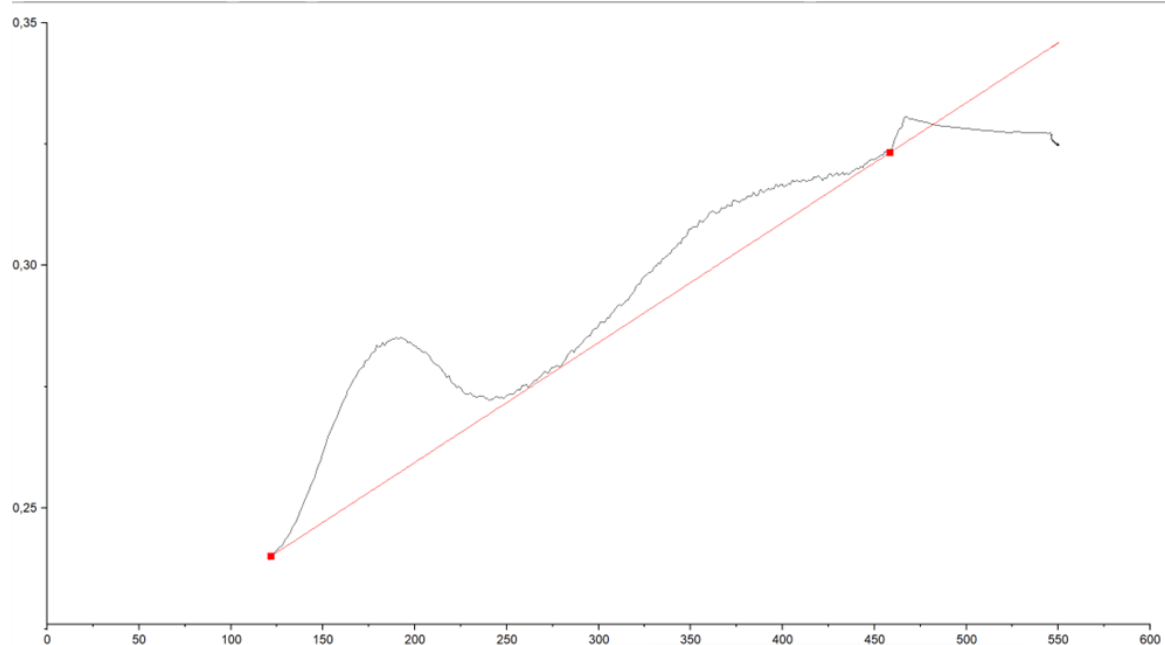


Figure 42: baseline correction for commercial ZSM-5

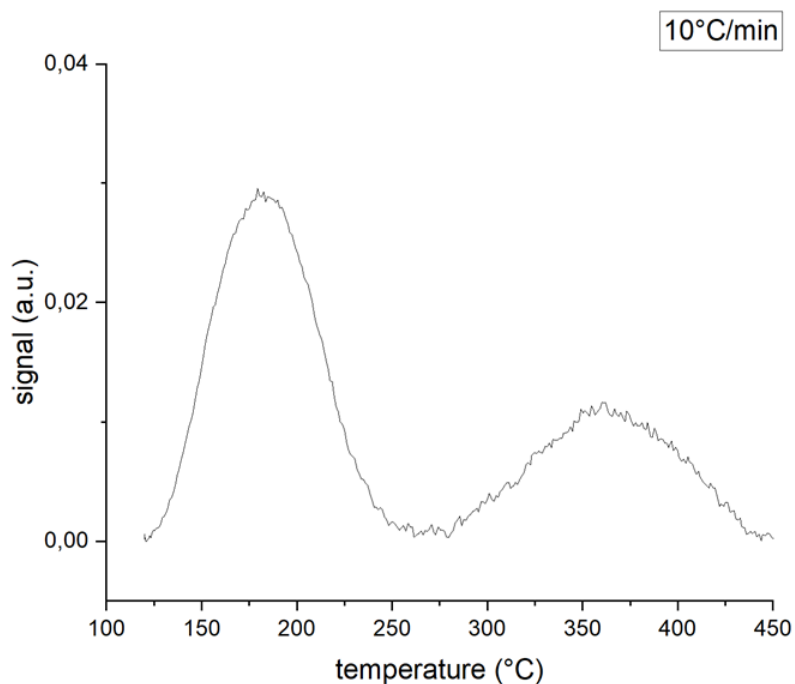


Figure 43: corrected spectrum for commercial ZSM-5

As visible, the minimum between the two peaks is close to zero, which in reality is not the case. The height of this point is however impossible to predict, so that this point is taken to be around zero or slightly higher than zero for all the spectra.

For some spectra, the former method (left and right point determination on the graph to construct a linear baseline) leads to a minimum value between the two peaks that is lower than zero. In this case, a slight angle in the baseline is taken to make sure that the signal is higher than zero at all times. This is shown for ZSM-5@25_B in Figure 44 and Figure 45.

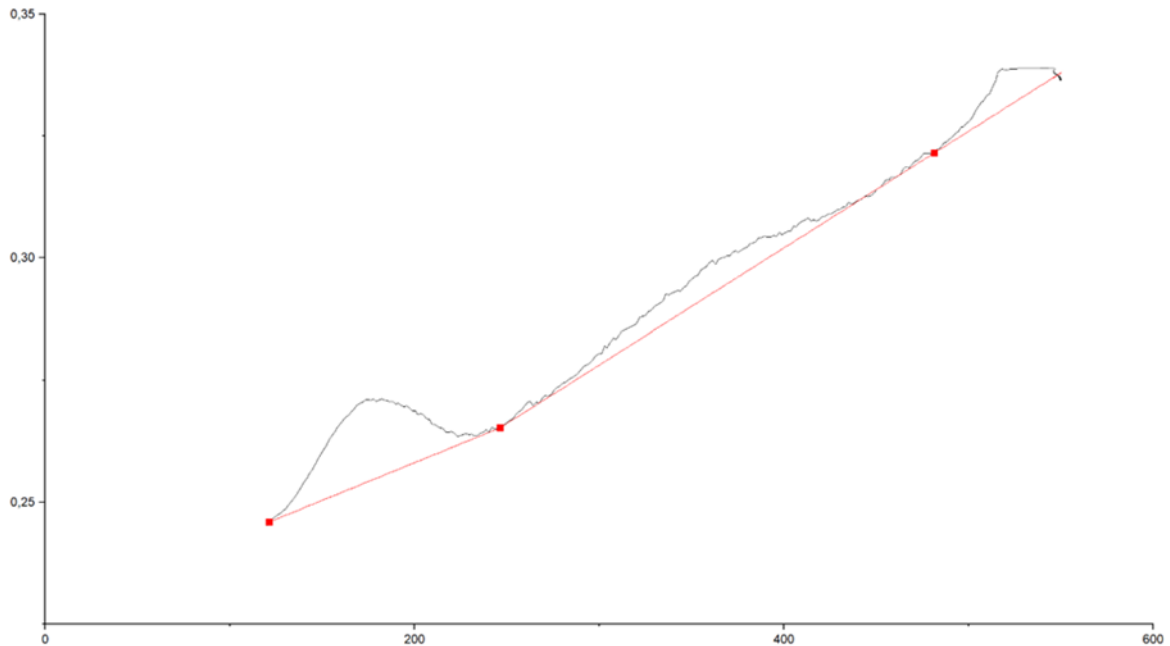


Figure 44: baseline correction for ZSM-5@25_B

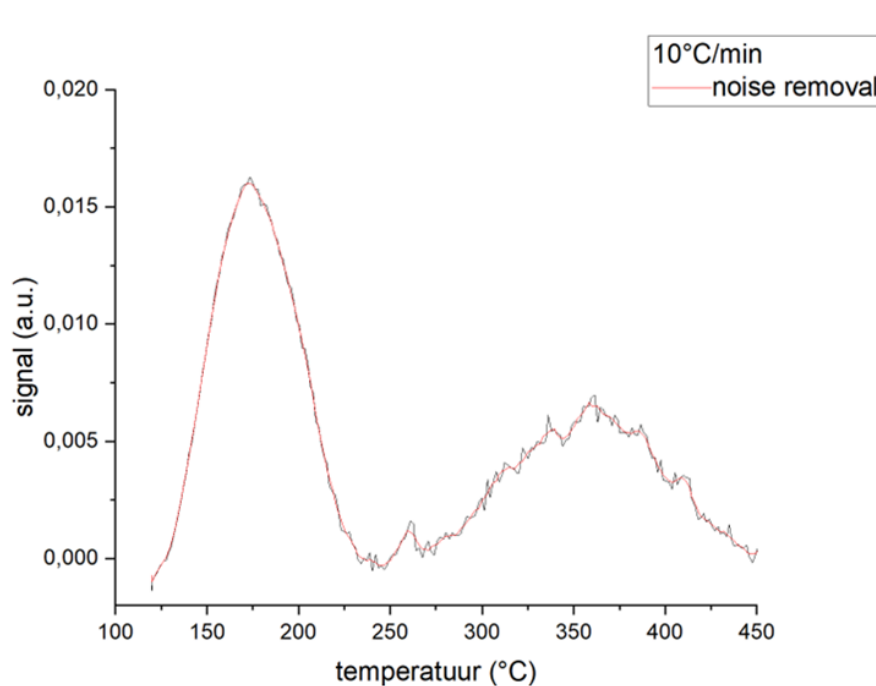


Figure 45: corrected spectrum for ZSM-5@25_B

Because the minimum between the two peak is always at or close to zero, it was chosen to only model two Gaussian peaks on each spectrum. The one at lower temperature corresponds to weak acidic sites and the one at high temperature to the strong acidic sites. With these method, a comparison between the samples is tried to be made.

It is very important to note that the found concentration of the active sites in this thesis are only valuable as a comparative tool between the catalysts, and the absolute values of the active sites are not at all correct. Quantitative results of NH₃-TPD on some of the samples at the INCAT research group (at UGhent by doctoral student Loïc Eloi) can be found in Appendix C: NH₃-TPD acidity results from Ghent campus and Appendix D: NH₃-TPD spectra from Ghent campus. For completeness, the analysis conditions of these experiments are included in Appendix F: analysis conditions for NH₃-TPD at the home campus (Ghent). Because the results in this thesis are subjected to the mentioned problems, the results from the home campus will also be discussed in order to be able to draw a more complete and trustworthy conclusion regarding the catalysts samples.

3.2.2.2 CO₂-TPD

The CO₂-TPD experiments have the same unstable baseline and nod, although the latter issue is not as much as a problem because the desorption of CO₂ occurred for all the samples at lower temperature (<200°C). Because only one peak is observed in the TPD spectrum, the baseline correction is probably more correctly performed than for the NH₃-TPD spectra. Hence, the obtained density values are quantitatively more valuable than those of the NH₃-TPD study. The baseline correction is done by drawing a line between the start of the spectrum and the apparent end of the peak.

3.2.2.3 Possible solutions to obtain qualitative spectra

The problems discussed earlier were not solved during the study. The unstable baseline and the nod were tried to be avoided by trial-and-error, however with no positive result. Some attempted and possible future solutions will be shortly discussed in this chapter.

A gas leak could lead to an unstable baseline. This was however not detected. The gasses were all reconnected and flushed to ensure all the connections were gastight. This did not led to a difference in the obtained spectra. A further investigation by an expert on the equipment could possibly be useful to find any hidden issues regarding the gas connections and gasses.

By giving the TCD detector a long time to stabilize the baseline, better results could possibly be obtained. However, even after a long stabilization period of more than a week under He, the unstable baseline with nod was still observed.

The nod only appears at a varying, elevated temperature of around 450°C. Repeated experiments were conducted to try to avoid this nod. Analyses with lower and higher temperature rates did not show a clear difference.

A possible solution is replacing some of the critical components of the equipment. However, the TCD detector was replaced less than a year prior to the research. The six-way valve was replaced at the start of the analyses. The replacement of other components should be discussed with an expert from the equipment manufacturer (Micromeritics).

Correcting each spectrum with a specific baseline correction was attempted by recording the spectrum on an empty tube with quartz wool at different temperature rates. If the baseline would be predictable this data can be subtracted from the obtained TPD spectra on the samples. However, when repeating the recording on an empty tube, the signal was not constant and gave a different observed baseline, with the nod at a different temperature, at each analysis. This method is thus not reproducible. In the future, new attempts could be made to find a correlation between the heating rate, temperature and obtained baseline. Advanced signal processing techniques like Fourier Transform analysis can be used. A data treatment model can then correct the obtained spectra to make them more qualitative and possibly enable for quantitative analysis of the active sites, rather than comparative.

The appearance of the nod is very unexpected, and could potentially be a software issue. The equipment company (Micromeritics) was contacted to present this problem. The raw data (TCD signal versus temperature) of a NH₃-TPD experiment from the Ghent campus which gave good results and from this research which gave bad results was attached. No answer from the company was received at the time of the submission of this thesis.

Sadly, due to the problems, no good spectra and subsequent quantitative results were obtained during this research. Hopefully, the problem can be solved in the future, with the help of experts from the equipment company. An attempt was still made for drawing conclusions from the results, although these are not ideal and uncertain.

3.2.3 Acidity study with NH₃-TPD

The corrected NH₃-TPD spectra of all samples for the three different heating rates (10, 15, 20°C/min) are shown in Appendix G: corrected and deconvoluted NH₃-TPD spectra. The modeled peaks from the deconvolution are visible. Because a gas concentration calibration was performed, the area under the peaks can be correlated to the amount of desorbed NH₃ per gram catalyst. It is a unit for the acidic active sites concentration on the sample. This acidic concentration is determined for all the heating rates and a mean value with standard deviation on the experimental values is obtained. The results are summarized in Table 17.

Table 17: acid density results from NH₃-TPD experiments

Catalyst	Weak sites ($\mu\text{mol}/\text{g}_{\text{cat}}$)	Strong sites ($\mu\text{mol}/\text{g}_{\text{cat}}$)	Total sites ($\mu\text{mol}/\text{g}_{\text{cat}}$)
Comm. ZSM-5	201 ± 10	83 ± 11	284 ± 15
ZSM-5@25	162 ± 4	43 ± 6	205 ± 7
ZSM-5@150	29 ± 2	21 ± 10	50 ± 10
ZSM-5@25_B	101 ± 3	63 ± 6	164 ± 7
ZSM-5@150_B	14 ± 3	6 ± 1	20 ± 3
CeO₂/ZSM-5	63 ± 4	9 ± 3	72 ± 5
ZSM-5@CeO₂	213 ± 17	65 ± 12	278 ± 20

As stated earlier, these values are only valuable for comparative purposes between the catalysts and cannot be reported as correct absolute values. In the next chapters, the catalysts will be compared in regard to the relation between their modification (Si/Al ratio, B incorporation, hybrid catalysts) and the observed acidity. The results of the analysis at the Ghent campus, are also discussed. For a visual comparison between the samples, the shown spectra are those of 15°C/min for all the catalysts. The determined acidic concentrations are however determined from the TPD data of all the heating rates. The standard deviation on the acid density is calculated.

By performing the TPD at three different heating ratio's, the desorption energy (E_d) of the strong acid peak, which is a parameter for the strength of the strong acidic sites, was calculated by using equation (10). The plotted Arrhenius curves for all the samples are placed in Appendix H: Arrhenius plots for E_d determination of the strong acid sites. The derived E_d results are listed in Table 18. The analysis on commercial ZSM-5 was repeated to enable for an estimation of the experimental error (the standard deviation was used for this). This error is used as an estimation for the error for all the samples, although only the commercial ZSM-5 was repeated.

Table 18: NH₃-TPD desorption energy results

Catalyst	T _{max} (10°C/min, °C)	T _{max} (15°C/min, °C)	T _{max} (20°C/min, °C)	E_d (kJ/mol)
Comm. ZSM-5 (1)	360.2	371.3	375.9	135.12
Comm. ZSM-5 (2)	350.8	362.4	366.3	130.10
Comm. ZSM-5 (mean value)	355.5 ± 4.70	366.85 ± 4.45	371.1 ± 4.80	132.59 ± 2.51
ZSM-5@25	356.3	365.7	372.5	133.95 ± 2.51
ZSM-5@150	339.4	351.2	/ (strong deviation)	98.97 ± 2.51
ZSM-5@25_B	363.5	374.7	/ (strong deviation)	113.46 ± 2.51
ZSM-5@150_B	/ (strong deviation)	342.4	352.1	84.58 ± 2.51
CeO₂/ZSM-5	349.6	361.8	/ (strong deviation)	98.80 ± 2.51
ZSM-5@CeO₂	364.5	370.5	380.5	134.6 ± 2.51

When comparing this E_d values, some conclusions can be made. One can observe that the E_d values for the strong acid site differ significantly between the samples. The highest values are found for commercial and prepared ZSM-5, respectively 132.59 and 133.95 ± 2.51 kJ/mol. The strength of the strong acid site for these standard ZSM-5 samples (commercial and prepared) is, considering the error, not significantly different. The modified and hybrid samples however, generally show a significant decrease in the acidic site strength. Only the hybrid ZSM-5@CeO₂ has a strength that corresponds those of the standard ZSM-5. In conclusion for the global results, the modifications and hybrid catalysts change the acid density and acid strength. The E_d values and site concentrations for all the catalysts will be further discussed in the following chapters, where all the modifications and hybrid catalysts will be reviewed on their acidity.

The found E_d values are compared with those from the literature, to confirm that these are realistic. The amount of acidic sites will not be compared, as the values for this thesis are too low and only for comparative purposes (see earlier). For completion, reported values will be given. In other studies, total active site concentrations for ZSM-5 of 100-700 $\mu\text{mol}/\text{g}_{\text{cat}}$, depending on Si/Al ratio, have been reported [110][111]. E_d values of 100-170 kJ/mol are found for zeolite samples with a Si/Al from 10 to 150. The E_d values in this thesis range between 85-135 kJ/mol, and can, although relatively low compared to other reported values, possibly be realistic [110], [111], [141].

For comparison, the T_{max} values for a heating ratio of 10°C/min obtained at the home campus by doctoral student Loïc Eloï compared by the ones from this thesis are included in Table 19. The NH₃ loading at the home campus (Ghent) was done at a temperature of 150°C, thus higher than the temperature of 120°C in this thesis. The big difference is remarkable. The shift to higher temperature when loading at higher temperature is expected, but the high shift of around 40 to 70°C for each sample cannot be explained. This difference once again leads to the conclusion that the experiments in this thesis differ significantly from the similar experiments at the home campus in Ghent. The slightly different analysis conditions, bad spectra, baseline problems and the fact that only comparative values in this thesis can be used all have their part in this differentiation.

Table 19: comparison for T_{max} in this thesis and at home campus Ghent (at 10°C/min)

Catalyst	T_{max} (10°C/min: this thesis)	T_{max} (10°C/min: at home campus Ghent)
ZSM-5@25	356.3	405
ZSM-5@150	339.4	395
ZSM-5@25_B	363.5	435
ZSM-5@150_B	344.3	385
CeO₂/ZSM-5	349.6	418
ZSM-5@CeO₂	364.5	405

3.2.3.1 Acidity of prepared ZSM-5@25 in comparison to commercial ZSM-5@25

Both commercial and prepared ZSM-5@25 were analyzed. The NH₃-TPD spectra, acid site concentration and E_d results for commercial ZSM-5@25 and prepared ZSM-5@25 are shown in Figure 46 and Table 20.

Table 20: acid site concentration results of commercial and prepared ZSM-5@25

Catalyst	Weak sites (μmol/g _{cat})	Strong sites (μmol/g _{cat})	Total sites (μmol/g _{cat})	E _d (kJ/mol)
Comm. ZSM-5	201 ± 10	83 ± 11	284 ± 15	132.59 ± 2.51
ZSM-5@25	162 ± 4	43 ± 6	205 ± 7	133.95 ± 2.51

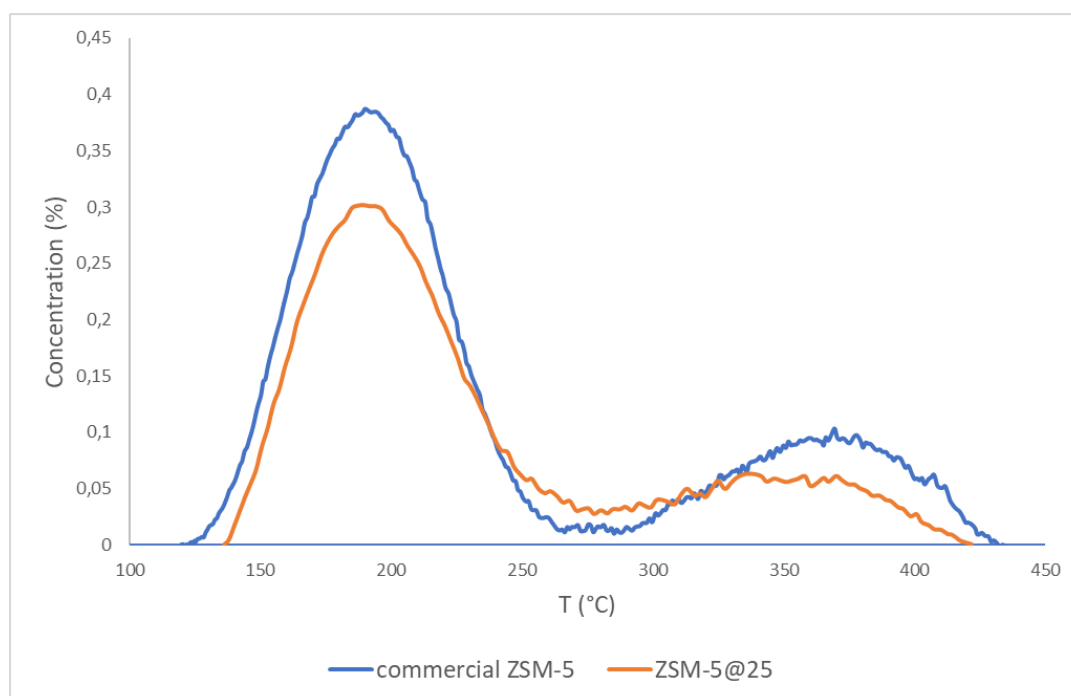


Figure 46: NH₃-TPD spectra of commercial and prepared ZSM-5@25

It is clear from the acid density and TPD spectra that both the amount of weak and strong acidic sites are lower for the prepared ZSM-5@25 catalyst. A possible reason could be that the preparation in the lab is not as ideal as the industrial production on larger scale. The difference in weak and strong sites is 19.4% and 48.2% respectively. The total acid density is 27.8% lower. It should also be taken into account that the real Si/Al ratio of these samples are 24 for the commercial ZSM-5 and 15 for the prepared ZSM-5. A higher acidity is expected (see literature study) for ZSM-5 with lower Si/Al ratio.

The difference between the acidity of the prepared and commercially bought ZSM-5 will thus be even higher, when taking into account the difference in Si/Al ratio.

The strength of the strong acidic sites does not differ significantly between the two samples, with values of 132.59 and 133.95 ± 2.51 kJ/mol for commercial and prepared ZSM-5 respectively. The actual Si/Al ratios for the samples are respectively 24 and 15. As stated in the literature study, a higher ratio generally leads to weaker acidic sites. The prepared ZSM-5 has the lowest ratio, but this does not lead to a stronger acidic site. When taking into account the difference in Si/Al ratio, it is thus probable that the commercial ZSM-5 has slightly stronger acidic sites than the prepared ZSM-5.

The commercial ZSM-5 was not characterized at the home campus, so that no comparison between the result of this thesis and those from the research group can be made.

In conclusion, the prepared ZSM-5 has a lower acidic concentration for both the weak and strong acidic sites. The strength of the strong acidic site, when taking into account the difference in Si/Al, is probably slightly higher for the commercially bought ZSM-5 when the samples would have the same Si/Al ratio. To ensure that this statement is correct, a prepared ZSM-5 sample with the same Si/Al ratio as the commercial one should be analyzed.

3.2.3.2 Influence of the ZSM-5 SiO₂/Al₂O₃ ratio

A higher Si/Al ratio generally leads to a lower concentration of acidic sites and a decrease in acid strength, as reported in other researches (see literature study). The NH₃-TPD spectra, acid site concentration and E_d results for ZSM-5@25 and prepared ZSM-5@150 are shown in Figure 47 and Table 21.

Table 21: acid site concentration results of ZSM-5@25 and ZSM-5@150

Catalyst	Weak sites ($\mu\text{mol}/\text{g}_{\text{cat}}$)	Strong sites ($\mu\text{mol}/\text{g}_{\text{cat}}$)	Total sites ($\mu\text{mol}/\text{g}_{\text{cat}}$)	E _d (kJ/mol)
ZSM-5@25	162 ± 4	43 ± 6	205 ± 7	133.95 ± 2.51
ZSM-5@150	29 ± 2	21 ± 10	50 ± 10	98.97 ± 2.51

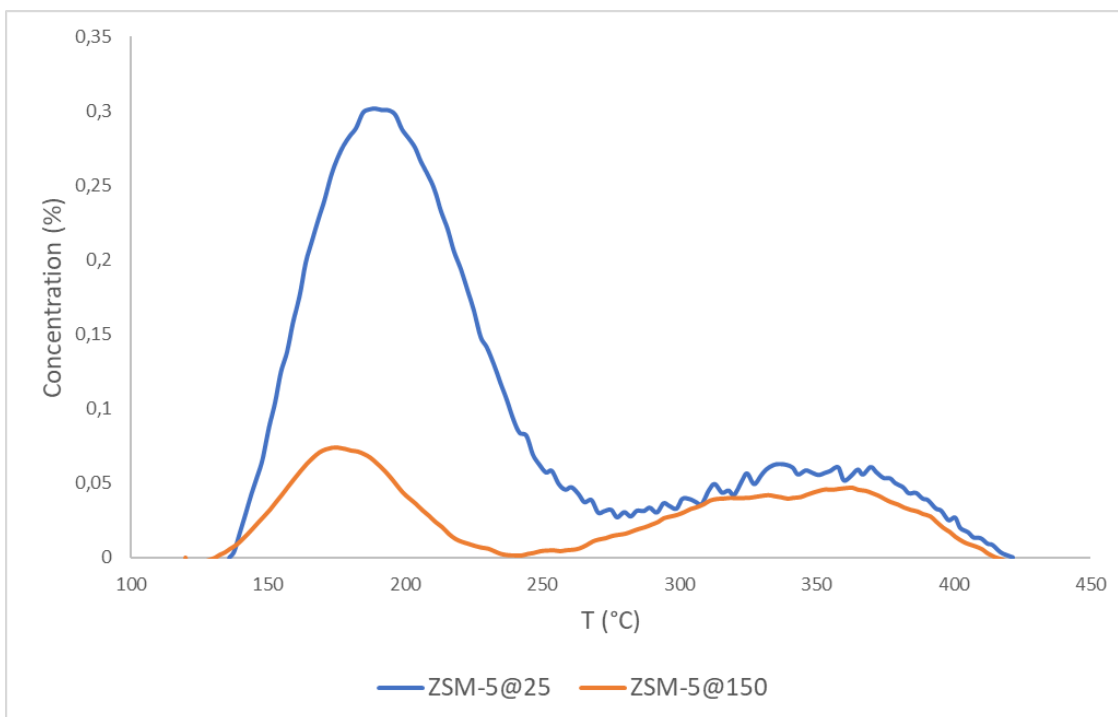


Figure 47: NH_3 -TPD spectra ZSM-5@25 and ZSM-5@150

A drastic decrease in weak acidic sites (-82.1%) and in strong acidic sites (-51.2%) is observed when the Si/Al is raised from 15 to 150. The most significant decrease is thus observed for the weak acidic sites. The total acid density decreases by 75.6%.

The found E_d values for ZSM-5@25 and ZSM-5@150 are respectively 133.95 and 98.97 ± 2.51 kJ/mol. These correspond with the reported E_d values in the study of Gunst et al. (2020), where values of 135.1 kJ/mol and 103.3 kJ/mol were reported for ZSM-5 with Si/Al ratio of 15 and 140 respectively [141]. These ratios are similar to the actual Si/Al ratios in this thesis. These E_d values are thus realistic. A very slight shift in peak maxima to a lower temperature is also visible in the TPD spectrum for ZSM-5@150 compared to ZSM-5@25. This means that the strength of the strong acidic site is decreased for ZSM-5@150 compared to ZSM-5@25.

Discussion of the acidity results from the Ghent campus

The results of the research at the Ghent campus are discussed, in order to be able to give conclusions with more certainty and also give quantitative values for the acid density in the samples. The spectra do not have the baseline problem, and the deconvolution was performed for four peak strengths, being weak, medium, strong and very strong sites. The results are summarized in Table 22 and the deconvoluted TPD spectra of ZSM-5@25 and ZSM-5@150 are shown in Figure 48 and Figure 49 respectively. E_d was only determined for ZSM-5@25, the Arrhenius plot can be found in Figure 82 (appendix E).

Table 22: acid site concentration results of ZSM-5@25 and ZSM-5@150 (Ghent campus)

Catalyst	Weak sites ($\mu\text{mol/g}_{\text{cat}}$)	Medium sites ($\mu\text{mol/g}_{\text{cat}}$)	Strong sites ($\mu\text{mol/g}_{\text{cat}}$)	Very strong sites ($\mu\text{mol/g}_{\text{cat}}$)	Total sites ($\mu\text{mol/g}_{\text{cat}}$)	E_d (kJ/mol)
ZSM-5@25	120	120	112	66	419	115
ZSM-5@150	13	13	38	23	86	/

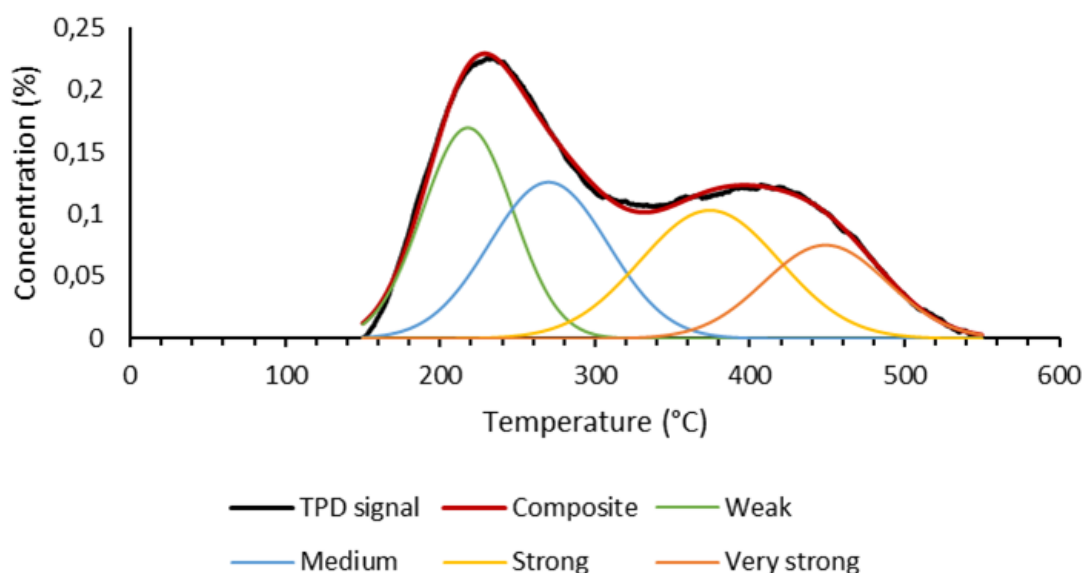


Figure 48: NH_3 -TPD spectrum for ZSM-5@25 (Ghent campus)

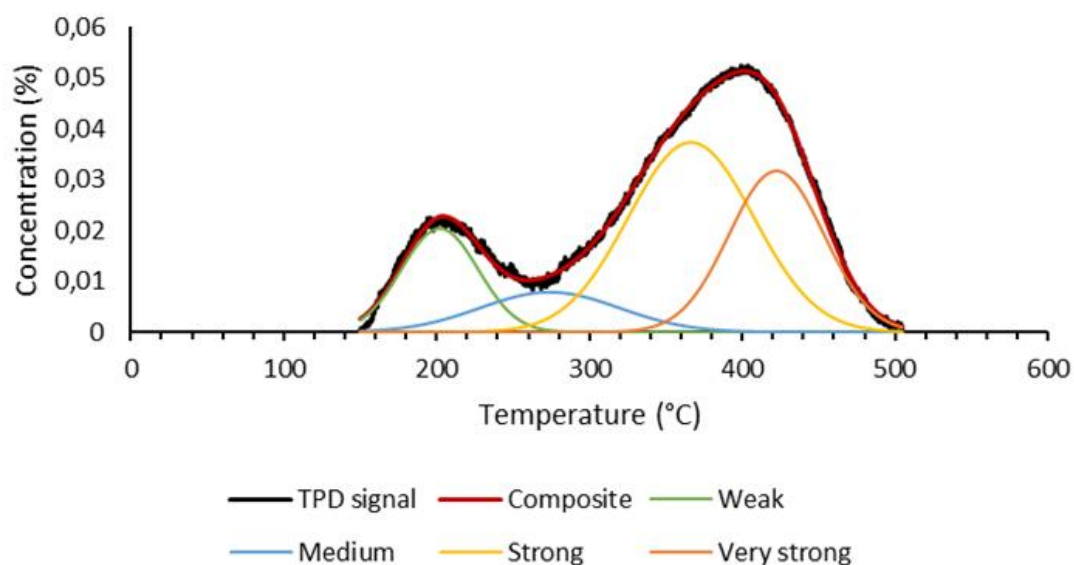


Figure 49: NH_3 -TPD spectrum for ZSM-5@150 (Ghent campus)

It is clear that the amount of acid sites decreases significantly when the Si/Al ratio is 150 compared to 25. The impact is the highest on the weak and medium acid sites, with a decrease from 120 to 13 $\mu\text{mol/g}$ for both the sites, which corresponds to a decrease of 89.2%. The strong acid site density decreases from 112 to 38 $\mu\text{mol/g}$ (decrease of 66.1%) and the very strong sites from 66 to 23 $\mu\text{mol/g}$ (decrease of 65.2%) The total acid density of ZSM-5@150 is 86 $\mu\text{mol/g}$ compared to 419 $\mu\text{mol/g}$ for ZSM-5@25, which is a decrease of 79.5%. Increasing the Si/Al thus has a great impact on the acid site density of all strengths. The impact is the highest on the weak and medium acidic sites. This is also visible from the TPD spectra, shown in Figure 48 and Figure 49. In ZSM-5@25, the weak and medium sites are most present, while in ZSM-5@150, the strong and very strong sites have a relatively higher share of the total sites.

Comparison of results at Ghent campus with this thesis

Both this research and the research at the Ghent campus found similar results, being it not a quantitative way as explained earlier. The density in weak sites in this thesis was found to decrease with 82.1% when increasing the Si/Al ratio from 25 to 150. The decrease in strong sites is 51.2%. The total amount of acid sites decreases with 75.6% The reported decrease at the Ghent campus was 89.2% for the weak and medium sites and 66.1% and 65.2% for the strong and very strong sites respectively. The total acid density decrease is 79.5%. The quantitative values are not comparable, but the relative decrease of the sites acid density show the same trends for both the studies.

The E_d value of ZSM-5@25 reported on the Ghent campus is lower than in this thesis, with values of respectively 115 and 133.95 kJ/mol. It should be noted that in the study in Ghent, four data points were obtained instead of three in this thesis. Having only three data points comes with a great uncertainty, as a small change in T_{max} lead to a significant shift in E_d value. However, a study De Saegher et al. (2020) reported for ZSM-5 with the same actual Si/Al ratio of 15 a E_d value of 135.1 kJ/mol [141]. This value is very close to the found value of 133.95 kJ/mol in this thesis, which leads to believe that this is a realistic value.

In conclusion, using a higher Si/Al ratio for the ZSM-5 leads to a successful lowering of acid site density. The highest decrease is observed for the weak and medium acidic sites with a lower decrease for the strong and very strong acidic sites. This trend was confirmed by both studies.

In this thesis, it was found that increasing the Si/Al ratio decreased the strength of the strong acidic site, with a decrease from 133.95 to 98.97 kJ/mol. This indicates that not only the acid density on the catalysts decreased, but also the strength of the sites. This modification is thus useful in the tempering of the acidity in the ZSM-5 catalyst, both in acid density and strength.

3.2.3.3 Influence of Boron incorporation in ZSM-5

The goal of the B incorporation is tempering the acidity. The NH₃-TPD spectra, acid site concentration and E_d results for ZSM-5@25, ZSM-5@25_B, ZSM-5@150 and ZSM-5@150_B are shown in Figure 50, Figure 51 and Table 23.

Table 23: acid site concentration results of ZSM-5@25, ZSM-5@150 and the Boron incorporated catalysts

Catalyst	Weak sites (μmol/g _{cat})	Strong sites (μmol/g _{cat})	Total sites (μmol/g _{cat})	E _d (kJ/mol)
ZSM-5@25	162 ± 4	43 ± 6	205 ± 7	133.95 ± 2.51
ZSM-5@25_B	101 ± 3	63 ± 6	164 ± 7	113.46 ± 2.51
ZSM-5@150	29 ± 2	21 ± 10	50 ± 10	98.97 ± 2.51
ZSM-5@150_B	14 ± 3	6 ± 1	20 ± 3	84.58 ± 2.51

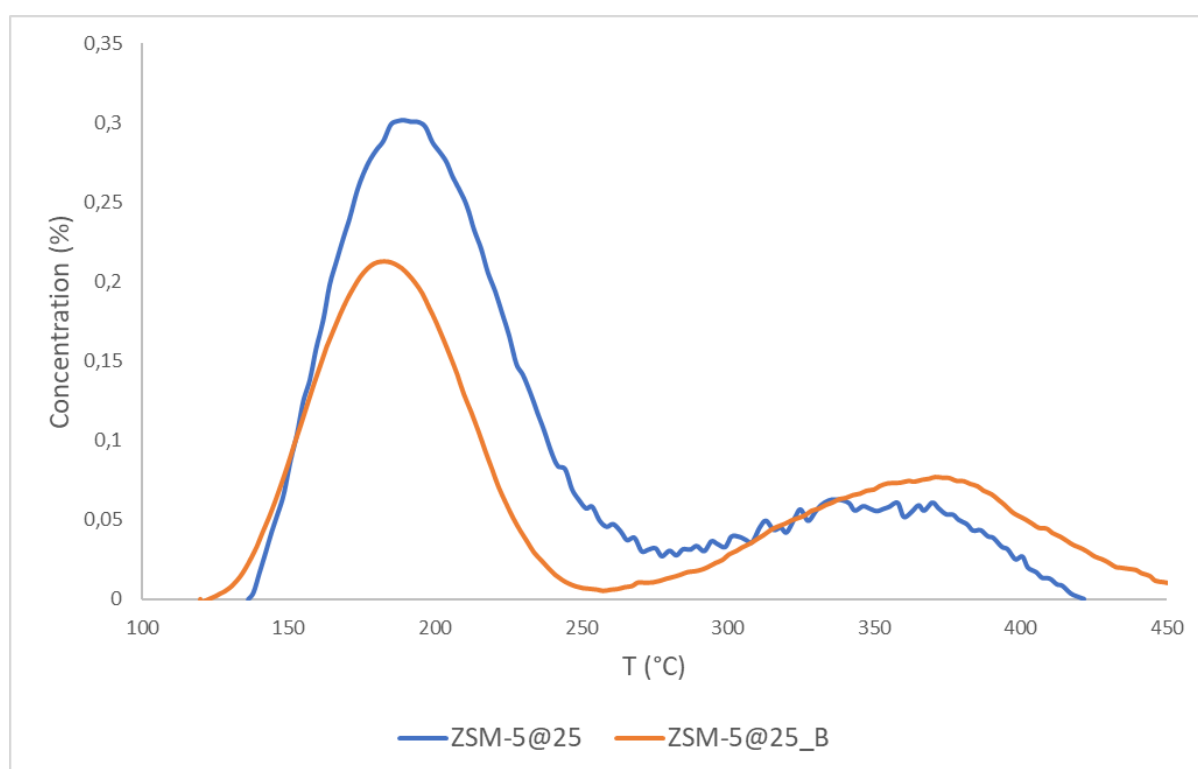


Figure 50: NH₃-TPD spectra of ZSM-5@25 and ZSM-5@25_B

For the B incorporated ZSM-5@25, a 37.7% decrease in weak acidic sites is observed. A decrease in strong acidic sites is expected, however this is not found. Instead an increase of 46.5% is reported. This is an unexpected result and cannot be explained with certainty. A possible explanation is a big error on the measurements (most by the data treatment and baseline correction, although this was repeated several times). OES data revealed that ZSM-5@25_B only has a B/Al ratio of 0.2 instead of 1 at which is aimed. The B incorporation effect is probably lowered by this, but this still does not explain the slight increase in strong acidic sites. The total acid density decreases by 20%.

The strength of the strong acidic sites is lower for ZSM-5@25_B compared to ZSM-5@25, with values of 113.46 and 133.95 ± 2.51 kJ/mol. The B incorporation does thus lower the acidic strength of the catalyst. The total acid density also decreases, but the rise in strong acid density cannot be explained and is very unlikely to be correct.

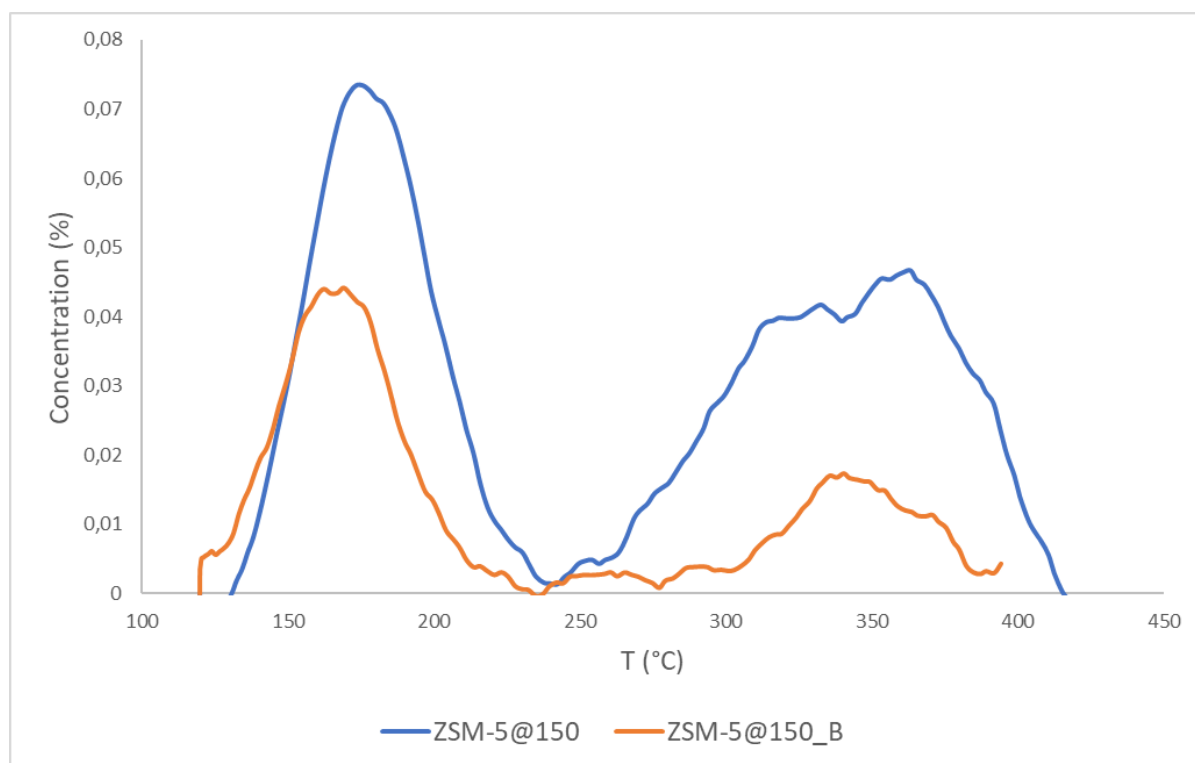


Figure 51: NH₃-TPD spectra of ZSM-5@150 and ZSM-5@150_B

The effect of the B incorporation in this thesis is more clear for ZSM-5@150. A decrease of 51.7% and 71.4% for the weak and strong acid sites respectively is observed in the B modified sample. The total acid density decreases by 60%. The OES showed that a B/Al ratio of 0.9 is achieved, which is almost the wanted value. When the B incorporation is achieved with high efficiency (almost half of the Al is replaced by B), the tempering of the acidity is very clear, both in weak and strong acidic sites.

The E_d of the strong acidic sites in ZSM-5@150_B is found to be lower than those of ZSM-5@150, with values of 84.58 and 98.97 ± 2.51 kJ/mol. The B incorporation shows thus a clear decrease in acid strength.

In conclusion, the incorporation of B in the ZSM-5 catalysts lead to a tempering of the acidity. A decrease in weak and strong acidic sites is observed, and the strength of the acidic sites is lowered.

The result in this thesis for ZSM-5@25_B contradicts this and seems to be incorrect. An increase in strong acidic site density was found compared to ZSM-5@25, which is unexpected. At the home campus in Ghent, this anomaly was not reported and because this is in contradiction with other studies (see literature study), it is concluded that the increase in strong acid site density for ZSM-5@25_B compared to ZSM-5@25 is not correct and should be refuted.

Discussion of the acidity results from the Ghent campus

The results of the research at the Ghent campus are discussed, in order to be able to give conclusions with more certainty and also give quantitative values for the acid density in the samples. The spectra do not have the baseline problem, and the deconvolution was performed for four peak strengths, being weak, medium, strong and very strong sites. The results are summarized in Table 24 and the deconvoluted TPD spectra of ZSM-5@25_B and ZSM-5@150_B are shown in Figure 52 and Figure 53 respectively. E_d was only determined for ZSM-5@25_B, the Arrhenius plot can be found in Figure 83 (appendix E).

Table 24: acid site concentration results of ZSM-5@25_B and ZSM-5@150_B (Ghent campus)

Catalyst	Weak sites ($\mu\text{mol}/g_{\text{cat}}$)	Medium sites ($\mu\text{mol}/g_{\text{cat}}$)	Strong sites ($\mu\text{mol}/g_{\text{cat}}$)	Very strong sites ($\mu\text{mol}/g_{\text{cat}}$)	Total sites ($\mu\text{mol}/g_{\text{cat}}$)	E_d (kJ/mol)
ZSM-5@25	120	120	112	66	419	115
ZSM-5@25_B	80	80	36	78	274	84
ZSM-5@150	13	13	38	23	86	/
ZSM-5@150_B	6	6	29	8	49	/

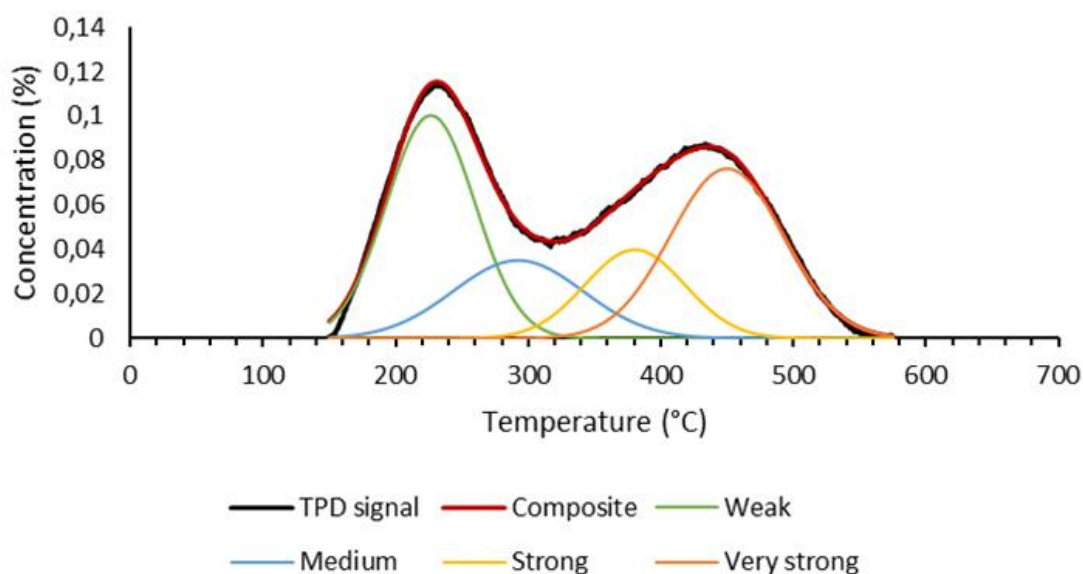


Figure 52: NH_3 -TPD spectrum for ZSM-5@25_B (Ghent campus)

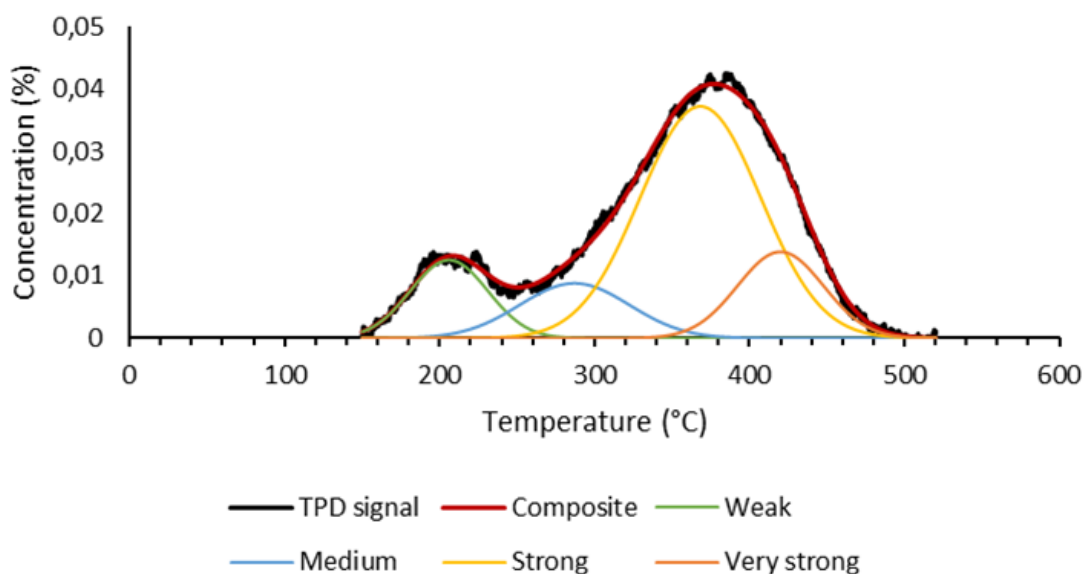


Figure 53: NH_3 -TPD spectrum for ZSM-5@150_B (Ghent campus)

When comparing ZSM-5@25_B with ZSM-5@25, a decrease from 120 to 80 $\mu\text{mol/g}$ for both the weak and medium sites is reported, which corresponds to a decrease of 33.3%. The strong acid site density decreases from 112 to 36 $\mu\text{mol/g}$ (decrease of 67.9%). Strangely, the very strong site density increases from 66 to 78 $\mu\text{mol/g}$ (increase of 18.2%). This could be a result of the deconvolution choice, and because the strong and very strong acidic peaks are localized close to each other, it is chosen to discuss this as one peak: the combined strong acidic peak. The strong acidic peak then shows a decrease from 178 to 114 kJ/mol, when incorporating B in the ZSM-5. This corresponds to a decrease of 36.0%. The total acidic density decreases from 419 to 274 kJ/mol (decrease of 34.6%). The weak, medium and strong acidic density thus decreases all in a similar manner, with a decrease of around 35%.

The reported E_d values by the Ghent study are 115 and 84 kJ/mol for ZSM-5@25 and ZSM-5@25_B respectively. The B incorporation thus decreases the strength of the strong acidic peak.

When comparing ZSM-5@150_B with ZSM-5@150, a decrease from 13 to 6 $\mu\text{mol/g}$ for both the weak and medium sites is reported, which corresponds to a decrease of 55.8%. This is more than the decrease for the ZSM-5@25 sample, which had a decrease for the weak and medium sites of 33.3% when incorporating B. The strong and very strong acid site density decreases from 38 to 29 $\mu\text{mol/g}$ (decrease of 23.7%) and 23 to 8 $\mu\text{mol/g}$ (decrease of 65.2%) respectively. The combined strong acidic peak (strong and very strong) has a decrease of 39.3%. This is almost the same as the decrease in the B incorporated ZSM-5@25, which had a decrease of 36% for the combined strong site. The total acidic density of ZSM-5@150_B compared to ZSM-5@150 decreases from 86 to 49 kJ/mol (decrease of 43.0%).

Comparison of results at Ghent campus with this thesis

As stated earlier, the results of ZSM-5@25_B in this thesis seem to be incorrect. The increase in strong acidic sites in the B incorporated sample cannot be explained. The results of the ZSM-5@150_B are more in line with the expectations, and will be compared to those obtained in the Ghent research.

The density in weak sites in this thesis was found to decrease with 51.7% when incorporating B in ZSM-5@150. The decrease in strong sites is 71.4%. The total amount of acid sites decreased with 60%. The reported decrease at the Ghent campus was 55.8% for the weak and medium sites and 36% and for the combined strong sites. The total acid density decrease from the Ghent study is 43%. The decrease in weak and medium sites is similar. The decrease in strong acidic sites however, deviates significantly with values of 71.4% and 36% for this thesis and the Ghent research respectively. This could indicate that the found decrease for the strong acidic sites is too high.

In conclusion, incorporating B in ZSM-5 leads to a successful lowering of acid site density. In this thesis, the highest decrease was found for the stronger sites, while in the Ghent research the weak sites show a higher decrease in acid density. The Ghent results are quantitatively correct and thus probably more trustworthy.

In both the researches, it was found that incorporating B decreased the strength of the strong acidic site. In this thesis, B incorporation in ZSM-5@25 led to a decrease from 133.95 to 113.46 kJ/mol. B incorporation in ZSM-5@150 showed a decrease from 98.97 to 84.58 kJ/mol. The Ghent research only analyzed the E_d of ZSM-5@25 with B incorporation. A decrease from 115 to 84 kJ/mol was reported. The trends of these results are thus similar, but the absolute values differentiate from each other. It is however clear that the B incorporation lowers the acid strength significantly. This indicates that not only the acid density on the catalysts decreased, but also the strength of the sites. This modification is thus useful in the tempering of the acidity in the ZSM-5 catalyst, both in acid density and strength.

3.2.3.4 Influence of using hybrid ZSM-5 with CeO₂

Two methods were used to prepare a hybrid catalyst containing ZSM-5 and CeO₂ with the aim of tempering the acidity. The NH₃-TPD spectra, acid site concentration and E_d results for ZSM-5@25, CeO₂/ZSM-5 and ZSM-5@CeO₂ are shown in Figure 54, Figure 55 and Table 25.

Table 25: acid site concentration results of ZSM-5@25 and the hybrid catalysts

Catalyst	Weak sites ($\mu\text{mol/g}_{\text{cat}}$)	Strong sites ($\mu\text{mol/g}_{\text{cat}}$)	Total sites ($\mu\text{mol/g}_{\text{cat}}$)	E_d (kJ/mol)
ZSM-5@25	162 ± 4	43 ± 6	205 ± 7	133.95 ± 2.51
CeO₂/ZSM-5	63 ± 4	9 ± 3	72 ± 5	98.80 ± 2.51
ZSM-5@CeO₂	213 ± 17	65 ± 12	278 ± 20	134.60 ± 2.51

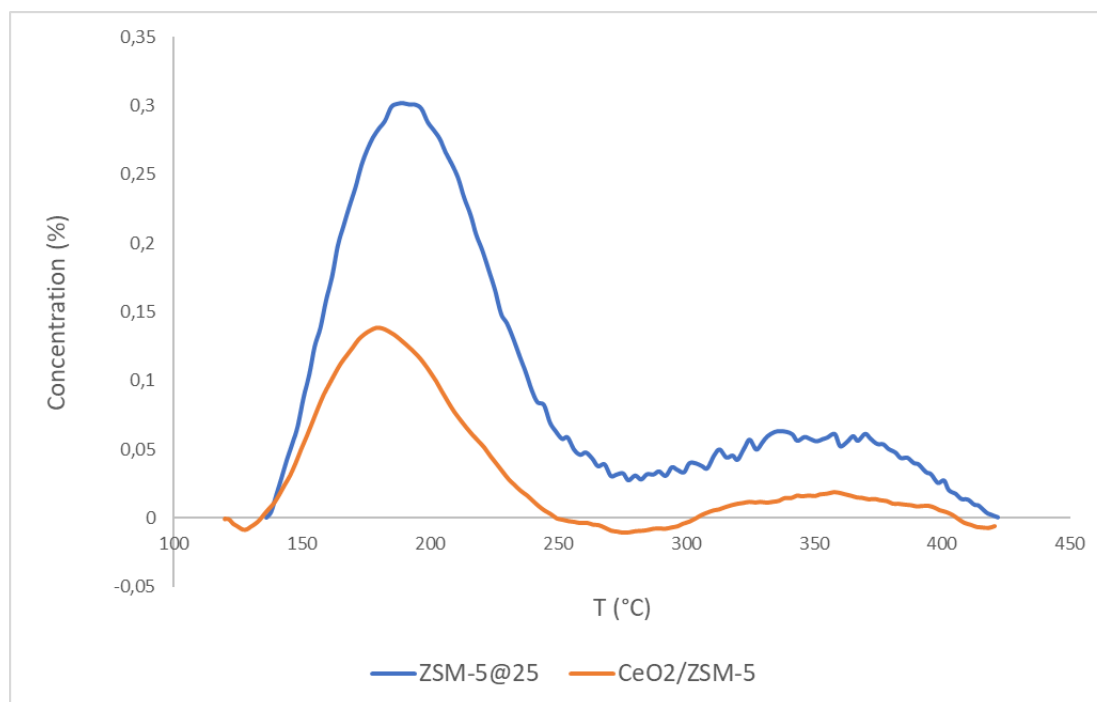


Figure 54: NH₃-TPD spectra of ZSM-5@25 and CeO₂/ZSM-5

The hybrid CeO₂/ZSM-5, where ZSM-5 is dispersed on CeO₂, shows a successful tempering in acidity of the catalyst. A decrease of 61.1%, 79.6% and 64.9% is found for the weak, strong and total acidic sites respectively. The strength of the strong acidic sites decreases to 98.80 ± 2.51 kJ/mol compared to 133.95 ± 2.51 kJ/mol of the pure ZSM-5. This hybrid method seems thus to be an efficient way to obtain a decrease in acidic concentration and acidic site strength in ZSM-5.

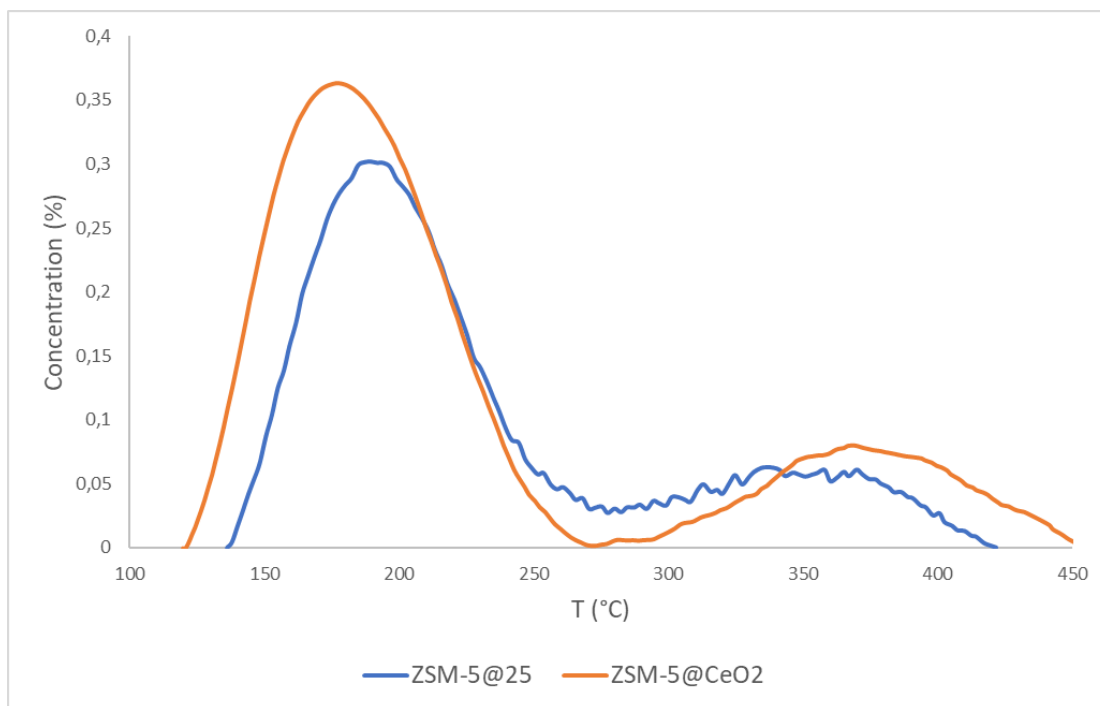


Figure 55: NH_3 -TPD spectra of ZSM-5@25 and ZSM-5@CeO₂

An unexpected result is obtained for the ZSM-5@CeO₂ hybrid catalysts. Here, a core-shell topology is obtained, with ZSM-5 being the core and CeO₂ the shell. A significant increase in both weak acidic (31.5%) and strong acidic sites (51.2%) is observed. A similar E_d value of 134.60 ± 2.51 kJ/mol as for ZSM-5 is found, which has a value of 133.95 ± 2.51 kJ/mol. These results appear to show that the tempering of the acidity has not been achieved. On the contrary, an increase in acid site density is observed. This result is unlikely, and does not correspond with the result from the Ghent study. This should thus probably be refuted.

Discussion of the acidity results from the Ghent campus

The results of the research at the Ghent campus are discussed, in order to be able to give conclusions with more certainty and also give quantitative values for the acid density in the samples. The spectra do not have the baseline problem, and the deconvolution was performed for four peak strengths, being weak, medium, strong and very strong sites. The results are summarized in Table 26 and the deconvoluted TPD spectra of CeO₂/ZSM-5 and ZSM-5@CeO₂ are shown in Figure 56 and Figure 57 respectively. The E_d values were not determined for the hybrid catalysts.

Table 26: acid site concentration results of ZSM-5@25 and hybrid catalysts (Ghent campus)

Catalyst	Weak sites ($\mu\text{mol}/\text{g}_{\text{cat}}$)	Medium sites ($\mu\text{mol}/\text{g}_{\text{cat}}$)	Strong sites ($\mu\text{mol}/\text{g}_{\text{cat}}$)	Very strong sites ($\mu\text{mol}/\text{g}_{\text{cat}}$)	Total sites ($\mu\text{mol}/\text{g}_{\text{cat}}$)
ZSM-5@25	120	120	112	66	419
CeO ₂ /ZSM-5	36	32	69	37	174
ZSM-5@CeO ₂	80	81	92	50	304

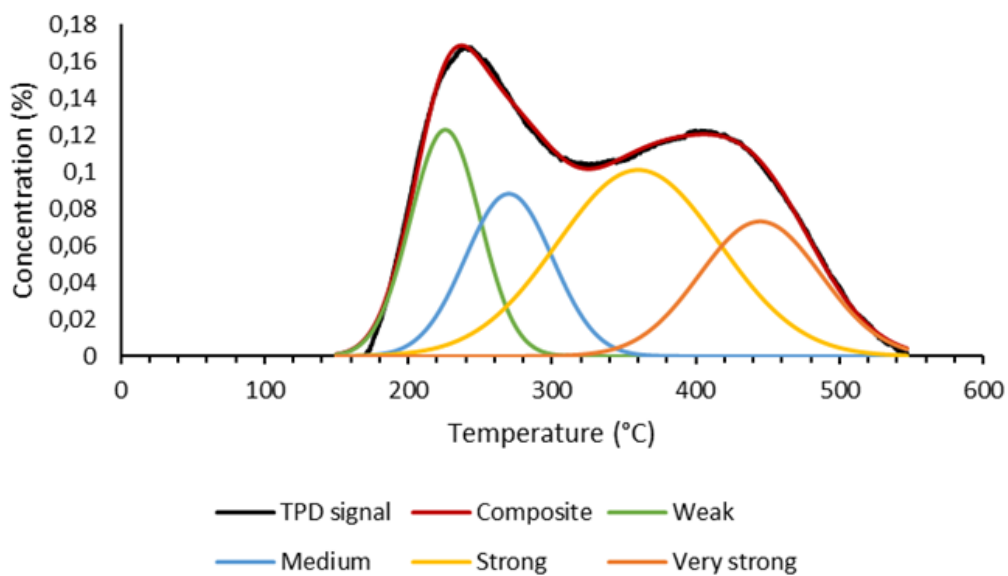


Figure 56: NH₃-TPD spectrum for CeO₂/ZSM-5 (Ghent campus)

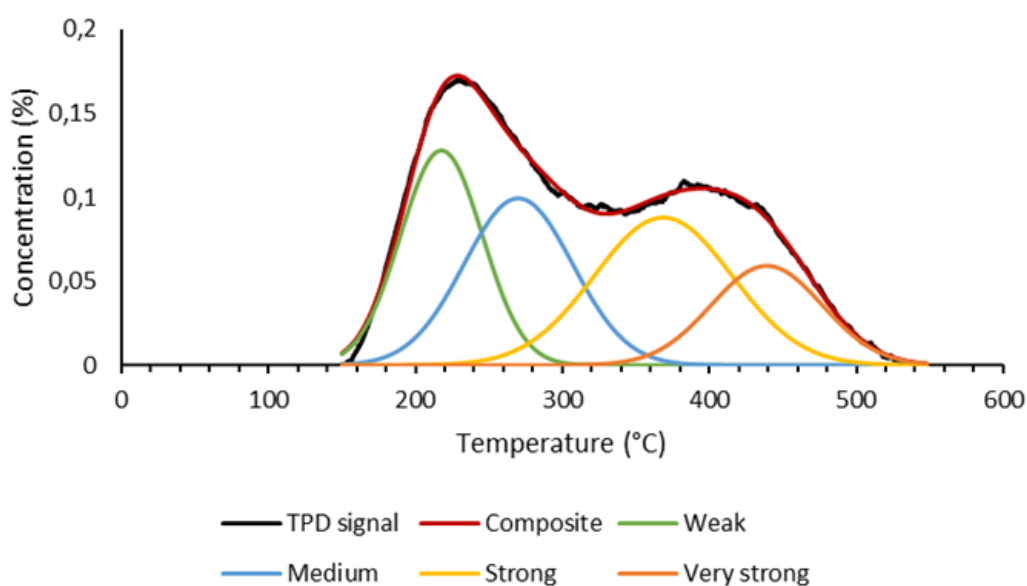


Figure 57: NH₃-TPD spectrum for ZSM-5@CeO₂ (Ghent campus)

When comparing CeO₂/ZSM-5 with ZSM-5@25, a decrease from 120 to 36 μmol/g and from 120 to 32 μmol/g for the weak and medium sites respectively is reported, which corresponds to a decrease of 70% and 73.3%. The strong acid site density decreases from 112 to 69 μmol/g (decrease of 38.4%) and the very strong site from 66 to 37 μmol/g (decrease of 43.9%). The combined strong acidic peak (strong and very strong) shows a decrease of 40.4%. The total acidic density decreases from 419 to 174 μmol/g (decrease of 58.5%). The most significant decrease is thus observed for the weak and medium acidic sites.

When comparing ZSM-5@CeO₂ with ZSM-5@25, a decrease from 120 to 80 μmol/g and from 120 to 82 μmol/g is found for the acid density of the weak and medium site respectively. The strong and very strong acid site density decreases from 112 to 92 μmol/g (decrease of 17.9%) and 66 to 50 μmol/g (decrease of 24.2%) respectively. The combined strong acidic peak (strong and very strong) shows a decrease of 20.2%. The total acidic density of ZSM-5@CeO₂ compared to ZSM-5@25 decreases from 419 to 304 μmol/g (decrease of 27.4%). A lower decrease in acid density is thus reported, compared to the CeO₂/ZSM-5 catalyst.

Comparison of results at Ghent campus with this thesis

The density in weak sites of CeO₂/ZSM-5 in this thesis was found to decrease with 61.1% compared to ZSM-5@25. The decrease in strong sites is 79.6% and the total amount of acid sites decreased with 64.9%. The reported decrease at the Ghent campus was ca. 72% for the weak and medium sites and 40.4% for the combined strong sites. The total acid density decrease from the Ghent study is 58.5%. In this thesis, the highest decrease was found for the strong sites. In the Ghent study however, the highest decrease was found for the weak and medium acidic sites. The result of the Ghent study are probably more reliable. The total sites show a more similar decrease, with a value of 64.9 and 58.5% for this thesis and the Ghent study respectively. It can be concluded that the use of the CeO₂/ZSM-5 leads to a successful lowering of both the weak and stronger acid site density.

The E_d value for CeO₂/ZSM-5 was only determined in this thesis, and showed a decrease from 133.95 to 98.80 kJ/mol for the CeO₂/ZSM-5 catalysts compared to ZSM-5@25. This indicates that not only the acid density on the catalyst decreased, but also the strength of the sites. This modification is thus useful in the tempering of the acidity in the ZSM-5 catalyst, both in acid density and strength.

The density in acidic sites of ZSM-5@CeO₂ in this thesis was found to increase significantly, with 31.5% and 51.2% for the weak and strong acidic sites respectively. This unexpected result is different from the one in the Ghent study, where the expected decrease was observed. This is a remarkable finding and does not correspond with the results of the home campus (Ghent), where a decrease in acidic sites is found, although not as high a decrease as in the hybrid CeO₂/ZSM-5. For comparison, at the home campus a decrease in total acid sites for CeO₂/ZSM-5 of 58.5% is found. The decrease in total acid sites of ZSM-5@CeO₂ was only 27.4%. Why the decrease for ZSM-5@CeO₂ is not visible in this thesis is not clear. It is possible that a big error on the experiment led to these uncertain results.

As the results at the home campus are more trustworthy (e.g. no spectra and base line issues), it can be concluded that the tempering of the acidity is achieved for both of the hybrid catalysts, although in this research, it was only confirmed for the CeO₂/ZSM-5 catalyst. The method for CeO₂/ZSM-5 led to the highest decrease in acid sites. This conclusion is made by using the data obtained at the home campus, as the data in this thesis for ZSM-5@CeO₂ does not seem to be representative.

The E_d value for ZSM-5@CeO₂ was only determined in this thesis, and showed no decrease in strength of the strong acidic site with values of 133.95 and 134.60 kJ/mol for the ZSM-5 and ZSM-5@CeO₂ catalyst respectively. It is unclear if this result is valuable, as it could not be confirmed by the data from the Ghent research.

3.2.4 Basicity study with CO₂-TPD

The corrected CO₂-TPD spectra of all samples for the three different heating rates (10, 15, 20°C/min) are shown in Appendix I: corrected and deconvoluted CO₂-TPD spectra. The modeled peaks from the deconvolution are visible. Because a gas concentration calibration was performed, the area under the peaks can be correlated to the amount of desorbed CO₂ per gram catalyst. It is a unit of the basic active sites concentration on the sample. This basic concentration is determined for all the heating rates and a mean value with standard deviation on the experimental values is obtained.

In the next chapter, the basic properties of the hybrid catalysts will be discussed. For a visual comparison between the samples, the shown spectra are those of 15°C/min for all the catalysts. The determined basic concentrations are however determined from the TPD data of all the heating rates.

By performing the TPD at three different heating ratio's, the desorption energy (E_d) of the basic peak, which is a parameter for the strength of the strong acidic sites, was calculated by using equation (10). The plotted Arrhenius curves for all the samples are placed in Appendix J: Arrhenius plots for E_d determination of the basic sites. The derived E_d results are listed in Table 27. For CeO₂/ZSM-5, no E_d value was obtained because the spectra for 20°C/min was lost and the data of the other heating ratios did not led to a rising slope. None of the experiments were repeated, hence no experimental error was calculated. The samples were not characterized at the Ghent campus, so no discussion of these results to obtain a more certain conclusion is possible. The obtained values and conclusions are thus not very trustworthy and only give an rough estimation without much certainty of the result.

Table 27: CO₂-TPD desorption energy results

Catalyst	T _{max} (10°C/min, °C)	T _{max} (15°C/min, °C)	T _{max} (20°C/min, °C)	E _d (kJ/mol)
CeO₂	78.9	81.8	85.1	110.83
CeO₂/ZSM-5	74.2	69.6	/	/
ZSM-5@CeO₂	78.2	81.8	85.1	99.45

3.2.4.1 Basic properties of the hybrid catalysts

The basic density results are summarized in Table 28. Figure 58 and Figure 59 compare the TPD spectra of pure CeO₂ with CeO₂/ZSM-5 and ZSM-5@CeO₂ respectively. Pure CeO₂ shows a basic peak at a low temperature (around 80°C). This basic peak is tried to be incorporated in the ZSM-5 catalysts to achieve basic properties.

Table 28: basic density results from CO₂-TPD experiments

Catalyst	Basic sites (μmol/g _{cat})
CeO₂	11.82 ± 0.13
CeO₂/ZSM-5	0.81 ± 0.14
ZSM-5@CeO₂	4.41 ± 1.37

Analogue as with NH₃-TPD, these values are mostly valuable for comparative purposes between the catalysts and cannot be reported as correct absolute values. However, because only one peak is obtained in the TPD spectrum, the baseline correction is probably performed more correctly than on the NH₃-TPD spectra. Hence, the obtained basic site density values for the CO₂-TPD are expected to be more quantitatively valuable than those of the NH₃-TPD study.

Pure CeO₂ shows a basic peak at a low temperature (around 80°C). This is a lower temperature than the reported temperature of 110°C by Yoshikawa et al. (2016) for a heating rate of 10°C/min [142]. The basic density of the basic peak is 11.82 μmol/g_{cat}. This basic peak is tried to be incorporated in the ZSM-5 catalysts to achieve basic properties.

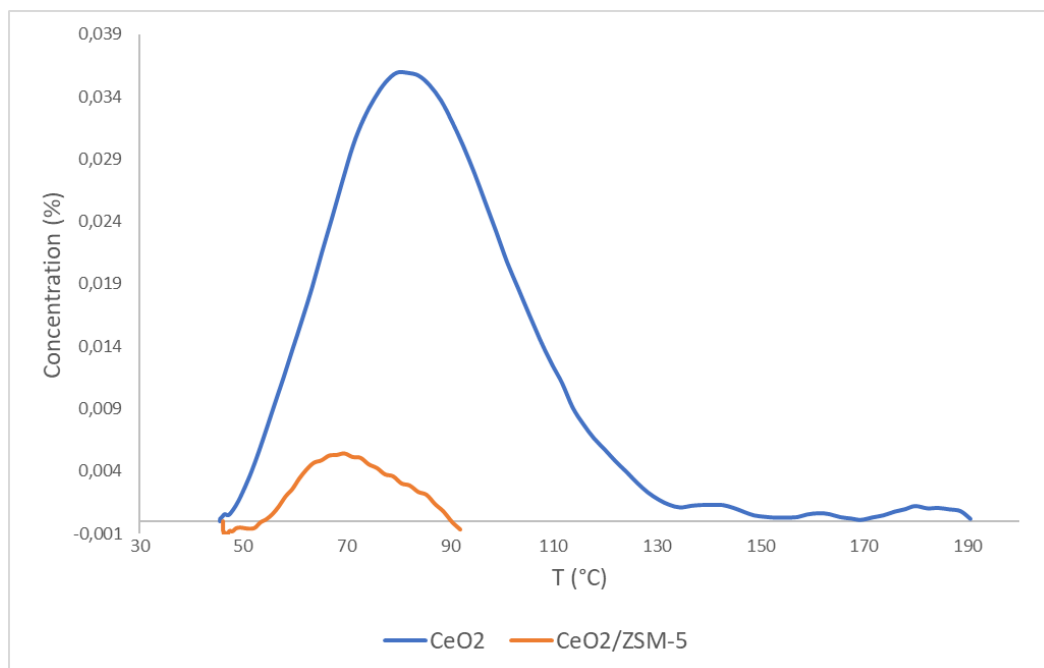


Figure 58: CO_2 -TPD spectra of CeO_2 and $\text{CeO}_2/\text{ZSM-5}$

The hybrid $\text{CeO}_2/\text{ZSM-5}$ shows only a very small basic peak. The concentration of basic sites is less than 6% of the value for pure CeO_2 , with a density of $0.81 \mu\text{mol}/\text{g}_{\text{cat}}$. Half of the catalyst is CeO_2 and half is ZSM-5 which means that if all the basic properties were incorporated in the ZSM-5, the basic concentration would be half of the value for CeO_2 . It is however far lower, which means that the basic properties of CeO_2 is not significantly inhibited in the catalyst. In this hybrid structure, ZSM-5 is dispersed on CeO_2 . This could mean that the CeO_2 particles are not very available on the surface of the catalyst. The basic peak is shifted to a lower temperature, and thus seems to have a lower strength than in pure CeO_2 . The reason for this is not certain. It is possible that the addition of ZSM-5 to CeO_2 alters the surface composition and create new surface species. The acidic sites of ZSM-5 possibly interact with the basic sites of CeO_2 which leads to a decrease in basic strength. The surface structural properties could also be altered. This are only possibilities, and could be researched in the future by surface analysis techniques.

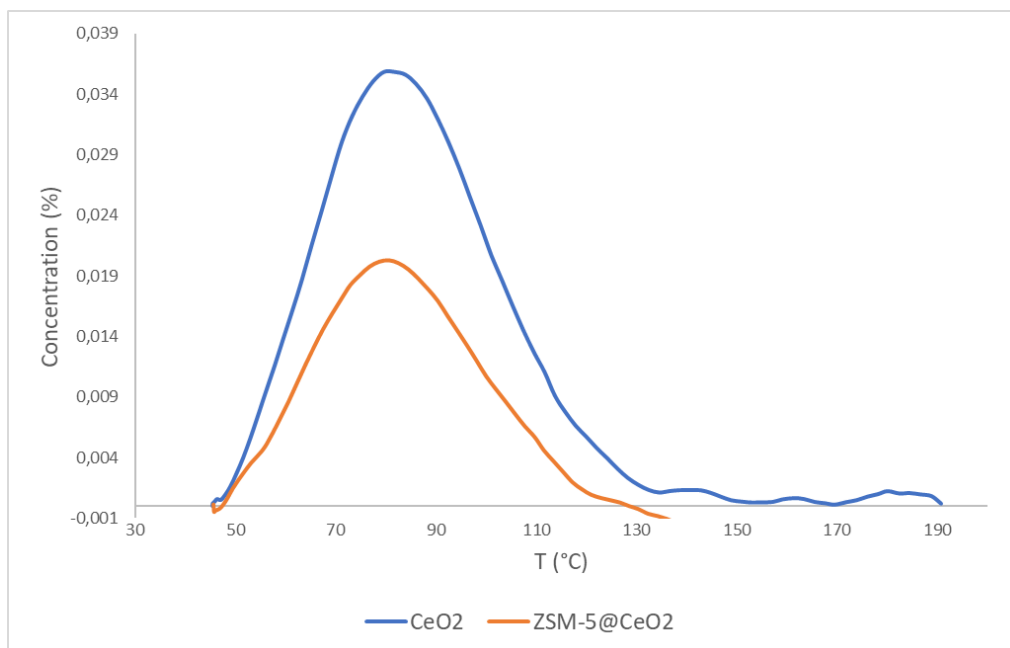


Figure 59: CO_2 -TPD spectra of CeO_2 and ZSM-5@CeO_2

ZSM-5@CeO_2 shows a far less decrease in basic sites compared to $\text{CeO}_2/\text{ZSM-5}$, with a basic site density of $4.41 \mu\text{mol/g}_{\text{cat}}$. The concentration of basic sites is 37.3% of those in CeO_2 . A slightly lower E_d value for ZSM-5@CeO_2 is obtained in comparison to pure CeO_2 , with values of 99.45 and 110.83 kJ/mol. The basic sites (obtained from the CeO_2) thus have a slightly decreased strength in the hybrid ZSM-5@CeO_2 catalyst. This is not clearly visible on the TPD spectra, where the peak of the hybrid catalyst is located at the same temperature of the one for pure CeO_2 . The minor shift indicates that the basic strength does not decrease as much as with the $\text{CeO}_2/\text{ZSM-5}$ catalyst.

This method for the preparation of the hybrid catalyst is superior in incorporating the basic sites of CeO_2 into the ZSM-5 catalysts compared to $\text{CeO}_2/\text{ZSM-5}$. The basic sites are readily available on the surface of the catalyst, which probably is due to the fact that the CeO_2 is the shell in the core-shell structure. The species is thus more exposed at the surface of the catalyst.

3.2.5 ZSM-5 modifications and hybrid catalysts effect on the dehydration of 1,3-BDO

In the literature study, it was discussed that ZSM-5 is a performant catalyst for the dehydration of 1,3-butanediol to butadiene. It was reported that catalysts with decreased acid density and strength showed the highest conversion and selectivity to butadiene. Tempering the acidity of ZSM-5 , by lowering the acid density and strength is beneficial to obtain a more efficient catalysts, with the aim of maximizing the butadiene output of the reaction. ZSM-5 was modified by increasing the Si/Al ratio and incorporating B. Hybrid CeO_2 with ZSM-5 catalysts were also prepared.

Increasing the Si/Al from 25 to 150 has proven to significantly lower the acid density and strength, with a decrease of 75.6% and 79.5% in acid sites for this thesis and the Ghent study respectively. The E_d value decreases from 133.95 to 98.97 kJ/mol. The modification thus lowered the acid density and acid strength, which has been reported to promote the dehydration of 1,3-BDO to BD.

When B is incorporated in ZSM-5@25, a decrease in total acid sites of 34.6% was found in the Ghent study. The density result from this thesis seemed to be incorrect. The reported change in E_d is 133.95 to 113.46 kJ/mol and 115 to 84 kJ/mol for this and the Ghent research respectively. This thesis found higher E_d values than the Ghent research, but the decreasing trend with the incorporation of B is similar. A significant decrease in acid strength is observed. The modification thus also lowered the acid density and acid strength, which has been reported to promote the dehydration of 1,3-BDO to BD.

When B is incorporated in ZSM-5@150, a decrease in total acid sites of 60% was found in this thesis while 43% is reported in the Ghent study. The change in E_d reported in this thesis is 98.97 to 84.58 kJ/mol. Again, the acid density and strength was successfully lowered.

When the two modifications are combined (thus comparing ZSM-5@25 with ZSM-5@150_B), a decrease of 90.2% and 88.3% in this thesis and the Ghent thesis respectively was found. The E_d value decreases from 133.95 to 84 kJ/mol. A very high degree of acidic tempering is obtained, and can probably improve the reaction with a high selectivity to butadiene.

The hybrid CeO₂/ZSM-5 shows a decrease in total acid sites of 64.9% and 38.4% in this thesis and the Ghent research respectively. The change in E_d reported in this thesis is 133.95 kJ/mol to 98.80 kJ/mol compared to ZSM-5@25. A significant decrease in acid density and strength is observed.

The hybrid ZSM-5@CeO₂ shows a decrease in total acid sites of 27.4% in the Ghent research. In this thesis, an increase was found and the results were refuted. No change in E_d is reported in this thesis with values 133.95 kJ/mol and 134.60 kJ/mol for ZSM-5@25 and ZSM-5@CeO₂ respectively. This can however not be confirmed by data from the Ghent campus, and is not likely to be correct. The decrease in acid density of the Ghent campus is the most trustworthy result. The decrease is lower than the decrease in the hybrid CeO₂/ZSM-5. The most effective method for the hybrid catalyst is thus the CeO₂/ZSM-5. In this case, the acidity is tempered the most, with a significant lowering of both the acid density and strength

The basicity of pure CeO₂ and the hybrid catalysts was also characterized. ZSM-5@CeO₂ showed a good basic site incorporation compared to CeO₂/ZSM-5, but as stated before a lower acid tempering was found. An optimal balance between acidic tempering and base incorporation should be found for the hybrid catalysts and has to be further investigated.

In conclusion, these ZSM-5 modifications and the use of hybrid CeO₂ and ZSM-5 catalysts were found to be successful in tempering the acidity. The hybrid ZSM-5@CeO₂ also has a good basic site incorporation.

These modification probably improve the dehydration reaction of 1,3-BD and selectivity to BD. To be able to confirm if these catalysts have good activity and stability, reactor tests should be performed. The selectivity to BD is very important, as the goal is to maximize this output stream.

3.3 Future research

3.3.1 Supported metal catalysts for the depolymerization of lignin

The Pd dispersion of Pd and PdCu catalysts supported on Al_2O_3 , SiO_2 and AC has been investigated. The results were discussed and an attempt was made to link the dispersion results to provided reactor results for the lignin depolymerization with these catalysts. A hypothesis for the best performing catalysts was made. It was stated that the catalyst with the highest reported dispersion in this research on a non-acidic support, which is the Pd/AC catalyst, reached the highest M_w reduction in the shortest amount of time. The fastest initial depolymerization rate is found for PdCu/ Al_2O_3 , that has an acidic support and the highest reported dispersion of all the catalysts in this thesis. However, the depolymerization rate slows down and a high M_w reduction rate is reached after a far longer reaction time.

Further research is thus needed to confirm whether a catalyst with medium to high dispersion on a non-acidic support is indeed beneficial for this reaction. How the reaction-mechanism is affected by the catalyst properties should also be further investigated. The reactor study was performed, but a clear correlation between the catalyst properties and the performance for the lignin depolymerization was not yet found. This should be further researched, by performing more characterization studies and possibly reactor studies.

The catalyst can be further varied in terms of metal loading, Pd/Cu ratio or preparation method. These factors will have influence on the properties like the Pd dispersion and can possibly improve the activity for the lignin depolymerization reaction.

3.3.2 ZSM-5 catalysts for the dehydration of 1,3-BDO

By combining the (comparative) results of this thesis and the results from the Ghent study on the same catalyst samples, it was confirmed that using ZSM-5 with a increases Si/Al ratio, B incorporation or the use of hybrid ZSM-5 with CeO_2 , decreased the acid density. For most of the samples, the acidic strength also decreased.

This was not reported for ZSM-5@CeO₂, as the result in this thesis for the sample was uncertain, and the Ghent study did not investigate the site strength for this sample. No certain statement of the acid strength of ZSM-5@CeO₂ could thus be made.

These tempered catalysts are expected to have a beneficial effect on the dehydration reaction of 1,3-BDO to BD. This should be confirmed by performing a reactor study. The modified and hybrid ZSM-5 should have an increased conversion of 1,3-BDO and selectivity to BD. When this is achieved, a great step to a viable catalysts is made. A selection can then be made of the best performing catalyst for this reaction.

When a performant ZSM-5 catalyst is selected, an attempt can be made to further improve the catalyst. Possible improvements can be made by further increasing the Si/Al ratio, using different amounts of B in the sample and improving the incorporation method, using different amount of CeO₂... Repeated characterization in regard to their acidity and basicity and reactor studies can then again select an efficient catalyst, so that a very performant catalyst can be found for the dehydration of 1,3-BDO.

The basicity of pure CeO₂ and hybrid CeO₂ with ZSM-5 was characterized. The impact of the basic properties that are apparent in ZSM-5@CeO₂ should be further investigated. This hybrid catalyst showed a good basic site incorporation compared to CeO₂/ZSM-5, but a lower acid tempering. A optimal balance between acidic tempering and base incorporation should be found for the hybrid catalysts. This should be done by analyzing future reactor studies, so that a better understanding of the basic properties can be achieved.

4 Conclusion

This thesis aimed to characterize important active sites on some promising catalysts for two different reactions, the mild reductive lignin depolymerization and the dehydration of 1,3-BDO. For the former reaction, the Pd dispersion on Pd and PdCu supported on Al_2O_3 , SiO_2 and AC was determined with CO pulse chemisorption. For the dehydration of 1,3-BDO, the modified and hybrid ZSM-5 catalysts were analyzed with NH_3 - and CO_2 -TPD to characterize their acid and basic properties respectively. For both reactions, an attempt was made to link the reported properties to the reaction and select some promising catalysts samples. The results for both studies are summarized in the following sections.

4.1 Supported metal catalysts for the depolymerization of lignin

The CO pulse chemisorption study led to the following dispersion results. The Pd dispersion is found to be greatly influenced by both the catalyst support and the presence of the co-metal Cu. Of the monometallic Pd catalysts, the dispersion is the highest for Pd/AC, followed by Pd/ Al_2O_3 and Pd/ SiO_2 with values of respectively 12.68%, 8.89%, and 2.13%. The bimetallic PdCu samples demonstrate a different dispersion trend. Of the bimetallic catalysts, PdCu/ Al_2O_3 exhibits the highest dispersion, followed by PdCu/AC and PdCu/ SiO_2 , with values of 22.17%, 10.46%, and 1.58%, respectively. Based on these findings, some remarks can be made. Notably, the SiO_2 supported catalysts show a remarkably low dispersion. The highest reported Pd dispersion value is 22.17% on PdCu/ Al_2O_3 . However, the monometallic Pd/ Al_2O_3 exhibits a far lower dispersion of 8.89%. The AC supported samples displayed an intermediate dispersion value, with only a slight variation in the mono and bimetallic catalyst. Pd/AC showed a slightly higher dispersion of 12.68% compared to 10.46% for PdCu/AC. The dispersion values were tried to be correlated with the catalysts properties and compared to values reported in other studies. These observations shed light on the critical role played by the catalyst support type and the inclusion of a co-metal in modulating the dispersion of the Pd-based catalysts.

The dispersion results were linked to a particle size study by TEM-EDX (not performed by the writer of this thesis). The global trend that smaller observed surface particles led to a higher determined Pd dispersion was confirmed, with some slight deviations. Only the Pd/ Al_2O_3 catalysts did not comply with this theory, with a far too low dispersion. The reason for this is yet unknown and needs further research. The deviations are possibly due to the many assumptions in the used correlation between particle size and dispersion, and due to the fact that the particle size is influenced by the Cu addition, while the dispersion is only determined in regard to the Pd particles.

A reactor study (from the Ghent campus) was also analyzed. It was observed that Pd/AC, the catalyst with the highest dispersion value of the non-acidic supported catalysts, displayed the fastest depolymerization to a high M_w reduction of around 85%. The fastest initial depolymerization rate is observed for PdCu/Al₂O₃, which possesses an acidic support and has the highest reported dispersion among all the catalysts characterized in this study. However, as the reaction progresses, the depolymerization rate decreases, ultimately reaching a high M_w reduction but after a significantly longer reaction time than Pd/AC. It is noteworthy that the monometallic Pd/Al₂O₃ catalyst does not exhibit this rapid initial phase of depolymerization, although also having the acidic support. The low dispersion value compared to PdCu/Al₂O₃ could be the reason for this. Interestingly, a similar fast initial rate of M_w reduction is observed for the non-acidic PdCu/SiO₂ catalyst, while showing a very low dispersion. Consequently, it becomes apparent that the fast initial M_w reduction is not solely influenced by the acidity and dispersion of the catalyst. In conclusion, Pd/AC, with a non-acidic support and a relatively high dispersion of 12.68% compared to the other non-acidic catalysts, seems the most efficient for the depolymerization of lignin to a high M_w reduction. The initial rate is not the fastest, but the depolymerization rate stays high for a long time.

To confirm whether a catalyst with medium to high Pd dispersion on a non-acidic support is indeed beneficial for the mild reductive depolymerization of lignin and how the reaction mechanism is influenced by the catalysts properties, further research is needed.

This thesis tries to contribute in the understanding of catalysis for the lignin depolymerization. It focusses on the importance of catalyst characteristics, particularly dispersion and support acidity, in enhancing the efficiency of this reaction.

4.2 ZSM-5 catalysts for the dehydration of 1,3-BDO

The literature study discussed the effectiveness of ZSM-5 as a catalyst for the dehydration of 1,3-butanediol to butadiene. It was observed that catalysts with reduced acid density and strength exhibited higher conversion rates and selectivity towards butadiene. In this thesis, the acidity of ZSM-5 was tempered by decreasing the acid density and strength, aiming to enhance the efficiency of the catalyst and maximize the butadiene output. This was achieved through modifications such as increasing the Si/Al ratio and incorporating Boron. Additionally, hybrid CeO₂ with ZSM-5 catalysts were prepared.

When the Si/Al ratio was increased from 25 to 150, a significant decrease in acid density and strength was observed. This thesis reported a reduction of 75.6% in acid sites, while the Ghent study reported a decrease of 79.5%. The energy of desorption (E_d) value decreased from 133.95 to 98.97 kJ/mol. This indicates that the modification successfully lowered the acid density and strength.

Incorporating B in ZSM-5@25 led to a decrease of 34.6% in total acid sites according to the Ghent study. The density result in this thesis appeared to be incorrect. The reported change in E_d was 133.95 to 113.46 kJ/mol in this thesis and 115 to 84 kJ/mol in the Ghent research.

Despite the difference in E_d values, both studies demonstrated a significant decrease in acid strength. The modification with B effectively lowered the acid density and strength.

For ZSM-5@150, incorporating B resulted in a decrease of 60% in total acid sites in this thesis, while the Ghent study reported a decrease of 43%. The change in E_d reported in this thesis was 98.97 to 84.58 kJ/mol. Once again, the acid density and strength were successfully reduced, concluding that the B incorporation tempers the acidity for ZSM-5 samples with varying Si/Al ratio.

When comparing the combined modifications (ZSM-5@25 with ZSM-5@150_B), a decrease of 90.2% and 88.3% in total acid sites was observed in this thesis and the Ghent thesis, respectively. The E_d value decreased from 133.95 to 84 kJ/mol. A high degree of acidic tempering is thus obtainable.

The hybrid CeO₂/ZSM-5 catalyst showed a decrease of 64.9% and 38.4% in total acid sites in this thesis and the Ghent research, respectively. The change in E_d reported in this thesis was 133.95 kJ/mol to 98.80 kJ/mol compared to ZSM-5@25.

The hybrid ZSM-5@CeO₂ showed conflicting results regarding the decrease in total acid sites. In this thesis, an increase was found, but these results were refuted and considered incorrect. No change in E_d was reported in this thesis for ZSM-5@CeO₂. The most reliable result was the decrease in acid density from the Ghent study, although it was lower than the decrease observed in the hybrid CeO₂/ZSM-5 catalyst. Therefore, the hybrid CeO₂/ZSM-5 catalyst appears to be the most effective method for tempering the acidity. However, a far higher basic density was found in ZSM-5@CeO₂ compared to CeO₂/ZSM-5, with values of respectively 4.41 and 0.81 $\mu\text{mol/g}_{\text{cat}}$. This possibly also has a beneficial influence on the conversion and selectivity to BD. A good balance between the acidity and basicity has to be found in future research.

In conclusion, the proposed ZSM-5 modifications and the use of hybrid CeO₂ and ZSM-5 catalysts were found to be successful in tempering the acidity. The hybrid ZSM-5@CeO₂ also has a good basic site incorporation, but has a lower acidic tempering than the hybrid CeO₂/ZSM-5. A good balance between this has to be found. The tempering of the acidity and adding of a basic site possibly leads to an improved conversion and selectivity to BD in the dehydration of 1,3-BDO. This should be confirmed by reactor studies in the future.

5 Sustainability review

5.1 Green catalysis

This research tries to help in developments in the field of green chemistry, more specifically green catalysis. Green catalysis can be defined as the use of catalysts to enable chemical reactions that reduce or completely avoid harm to the environment. Green catalysts can considerably lower energy and/or use new reaction pathways that use waste streams from other processes, resulting in more ecologically friendly and long-lasting chemical processes. However, it is essential to comprehend the characteristics and behavior of catalysts, which necessitates catalyst characterization, in order to optimize catalysis and obtain the best results. This thesis focusses on the characterization of catalysts that can be used for renewable reaction pathways to sustainable platform chemicals, more specific the depolymerization of lignin to monomeric phenols (used for a large amount of products such as polymers, fuels, lubricants, additives...) and the dehydration of 1,3-butanediol to butadiene (mostly used for the production of butadiene rubber). How these reaction pathways can help in the production of green chemicals, is discussed earlier in the literature study.

12 principles of green chemistry have been formulated, which are shown in Figure 60 [143]–[145].



Figure 60: 12 principles of green chemistry

Some key principles of green chemistry and catalysis will be shortly discussed [145]. An important concept is the atom economy of a reaction, it corresponds with how efficient the reaction is. Basically, the more atoms of the reactants that are incorporated into the final products, the more efficient the reaction. Even if the yield of a reaction is very high, a low atom economy value (%) can be observed if a lot of the reactant atoms are converted to non-desired byproducts. The atom economy is defined as the percentage of reactant atoms which end up in the wanted product. The higher this value (max. 100% if all the atoms are incorporated in the useful products), the more efficient the feedstock is used and the smaller the amount of waste products [145]. The higher the selectivity to the desired product, the higher the atom economy will be. It has been discussed in the literature study how the selectivity for the wanted products can be increased. In the depolymerization of lignin, monomeric phenols are the wanted products. In the dehydration of 1,3-BDO, butadiene is the wanted product. By characterizing and testing the catalysts in a reactor study, the catalysts that leads to the highest activity and selectivity is tried to be found. In this thesis, only the characterizing part has been performed and hypothesis for efficient catalysts is tried to be made. Follow-up research is needed to confirm the promising catalysts and find the optimal reaction condition. This research thus helps in optimizing the atom economy of the discussed reaction.

The use of renewable feedstocks is also an important aspect in green chemistry and catalysis. Examples are biomass, carbon dioxide or water as sources for the reaction. This reduces the need for non-renewable sources like hydrocarbons. In this thesis, the feedstocks satisfy these goals. Lignin and 1,3-BDO are very abundant sources, as discussed in the literature study.

Green catalysts should be non-toxic, do not cause harm to the environment, are readily available and abundant and can be recycled. The catalyst should also be stable to enable for a long time of use. Good examples are zeolites, metal-organic frameworks (MOF) or enzymes. In the relation to the working of the catalyst, the use of solvents for the reactions should be minimized, because these solvents are often toxic and cause harm to the environment [144].

A very important aspect of green chemistry and catalysis is the reduction of energy consumption. Catalysis can significantly lower the required energy by using reaction pathways at lower temperatures and pressure [144].

Overall, the concepts of green chemistry and catalysis have the goal to develop more sustainable chemical processes that minimize waste and harm to the environment, reduce energy consumption, and promote the use of renewable feedstocks. This thesis tries to help in developments for the two discussed reactions, that aim to fulfill these goals.

5.2 The SDG's and green catalysis

The Sustainable Development Goals (SDG's) are an important worldwide agenda that cover a variety of topics, from environmental preservation to the eradication of poverty [146]. The SDG's offer a roadmap for attaining sustainable development, which supports social inclusion, economic expansion, and environmental preservation [147]. The 17 SDG's are listed in Figure 61 [148]. These objectives demand innovation and progress across many industries, including the industrial chemical sector. The chemical sector has a significant direct or indirect influence on almost all of the SDG's. Advances can lead to important steps for reaching the following goals: no poverty; zero hunger; good health and well-being; clean water and sanitation; affordable and clean energy; decent work and economic growth; industry, innovation and infrastructure; sustainable cities and communities; responsible consumption and production; climate action and life below water and on land (SDG's 1, 2, 3, 6, 7, 8, 9, 10, 11, 12, 13, 14, 15, 16). The chemical industry thus has an enormous opportunity to make a difference in these fields. For example on climate action: the chemical industry is the largest industrial energy consumer and the third largest industry subsector in terms of direct CO₂ emissions [149].



Figure 61: sustainable development goals

In many different ways, green catalysis and catalyst characterization are related to the SDG's. For instance, SDG 7 seeks to guarantee that everyone has access to reasonably priced, dependable, sustainable, and modern energy. By enabling more effective and environmentally friendly energy production, green catalysis can significantly contribute to the achievement of this objective. SDG 12 also emphasizes maintaining sustainable production and consumption habits.

By encouraging the use of renewable resources and minimizing waste in industrial processes, green catalysis and catalyst characterization can aid in the achievement of this objective [3]. This thesis, with focus on two reactions that produce useful bulk chemicals from renewable sources, is largely dedicated to this SDG 12

SDG 13 attempts to mitigate the effects of climate change. Utilizing green catalysis and characterizing catalysts can help to lower greenhouse gas emissions and lessen the consequences of climate change. It is possible to increase yields and selectivity while lowering the energy and raw material requirements for chemical production and minimizing the carbon footprint by enhancing catalyst performance. The use of waste streams from other processes or very abundant feed compounds as starting reagent, also is a promising option [150]. If a fossil hydrocarbon feed stream can be replaced by lignin, which is a waste stream of the paper industry, a great improvement is achieved. This is tried to be accomplished by the reductive catalytic depolymerization of lignin into monomeric phenols, for which in this thesis some promising catalysts are characterized.

In conclusion, green catalysis and catalyst characterization are critical instruments for reaching the SDG's because they provide an important foundation for encouraging sustainable development. This thesis helps in the research of useful catalysts that will make the production of the discussed products renewable, green, viable and efficient.

References

- [1] D. Sun, Y. Li, C. Yang, Y. Su, Y. Yamada, and S. Sato, "Production of 1,3-butadiene from biomass-derived C4 alcohols," *Fuel Processing Technology*, vol. 197. Elsevier B.V., Jan. 01, 2020. doi: 10.1016/j.fuproc.2019.106193.
- [2] BP Statistical Review of World Energy, "Years of fossil fuel reserves left," 2020.
- [3] G. Centi and S. Perathoner, "Catalysis and sustainable (green) chemistry," *Catal Today*, vol. 77, no. 4, pp. 287–297, Jan. 2003, doi: 10.1016/S0920-5861(02)00374-7.
- [4] A. N. (viaf)4775102 Glazer and H. (viaf)21366932 Nikaido, *Microbial biotechnology: fundamentals of applied microbiology*. New York (N.Y.) : Freeman, 1995. [Online]. Available: <http://lib.ugent.be/catalog/rug01:000685407>
- [5] A. Margellou and K. S. Triantafyllidis, "Catalytic transfer hydrogenolysis reactions for lignin valorization to fuels and chemicals," *Catalysts*, vol. 9, no. 1. MDPI, Jan. 01, 2019. doi: 10.3390/catal9010043.
- [6] F. G. Calvo-Flores and J. A. Dobado, "Lignin as Renewable Raw Material," *ChemSusChem*, vol. 3, no. 11, pp. 1227–1235, Nov. 2010, doi: <https://doi.org/10.1002/cssc.201000157>.
- [7] Ł. Klapiszewski, T. J. Szalaty, and T. Jesionowski, "Depolymerization and Activation of Lignin: Current State of Knowledge and Perspectives," *Lignin - Trends and Applications*, 2018, doi: 10.5772/intechopen.70376.
- [8] I. Haq, P. Mazumder, and A. S. Kalamdhad, "Recent advances in removal of lignin from paper industry wastewater and its industrial applications – A review," *Bioresour Technol*, vol. 312, p. 123636, Sep. 2020, doi: 10.1016/J.BIORTECH.2020.123636.
- [9] J. Ralph *et al.*, "Lignins: Natural polymers from oxidative coupling of 4-hydroxyphenylpropanoids," *Phytochemistry Reviews*, vol. 3, pp. 29–60, Jan. 2004, doi: 10.1023/B:PHYT.0000047809.65444.a4.
- [10] C. Xu, R. A. D. Arancon, J. Labidi, and R. Luque, "Lignin depolymerisation strategies: towards valuable chemicals and fuels," *Chem Soc Rev*, vol. 43, no. 22, pp. 7485–7500, Oct. 2014, doi: 10.1039/C4CS00235K.
- [11] X. Erdocia, F. Hernández-Ramos, A. Morales, N. Izaguirre, P. L. de Hoyos-Martínez, and J. Labidi, "Lignin extraction and isolation methods," *Lignin-based Materials for Biomedical Applications: Preparation, Characterization, and Implementation*, pp. 61–104, Jan. 2021, doi: 10.1016/B978-0-12-820303-3.00004-7.
- [12] D. Tian, R. P. Chandra, J. S. Lee, C. Lu, and J. N. Saddler, "A comparison of various lignin-extraction methods to enhance the accessibility and ease of enzymatic hydrolysis of the cellulosic component of steam-pretreated poplar," *Biotechnol Biofuels*, vol. 10, no. 1, pp. 1–10, Jun. 2017, doi: 10.1186/S13068-017-0846-5/FIGURES/4.

- [13] X. Liu, F. P. Bouxin, J. Fan, V. L. Budarin, C. Hu, and J. H. Clark, "Recent Advances in the Catalytic Depolymerization of Lignin towards Phenolic Chemicals: A Review," *ChemSusChem*, vol. 13, no. 17, pp. 4296–4317, Sep. 2020, doi: 10.1002/CSSC.202001213.
- [14] Virginia. M. Roberts, V. Stein, T. Reiner, A. Lemonidou, X. Li, and J. A. Lercher, "Towards Quantitative Catalytic Lignin Depolymerization," *Chemistry – A European Journal*, vol. 17, no. 21, pp. 5939–5948, May 2011, doi: <https://doi.org/10.1002/chem.201002438>.
- [15] M. P. Pandey and C. S. Kim, "Lignin Depolymerization and Conversion: A Review of Thermochemical Methods," *Chem Eng Technol*, vol. 34, no. 1, pp. 29–41, Jan. 2011, doi: <https://doi.org/10.1002/ceat.201000270>.
- [16] M. Fache, B. Boutevin, and S. Caillol, "Vanillin Production from Lignin and Its Use as a Renewable Chemical," 2015, doi: 10.1021/acssuschemeng.5b01344.
- [17] "Vanillin | C₈H₈O₃ - PubChem." <https://pubchem.ncbi.nlm.nih.gov/compound/Vanillin#section=Use-and-Manufacturing> (accessed Dec. 03, 2022).
- [18] M. Fache, B. Boutevin, and S. Caillol, "Vanillin Production from Lignin and Its Use as a Renewable Chemical," *ACS Sustain Chem Eng*, vol. 4, no. 1, pp. 35–46, Jan. 2016, doi: 10.1021/ACSSUSCHEMENG.5B01344/ASSET/IMAGES/MEDIUM/SC-2015-01344P_0017.GIF.
- [19] Erik. Dahlquist, "Biomass as energy source : resources, systems and applications," 2013.
- [20] F. Matos and P. Lima, "Lignin valorization through heterogeneous photocatalysis towards a sustainable circular-economy mindful approach".
- [21] J. M. Ha *et al.*, "Recent progress in the thermal and catalytic conversion of lignin," *Renewable and Sustainable Energy Reviews*, vol. 111, pp. 422–441, Sep. 2019, doi: 10.1016/J.RSER.2019.05.034.
- [22] C. Cheng *et al.*, "Catalytic Oxidation of Lignin in Solvent Systems for Production of Renewable Chemicals: A Review," *Polymers 2017, Vol. 9, Page 240*, vol. 9, no. 6, p. 240, Jun. 2017, doi: 10.3390/POLYM9060240.
- [23] X. Meng *et al.*, "Chemical Transformations of Poplar Lignin during Cosolvent Enhanced Lignocellulosic Fractionation Process," *ACS Sustain Chem Eng*, vol. 6, no. 7, pp. 8711–8718, Jul. 2018, doi: 10.1021/ACSSUSCHEMENG.8B01028/SUPPL_FILE/SC8B01028_SI_001.PDF.
- [24] S. G. Parto *et al.*, "Solvent assisted catalytic conversion of beech wood and organosolv lignin over NiMo/ γ -Al₂O₃," *Sustain Energy Fuels*, vol. 4, no. 4, pp. 1844–1854, Mar. 2020, doi: 10.1039/C9SE00375D.

- [25] X. Liu, F. P. Bouxin, J. Fan, V. L. Budarin, C. Hu, and J. H. Clark, "Recent Advances in the Catalytic Depolymerization of Lignin towards Phenolic Chemicals: A Review," *ChemSusChem*, vol. 13, no. 17, pp. 4296–4317, Sep. 2020, doi: 10.1002/CSSC.202001213.
- [26] H. Ma *et al.*, "Selective depolymerization of lignin catalyzed by nickel supported on zirconium phosphate," *Green Chemistry*, vol. 21, no. 3, pp. 658–668, Feb. 2019, doi: 10.1039/C8GC03617A.
- [27] T. Renders *et al.*, "Catalytic lignocellulose biorefining in n-butanol/water: a one-pot approach toward phenolics, polyols, and cellulose," *Green Chemistry*, vol. 20, no. 20, pp. 4607–4619, Oct. 2018, doi: 10.1039/C8GC01031E.
- [28] S. Wang, L. Shuai, B. Saha, D. G. Vlachos, and T. H. Epps, "From Tree to Tape: Direct Synthesis of Pressure Sensitive Adhesives from Depolymerized Raw Lignocellulosic Biomass," *ACS Cent Sci*, vol. 4, no. 6, pp. 701–708, Jun. 2018, doi: 10.1021/ACSCENTSCI.8B00140.
- [29] T. Zell and R. Langer, "Iron-catalyzed hydrogenation and dehydrogenation reactions with relevance to reversible hydrogen storage applications," *Recyclable Catalysis*, vol. 2, no. 1, Mar. 2016, doi: 10.1515/RECAT-2015-0010.
- [30] A. Karnitski *et al.*, "Roles of metal and acid sites in the reductive depolymerization of concentrated lignin over supported Pd catalysts," *Catal Today*, 2022, doi: 10.1016/J.CATTOD.2022.07.012.
- [31] M. Kim *et al.*, "Production of phenolic hydrocarbons using catalytic depolymerization of empty fruit bunch (EFB)-derived organosolv lignin on H β -supported Ru," *Chemical Engineering Journal*, vol. 309, pp. 187–196, Feb. 2017, doi: 10.1016/J.CEJ.2016.10.011.
- [32] S. An *et al.*, "Efficient lignin depolymerization with Ru- and W- modified bi-functional solid acid catalyst," *Bioresources*, vol. 17, no. 1, pp. 1062–1089, Dec. 2021, doi: 10.15376/biores.17.1.1062-1089.
- [33] F. Liu, G. Xuan, L. Ai, Q. Liu, and L. Yang, "Key factors that affect catalytic activity of activated carbon-based catalyst in chemical looping methane decomposition for H₂ production," *Fuel Processing Technology*, vol. 215, p. 106745, May 2021, doi: 10.1016/J.FUPROC.2021.106745.
- [34] Titin S. Fatimah, "Characterization of the γ , α -alumina and its adsorption capability to adsorb nickel (ii) and magnesium (ii) from nickel sulfate as a result of solvent differences," *Materials Science and Engineering*, 2021, Accessed: Mar. 08, 2023. [Online]. Available: <https://iopscience.iop.org/article/10.1088/1757-899X/1034/1/012151/pdf>
- [35] F. C. Hendriks, D. Valencia, P. C. A. Bruijninx, and B. M. Weckhuysen, "Zeolite molecular accessibility and host–guest interactions studied by adsorption of organic probes of tunable size," *Physical Chemistry Chemical Physics*, vol. 19, no. 3, pp. 1857–1867, Jan. 2017, doi: 10.1039/C6CP07572J.

- [36] G. Bergeret and P. Gallezot, "Particle Size and Dispersion Measurements," vol. 2, p. 10, 2008, doi: 10.1002/9783527610044.hetcat0038i.
- [37] A. M. Robinson, J. E. Hensley, and J. Will Medlin, "Bifunctional Catalysts for Upgrading of Biomass-Derived Oxygenates: A Review," *ACS Catalysis*, vol. 6, no. 8. American Chemical Society, pp. 5026–5043, Aug. 05, 2016. doi: 10.1021/acscatal.6b00923.
- [38] D. M. Alonso, S. G. Wettstein, and J. A. Dumesic, "Bimetallic catalysts for upgrading of biomass to fuels and chemicals," *Chem Soc Rev*, vol. 41, no. 24, p. 8075, 2012, doi: 10.1039/c2cs35188a.
- [39] B. Jiang, J. Hu, Y. Qiao, X. Jiang, and P. Lu, "Depolymerization of Lignin over a Ni–Pd Bimetallic Catalyst Using Isopropanol as an in Situ Hydrogen Source," *Energy & Fuels*, vol. 33, no. 9, pp. 8786–8793, Sep. 2019, doi: 10.1021/acs.energyfuels.9b01976.
- [40] S. Sitthisa, T. Pham, T. Prasomsri, T. Sooknoi, R. G. Mallinson, and D. E. Resasco, "Conversion of furfural and 2-methylpentanal on Pd/SiO₂ and Pd–Cu/SiO₂ catalysts," *J Catal*, vol. 280, no. 1, pp. 17–27, May 2011, doi: 10.1016/j.jcat.2011.02.006.
- [41] Grub J and Loser E, "Butadiene," in *Ullmann's Encyclopedia of Industrial Chemistry*, 7th ed. New York: John Wiley & Sons, 2011.
- [42] E. v. Makshina, M. Dusselier, W. Janssens, J. Degrève, P. A. Jacobs, and B. F. Sels, "Review of old chemistry and new catalytic advances in the on-purpose synthesis of butadiene," *Chemical Society Reviews*, vol. 43, no. 22. Royal Society of Chemistry, pp. 7917–7953, Nov. 21, 2014. doi: 10.1039/c4cs00105b.
- [43] F. Jing *et al.*, "Direct dehydration of 1,3-butanediol into butadiene over aluminosilicate catalysts," *Catal Sci Technol*, vol. 6, no. 15, pp. 5830–5840, 2016, doi: 10.1039/c5cy02211h.
- [44] N. Kataoka, A. S. Vangnai, T. Tajima, Y. Nakashimada, and J. Kato, "Improvement of (R)-1,3-butanediol production by engineered *Escherichia coli*," *J Biosci Bioeng*, vol. 115, no. 5, pp. 475–480, May 2013, doi: 10.1016/J.JBIOSC.2012.11.025.
- [45] J. H. Lee and S. B. Hong, "Dehydration of 1,3-butanediol to butadiene over medium-pore zeolites: Another example of reaction intermediate shape selectivity," *Appl Catal B*, vol. 280, Jan. 2021, doi: 10.1016/j.apcatb.2020.119446.
- [46] B. Braidia, V. Prana, and P. C. Hiberty, "The physical origin of saytzeff's rule," *Angewandte Chemie - International Edition*, vol. 48, no. 31, pp. 5724–5728, Jul. 2009, doi: 10.1002/ANIE.200901923.
- [47] S. Sato, F. Sato, H. Gotoh, and Y. Yamada, "Selective dehydration of alkanediols into unsaturated alcohols over rare earth oxide catalysts," *ACS Catalysis*, vol. 3, no. 4. pp. 721–734, Apr. 05, 2013. doi: 10.1021/cs300781v.
- [48] C. Woodford, "Zeolites," Aug. 24, 2021. <https://www.explainthatstuff.com/zeolites.html> (accessed Dec. 07, 2022).

- [49] "mordenite | mineral | Britannica." <https://www.britannica.com/science/mordenite> (accessed Dec. 07, 2022).
- [50] W. R. Grace, "Synthetic Non-fibrous Zeolites Product Stewardship Summary," *Grace*.
- [51] ExxonMobil, "Simple, scalable gasoline production. Produce transportation fuels with low technical and project risk."
- [52] "The Zeolite Cage Structure on JSTOR." <https://www.jstor.org/stable/1696781> (accessed Dec. 07, 2022).
- [53] Jiu Long, "Zeolite ZSM-5," *Jiulong Chemical*, 2017.
- [54] ACS Material LCC, "ZSM-5 - Zeolite Socony Mobil-5," 2019. <https://www.acsmaterial.com/blog-detail/zsm-5-molecular-seive.html> (accessed Dec. 07, 2022).
- [55] R. Szostak, "Molecular Sieves for Use in Catalysis," *Molecular Sieves*, pp. 1–50, 1989, doi: 10.1007/978-94-010-9529-7_1.
- [56] I. v. Kozhevnikov, "Heterogeneous acid catalysis by heteropoly acids: Approaches to catalyst deactivation," *J Mol Catal A Chem*, vol. 305, no. 1–2, pp. 104–111, Jun. 2009, doi: 10.1016/J.MOLCATA.2008.11.029.
- [57] D. T. Yazici and C. Bilgiç, "Determining the surface acidic properties of solid catalysts by amine titration using Hammett indicators and FTIR-pyridine adsorption methods," in *Surface and Interface Analysis*, Jun. 2010, pp. 959–962. doi: 10.1002/sia.3474.
- [58] M. B. Sayed, A. Auroux, and J. C. Védrine, "The effect of boron on ZSM-5 zeolite shape selectivity and activity: II. Coincorporation of aluminium and boron in the zeolite lattice," *J Catal*, vol. 116, no. 1, pp. 1–10, Mar. 1989, doi: 10.1016/0021-9517(89)90070-5.
- [59] B. Imelik, Institut de recherches sur la catalyse (France), and Centre national de la recherche scientifique (France), "Catalysis by acids and bases : proceedings of an international symposium ...," p. 445, 1985.
- [60] G. Li, C. Wu, D. Ji, P. Dong, Y. Zhang, and Y. Yang, "Acidity and catalyst performance of two shape-selective HZSM-5 catalysts for alkylation of toluene with methanol," *Reaction Kinetics, Mechanisms and Catalysis*, vol. 129, no. 2, pp. 963–974, Apr. 2020, doi: 10.1007/S11144-020-01732-9/FIGURES/7.
- [61] A. Igarashi, N. Ichikawa, S. Sato, R. Takahashi, and T. Sodesawa, "Dehydration of butanediols over CeO₂ catalysts with different particle sizes," *Appl Catal A Gen*, vol. 300, no. 1, pp. 50–57, Jan. 2006, doi: 10.1016/J.APCATA.2005.10.054.
- [62] S. Ohtsuka *et al.*, "Vapor-phase catalytic dehydration of butanediols to unsaturated alcohols over yttria-stabilized zirconia catalysts," *Appl Catal A Gen*, vol. 575, pp. 48–57, Apr. 2019, doi: 10.1016/J.APCATA.2019.02.013.

- [63] S. Tsunekawa, T. Fukuda, and A. Kasuya, "X-ray photoelectron spectroscopy of monodisperse CeO_{2-x} nanoparticles," *Surf Sci*, vol. 457, no. 3, pp. L437–L440, Jun. 2000, doi: 10.1016/S0039-6028(00)00470-2.
- [64] S. Sato, R. Takahashi, T. Sodesawa, and N. Honda, "Dehydration of diols catalyzed by CeO₂," *J Mol Catal A Chem*, vol. 221, no. 1–2, pp. 177–183, Nov. 2004, doi: 10.1016/J.MOLCATA.2004.07.004.
- [65] S. Sato, R. Takahashi, T. Sodesawa, and N. Honda, "Dehydration of diols catalyzed by CeO₂," *J Mol Catal A Chem*, vol. 221, no. 1–2, pp. 177–183, Nov. 2004, doi: 10.1016/J.MOLCATA.2004.07.004.
- [66] D. Sun, S. Arai, H. Duan, Y. Yamada, and S. Sato, "Vapor-phase dehydration of C₄ unsaturated alcohols to 1,3-butadiene," *Appl Catal A Gen*, vol. 531, pp. 21–28, Feb. 2017, doi: 10.1016/J.APCATA.2016.11.035.
- [67] L. Fang, F. Jing, J. Lu, B. Hu, and M. Pera-Titus, "Supporting Information Nano-flowered Ce@MOR hybrids with modulated acid properties for the vapor-phase dehydration of 1,3-butanediol into butadiene," 2017.
- [68] S. Prabhu *et al.*, "Synthesis and characterization of CeO₂ supported ZSM-5 zeolite for organic dye degradation," *Journal of Materials Science: Materials in Electronics*, vol. 33, no. 12, pp. 9211–9223, Apr. 2022, doi: 10.1007/S10854-021-07216-3/FIGURES/12.
- [69] M. A. Reiche, M. Maciejewski, and A. Baiker, "Characterization by temperature programmed reduction," *Catal Today*, vol. 56, no. 4, pp. 347–355, 2000, doi: 10.1016/S0920-5861(99)00294-1.
- [70] Micromeritics, "Temperature-Programmed Reduction Using the AutoChem," *One Micromeritics Drive*, no. 770, pp. 2–3.
- [71] S. Bhatia, J. Beltramini, and D. D. Do, "Temperature programmed analysis and its applications in catalytic systems," *Catal Today*, vol. 7, no. 3, pp. 309–438, 1990, doi: 10.1016/0920-5861(90)87001-J.
- [72] Hiden Analytical, "What is TPR?," 2018. [hidenanalytical.com/blog/what-is-tp/](https://www.hidenanalytical.com/blog/what-is-tp/)
- [73] "Notes - EFFECT OF SOME EXPERIMENTAL PARAMETERS ON TPR PROFILES | Altamira Instruments." <https://www.altamirainstruments.com/notes/13-effect-of-some-experimental-parameters-on-tp-profiles.html> (accessed Dec. 17, 2022).
- [74] Hiden Analytical, "Temperature Programmed Oxidation - A Guide," 2018. Temperature Programmed Oxidation - A Guide
- [75] C. A. Querini and S. C. Fung, "Temperature-programmed oxidation technique: kinetics of coke-O₂ reaction on supported metal catalysts," *Appl Catal A Gen*, vol. 117, no. 1, pp. 53–74, 1994, doi: 10.1016/0926-860X(94)80158-4.

- [76] R. J. Cvetanović and Y. Amenomiya, "A Temperature Programmed Desorption Technique for Investigation of Practical Catalysts," *Catalysis Reviews*, vol. 6, no. 1, pp. 21–48, Jan. 1972, doi: 10.1080/01614947208078690.
- [77] T. Ishii and T. Kyotani, *Temperature Programmed Desorption*. Tsinghua University Press Limited, 2016. doi: 10.1016/B978-0-12-805256-3.00014-3.
- [78] B. Mozgawa *et al.*, "Analysis of NH₃-TPD Profiles for CuSSZ-13 SCR Catalyst of Controlled Al Distribution – Complexity Resolved by First Principles Thermodynamics of NH₃ Desorption, IR and EPR Insight into Cu Speciation**," *Chemistry – A European Journal*, vol. 27, no. 68, pp. 17159–17180, Dec. 2021, doi: <https://doi.org/10.1002/chem.202102790>.
- [79] P. Kuśtrowski, L. Chmielarz, E. Bozek, M. Sawalha, and F. Roessner, "Acidity and basicity of hydrotalcite derived mixed Mg-Al oxides studied by test reaction of MBOH conversion and temperature programmed desorption of NH₃ and CO₂," *Mater Res Bull*, vol. 39, no. 2, pp. 263–281, 2004, doi: 10.1016/j.materresbull.2003.09.032.
- [80] K. Leistner, K. Xie, A. Kumar, K. Kamasamudram, and L. Olsson, "Ammonia Desorption Peaks Can Be Assigned to Different Copper Sites in Cu/SSZ-13," *Catal Letters*, vol. 147, no. 8, pp. 1882–1890, 2017, doi: 10.1007/s10562-017-2083-8.
- [81] M. Niwa and N. Katada, "Measurements of acidic property of zeolites by temperature programmed desorption of ammonia".
- [82] P. Kuśtrowski, L. Chmielarz, E. Bozek, M. Sawalha, and F. Rößner, "Acidity and basicity of hydrotalcite derived mixed Mg–Al oxides studied by test reaction of MBOH conversion and temperature programmed desorption of NH₃ and CO₂," *Mater Res Bull*, vol. 39, pp. 263–281, Feb. 2004, doi: 10.1016/j.materresbull.2003.09.032.
- [83] A. S. Al-Fatesh *et al.*, "Combined magnesia, ceria and nickel catalyst supported over γ -alumina doped with titania for dry reforming of methane," *Catalysts*, vol. 9, no. 2, Feb. 2019, doi: 10.3390/CATAL9020188.
- [84] J. Friedland, B. Kreitz, H. Grimm, T. Turek, and R. Güttel, "Measuring Adsorption Capacity of Supported Catalysts with a Novel Quasi-Continuous Pulse Chemisorption Method," *ChemCatChem*, vol. 12, no. 17, pp. 4373–4386, 2020, doi: 10.1002/cctc.202000278.
- [85] M. A. Fortunato *et al.*, "Dispersion measurement of platinum supported on Yttria-Stabilised Zirconia by pulse H₂ chemisorption," *Appl Catal A Gen*, vol. 403, no. 1, pp. 18–24, 2011, doi: <https://doi.org/10.1016/j.apcata.2011.06.005>.
- [86] Altamira Instruments, "Pulse Chemisorption," *Altamira Notes vol 1.5*. <https://www.altamirainstruments.com/notes/7-pulse-chemisorption.html>
- [87] Micromeritics, "Pulse Chemisorption Analysis," *AutoChem II 2920*, 2000.

- [88] G. Bergeret and P. Gallezot, "Particle Size and Dispersion Measurements," in *Handbook of Heterogeneous Catalysis*, 2008, pp. 738–765. doi: <https://doi.org/10.1002/9783527610044.hetcat0038>.
- [89] T. Ge, B. Zhu, Y. Sun, W. Song, Q. Fang, and Y. Zhong, "Investigation of low-temperature selective catalytic reduction of NO_x with ammonia over Cr-promoted Fe/AC catalysts," *Environmental Science and Pollution Research*, vol. 26, no. 32, pp. 33067–33075, Nov. 2019, doi: 10.1007/S11356-019-06301-9.
- [90] M. Gnanamani, R. Garcia, and G. Jacobs, "Effect of pretreatment conditions on acidity and dehydration activity of CeO₂-MeO_x catalysts." Accessed: Apr. 16, 2023. [Online]. Available: <https://www.osti.gov/servlets/purl/1756860>
- [91] B. Kraushaar-Czarnetzki and S. P. Müller, "Shaping of Solid Catalysts Objectives of Catalyst Shaping," *Synthesis of Solid Catalysts*, pp. 173–199, 2009, Accessed: Jan. 16, 2023. [Online]. Available: https://books.google.com/books/about/Synthesis_of_Solid_Catalysts.html?hl=nl&id=5ejCa9HGf2oC
- [92] W. Samoy, "Characterization of catalytic active sites via temperature-programmed techniques," Ghent, 2022.
- [93] "Inductively Coupled Plasma Atomic Emission Spectroscopy - an overview | ScienceDirect Topics." <https://www.sciencedirect.com/topics/materials-science/inductively-coupled-plasma-atomic-emission-spectroscopy> (accessed Feb. 08, 2023).
- [94] A. de Reviere, T. Vandevyvere, M. K. Sabbe, and A. Verberckmoes, "Renewable Butene Production through Dehydration Reactions over Nano-HZSM-5/ γ -Al₂O₃ Hybrid Catalysts," *Catalysts 2020, Vol. 10, Page 879*, vol. 10, no. 8, p. 879, Aug. 2020, doi: 10.3390/CATAL10080879.
- [95] T. De Saegher *et al.*, "Monometallic Cerium Layered Double Hydroxide Supported Pd-Ni Nanoparticles as High Performance Catalysts for Lignin Hydrogenolysis," *Materials 2020, Vol. 13, Page 691*, vol. 13, no. 3, p. 691, Feb. 2020, doi: 10.3390/MA13030691.
- [96] Z. Di, H. Wang, R. Zhang, H. Chen, Y. Wei, and J. Jia, "ZSM-5 core-shell structured catalyst for enhancing low-temperature NH₃-SCR efficiency and poisoning resistance," *Appl Catal A Gen*, vol. 630, p. 118438, Jan. 2022, doi: 10.1016/J.APCATA.2021.118438.
- [97] "PubChem." <https://pubchem.ncbi.nlm.nih.gov/> (accessed Apr. 09, 2023).
- [98] "AutoChem II 2920 Operator Manual," Jan. 2018.
- [99] "Thermal Conductivity Detector (TCD) Principle - Inst Tools." <https://instrumentationtools.com/thermal-conductivity-detector-tcd-principle/> (accessed Apr. 06, 2023).

- [100] “Thermal conductivity detector (TCD) | HiQ.” http://hiq.linde-gas.com/en/analytical_methods/gas_chromatography/thermal_conductivity_detector.html (accessed Apr. 06, 2023).
- [101] T. Adamo, “Thermal Conductivity Detector (TCD).” Accessed: Apr. 06, 2023. [Online]. Available: <https://www.utsc.utoronto.ca/~traceslab/PDFs/GC%20TCD.pdf>
- [102] X. Yang, M. v. Pereira, B. Neupane, G. C. Miller, S. R. Poulson, and H. Lin, “Upgrading Biocrude of *Grindelia Squarrosa* to Jet Fuel Precursors by Aqueous Phase Hydrodeoxygenation,” *Energy Technology*, vol. 6, no. 9, pp. 1832–1843, Sep. 2018, doi: 10.1002/ente.201700977.
- [103] G. R. Heal and L. L. Mkyayula, “The preparation of palladium metal catalysts supported on carbon part II: Deposition of palladium and metal area measurements,” *Carbon N Y*, vol. 26, no. 6, pp. 815–823, 1988, doi: 10.1016/0008-6223(88)90104-2.
- [104] T. A. Dorling and R. L. Moss, “The structure and activity of supported metal catalysts: II. Crystallite size and CO chemisorption on platinum/silica catalysts,” *J Catal*, vol. 7, no. 4, pp. 378–385, Apr. 1967, doi: 10.1016/0021-9517(67)90166-2.
- [105] P. Canton, G. Fagherazzi, M. Battagliarin, F. Menegazzo, F. Pinna, and N. Pernicone, “Pd/CO Average Chemisorption Stoichiometry in Highly Dispersed Supported Pd/ γ -Al₂O₃ Catalysts,” *Langmuir*, vol. 18, no. 17, pp. 6530–6535, Aug. 2002, doi: 10.1021/LA015650A.
- [106] G. Bergeret and P. Gallezot, “Particle Size and Dispersion Measurements,” vol. 2, p. 10, 2008, doi: 10.1002/9783527610044.hetcat0038i.
- [107] Micromeritics, “ammonia TPD for zeolite characterization on the autochem III.” Accessed: Mar. 02, 2023. [Online]. Available: <https://www.micromeritics.com/wp-content/uploads/20220527-AutoChem-III-app-note.pdf>
- [108] “Help Online - Origin Help - Algorithms (Smooth).” <https://www.originlab.com/doc/Origin-Help/Smooth-Algorithm> (accessed Apr. 08, 2023).
- [109] “Origin: Data Analysis and Graphing Software.” <https://www.originlab.com/origin> (accessed Apr. 08, 2023).
- [110] L. Rodríguez-González, F. Hermes, M. Bertmer, E. Rodríguez-Castellón, A. Jiménez-López, and U. Simon, “The acid properties of H-ZSM-5 as studied by NH₃-TPD and 27Al-MAS-NMR spectroscopy,” *Appl Catal A Gen*, vol. 328, no. 2, pp. 174–182, Sep. 2007, doi: 10.1016/J.APCATA.2007.06.003.
- [111] J. G. Post and J. H. C. Van Hooff, “Acidity and activity of H-ZSM-5 measured with NH₃-TPD and n-hexane cracking Acidity and activity of H-ZSM-5 measured with NH₃-t.p.d. and n-hexane cracking”, doi: 10.1016/0144-2449(84)90065-4.

- [112] M. Niwa and N. Katada, "New Method for the Temperature- Programmed Desorption (TPD) of Ammonia Experiment for Characterization of Zeolite Acidity: A Review," *The Chemical Record*, vol. 13, no. 5, pp. 432–455, Oct. 2013, doi: 10.1002/TCR.201300009.
- [113] K. Yoshikawa, M. Kaneeda, and H. Nakamura, "Development of Novel CeO₂-based CO₂ adsorbent and analysis on its CO₂ adsorption and desorption mechanism," *Energy Procedia*, vol. 114, pp. 2481–2487, 2017, doi: 10.1016/J.EGYPRO.2017.03.1400.
- [114] H. Jin, C. Miao, Y. Yue, C. Tian, W. Hua, and Z. Gao, "Sm-CeO₂/Zeolite Bifunctional Catalyst for Direct and Highly Selective Conversion of Bioethanol to Propylene," *Catalysts*, vol. 12, no. 4, p. 407, Apr. 2022, doi: 10.3390/CATAL12040407/S1.
- [115] C. C. Ilie *et al.*, "Activated water desorption from poly(methylvinylidene cyanide)," *Journal of Physical Chemistry B*, vol. 111, no. 27, pp. 7742–7746, Jul. 2007, doi: 10.1021/JP071661M.
- [116] R. S. Smith and B. D. Kay, "Desorption Kinetics of Benzene and Cyclohexane from a Graphene Surface," 2017, doi: 10.1021/acs.jpcc.7b05102.
- [117] P. A. Webb, "Introduction to Chemical Adsorption Analytical Techniques and their Applications to Catalysis," 2003.
- [118] M. Y. Byun, J. S. Kim, D. W. Park, and M. S. Lee, "Influence of calcination temperature on the structure and properties of Al₂O₃ as support for Pd catalyst," *Korean Journal of Chemical Engineering*, vol. 35, no. 5, pp. 1083–1088, May 2018, doi: 10.1007/s11814-018-0015-y.
- [119] M. K. Van Der Lee, A. Van Jos Dillen, J. H. Bitter, and K. P. De Jong, "Deposition precipitation for the preparation of carbon nanofiber supported nickel catalysts," *J Am Chem Soc*, vol. 127, no. 39, pp. 13573–13582, Oct. 2005, doi: 10.1021/ja053038q.
- [120] B. A. T. Mehrabadi, S. Eskandari, U. Khan, R. D. White, and J. R. Regalbuto, "A Review of Preparation Methods for Supported Metal Catalysts," in *Advances in Catalysis*, Academic Press Inc., 2017, pp. 1–35. doi: 10.1016/bs.acat.2017.10.001.
- [121] M. N. S. C. Roma, D. S. Cunha, G. M. Cruz, and A. J. G. Cobo, "Effects of Cu over Pd based catalysts supported on silica or niobia," *Brazilian Journal of Chemical Engineering*, vol. 17, no. 4–7, pp. 937–946, Dec. 2000, doi: 10.1590/S0104-66322000000400058.
- [122] J. S. Kwon, "The Pd/SiO₂ catalysts for hydrogenation of D-glucose," University of Ulsan, Ulsan, 2018.
- [123] P. M. Carraro, A. A. García Blanco, C. Chanquía, K. Sapag, M. I. Oliva, and G. A. Eimer, "Hydrogen adsorption of nickel-silica materials: Role of the SBA-15 porosity," *Microporous and Mesoporous Materials*, vol. 248, pp. 62–71, 2017, doi: 10.1016/J.MICROMESO.2017.03.057.

- [124] B. D. Zdravkov, J. J. Čermák, M. Šefara, and J. Janků, "Pore classification in the characterization of porous materials: A perspective," *Central European Journal of Chemistry*, vol. 5, no. 2, pp. 385–395, Jun. 2007, doi: 10.2478/S11532-007-0017-9/MACHINEREADABLECITATION/RIS.
- [125] D. J. Macquarrie, D. B. Jackson, S. Tailland, and K. A. Utting, "Organically modified hexagonal mesoporous silicas (HMS)—remarkable effect of preparation solvent on physical and chemical properties," *J Mater Chem*, vol. 11, no. 7, pp. 1843–1849, Jan. 2001, doi: 10.1039/B100957P.
- [126] R. Lamber, N. Jaeger, and G. Schulz-Ekloff, "Metal-support interaction in the Pd/SiO₂ system: Influence of the support pretreatment," *J Catal*, vol. 123, no. 2, pp. 285–297, 1990, doi: 10.1016/0021-9517(90)90128-7.
- [127] K. V. R. Chary, D. Naresh, V. Vishwanathan, M. Sadakane, and W. Ueda, "Vapour phase hydrogenation of phenol over Pd/C catalysts: A relationship between dispersion, metal area and hydrogenation activity," *Catal Commun*, vol. 8, no. 3, pp. 471–477, Mar. 2007, doi: 10.1016/j.catcom.2006.07.017.
- [128] Y. T. Kim, E. D. Park, M. Kang, and J. E. Yie, "The effect of physicochemical treatment on Pd dispersion of carbon-supported Pd catalysts," in *Solid State Phenomena*, Trans Tech Publications Ltd, 2008, pp. 57–60. doi: 10.4028/www.scientific.net/SSP.135.57.
- [129] J. H. Baek, J. S. Kim, M. J. Moon, and M. S. Lee, "Improvements of Pd/C catalyst support characteristics by various physical dispersion methods," *J Nanosci Nanotechnol*, vol. 15, no. 7, pp. 5314–5317, Jul. 2015, doi: 10.1166/jnn.2015.10399.
- [130] P. Insorn and B. Kitiyanan, "Selective hydrogenation of concentrated vinyl acetylene mixed C₄ by modified Pd catalysts: Effect of Cu," *Catalysts*, vol. 6, no. 12, Dec. 2016, doi: 10.3390/catal6120199.
- [131] F. Skoda, M. P. Astier, M. Paj, and M. Primet, "Surface characterization of palladium-copper bimetallic catalysts by FTIR spectroscopy and test reactions," 1994.
- [132] L. Gucci, Z. Schay, G. Stefler, L. F. Liotta, G. Deganello, and A. M. Venezia, "Pumice-Supported Cu-Pd Catalysts: Influence of Copper on the Activity and Selectivity of Palladium in the Hydrogenation of Phenylacetylene and But-1-ene," 1999. [Online]. Available: <http://www.idealibrary.comon>
- [133] Y. Cai and R. R. Adzic, "Platinum monolayer electrocatalysts for the oxygen reduction reaction: Improvements induced by surface and subsurface modifications of cores," *Advances in Physical Chemistry*, vol. 2011. 2011. doi: 10.1155/2011/530397.
- [134] W. J. Kim and S. H. Moon, "Modified Pd catalysts for the selective hydrogenation of acetylene," in *Catalysis Today*, May 2012, pp. 2–16. doi: 10.1016/j.cattod.2011.09.037.

- [135] N. Barrabés *et al.*, "Catalytic reduction of nitrate on Pt-Cu and Pd-Cu on active carbon using continuous reactor: The effect of copper nanoparticles," *Appl Catal B*, vol. 62, no. 1–2, pp. 77–85, Jan. 2006, doi: 10.1016/j.apcatb.2005.06.015.
- [136] J. A. Conkling and C. Mocella, *Chemistry of pyrotechnics : basic principles and theory*, 3rd ed. Boca Raton FL: CRC Press Taylor & Francis Group, 2019.
- [137] G. Ertl, H. Knözinger, and J. Weitkamp, *Preparation of Solid Catalysts*. Wiley, 1999. doi: 10.1002/9783527619528.
- [138] M. Argyle and C. Bartholomew, "Heterogeneous Catalyst Deactivation and Regeneration: A Review," *Catalysts*, vol. 5, no. 1, pp. 145–269, Feb. 2015, doi: 10.3390/catal5010145.
- [139] "Characterization of Copper Catalysts Using Pulse Reactions and a Mass Spectrometer on the AutoChem 2910."
- [140] "Characterizing Copper Catalysts Using Pulsed Chemisorption."
<https://www.azom.com/article.aspx?ArticleID=14562> (accessed May 17, 2023).
- [141] D. Gunst, M. Sabbe, M. F. Reyniers, and A. Verberckmoes, "Study of n-butanol conversion to butenes: Effect of Si/Al ratio on activity, selectivity and kinetics," *Appl Catal A Gen*, vol. 582, Jul. 2019, doi: 10.1016/J.APCATA.2019.05.035.
- [142] K. Yoshikawa, M. Kaneeda, and H. Nakamura, "Development of Novel CeO₂-based CO₂ adsorbent and analysis on its CO₂ adsorption and desorption mechanism," *Energy Procedia*, vol. 114, pp. 2481–2487, Jul. 2017, doi: 10.1016/J.EGYPRO.2017.03.1400.
- [143] "Green Chemistry: How Does it Work? - Scientific Pakistan."
<https://scientificpakistan.com/chemistry/what-is-green-chemistry/> (accessed Apr. 20, 2023).
- [144] "Basics of Green Chemistry | US EPA." <https://www.epa.gov/greenchemistry/basics-green-chemistry> (accessed Apr. 20, 2023).
- [145] "12 Principles of Green Chemistry - American Chemical Society."
<https://www.acs.org/greenchemistry/principles/12-principles-of-green-chemistry.html> (accessed Apr. 20, 2023).
- [146] "Sustainable Development Goals | United Nations Development Programme."
<https://www.undp.org/sustainable-development-goals> (accessed Apr. 20, 2023).
- [147] "Sustainable Development Goals."
<https://www.who.int/data/gho/data/themes/sustainable-development-goals> (accessed Apr. 19, 2023).
- [148] "UNESCO and Sustainable Development Goals."
<https://en.unesco.org/sustainabledevelopmentgoals> (accessed Apr. 19, 2023).

- [149] “Chemicals - Fuels & Technologies - IEA.” <https://www.iea.org/fuels-and-technologies/chemicals> (accessed Apr. 19, 2023).
- [150] R. A. Sheldon, “Green and sustainable manufacture of chemicals from biomass: state of the art,” *Green Chemistry*, vol. 16, no. 3, pp. 950–963, Feb. 2014, doi: 10.1039/C3GC41935E.

Appendices

Appendix A: CO pulse chemisorption spectra

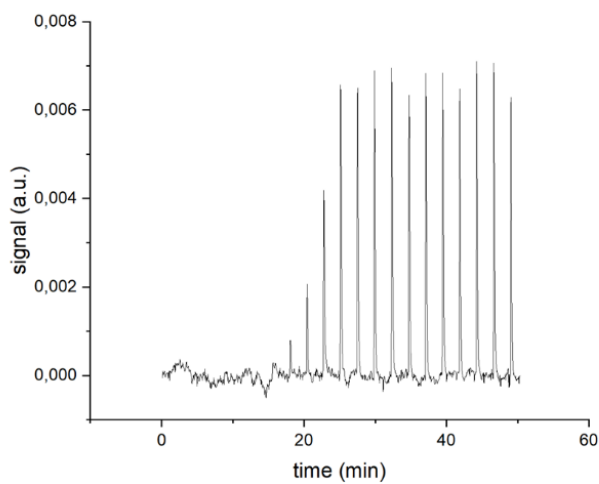


Figure 62: Pd/Al₂O₃ CO pulse chemisorption spectrum (1% CO)

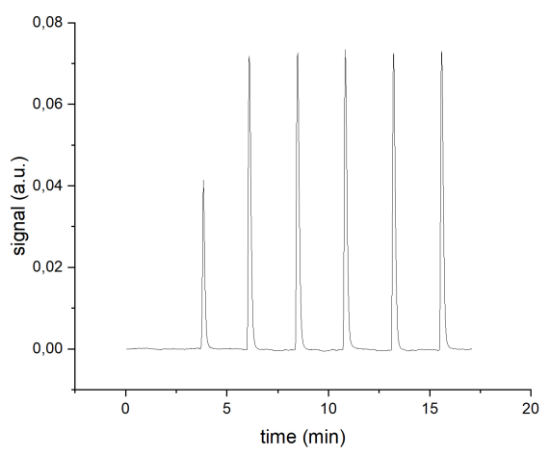


Figure 63: Pd/Al₂O₃ CO pulse chemisorption spectrum (10% CO)

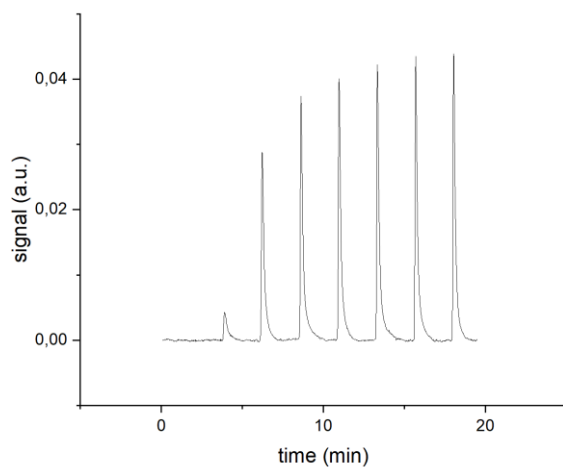


Figure 64: PdCu/Al₂O₃ CO pulse chemisorption spectrum (10% CO/He)

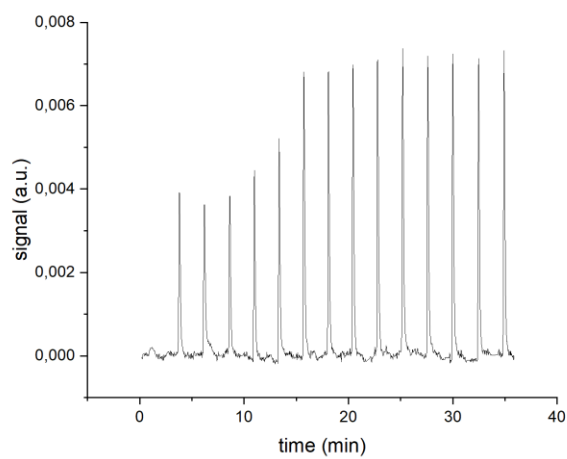


Figure 65: Pd/SiO₂ CO pulse chemisorption spectrum (1% CO/He)

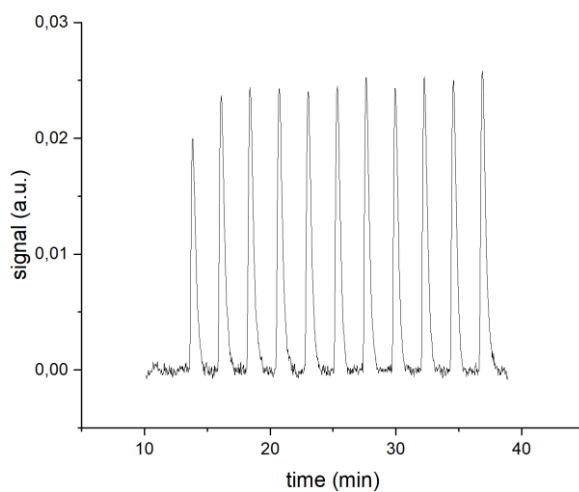


Figure 66: PdCu/SiO₂ CO pulse chemisorption spectrum (10% CO/He)

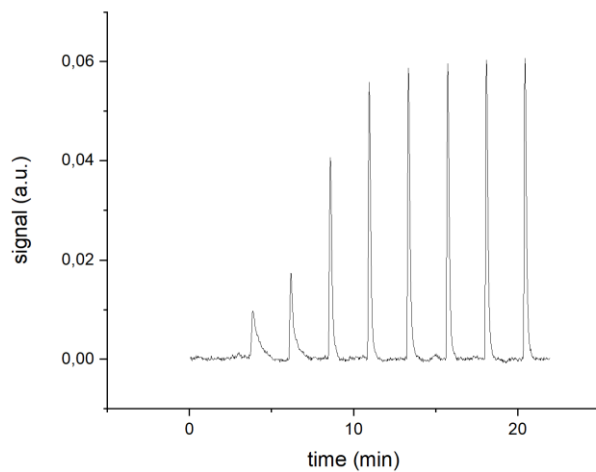


Figure 67: Pd/AC CO pulse chemisorption spectrum (10% CO/He)

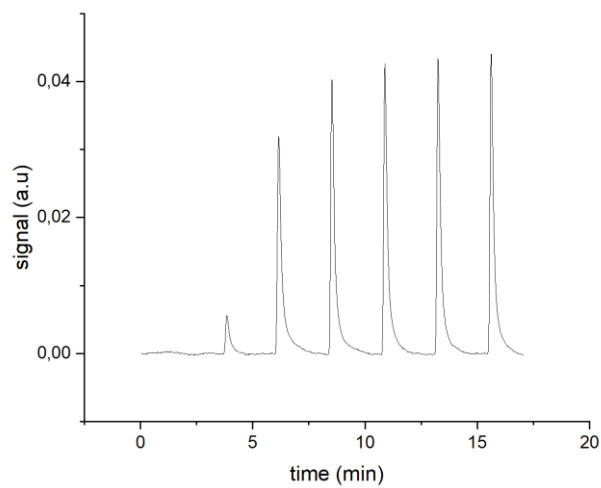


Figure 68: PdCu/AC CO pulse chemisorption spectrum (10% CO/He)

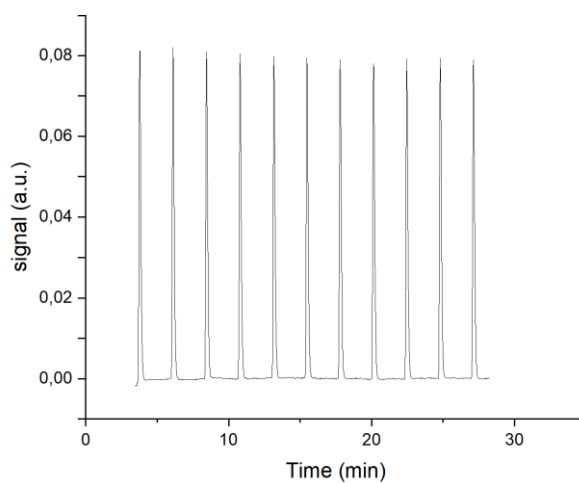


Figure 69: CO pulse chemisorption spectrum of an empty tube with quartz wool (10%CO/He)

Appendix B: TEM-EDX results on supported metal catalysts

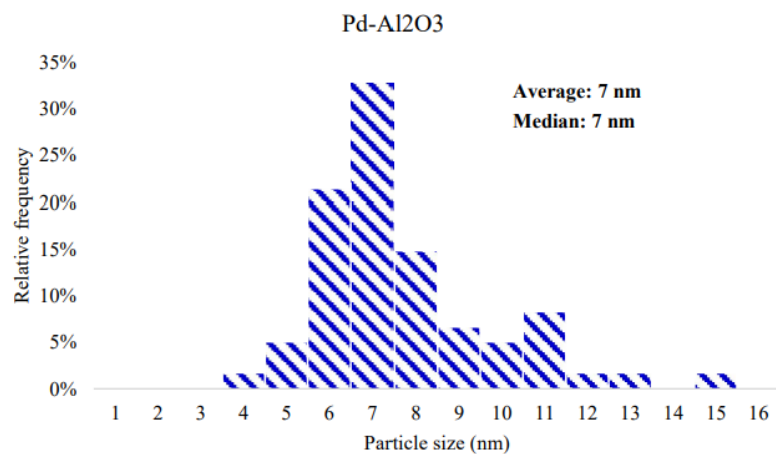


Figure 70: particle size distribution of Pd/Al₂O₃

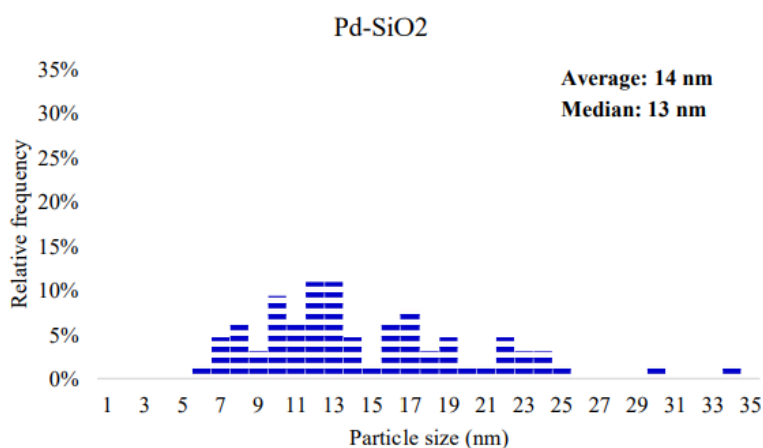


Figure 71: particle size distribution of Pd/SiO₂

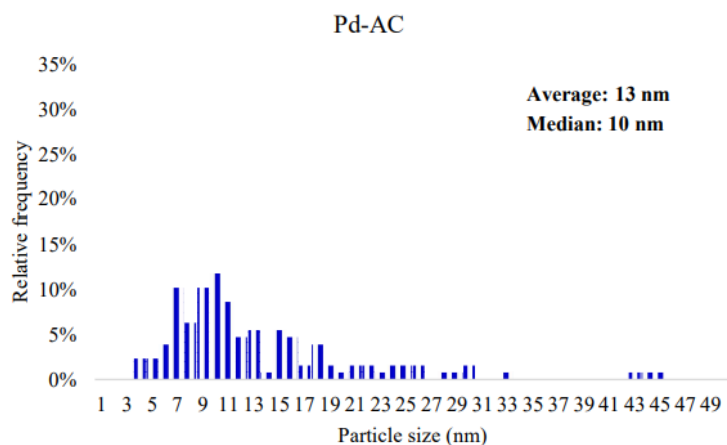


Figure 72: particle size distribution of Pd/AC

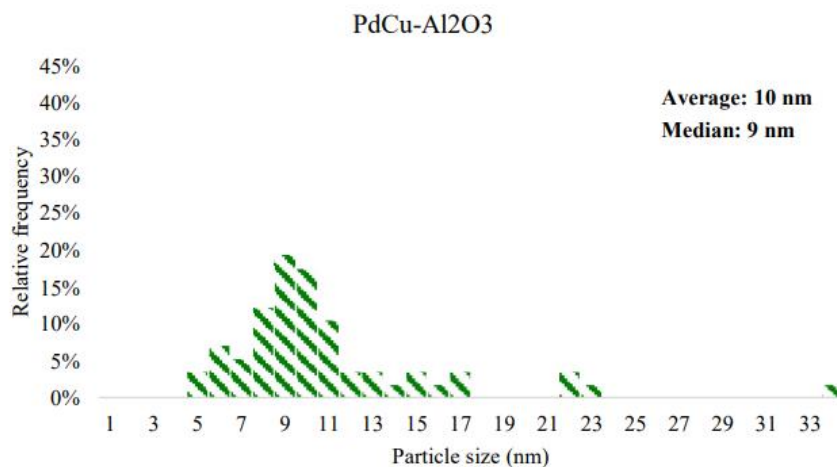


Figure 73: particle size distribution of PdCu/Al₂O₃

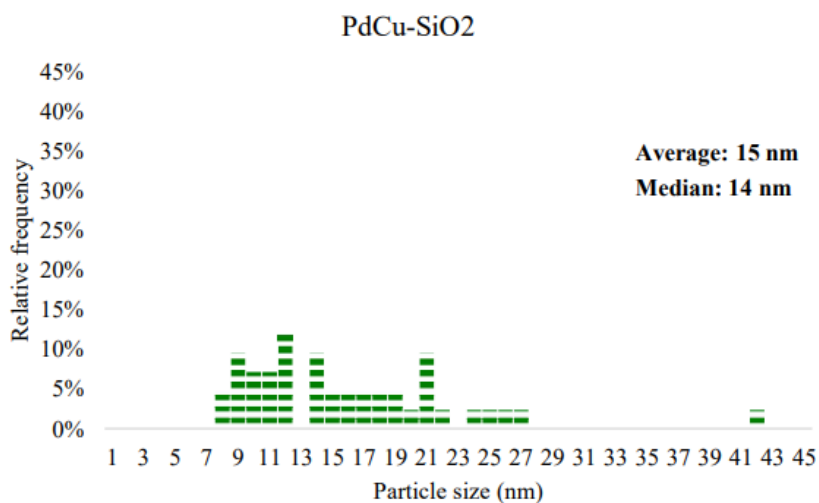


Figure 74: particle size distribution of PdCu/SiO₂

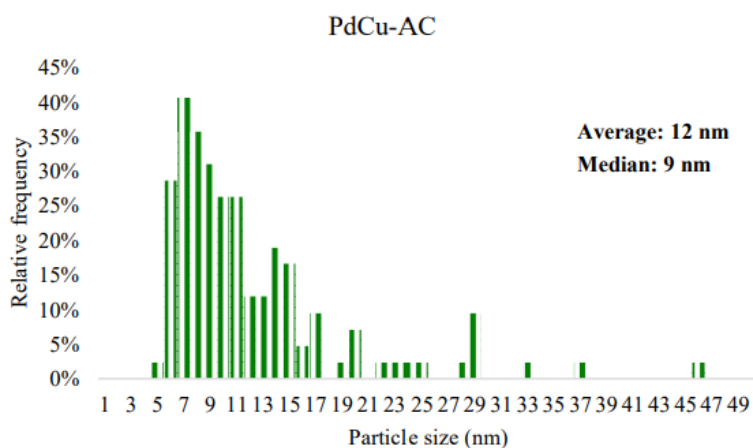


Figure 75: particle size distribution of PdCu/AC

Appendix C: NH₃-TPD acidity results from Ghent campus

Table 29: NH₃-TPD results of the samples, analyzed on Ghent campus

Sample	Amount of acid sites (μmol/g)				
	Weak	Medium	Strong	Very strong	Total
ZSM-5@25	120	120	112	66	419
ZSM-5@150	13	13	38	23	86
ZSM-5 @25_B	80	80	36	78	274
ZSM-5 @150_B	6	6	29	8	49
CeO ₂ /ZSM-5	36	32	69	37	174
ZSM-5@ CeO ₂	80	81	92	50	304

Table 30: peak temperature of spectra with heating ratio 10°C/min, from Ghent campus

Sample	Temperature (°C)			
	Weak	Medium	Strong	Very strong
ZSM-5@25	217	270	374	448
ZSM-5@150	202	274	366	422
ZSM-5@25_B	226	292	380	450
ZSM-5 @150_B	206	287	368	420
CeO ₂ /ZSM-5	225	270	360	445
ZSM-5@ CeO ₂	218	270	369	439

Appendix D: NH₃-TPD spectra from Ghent campus

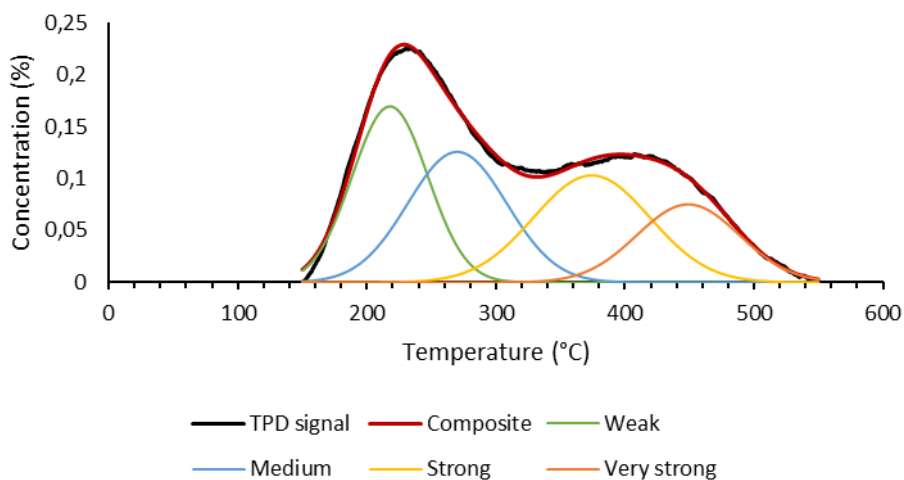


Figure 76: NH₃-TPD spectrum for ZSM-5@25 (Ghent campus)

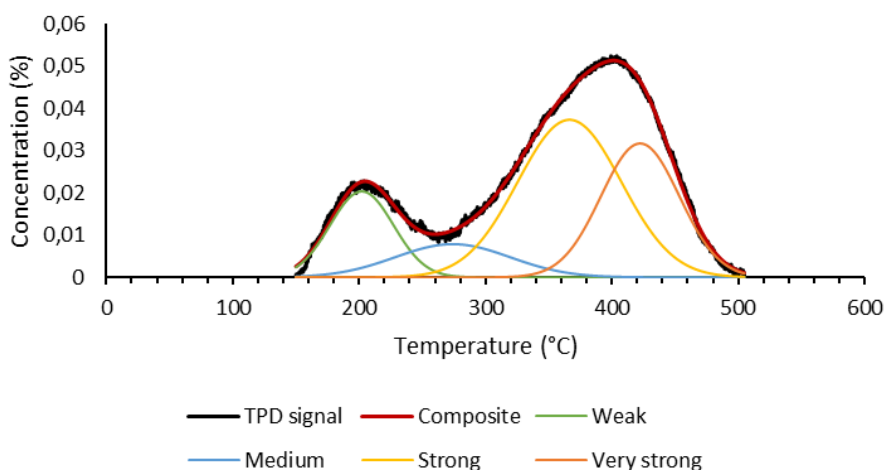


Figure 77: NH₃-TPD spectrum for ZSM-5@150 (Ghent campus)

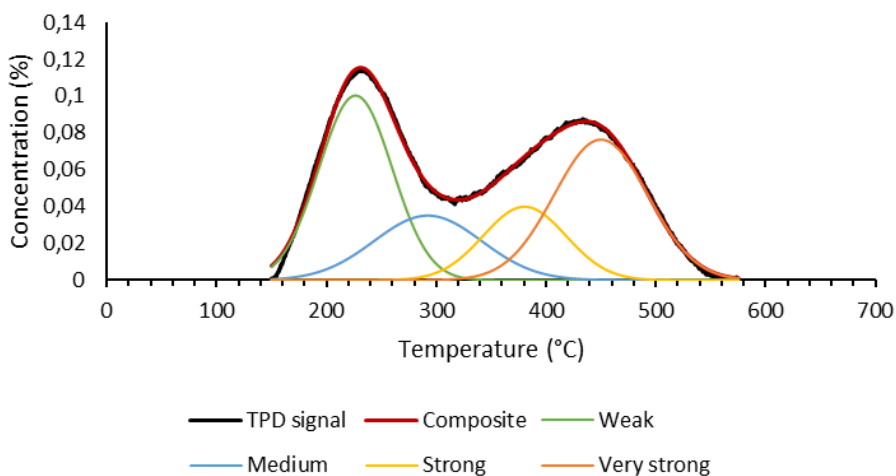


Figure 78: NH₃-TPD spectrum for ZSM-5@25_B (Ghent campus)

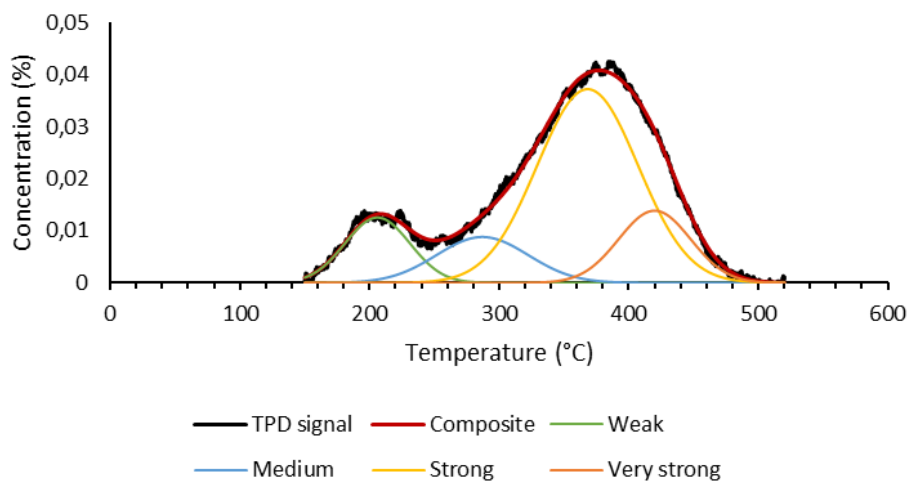


Figure 79: NH_3 -TPD spectrum for ZSM-5@150_B (Ghent campus)

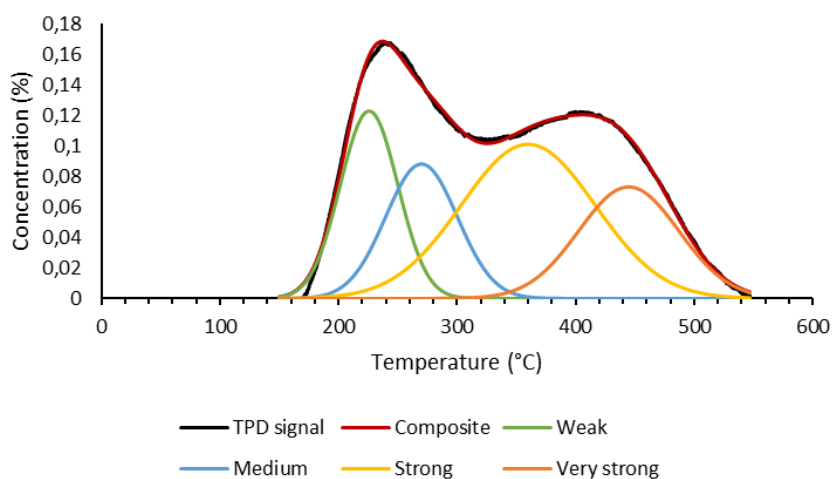


Figure 80: NH_3 -TPD spectrum for $\text{CeO}_2/\text{ZSM-5}$ (Ghent campus)

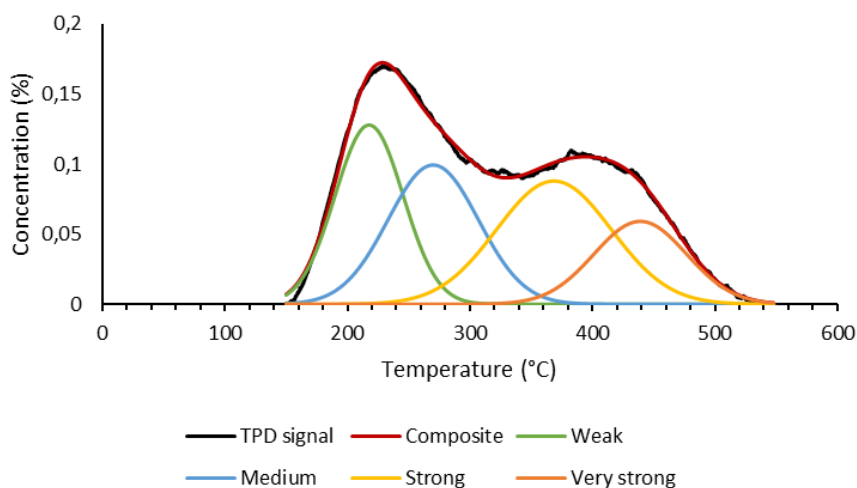


Figure 81: NH_3 -TPD spectrum for ZSM-5@ CeO_2 (Ghent campus)

Appendix E: Arrhenius plots for E_d determination of the strong acid sites (Ghent campus)

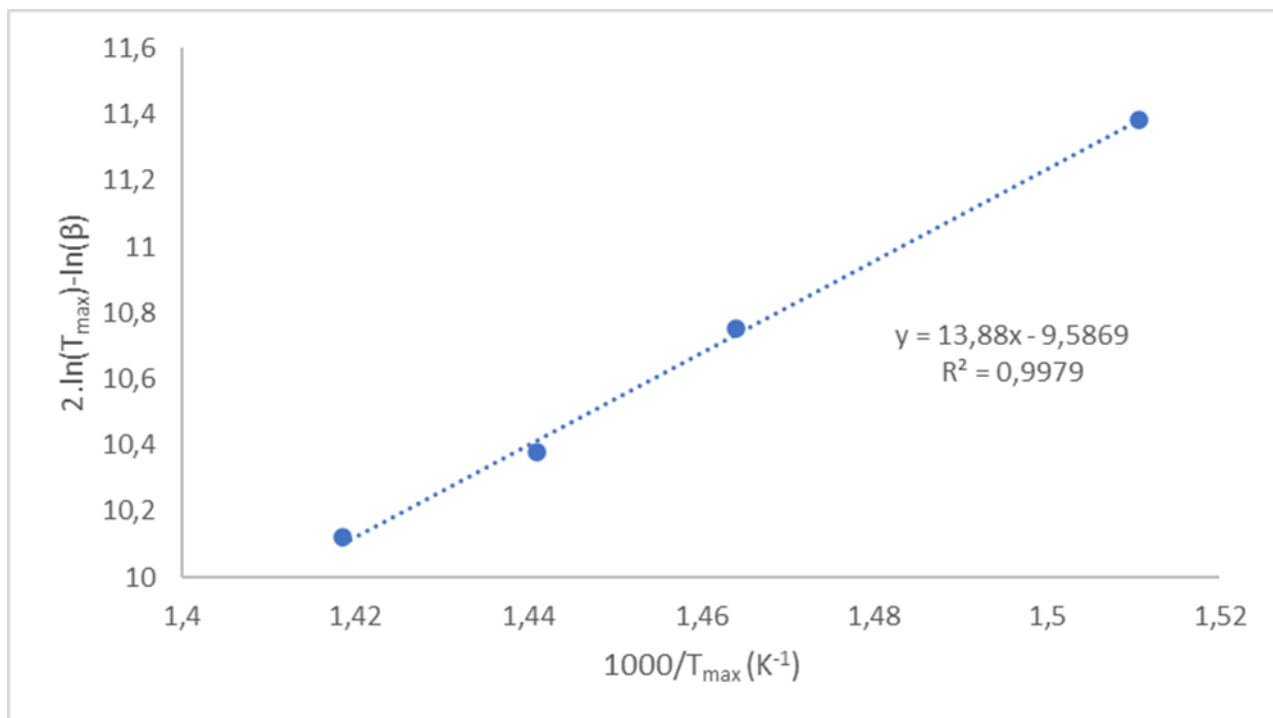


Figure 82: Arrhenius plot for ZSM-5@25 (acid site) at Ghent campus

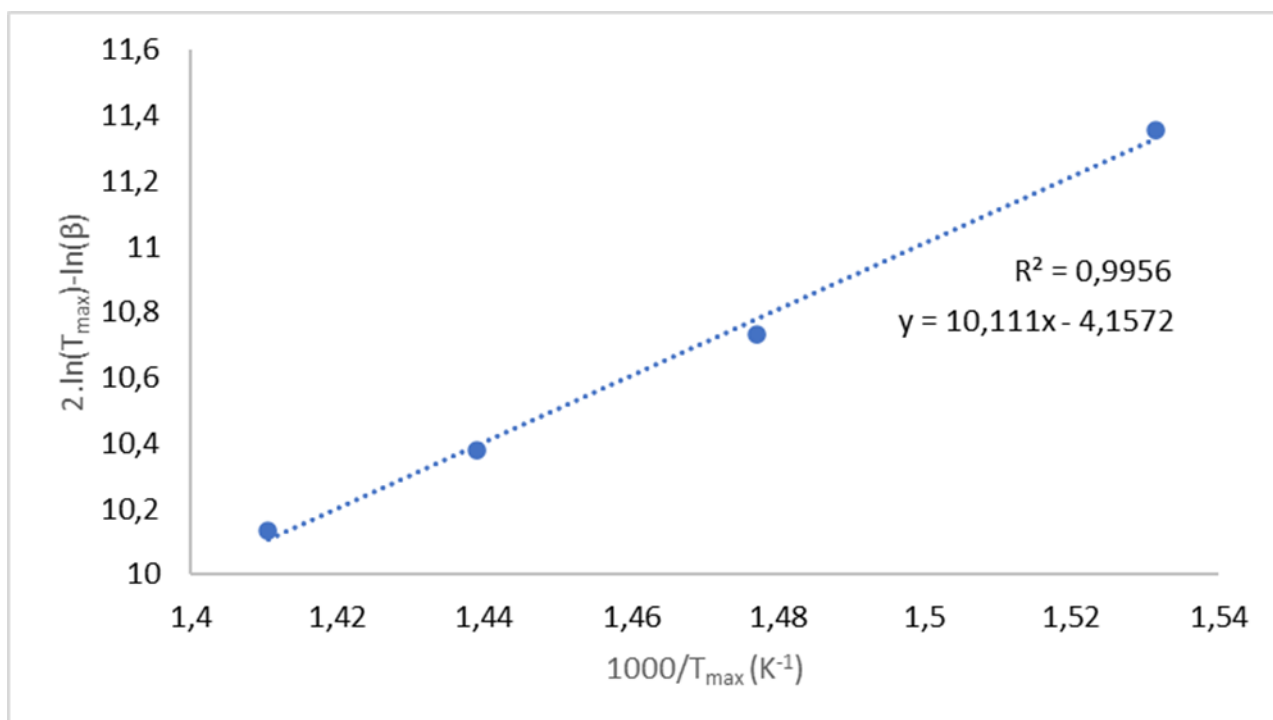


Figure 83: Arrhenius plot for ZSM-5@25_B (acid site) at Ghent campus

Appendix F: analysis conditions for NH₃-TPD at the home campus (Ghent)

The analysis conditions for the NH₃-TPD on the samples for which the results are shown in the former appendices are summarized. This for completeness and to be able to make a comparison between other studies and this thesis. The most important changes to the conditions in this thesis are the use of 4% NH₃/He instead of 5% and the loading at 150°C instead of 120°C.

Step 1: pretreatment (under inert He flow at 25 cm³/min)

- heating to 500°C at 2°C/min, wait 120 min
- cooling to 120°C at 20°C/min, wait 25 min

Step 2: NH₃ loading at 150°C (4% NH₃/He at 25 cm³/min)

- wait 30 min

Step 3: purging and NH₃-TPD (under inert He flow at 25 cm³/min)

- wait 30 min (purging non adsorbed NH₃)
- start recording with t= 1 s
- heating to 650°C at 10°C/min, wait 30 min
- stop recording
- return to 150°C (use Kwikcool on Autochem → fast cooling)

⇒ **Repeat loading and TPD steps for TPD heating rates of 15°C/min and 20°C/min**

Step 4: termination

- return to ambient temperature (use Kwikcool)

Appendix G: corrected and deconvoluted NH₃-TPD spectra (respective heating ratio of 10, 15, 20°C/min)

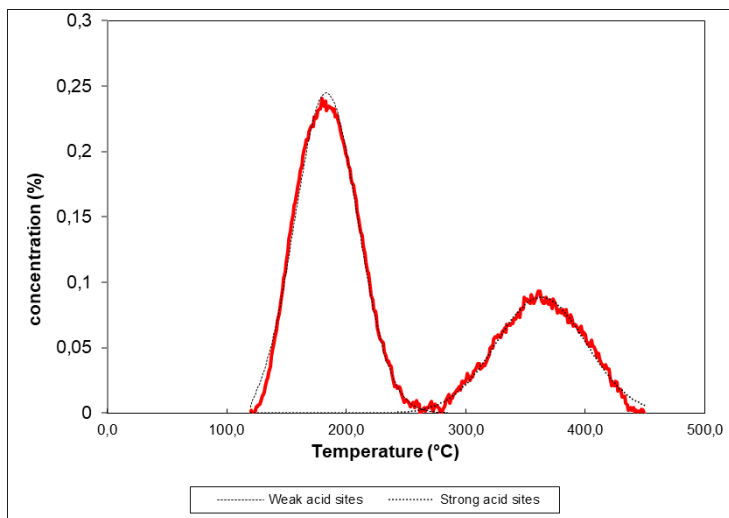


Figure 84: NH₃-TPD spectrum of commercial ZSM-5 (10°C/min)

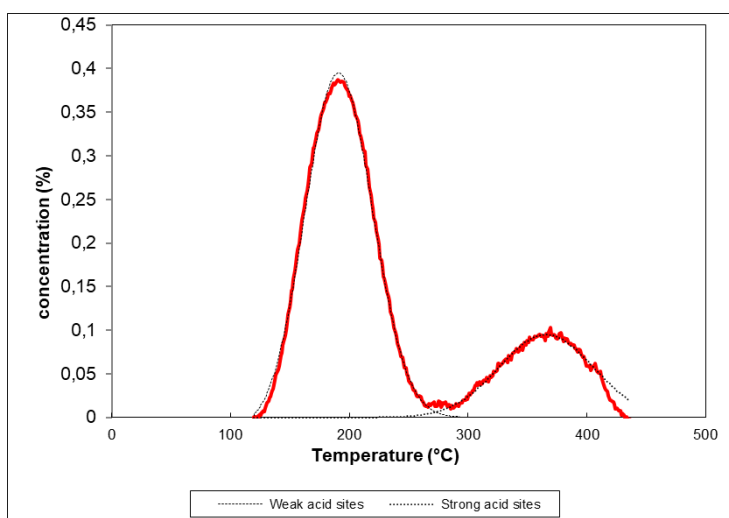


Figure 85: NH₃-TPD spectrum of commercial ZSM-5 (15°C/min)

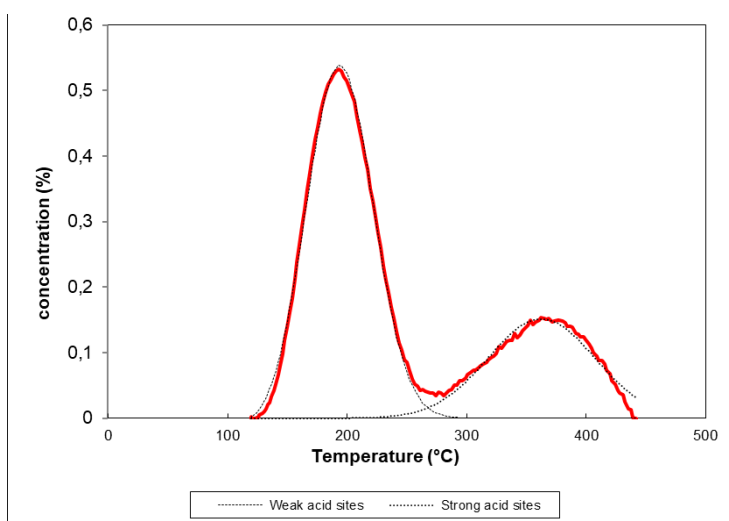


Figure 86: NH₃-TPD spectrum of commercial ZSM-5 (20°C/min)

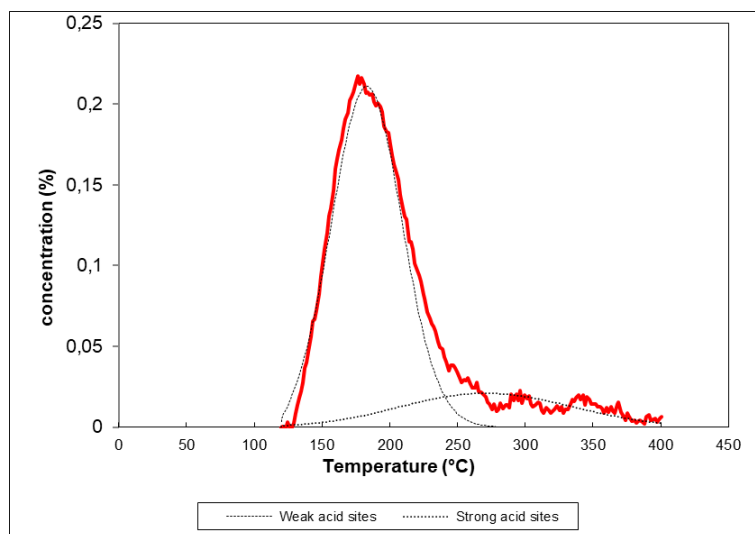


Figure 87: NH_3 -TPD spectrum of ZSM-5@25 (10°C/min)

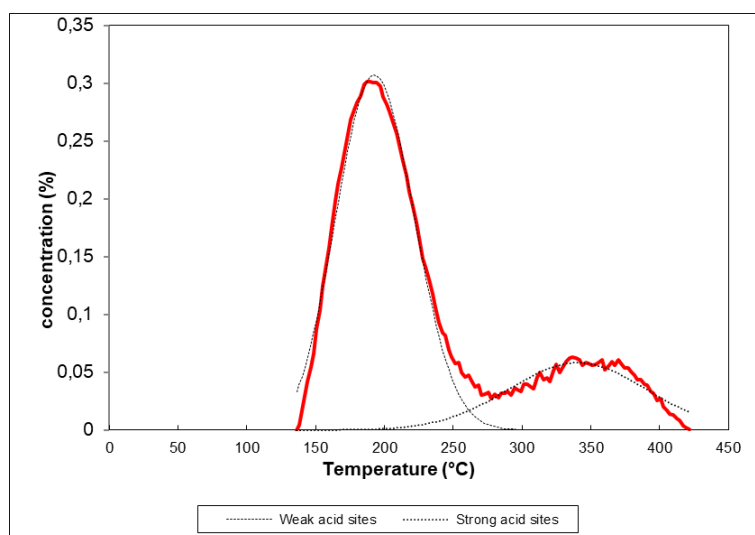


Figure 88: NH_3 -TPD spectrum of ZSM-5@25 (15°C/min)

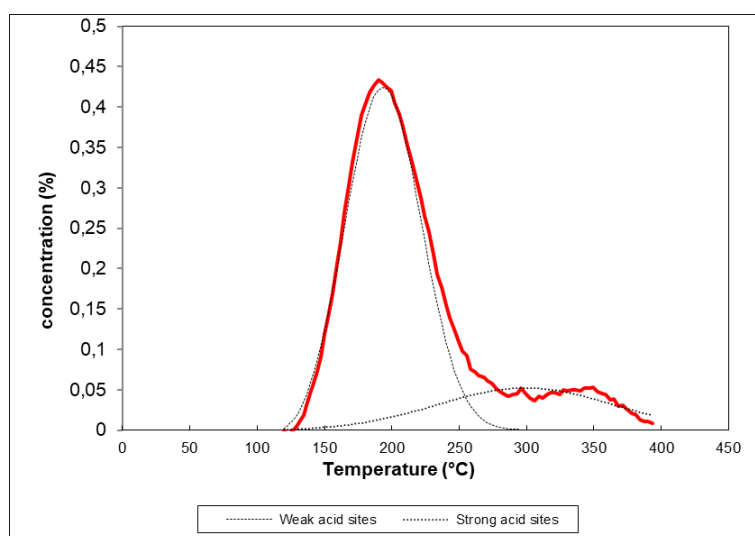


Figure 89: NH_3 -TPD spectrum of ZSM-5@25 (20°C/min)

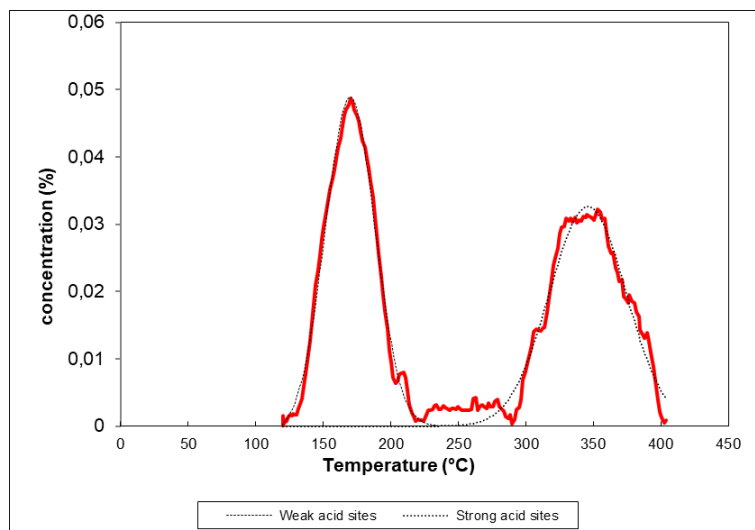


Figure 90: NH_3 -TPD spectrum of ZSM-5@150 (10°C/min)

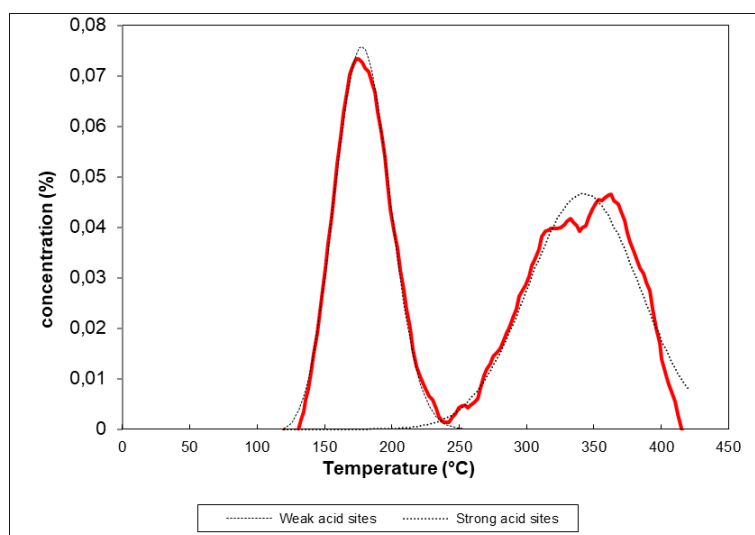


Figure 91: NH_3 -TPD spectrum of ZSM-5@150 (15°C/min)

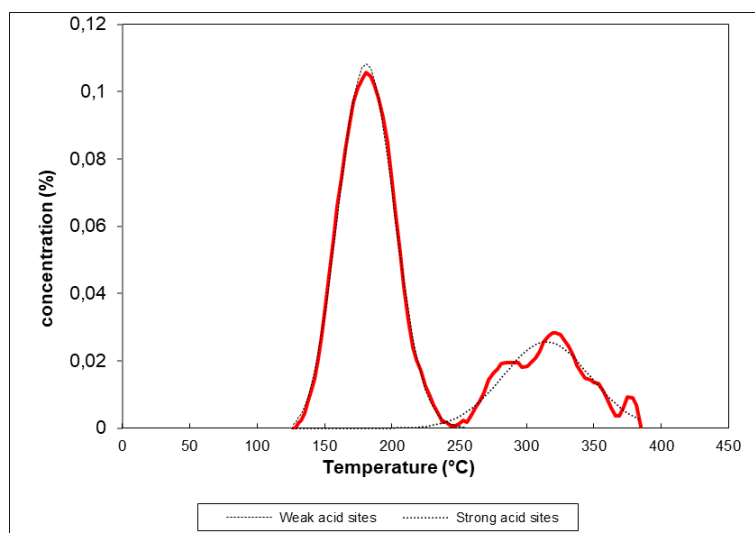


Figure 92: NH_3 -TPD spectrum of ZSM-5@150 (20°C/min)

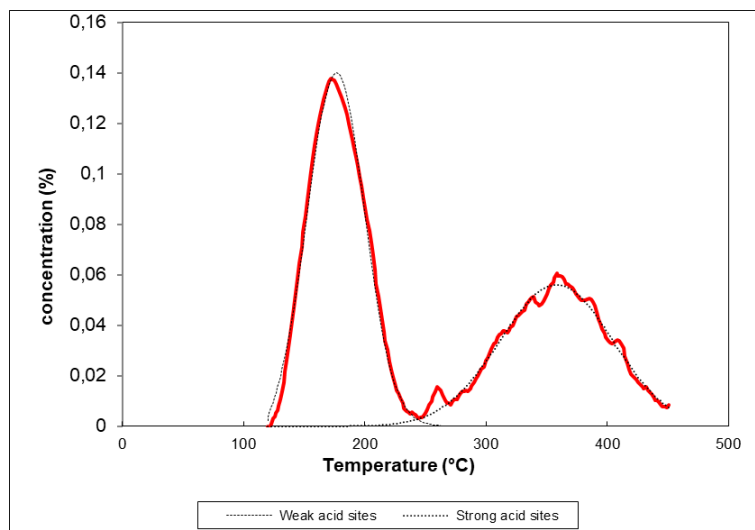


Figure 93: NH_3 -TPD spectrum of ZSM-5@25_B (10°C/min)

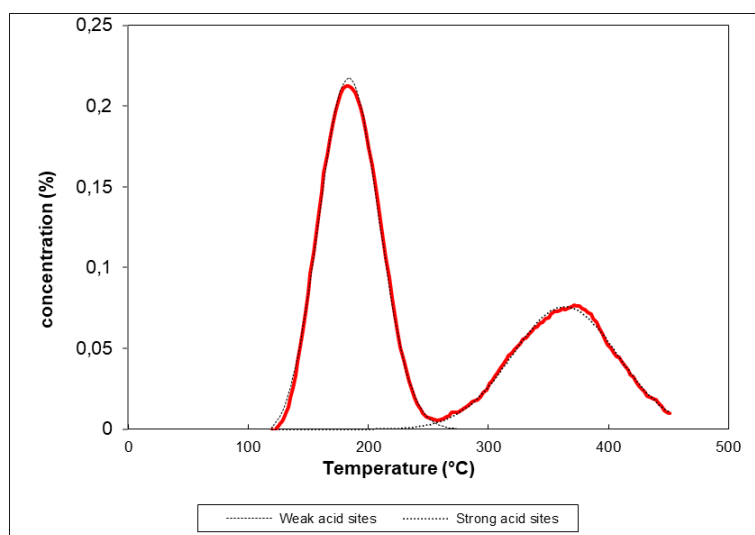


Figure 94: NH_3 -TPD spectrum of ZSM-5@25_B (15°C/min)

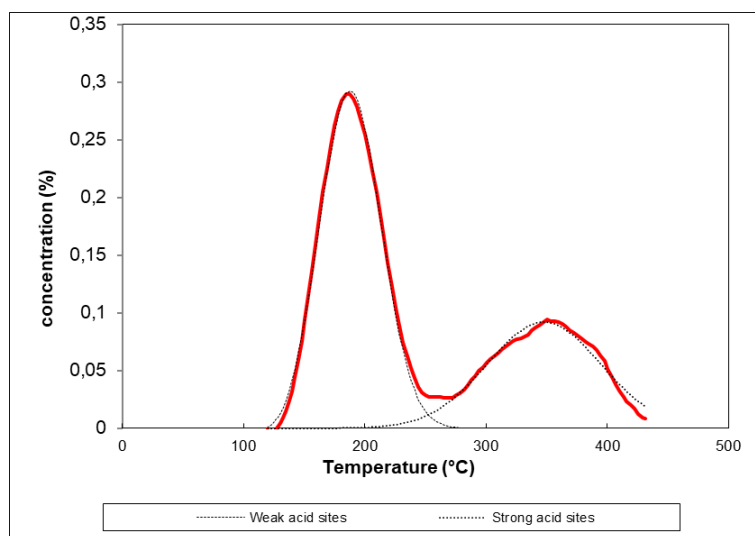


Figure 95: NH_3 -TPD spectrum of ZSM-5@25_B (20°C/min)

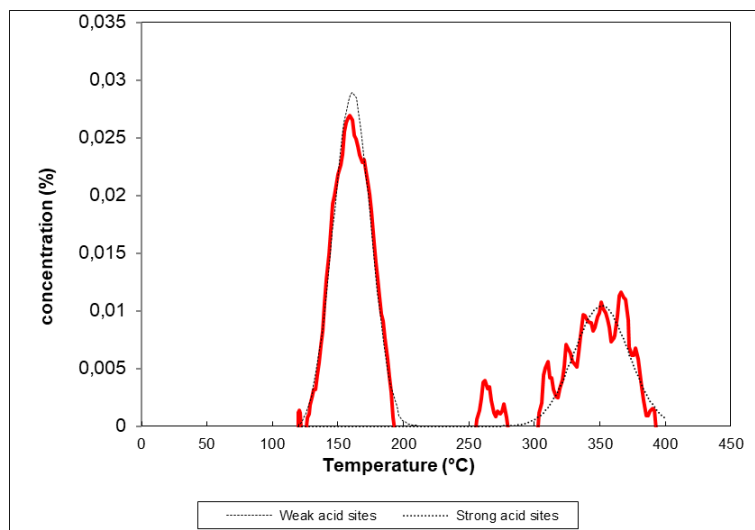


Figure 96: NH_3 -TPD spectrum of ZSM-5@150_B (10°C/min)

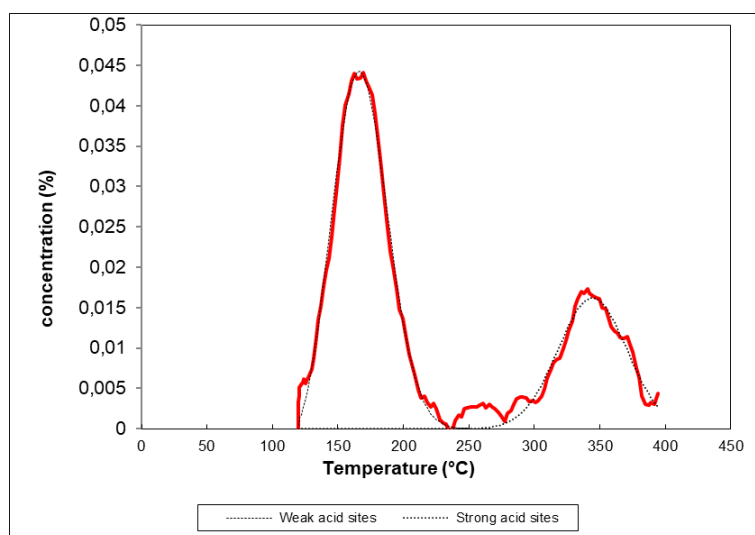


Figure 97: NH_3 -TPD spectrum of ZSM-5@150_B (15°C/min)

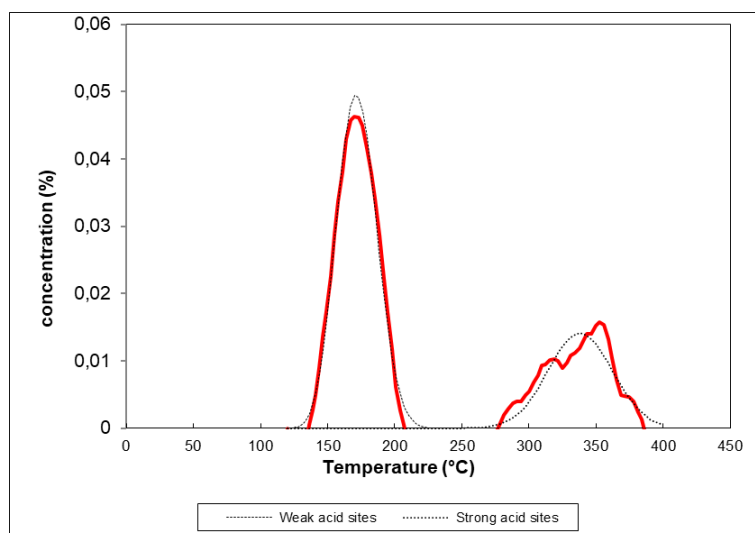


Figure 98: NH_3 -TPD spectrum of ZSM-5@150_B (20°C/min)

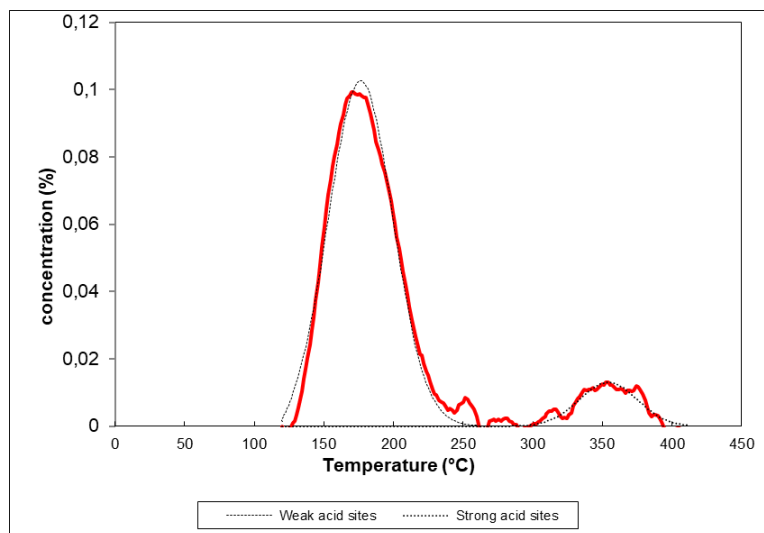


Figure 99: NH_3 -TPD spectrum of $\text{CeO}_2/\text{ZSM-5}$ ($10^\circ\text{C}/\text{min}$)

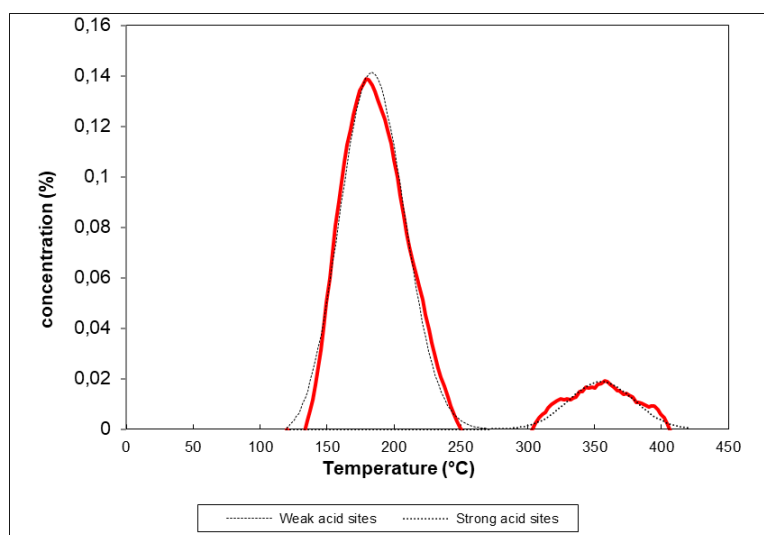


Figure 100: NH_3 -TPD spectrum of $\text{CeO}_2/\text{ZSM-5}$ ($15^\circ\text{C}/\text{min}$)

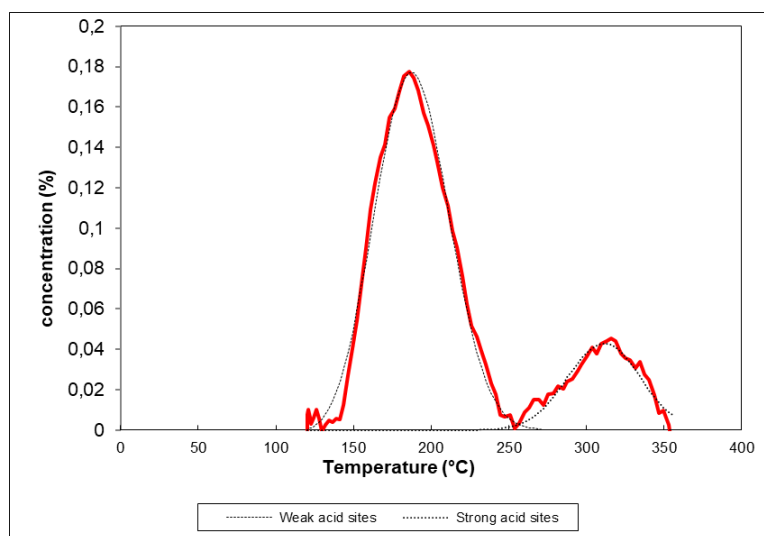


Figure 101: NH_3 -TPD spectrum of $\text{CeO}_2/\text{ZSM-5}$ ($20^\circ\text{C}/\text{min}$)

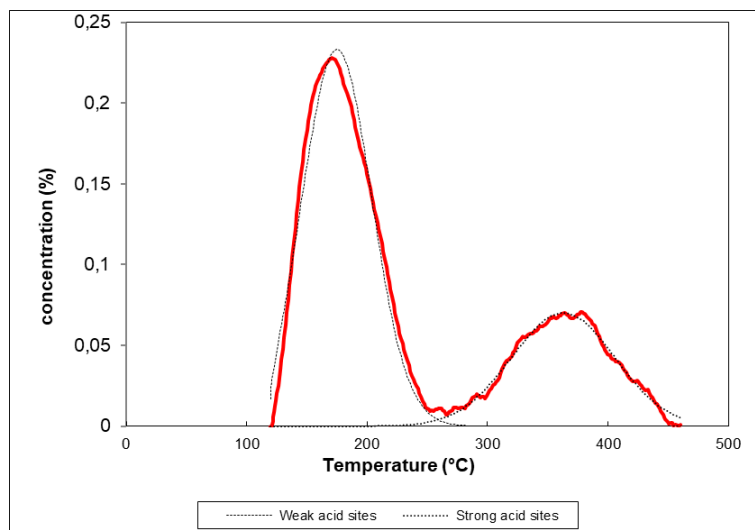


Figure 102: NH_3 -TPD spectrum of ZSM-5@ CeO_2 ($10^\circ\text{C}/\text{min}$)

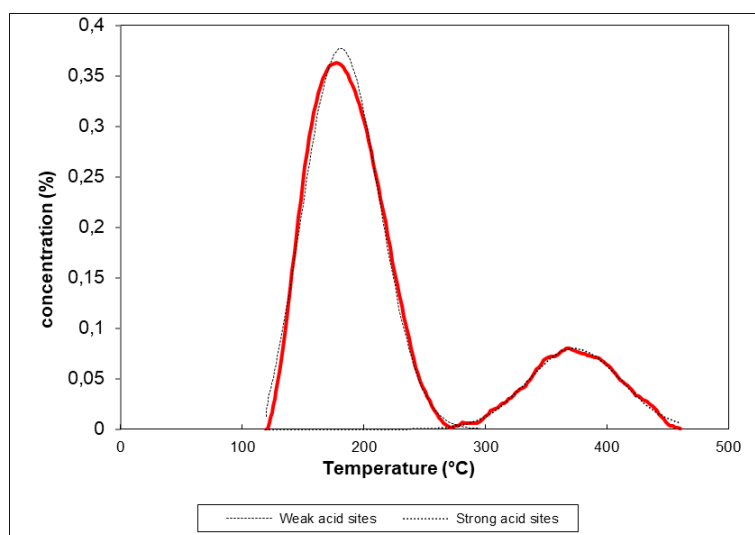


Figure 103: NH_3 -TPD spectrum of ZSM-5@ CeO_2 ($15^\circ\text{C}/\text{min}$)

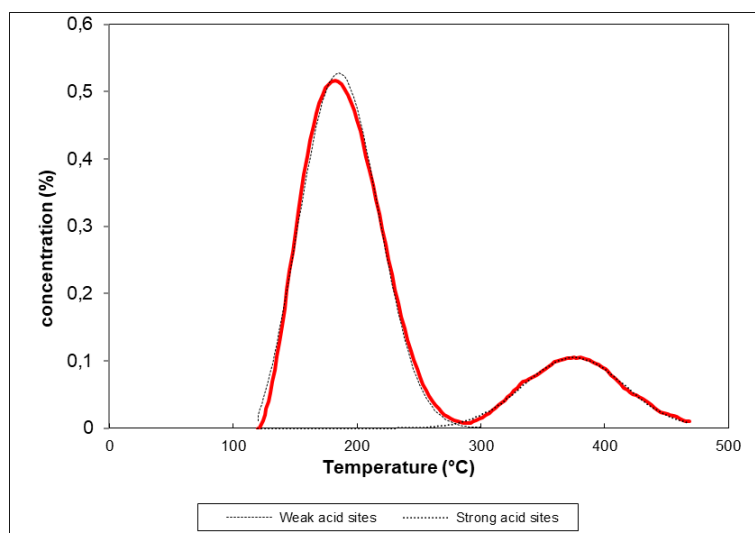


Figure 104: NH_3 -TPD spectrum of ZSM-5@ CeO_2 ($20^\circ\text{C}/\text{min}$)

Appendix H: Arrhenius plots for E_d determination of the strong acid sites

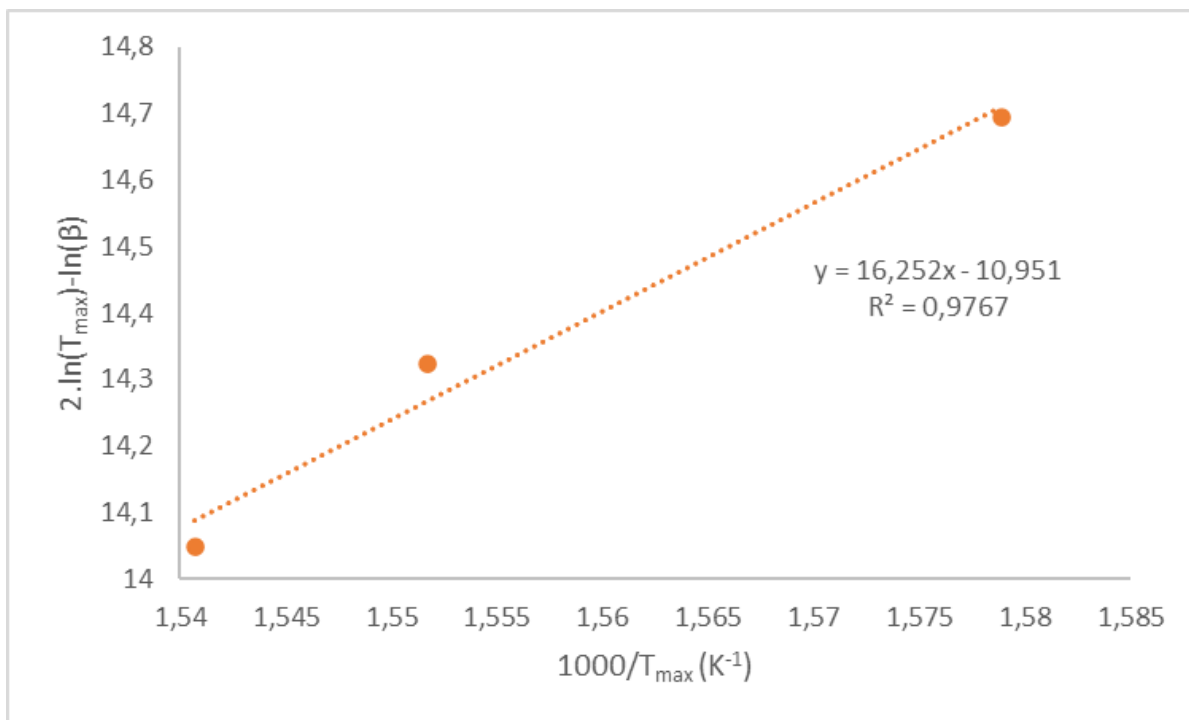


Figure 105: Arrhenius plot for commercial ZSM-5 (1) (acid site)

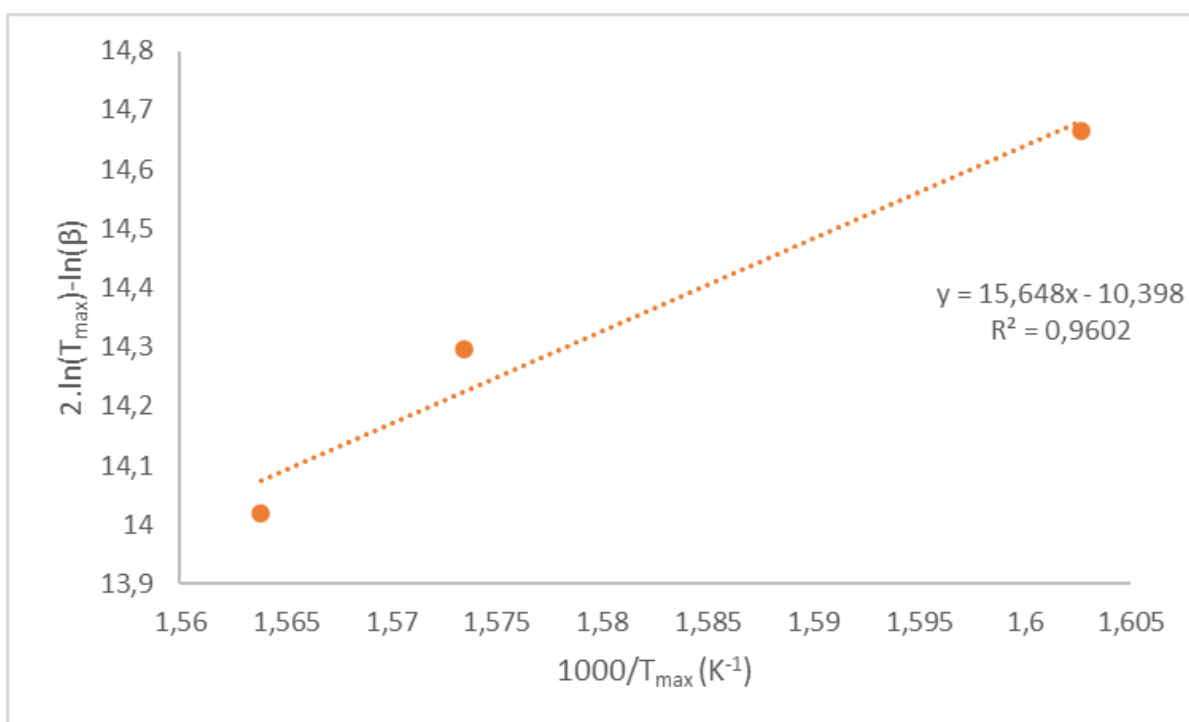


Figure 106: Arrhenius plot for commercial ZSM-5 (2) (acid site)

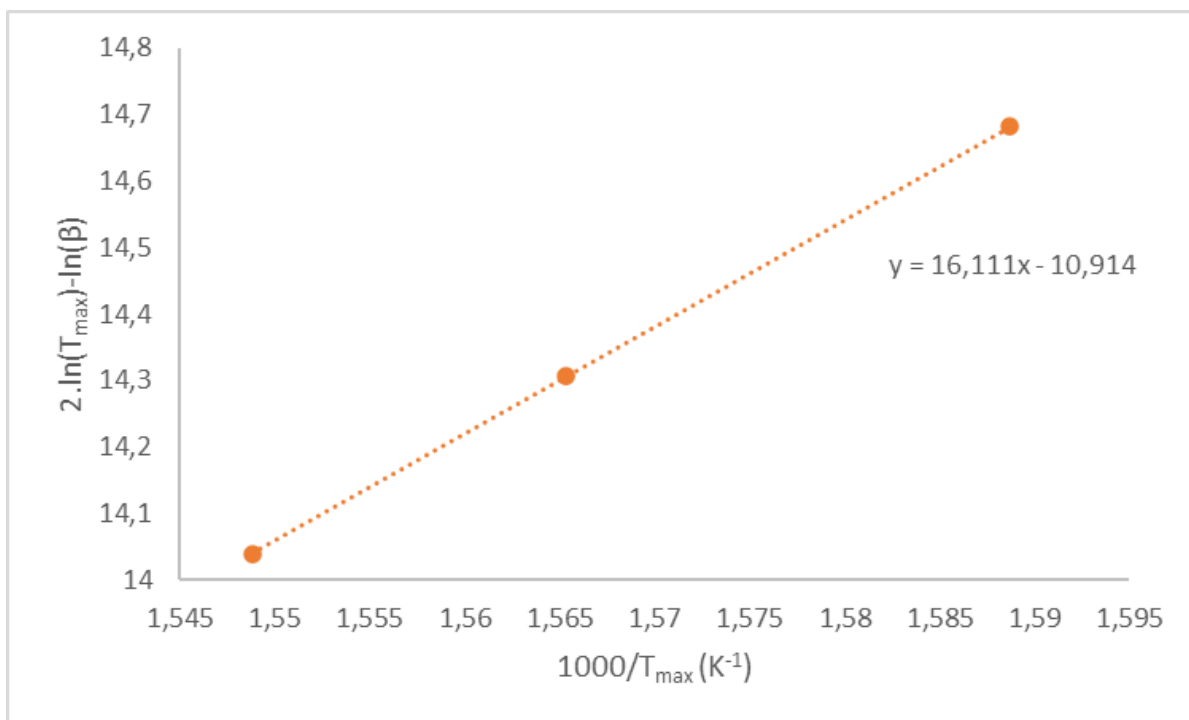


Figure 107: Arrhenius plot for ZSM-5@25 (acid site)

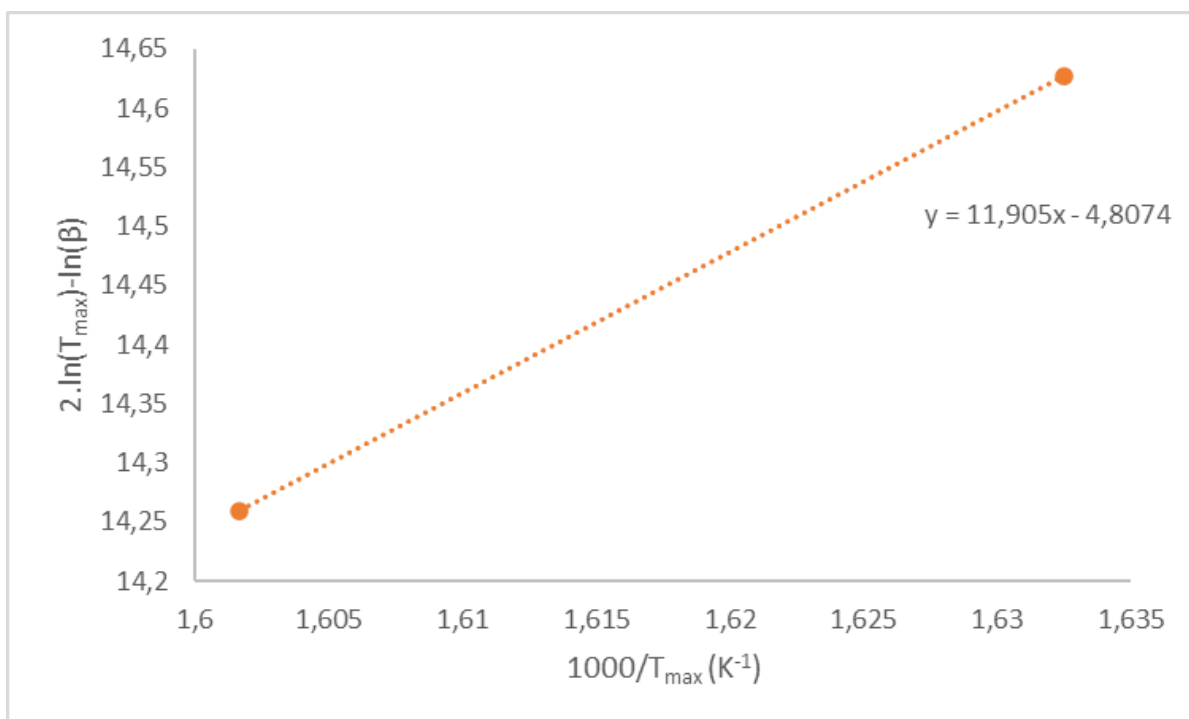


Figure 108: Arrhenius plot for ZSM-5@150 (acid site)

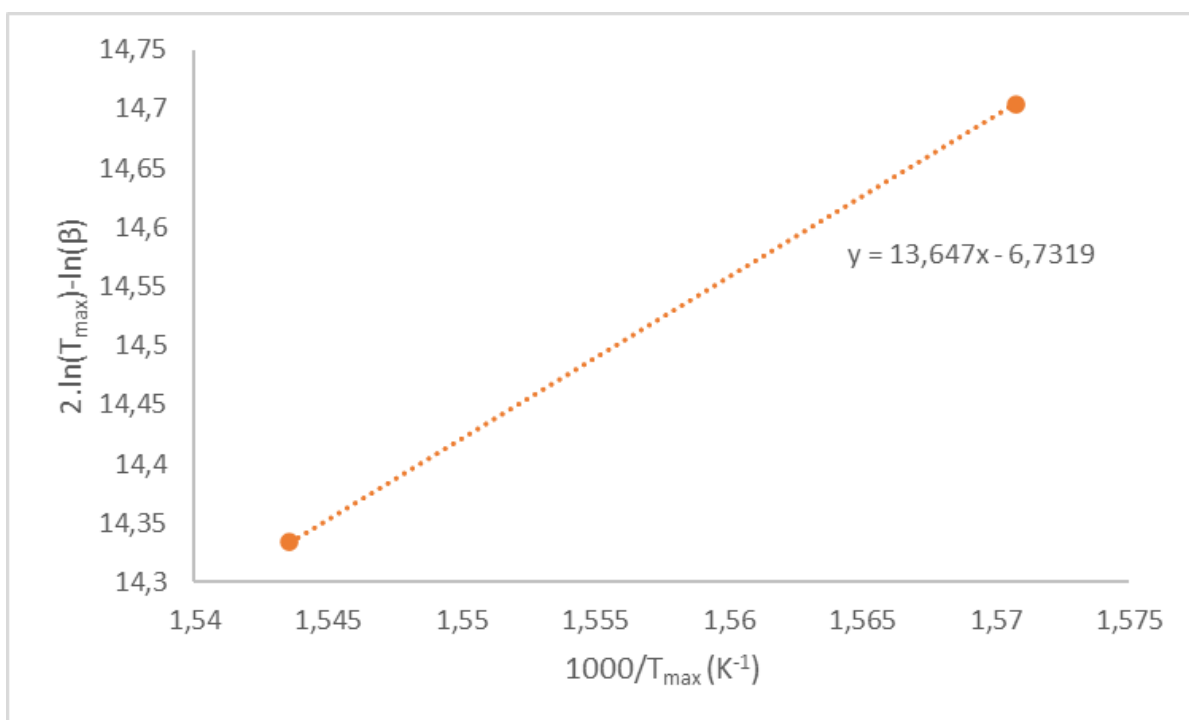


Figure 109: Arrhenius plot for ZSM-5@25_B (acid site)

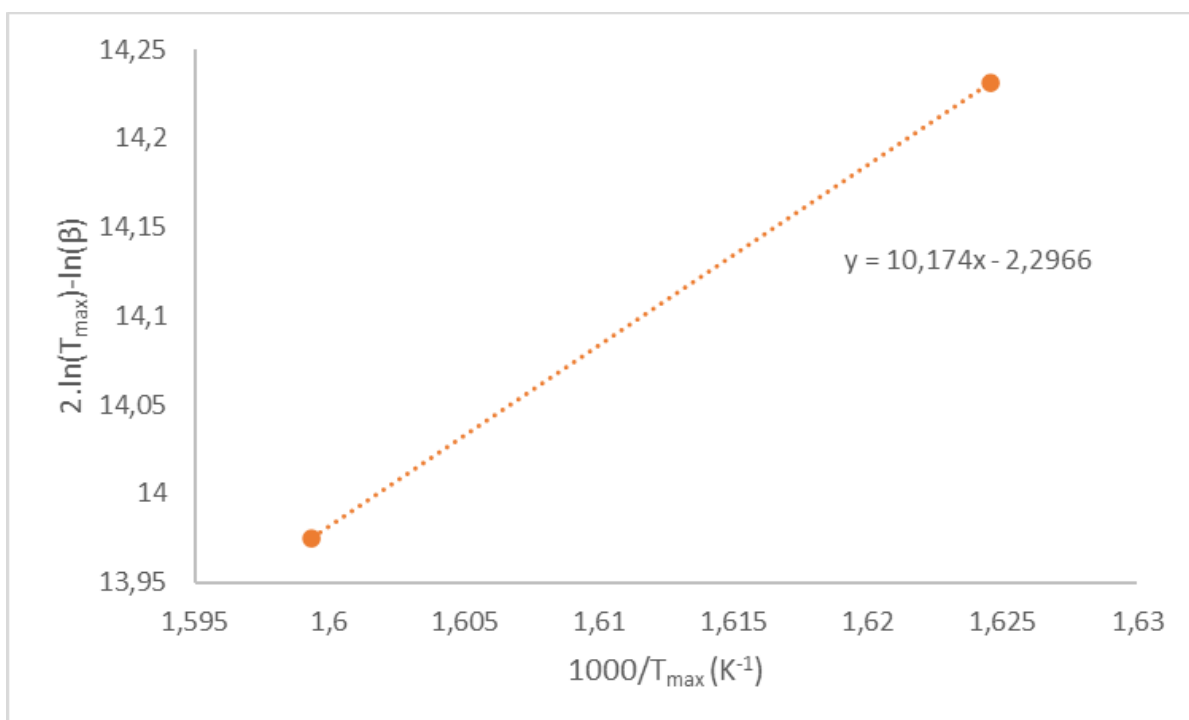


Figure 110: Arrhenius plot for ZSM-5@150_B (acid site)

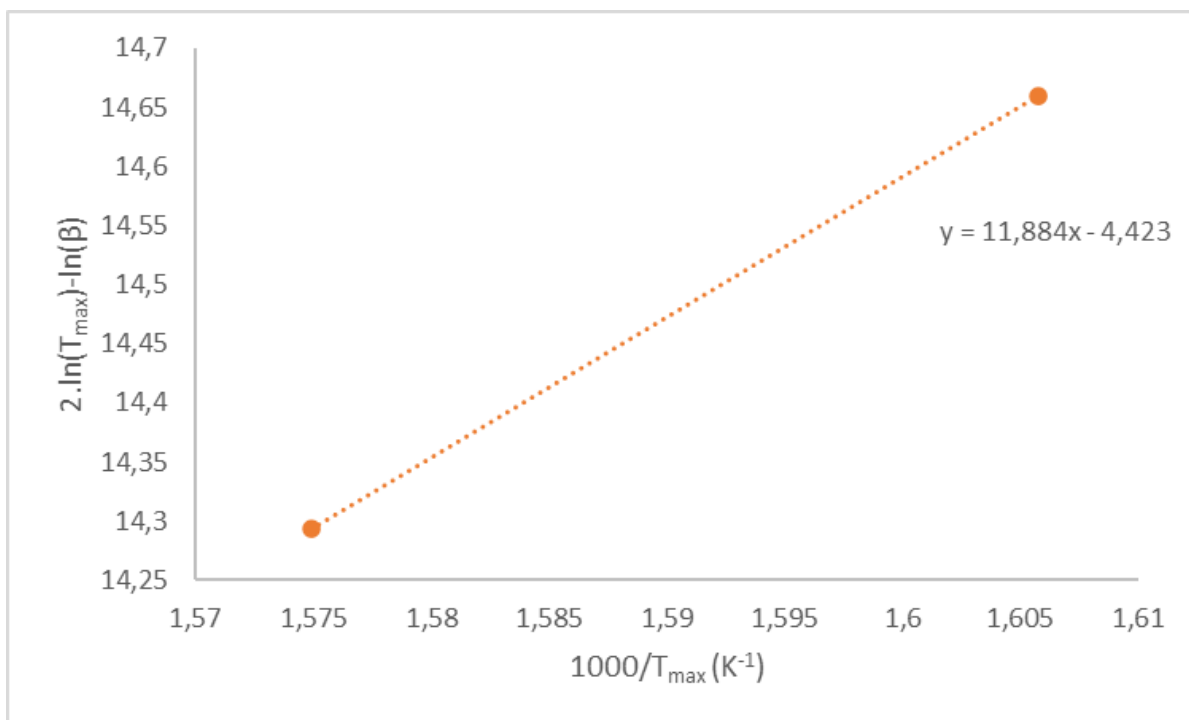


Figure 111: Arrhenius plot for CeO₂/ZSM-5 (acid site)

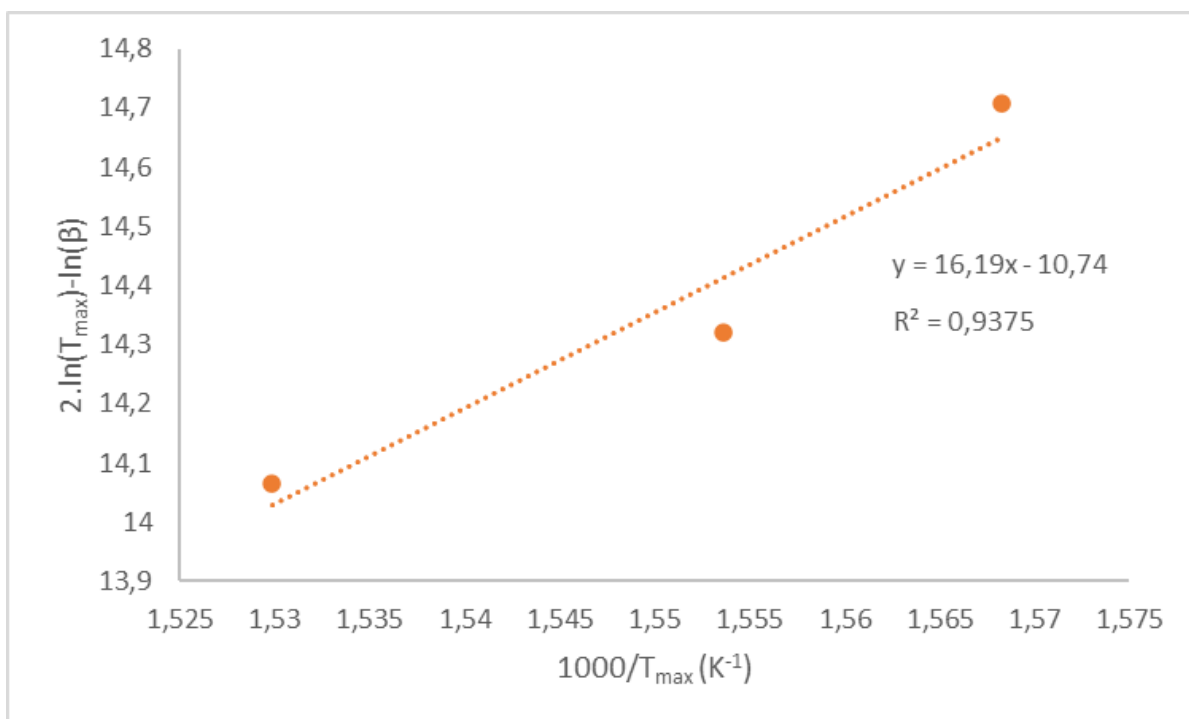


Figure 112: Arrhenius plot for ZSM-5@CeO₂ (acid site)

Appendix I: corrected and deconvoluted CO₂-TPD spectra (respective heating ratio of 10, 15, 20°C/min)

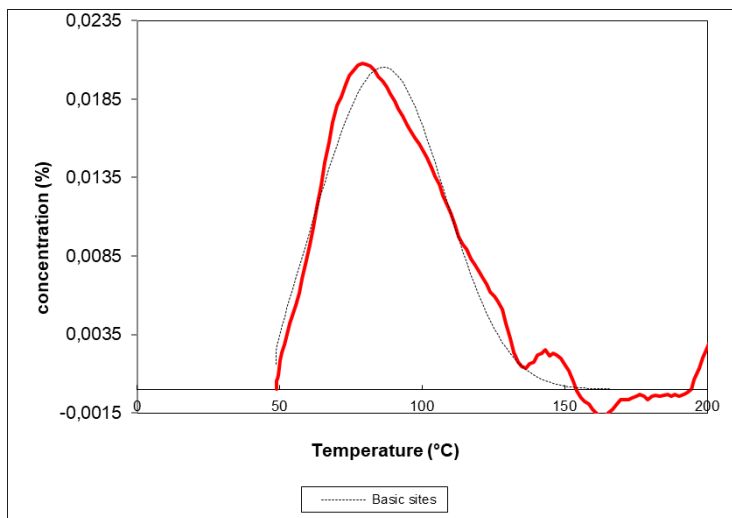


Figure 113: CO₂-TPD spectrum of CeO₂ (10°C/min)

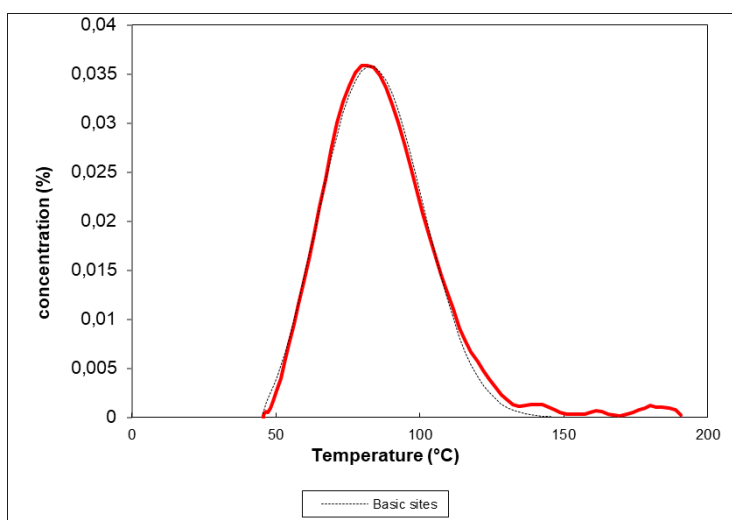


Figure 114: CO₂-TPD spectrum of CeO₂ (15°C/min)

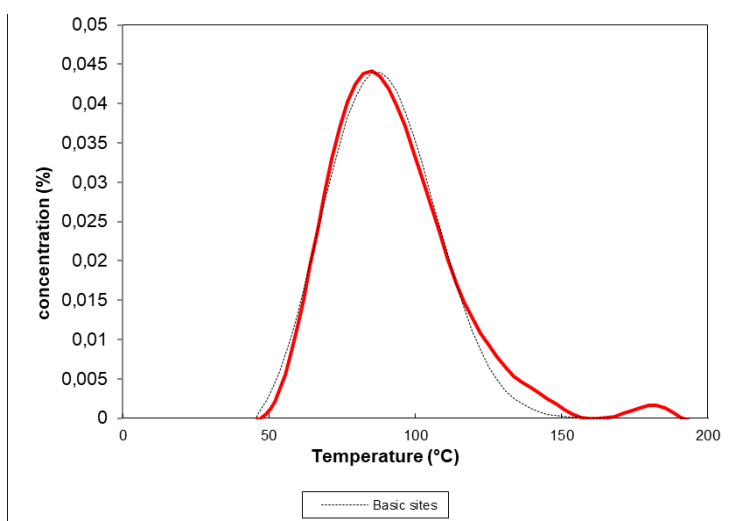


Figure 115: CO₂-TPD spectrum of CeO₂ (20°C/min)

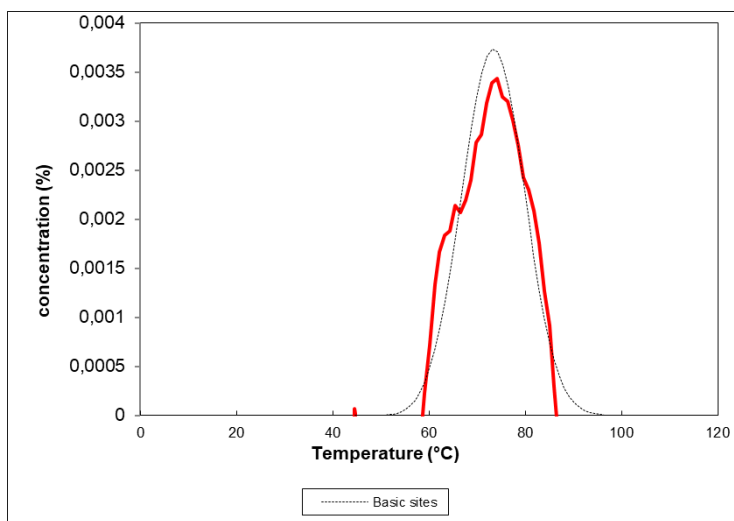


Figure 116: CO₂-TPD spectrum of CeO₂/ZSM-5 (10°C/min)

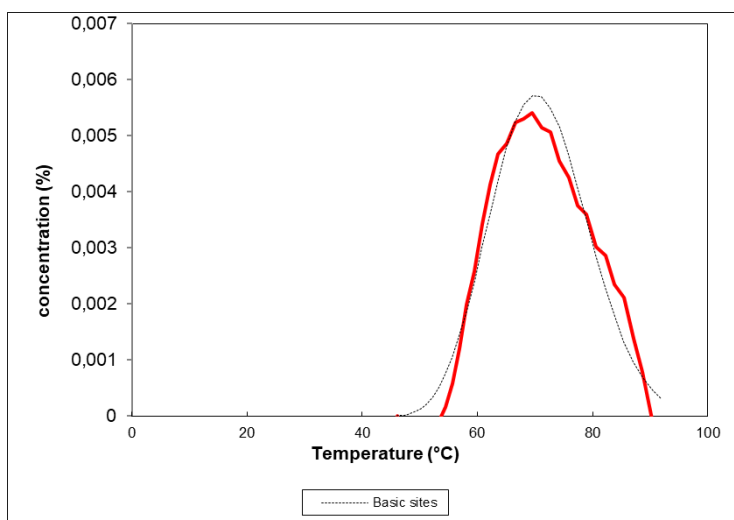


Figure 117: CO₂-TPD spectrum of CeO₂/ZSM-5 (15°C/min)

20°C/min: no useful recording due to software issue

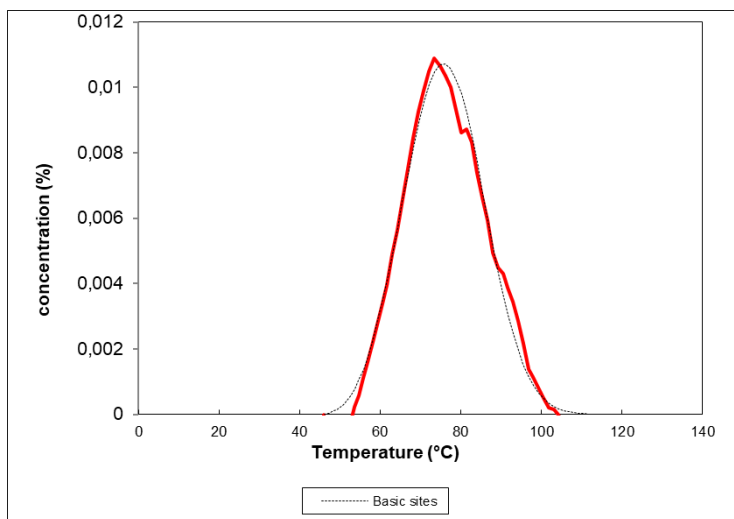


Figure 118: CO₂-TPD spectrum of ZSM-5@CeO₂ (10°C/min)

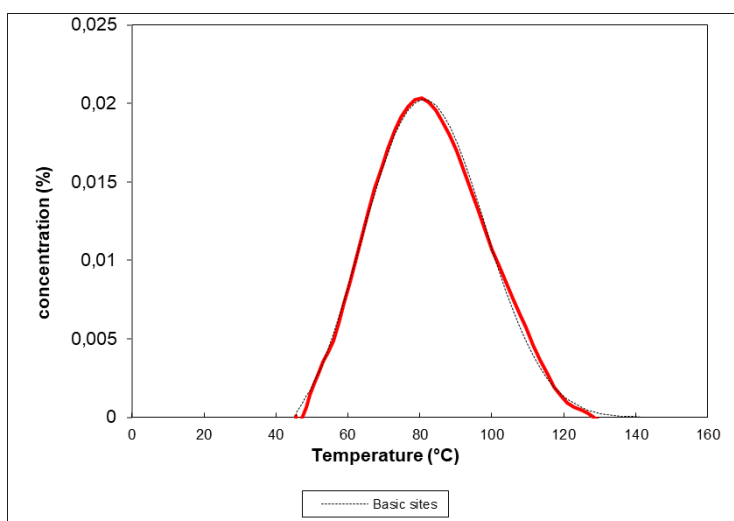


Figure 119: CO₂-TPD spectrum of ZSM-5@CeO₂ (15°C/min)

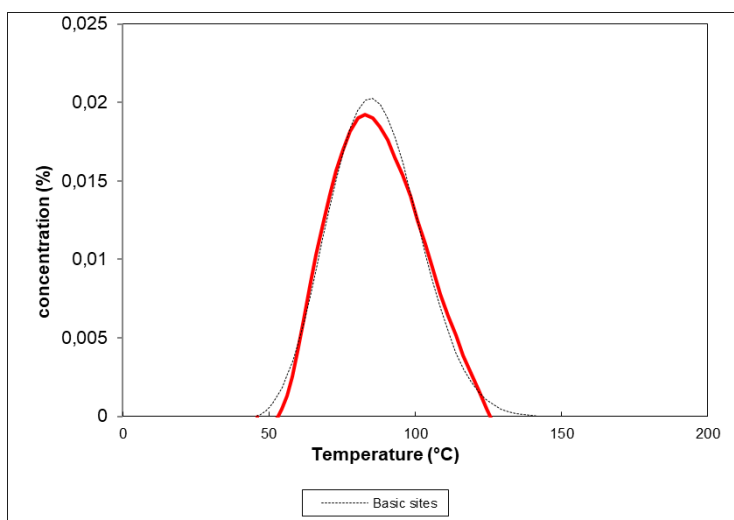


Figure 120: CO₂-TPD spectrum of ZSM-5@CeO₂ (20°C/min)

Appendix J: Arrhenius plots for E_d determination of the basic sites

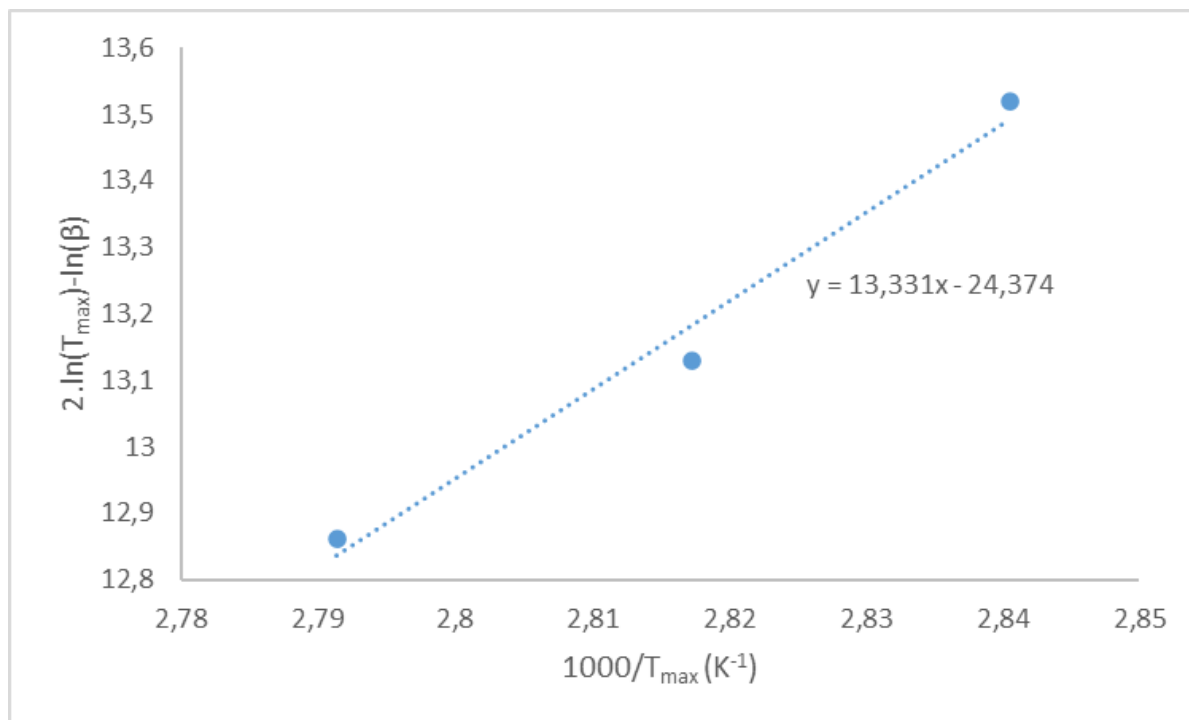


Figure 121: Arrhenius plot for CeO_2 (basic site)

$CeO_2/ZSM-5$:

- measurement of 20°C/min failed due to software issue
- two remaining points do not give rising slope

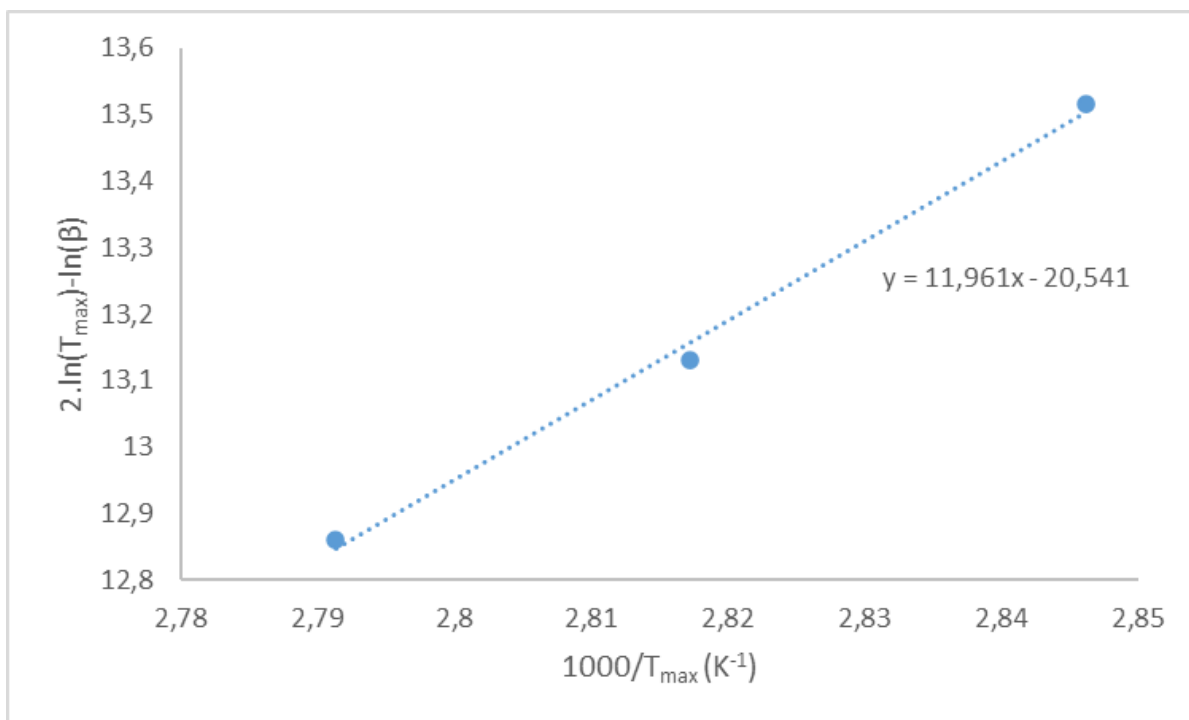


Figure 122: Arrhenius plot for ZSM-5@CeO₂ (basic site)

